The influence of potassium carbonate and potassium chloride during heat treatment of an inertinite-rich bituminous char

A Thesis submitted in fulfillment of the requirements for the degree

Master of Science in Chemistry

at the Potchefstroom Campus of the North-West University

by

Kelebogile Ancient Leeuw

Promoter: Prof. C. Strydom (North-West University)

Co-promoters: Prof. J. Bunt (North-West University)

Dr. D. van Niekerk (Sasol)

December 2012

Acknowledgements

I would like to extend my gratitude and appreciation to Prof Strydom, Prof Bunt and Dr Van Niekerk (Sasol) for their exceptional dedication, support, guidance and time spent throughout the study.

Dr Johan Van Dyk from Sasol Technology and Coal Processing Technologies is thanked for his contribution and insights.

Thanks to Sasol Research and Development for the financial support.

Dr Sabine Verryn of XRD laboratories is thanked for performing XRD analysis of the coal and char samples. Thank you to the ACT laboratories in Pretoria for performing proximate and ultimate analyses; and Sci-ba laboratories for XRF analysis of the samples.

To my family, the Leeuw's (Dad, Mom, Mumsy, Buti, Setty), thank you for your continued support and love. Special thanks to my mom for her prayers, and to my sister Setty for her encouragement and moral support through the trying times.

More importantly, to my Creator and Saviour, thank you for giving me the strength and patience, and for blessing me with the wisdom and intellect to successfully achieve my goals.

Abstract

Thermogravimetry, coupled with a mass spectrometer (TG-MS) was used to investigate the catalytic effect potassium carbonate (K_2CO_3) and potassium chloride (KCl), on the char conversion and the product gas composition of chars derived from a South African inertinite-rich bituminous coal. Sequential leaching of the coal with HCl-HF-HCl was performed to reduce the mineral matter present in the coal. This was done in order to reduce possible undesirable interactions between the minerals and inorganic compounds in the coal during heat treatments. The leaching process substantially reduced the ash content from 21.5% to less than 3%.

K_2CO_3 and KCl [0.5, 1, 3, 5 K-wt %] were loaded to the demineralized coal, raw coal and demineralized coal with added mineral mixture prior to charring. The mineral mixture was made up of kaolinite, quartz, pyrite, siderite, calcite, anastase and hydromagnesite. The 'doped' coal samples were then subjected to heat treatments in a CO_2 atmosphere up to 1200 °C. The results obtained showed that both K_2CO_3 and KCl exhibit a catalytic effect on the char conversion during heat treatments in CO_2 atmosphere and the char conversion was increased with increasing loadings up to 5 K-wt% of K_2CO_3 and KCl. The temperature ranges at which conversion occurred were found to be lower for K_2CO_3 than for KCl. Subsequently, char conversion occurred over a relatively narrower temperature range for K_2CO_3 than observed for KCl. The catalytic behaviour of K_2CO_3 and KCl was confirmed by the results obtained. The results also indicated that the catalytic influence of K_2CO_3 is greater than that of KCl and that KCl is more susceptible to deactivation by minerals and inorganic compounds present in the coal than K_2CO_3.

Different analytical techniques (XRF and XRD) were used to determine the extent of interaction of the catalysts used with the char material in the 5 K-wt% 'doped' coal samples. From the XRF results, it was observed that the K_2O content was reduced after heat treatments in CO_2, however, no potassium crystalline phases were observed in the XRD results after heat treatments in CO_2. The reduced K_2O content may be attributed to the potassium been taken up in other mineral matter during char reaction with CO_2, forming new amorphous inorganic complex compounds. Thus the potassium retained in the sample after heat treatment, indicated by the XRF results, may be in an amorphous phase.

Mass spectrometry (MS) indicated that temperatures at which the maximum rate of evolution of gaseous species occurred were relatively lower for K_2CO_3 loaded char samples

than observed for KCl loaded samples. In addition, no mass-to-charge ratio (m/z) peak at 39 atomic mass unit (amu) from the MS results was observed, indicating that no potassium was detected in the gaseous phases for all the char samples. The undetected potassium in the gaseous phase may be due to the detection limit of the MS equipment.

The MS results also indicated that addition of the catalyst facilitates the evolution of H_2 from the coal char samples. Addition of the catalysts to the samples lowered the temperature at which maximum H_2 was given off. The shift to lower temperatures was observed with increased catalyst loadings for both K_2CO_3 and KCl loaded samples.

Keywords: Catalytic, CO_2, Char, Inertinite, Potassium, TG-MS

Table of Contents

Acknowledgements ii

Abstract iii

Table of Contents v

List of Figures x

List of Tables xiv

List of Abbreviations xvi

List of Appendices xvii

CHAPTER 1 1

Introduction 1

1.1 Problem statement and substantiation 1

1.2 Hypothesis 3

1.3 Research aims and objectives 3

1.4 Method of investigation 4

CHAPTER 2 6

Literature Review 6

2.1 Introduction to coal 6

2.2 Maceral composition 8

2.2.1 Vitrinite 9

2.2.2 Liptinite (or exinite) 10

2.2.3 Inertinite 10

2.2.3.1 Inertodetrinite 11

2.2.3.2 Fusinite 11

2.2.3.3 Semifusinite 12

2.3 Mineral matter in coal 12
2.3.1 Mineral matter behaviour during coal processing 16
2.4 Potassium compounds 16
2.4.1 Reactions of potassium compounds with mineral matter 17
2.5 Coal gasification 18
2.5.1 Volatile product composition 19
2.5.2 Coal-char gasification 20
2.5.3 Mechanism of coal-char gasification in CO_2 21
2.5.4 Catalysed coal-char gasification in CO_2 22
2.5.3.1 Potassium Catalysed CO_2 gasification 25
CHAPTER 3 29
Analysis and Characterization Techniques 29
3.1 Proximate Analysis 29
3.2 Ultimate Analysis 30
3.3 Thermogravimetric (TG) Analysis 31
3.3.1 Derivative of Thermogravimetric (DTG) curves 32
3.4 Mass Spectrometry (MS) 32
3.5 X-Ray Fluorescence 34
3.6 X-Ray-Diffraction 35
CHAPTER 4 37
Experimental Procedures 37
4.1 Sample Preparation 37
4.1.1 Sequential leaching of coal 37
4.1.2 Dopant addition 38
4.1.2.1 Model Mineral Mixture 38

4.1.2.2 Inorganic salts 39
4.2 Thermogravimetry-Mass Spectrometry (TG-MS) 39
4.2.1 Thermogravimetric (TG) Analysis 40
4.2.2 Mass Spectrometer (MS) 41
4.3 Tube furnace experiments 43
4.3.1 Heat treatment in N_2 43
4.3.2 Heat treatment in CO_2 44
4.4 Sample Analysis 44
4.4.1 Proximate and Ultimate Analyses 45
4.4.2 X-Ray Fluorescence (XRF) 45
4.4.3 XRD (X-Ray-Diffraction) 46
4.5 Experimental Plan 46
CHAPTER 5 50
Results and Discussion 50
Characterization of coal samples and additives 50
5.1 Proximate and ultimate analyses 50
5.2 X-ray fluorescence (XRF) 51
5.2.1 Elemental analysis of the raw (untreated) and demineralized (treated/leached) coal 52
5.2.2 Elemental analysis of additives 53
5.2.3 XRF results of raw and demineralized coal after heat treatment in N_2 54
5.3 X-Ray Diffraction of coal and char samples 57
5.3.1 Demineralized coal and char samples with/without catalyst loadings 57
5.3.2 Raw coal and char samples with/without catalyst loadings 60
5.3.3 Demineralized coal and char samples with added mineral mixture, with/without catalyst loadings 63

CHAPTER 6 67

Results and Discussion 67

Thermogravimetric (TG) analysis of coal-char samples 67

6.1 Thermochemistry of K_2CO_3 and KCl 68

6.2 Effect of catalyst loadings on the coal-char derived from demineralized coal 70

6.2.1 TG curves 70

6.2.2 DTG curves 72

6.3 Effect of catalyst loadings on the coal-char derived from raw coal 77

6.3.1 TG curves 77

6.3.2 DTG curves 80

6.4 Effect of catalyst loadings on the coal-char derived from demineralized coal with added mineral mixture 83

6.4.1 TG curves 83

6.4.1 DTG curves 85

6.5 Comparisons of similar samples with/without K_2CO_3 and KCl loadings 88

6.5.1 Comparison of each char sample separately 89

6.5.2 Comparisons of char samples derived from a different coal sample 91

CHAPTER 7 94

Results and Discussion 94

Mass Spectroscopy (MS) of evolved gaseous species from coal-char 94

7.1 TG-MS application 94

7.2 Evolution of gaseous species during char heat treatments in a CO_2 atmosphere 94

7.3 Overview 95

7.3.1 Char formation 95

7.3.2 Typical reaction mechanism of C-CO_2 96

7.4 H_2 evolution profiles 97
7.5 CO evolution profiles 103
7.6 Gaseous carbon evolution profiles 109
7.7 The presence of potassium in the vapour phase of the product gas 115
7.8 Comparisons of the MS results between 5 K-wt% loaded samples 116
7.8.1 Effect of K_2CO_3 and KCl on the temperature ranges of evolution 116
7.8.1.1 H_2 evolution profiles 116
7.8.1.1 CO evolution profiles 121
7.8.2 Relationship between gas evolution temperatures and char conversion 124
CHAPTER 8 130
Summary, Conclusions and Recommendations 130
8.1 Coal Characterization 130
8.2 Thermogravimetric (TG) analyses of coal char 131
8.3 Mass Spectrometry analyses 133
8.4 Catalytic activity of potassium compounds 133
8.5 Recommendations 135
References 136

List of Figures

Figure 1.1 Outline of study ……5

Figure 2.1 Different types of coal ……7

Figure 2.2 Model structure of bituminous coal ……8

Figure 2.3 Model structure of coal during pyrolysis ……18

Figure 2.4 Volatile products evolved durng devolatilization of coal ……19

Figure 2.5 Pyrolysis process ……20

Figure 2.6 Mechanisms for potassium-catalyzed CO_2 gasification ……26

Figure 3.1 Components of a thermogravimetric analyzer ……32

Figure 3.2 Components of a mass spectrometer ……33

Figure 3.3 X-ray pathways during XRF analysis ……34

Figure 3.4 X-ray pathways during XRD analysis ……35

Figure 4.1 Acid leaching procedure with HCl and HF ……38

Figure 4.2 Thermogravimetric Analyzer ……40

Figure 4.3 TG thermobalance onto which the sample was loaded ……40

Figure 4.4 Mass Spectrometer connected to the TG instrument ……41

Figure 4.5 Horizontal tube furnace ……43

Figure 4.6 Sample loading into the tube furnace ……44

Figure 5.1 XRD diffractogram for the demineralized coal before heat treatment ……59

Figure 5.2 XRD diffractogram for the demineralized coal after N_2 heat treatment ……59

Figure 5.3 XRD diffractogram for the demineralized coal after CO_2 heat treatment ……60

Figure 5.4 XRD diffractogram for the raw coal before heat treatment ……62

Figure 5.5 XRD diffractogram of the raw coal after N_2 heat treatment ……62

Figure 5.6 XRD diffractogram for the raw coal after CO_2 heat treatment ……63

Figure 5.7 XRD diffractogram for the demineralized coal with added mineral mixture after N_2 heat treatment ……66

Figure 5.8 XRD diffractogram for demineralized coal with added mineral mixture after CO_2 heat treatment ……66

Figure 6.1 TG curve of K_2CO_3 in CO_2 ……68

Figure 6.2 TG curve of KCl in CO_2 ……70

Figure 6.3 TG curves of the char derived from the demineralized coal with K_2CO_3 loadings during heat treatment in CO_2 atmosphere ……71

Figure 6.4 TG curves of the char derived from the demineralized coal with KCl loadings during heat treatment in CO_2 atmosphere ……71

Figure 6.5 DTG curves of the char derived from the demineralized coal with K_2CO_3 loadings during heat treatment in CO_2 atmosphere ……72

Figure 6.6 TG curves of the char derived from the demineralized coal with KCl loadings during heat treatment in CO_2 atmosphere ……73

Figure 6.7 Illustration of characteristic temperatures by visual inspection of the DTG ……74

Figure 6.8 Illustration of the temperature at 50% mass loss ($T_{50\%}$) determination ……75

Figure 6.9 Reactivity at T_{max} of the char derived from the demineralized coal with K_2CO_3 and KCl loadings ……76

Figure 6.10 Reactivity at $T_{50\%}$ of the char derived from the demineralized coal with K_2CO_3 and KCl loadings ……76

Figure 6.11 TG curves of the char derived from the raw coal with K_2CO_3 loadings during heat treatment in CO_2 atmosphere ……78

Figure 6.12 TG curves of the char derived from the raw with KCl loadings during heat treatment in CO_2 atmosphere ……78

Figure 6.13 DTG curves of the char derived from the raw coal with K_2CO_3 loadings during heat treatment in CO_2 atmosphere ……80

Figure 6.14 DTG curves of the char derived from the raw coal (RC) with KCl loadings during heat treatment in CO_2 atmosphere ……80

Figure 6.15 Reactivity at T_{max} of char derived from the raw coal (RC) with K_2CO_3 and KCl loadings ……82

Figure 6.16 Reactivity at $T_{50\%}$ of the char derived from the raw coal (RC) with K_2CO_3 and KCl loadings ……82

Figure 6.17 DTG curves of the char derived from the demineralized coal with added mineral mixture with K_2CO_3 loadings during heat treatment in CO_2 atmosphere ……83

Figure 6.18 TG curves of the char derived from the demineralized coal with added mineral mixture with KCl loadings during heat treatment in CO_2 atmosphere ……..84

Figure 6.19 DTG curves of the char derived from the demineralized coal with added mineral mixture with K_2CO_3 loadings during heat treatment in CO_2 atmosphere ……85

Figure 6.20 DTG curves of the char derived from the demineralized coal with added mineral mixture with KCl loadings during heat treatment in CO_2 atmosphere……..86

Figure 6.21 Reactivity at T_{max} of the char derived from the demineralized coal with added mineral mixture(DC+MM) with K_2CO_3 and KCl loading ……87

Figure 6.22 Reactivity at $T_{50\%}$ of the char derived from the demineralized coal with added mineral mixture(DC+MM) with K_2CO_3 and KCl loading ……..88

Figure 6.23 TG curves of the char derived from the demineralized coal with 5 K-wt% catalyst loading ……89

Figure 6.24 TG curves of the char derived from the raw coal with 5 K-wt% catalyst loading ……89

Figure 6.25 TG curves of the char derived from the demineralized coal with added mineral mixture and 5 K-wt% catalyst loading ……90

Figure 6.26 TG curves of the char derived from 5 K-wt% K_2CO_3 loaded samples of the demineralized coal, raw coal and demineralized coal with added mineral mixture ……91

Figure 6.27 TG curves of the char derived from 5 K-wt% KCl loaded samples of the demineralized coal, raw coal and demineralized coal with added mineral mixture ……..92

Figure 7.1 Model structure of coal-char after pyrolysis ……..95

Figure 7.2 Illustration of CO_2 chemisorption during C-CO_2 reaction ……..96

Figure 7.3 Abstraction of hydrogen by the CO_2 molecular gas phase ……97

Figure 7.4 Mass spectra of H_2 for the char derived from the demineralized coal with/without catalyst loadings ……..100

Figure 7.5 Mass spectra of H_2 for the char derived from the raw coal with/without catalyst loadings ……101

Figure 7.6 Mass spectra of H_2 for the char derived from the demineralized coal with added mineral mixture, with/without catalyst loadings ……102

Figure 7.7 Mass spectra of CO for the char derived from the demineralized coal with/without catalyst loadings ……106

Figure 7.8 Mass spectra of CO for the char derived from the raw coal with/without catalyst loadings ……107

Figure 7.9 Mass spectra of CO for coal char derived from demineralized coal with added mineral mixture, with/without catalyst loadings ……108

Figure 7.10 Mass spectra of gaseous carbon for the char derived from demineralized coal with/without catalyst loadings ……112

Figure 7.11 Mass spectra of gaseous carbon for the char derived from the raw coal with/without catalyst loadings ……113

Figure 7.12 Mass spectra of gaseous carbon for the char derived from the demineralized coal with added mineral mixture, with/without catalyst loadings ……114

Figure 7.13 The effect of K_2CO_3 and KCl on the temperatures of H_2 evolution for the char derived from the demineralized ……118

Figure 7.14 The effect of K_2CO_3 and KCl on the temperatures of H_2 evolution for the char derived from the raw coal ……119

Figure 7.15 The effect of K_2CO_3 and KCl on the temperatures of H_2 evolution for the char derived from the demineralized coal with added mineral mixture ……120

Figure 7.16 The effect of K_2CO_3 and KCl on the temperatures of CO_2 evolution for the char derived from the demineralized coal ……121

Figure 7.17 The effect of K_2CO_3 and KCl on the temperatures of CO_2 evolution for the char derived from the raw coal ……122

Figure 7.18 The effect of K_2CO_3 and KCl on the temperatures of CO_2 evolution for the char derived from the demineralized coal with added mineral mixture ……123

Figure 7.19 DTG-MS analysis of the char derived from the demineralized coal with 5 K-wt% K_2CO_3 loading ……125

Figure 7.20 DTG-MS analysis of the char derived from the demineralized coal with 5 K-wt% KCl loading ……126

Figure 7.21 DTG-MS analysis of the char derived from the raw coal with 5 K-wt% K_2CO_3 loading ..127

Figure 7.22 DTG-MS analysis of the char derived from the raw coal with 5 K-wt% KCl loading ……127

Figure 7.23 DTG-MS analysis of the char derived from the demineralized coal with added mineral mixture and 5 K-wt% K_2CO_3 loading ……128

Figure 7.24 DTG-MS analysis of the char derived from the demineralized coal with added mineral mixture and 5 K-wt% KCl loading ……129

List of Tables

Table: 2.1 Summary of macerals found in hard coals 9

Table 2.2 Principal minerals found in coal 15

Table 2.3 Proposed models for gasification of carbon in CO_2 22

Table 4.1 Chemical compounds of the model mineral mixture 39

Table 4.2 List of samples prepared for TG-MS experiments 47

Table 4.3 List of samples prepared for tube furnace experiments 48

Table 4.4 Experimental conditions for TG-MS and tube furnace experiments 49

Table 5.1 Proximate and Ultimate analyses results of the raw coal and demineralised coal 51

Table 5.2 XRF results for the raw and demineralized coal 53

Table 5.3 XRF results for the catalysts and mineral mixture 54

Table 5.4 XRF results of samples with/without 5 K-wt% catalyst loadings before and after heat treatments in N_2 and CO_2 atmospheres 56

Table 5.5 XRD results of demineralized coal and char samples with/without 5 K-wt% catalyst loadings 58

Table 5.6 Carbon-free basis XRD results of the demineralized coal and char samples with/without 5 K-wt% catalyst loadings 58

Table 5.7 XRD results of the raw coal and char samples with/without 5 K-wt% catalyst loadings 61

Table 5.8 Carbon-free XRD results of raw coal and char samples with/without 5 K-wt% catalyst loadings 62

Table 5.9 XRD results of the demineralized coal and char samples with added mineral mixture, with/without 5 K-wt% catalyst loadings 64

Table 5.10 Carbon-free XRD results of the demineralized coal and char samples with added mineral mixture, with/without 5 K-wt% catalyst loadings 65

Table 6.1 Characteristic temperatures of the char derived from the demineralized coal with/without catalyst loadings 74

Table 6.2 Characteristic temperatures of the char derived from the raw coal with/without catalyst loadings 81

Table 6.3 Characteristic temperatures of the char derived from the demineralized coal with added mineral mixture, with/without catalyst loadings ……87

Table 7.1 Temperatures at maximum rate of H_2 evolution of the chars derived from the demineralized coal, with/without catalyst loadings ……98

Table 7.2 Temperatures at maximum rate of H_2 evolution of the chars derived from the raw coal, with/without catalyst loadings ……99

Table 7.3 Temperatures at maximum rate of H_2 evolution of the chars derived from the demineralized coal with added mineral mixture, with/without catalyst loadings ……..99

Table 7.4 Temperatures at maximum rate of CO evolution of the chars derived from the demineralized coal, with/without catalyst loadings ……104

Table 7.5 Temperatures at maximum rate of CO evolution of the chars derived from the raw coal, with/without catalyst loadings ……..105

Table 7.6 Temperatures at maximum rate of CO evolution of the chars derived from the demineralized coal with added mineral mixture, with/without catalyst loadings ……105

Table 7.7 Temperatures at maximum rate of gaseous carbon evolution of the chars derived from the demineralized coal, with/without catalyst loadings ……110

Table 7.8 Temperatures at maximum rate of gaseous carbon evolution of the chars derived from the raw coal with added mineral mixture, with/without catalyst loadings ……110

Table 7.9 Temperatures at maximum rate of gaseous carbon evolution of the chars derived from the demineralized coal, with/without catalyst loadings ……111

List of Abbreviations

ΔT	change in temperature
AMU	atomic mass unit
CO_2	carbon dioxide
DC	demineralized coal
DC+MM	demineralized coal with added mineral mixture
DTG	derivative of the thermogravimetric curve
HCl	hydrochloric acid
HF	hydrofluoric acid
ISO	International Standard Organization
K_2CO_3	potassium carbonate
KCl	potassium chloride
K-wt%	potassium weight percentage
LTA	low temperature ashing
M/Z	mass-to-charge-ratio
MM	mineral mixture
MS	mass spectrometry
N_2	nitrogen
RC	raw coal
$T_{50\%}$	temperature at 50% mass loss
T_f	final temperature
TG	thermogravimetry
TG-MS	thermogravimetry coupled with mass spectrometry
T_i	initial temperature
T_{max}	maximum temperature
Wt %	weight percentage
XRD	X-ray diffraction
XRF	X-ray fluorescence

List of Appendices

Appendix A

Table A1 Minor and trace elemental analysis of samples with/without 5 K-wt% K_2CO_3 and KCl loadings before and after heat treatments in N_2 and CO_2 atmospheres ……ii

Figure A1 XRD diffractogram of DC + 5 K-wt% K_2CO_3 after heat treatment in N_2 ……vii

Figure A2 XRD diffractogram of DC + 5 K-wt% K_2CO_3 after heat treatment in CO_2 ……vii

Figure A3 XRD diffractogram of DC + 5 K-wt% KCl after heat treatment in N_2 ……viii

Figure A4 XRD diffractogram of DC + 5 K-wt% KCl after heat treatment in CO_2 ……viii

Figure A5 XRD diffractogram of RC + 5 K-wt% K_2CO_3 after heat treatment in N_2 ……ix

Figure A6 XRD diffractogram of RC + 5 K-wt% K_2CO_3 after heat treatment in CO_2 ……ix

Figure A7 XRD diffractogram of RC + 5 K-wt% KCl after heat treatment in N_2 ……x

Figure A8 XRD diffractogram of RC + 5 K-wt% KCl after heat treatment in CO_2 ……x

Figure A9 XRD diffractogram of DC+MM + 5 K-wt% K_2CO_3 after heat treatment in N_2 ……xi

Figure A10 XRD diffractogram of DC+MM + 5 K-wt% K_2CO_3 after heat treatment in CO_2 ……xi

Figure A11 XRD diffractogram of DC+MM + 5 K-wt% KCl after heat treatment in N_2 ……xii

Figure A12 XRD diffractogram of DC+MM + 5 K-wt% KCl after heat treatment in CO_2 ……xii

Table A2 Temperature values at $T_{50\%}$ ……xiii

CHAPTER 1

Introduction

This chapter gives the aims and objectives of this study and the motivation thereof. The proposed method of investigation is also outlined in this chapter.

1.1 Problem statement and substantiation

Mineral matter present in coal is known to have a significant effect on coal utilization processes such as combustion, coking and gasification [Matjie et al., 2011]. Mineral matter comprises of all inorganic materials and elements present in coal as discrete (crystalline and non-crystalline) mineral phases [Ward, 2002], and may occur in coal as minerals, mineraloids and as organically-associated inorganic elements [Matjie, 2011]. During heat treatments, these minerals react and are transformed, resulting in newly formed mineral phases [Moulijn and Kapteijn, 1984; Vassileva and Vassilev, 2006]; that can have both negative effects (e.g. fouling, slagging, corrosion of equipment and the reduction in the overall rate of coal conversion processes) and positive effects (e.g. catalytic behavior of minerals and also act as dispersive agents) on coal conversion plants [Matjie et al., 2011; Vamvuka, 2006; Kershaw and Taylor, 1992].

Potassium compounds are some of the minerals that can act as catalysts and are known to be among the most effective in coal gasification. They have been shown to significantly enhance the reactivity of coal during processing [Rivera-Utrilla et al., 1987; Kyotani et al., 1993]. These compounds are found in naturally occurring potassium-bearing minerals in coal, and according to Spiro et al. [1986], the potassium compounds are commonly found in clay minerals such as muscovite [$KAl_2(AlSi_3O_{10})(OH)_2$], illite [$K_{0.66}Al_2(Al_{0.66}Si_{3.33}O_{10})(OH)_2$], leucite [$KAlSiO_6$] and feldspar [$KAlSi_3O_8$]. However, synthetic potassium compounds may also be deliberately added to coal to enhance its reactivity. The potassium additives may include strong bases, organic salts and inorganic salts. According to Formella et al. [1986], the higher the amount of clay minerals in coal; the larger the amount of catalyst that must be added to increase the coal's reactivity.

The associated precursor anion of the catalyst has also been reported to play an important role as to how effective the catalyst would be during coal heating [Lang, 1986; Huttinger and Minges, 1986]. According to Veraa and Bell [1978], oxides, hydroxides, bicarbonates and carbonates are more active than other salts. Huttinger and Minges [1986] reported that during steam gasification, the reactivity of the potassium salts have the following sequence: KOH ~ K_2CO_3 ($KHCO_2$, $K_2C_2O_4$, $KO_2C_2H_3$) ~ KNO_3 > K_2SO_4 > KCl. Marsh and Walker [1979] reported that the effect of the addition of potassium salts to coal may be due to their ability to destroy the coking and caking processes apparent in some coals, thus reducing the fluidity during heat treatments. In addition, the presence of some potassium salts result in increased oxygen content in coal during heat treatments and as a result, reactivity is enhanced. Furthermore, the reactivity of the resulting char is also enhanced because of the catalytic effect of the retained potassium.

On the other hand, potassium compounds are known to react with mineral matter in coal resulting in catalytically inactive silicates [Huttinger and Minges, 1986]. For instance, potassium reacts with clay minerals and pyrite forming inactive compounds such as $KAlSiO_4$ and $KFeS_2$, respectively [Lang, 1986]. According to Rivera-Utrilla et al. [1987], this behaviour may be overcome by increasing the catalyst loading.

South African coal reserves are said to produce over 95% bituminous coal (ranging from high to low volatile content), with inertinite as the dominating maceral [Kershaw and Taylor, 1992]. The maceral content of Highveld coals is reported to consist of about 88% inertinite maceral, and semifusinite is said to be the dominating inertinite maceral [Van Niekerk et al., 2010]. The high inertinite maceral in South African coals is known to pose problems when subjected to heat treatments [Malumbazo et al., 2011]. South African coals are also reported to have high mineral matter contents (more than 75%) and ash yields, sometimes in excess of 20% [Van Niekerk et al., 2008; Kershaw and Taylor, 1992]. The dominant minerals are clays, carbonates, sulphides, quartz and glauconite [Falcon and Snyman, 1986]; with kaolinite being the principal clay mineral (more than 80%) in South African coals [Kershaw and Taylor, 1992].

Catalysts are reported to play an important role in controlling the distribution and composition of the gaseous products, due to the ability to selectively promote a particular reaction during coal and coal char thermal processing [Veraa and Bell, 1978; Kim et al., 1989]. During conventional coal gasification, the main gaseous products are a mixture of H_2, CO, CO_2, CH_4 and other minor gases [Wang et al., 2009]; however, the presence of a catalyst has been shown to lower the formation rates of CO_2 [Huttinger and Minges, 1986]. During coal gasification

(in steam and oxygen), reaction temperatures higher than 1000°C are required, however studies have shown that when catalysts are used, the reaction temperatures are significantly lowered with simultaneous high coal throughputs [Wang et al., 2009; Veraa and Bell, 1978].

Although South Africa is the fifth largest coal producer worldwide [World Coal Institute, 2008], there is comparatively little scientific knowledge of its inertinite-rich coals, as most studies have mainly focused on the vitrinite-rich coals of the Northern hemisphere. It is only in recent years that studies have focused on South African coals [Hattingh et al., 2011; Van Niekerk et al., 2008; Van Niekerk et al., 2010; Van Niekerk and Matthews, 2010; Strydom et al., 2011; Malumbazo et al., 2011; Everson et al., 2008; Klopper et al., 2012]. However, there is still a need for more detailed studies in order to evaluate and understand the behaviour of South African coals in different utilization processes.

1.2 Hypothesis

Inorganic salts such as potassium carbonate (K_2CO_3) and potassium chloride (KCl) exhibit a catalytic effect on coal char conversion during heat treatments. The amount of K_2CO_3 and KCl may have a controlling effect on the volatile species formed during heat treatments of the coal char.

1.3 Research aims and objectives

The aims and objectives of this study include heat treatments of a char derived from a South African inertinite-rich coal, up to temperatures of 1200°C in a CO_2 atmosphere in order to:

- investigate the effects of K_2CO_3 and KCl loadings on char conversion during heat treatments in a CO_2 atmosphere ;
- identify some of the gaseous species formed during treatments of the coal char in a CO_2 atmosphere;
- investigate the effects of K_2CO_3 and KCl loadings on the composition of the volatile reaction products released from the coal-char during heat treatments in a CO_2 atmosphere;

- determine which inorganic salt exhibits a greater catalytic effect during heat treatment of the coal-char in a CO_2 atmosphere.

1.4 Method of investigation

Figure 1.1 below represents the outline of the study. Sequential leaching of an inertinite-rich bituminous coal was conducted using an acid treatment method using HCl-HF-HCl [Strydom et al., 2011; Van Niekerk et al., 2008, Van Niekerk et al., 2010; Ishihara et al., 2004]. Bituminous coals are well known to consist of inorganic salts and mineral matter of up to more than 30%; and the leaching process is known to reduce these minerals to less than 3% [Strydom et al., 2011; Van Niekerk et al., 2008; Van Niekerk et al., 2010]. The leaching process is essential in order to reduce mineral-mineral and mineral–coal interactions during the reaction conditions that will be employed in this study. Proximate and ultimate analyses of the raw (untreated) coal and of the leached (demineralized) coal were performed in order to determine the extent of the leaching process on the coal sample.

Various amounts of K_2CO_3 and KCl (0.5, 1, 3, and 5 K-wt%) were loaded to the demineralized coal, raw coal and the demineralized coal with an added model mineral mixture. The prepared mineral mixture was made up of 25% kaolin clay, 20% quartz, 20% Pyrite, 15% Calcite, 8% Siderite, 8% hydromagnesite, and 4% anastase [Nel et al., 2011]. The ‘doped’ coal samples were then subjected to heat treatments (up to 900°C in a N_2 atmosphere) in a thermogravimetric (TG) analyzer to prepare the respective chars. The resulting chars were further subjected to heat treatments up to 1200°C in a CO_2 atmosphere, in a thermogravimetric analyzer coupled with a mass spectrometer (TG-MS). The MS was used to simultaneously identify the gaseous products formed during heat treatments of the coal-char in temperatures of up to 1200°C in a CO_2 atmosphere. The influence of the inorganic salts and the level of loadings on the char conversion and the gas composition were investigated.

Tube furnace experiments were conducted on the 5 K-wt% loaded samples in N_2 and CO_2 atmospheres. XRD and XRF analyses of the coal samples before and after heat treatments in CO_2 were performed on the product samples.

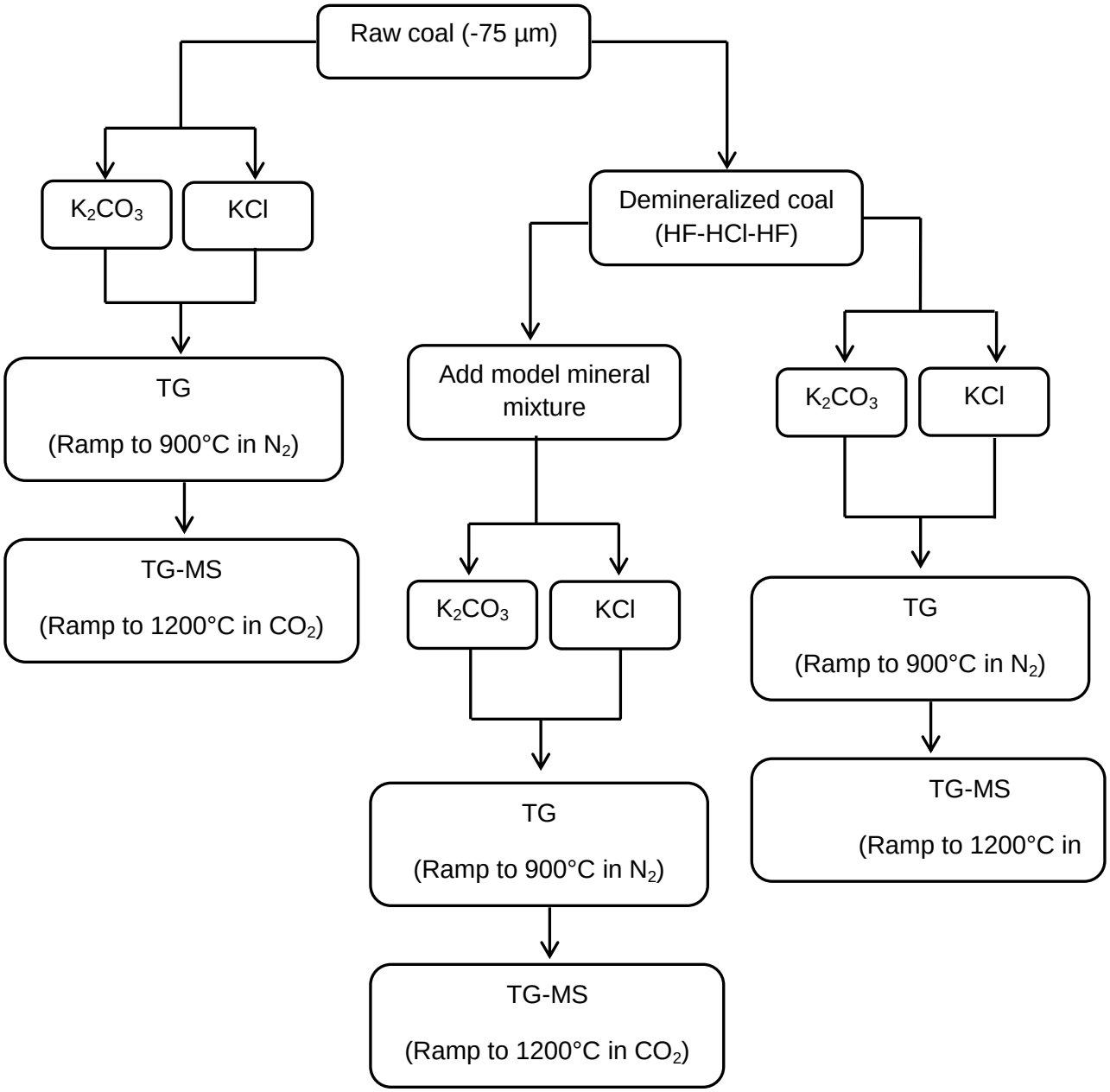

Figure 1.1 Outline of study

CHAPTER 2

Literature Review

This chapter gives a literature overview of coal composition and coal classification. It also focuses on the influence of mineral matter during coal processing, as well as catalyst behaviour and the influence of catalyst additions during coal heat treatments.

2.1 Introduction to coal

Coal, a heterogeneous, combustible sedimentary organic rock; is made up of fossilized plant material which has undergone chemical and physico-structural changes over a period of time [Falcon and Snyman, 1986; Van Niekerk et al., 2010; Oboirien et al., 2011; Snyman, 1998, Stach et al., 1982]. Coal is by far the largest and most complex natural raw material known, having adequate reserves to meet its expected demand as an energy source [Snyman, 1998; Falcon and Snyman, 1986].

Coal is made up of both organic (macerals) and inorganic (minerals) matter [Ward, 2002; Snyman, 1998]. The organic component of coal (which is consequential of plant debris) determines the nature of the coal (e.g. rank/maturity and type); hence all the benefits of coal during utilization processes are as a result of these constituents [Taylor and Liu, 1987; Ward, 2002]. On the other hand, the inorganic part of coal contributes little value to coal, and mostly poses problems during coal utilization processes [Ward, 2002]. According to Snyman [1998]: “more than 20 variables need to be determined in order to completely characterize a coal, these include: moisture, ash, volatile matter, carbon, hydrogen, oxygen, sulphur and nitrogen contents, specific heat content (or calorific value), several coking parameters, ash composition, ash fusion characteristics, etc”. Even with these above mentioned parameters known, there is still much debate as to what the actual structure of coal is. As a result, each coal is classified by three (independent) variables, namely: grade, type (organic or maceral composition), and rank/maturity [Snyman, 1998].

The grade of coal is inversely related to the percentage of inorganic matter in the coal, and the ash content of coal generally varies between 0.82 and 0.95 of the mineral matter content present in the coal [Snyman, 1998]. On the other hand, the type of coal is determined

by the degree of alteration of the plant material during coalification; and the rank of coal by the degree of metamorphism due to temperature and pressure increases after burial of the original organic material [Snyman, 1998]. Presented in Figure 2.1 are the different physical appearances of the different types of coals.

Figure 2.1 Different types of coal [Hlatshwayo, 2009]

The types of coal vary from lignite (soft brown-coal), sub-bituminous (hard brown-coal), bituminous coals, to anthracite and meta-anthracites and are characterized by their physical appearance and the amount of mineral matter present [Stach et al., 1975].

Many researchers have published what they consider to be the structure of coal but due to coal's complexity, the exact structure is still not known. However, various molecular and structural models are available that have been proposed to understand the structure of coal [Van Niekerk and Matthews, 2010; Narkiewicz and Matthews, 2008; Van Niekerk et al., 2008; Matthews and Chaffee, 2012]. Figure 2.2 presents one of the many structures that have been proposed to date. The structure of coal generally consists of three-dimensional macromolecular networks which consist of aromatic groups with various functional groups. These aromatic groups are cross-linked by weak hetero-aliphatic bridges [Van Niekerk et al., 2008; Veras et al., 2002; Shinn, 1984].

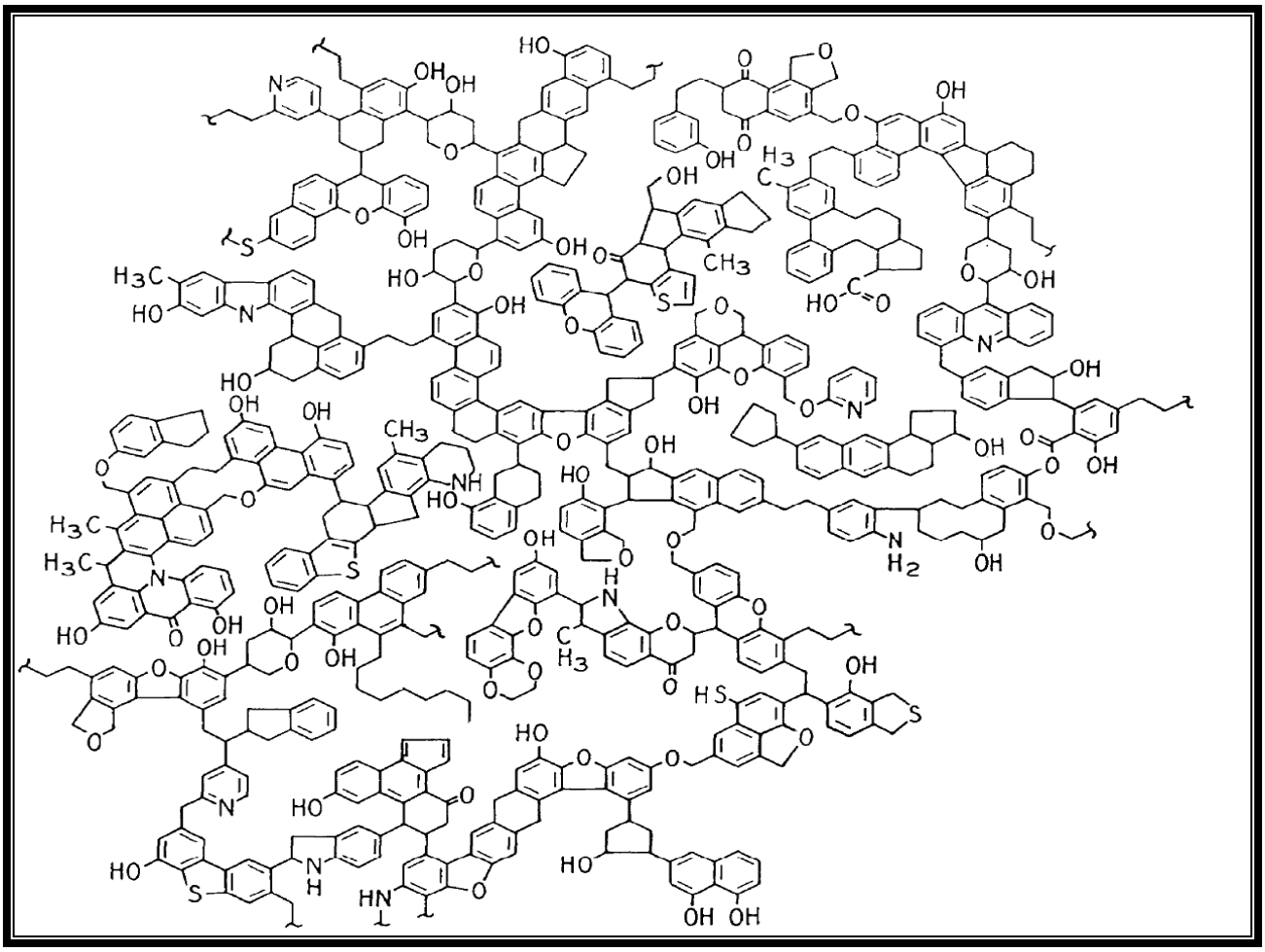

Figure 2.2 Model structure of bituminous coal [Shinn, 1984]

2.2 Maceral composition

Macerals are organic constituents (or optically homogeneous aggregates of organic substances) that developed from the original plant material buried during early coalification [Scott, 2002; Falcon and Snyman, 1986]. Macerals may also be described as coalified plant remains whose form and cell structure are still preserved (and also unrecognized degraded plant products) in the bituminous stage [Stach et al., 1982]. According to the whole coal community, maceral formation depends on factors such as the type of plant community, climatic controls, ecological conditions, acidity (pH) and redox or Eh value; and each maceral may be

distinguished from others by its colour, size, shape, morphology and reflectance [Falcon and Snyman,1998; Starch et al., 1982; Kershaw and Taylor, 1992].

Three maceral groups are known: vitrinite, liptinite (or exinite) and inertinite [Stach, 1982]. These group macerals are further divided into separate macerals and subgroups, as shown in Table 2.1.

Table: 2.1 Summary of macerals found in hard coals [ICCP System, 1998, 2001, Stach, 1982]

Maceral Group	***Vitrinite***	***Liptinite*** (or ***exinite***)	***Inertinite***
• Subgroup	Telinite, Collotelinite • *Telovitrinite* Vitrodetrinite, Collodetrinite • Detrovitrinite Corpogelinite, Gelinite • Gelovitrinite	Sporinite Cutinite Resinite Alginite Liptodetrinite	Fusinite Semifusinite Funginite Secretinite Macrinite Micrinite Inertodetrinite

2.2.1 Vitrinite

Northern Hemispheric coals are well known to contain a high percentage of vitrinite maceral. Vitrinite is reported to form mostly under moist conditions [Cai and Kandiyoti, 1995] and it frequently occurs in bituminous coals [Starch, 1982]. Vitrinite is formed from cell wall material and cell fillings of plants such as trunks, branches, twigs, roots and leaf tissue [Falcon and Snyman, 1986] and it is reactive during technological processes such as coke making

[Snyman, 1998]. In order for the vitrinite to be preserved from the beginning of coalification, the peat swamp needs to be rapidly covered by water to prevent severe biochemical transformations by oxidation [Falcon and Snyman, 1986]. Therefore, it is believed that vitrinization occurs under aerobic or relatively reducing conditions [Falcon and Snyman, 1986].

2.2.2 Liptinite (or exinite)

Liptinite is derived from hydrogen-rich plants (and their decomposition products) such as spores, cuticles, suberin cell walls, resins, polymerized waxes, fats and oils of vegetable origin [Scott, 2002; Falcon and Snyman, 1986]. Liptinite is a reactive maceral during coal processing and according to Snyman [1998], the reflectivity of this maceral increases with increasing coal rank, more than that of vitrinite. Falcon and Snyman [1986] also reported that liptinite releases the largest amount of volatile matter due to its carbon-rich and hydrogen-rich contents.

In South African coals, the liptinite maceral is reported to seldom exceed a volume of 7% of the total maceral composition (under incident white light analysis) and is therefore the least recognized maceral group [Kruszewska, 2003].

2.2.3 Inertinite

South African Permian coals are known to contain a high percentage of inertinite maceral compared to northern hemispheric coals, which are high in vitrinite [Hagelsakamp and Snyman, 1988]. There is still some debate regarding the origin of inertinite in Permian Gondwana coals. However, their presence in coal is indicative of the oxidation of fungal activity or peat, cold and dry climatic conditions and atmospheric exposure when the host sediment was deposited [Van Niekerk et al., 2008; Cai and Kandiyoti, 1995, Glasspool, 2003].

According to Glasspool [2003], inertinites may be thought of or interpreted as charcoal since wildfires was an important factor in their accumulation. In contrast to vitrinite and liptinite, inertinite is less reactive during coal processing and relatively poor in volatile matter [Snyman, 1998; Falcon and Snyman, 1986]; however, partly reactive inertinites have been observed in Gondwana coals [Scott, 2002].

During carbonization of coking coals, vitrinite and liptinite macerals are known to soften whereas fusibility of the inertinite maceral does not take place at all or it is very weak [Stach et al., 1982]. Inertinite is characterized by its high reflectance, high carbon and low hydrogen contents, and increased aromaticity [Stach et al., 1982].

2.2.3.1 Inertodetrinite

A very high concentration of the inertodetrinite maceral is found in many Gondwana coals and is a characteristic maceral in these coals [Stach et al., 1982]. Inertodetrinite is made up of reflecting fine particles, which generally originate from remains of fusinite, semifusinite, macrinite and sclerotinite. These particles may also originate from residues of cell fillings, remains of fungal hyphae and fragments of fungal spores or fusinitized microspores. However, inertodetrinite occurring in Tertiary soft and hard coals originates from fragments of fusinite and fungo-sclerotinite [Stach et al., 1982].

The physical and chemical properties of inertodetrinite include high reflectance of the particles (higher than the reflectance of vitrinite), white to pale-grey colour and a high carbon and low hydrogen content [Stach et al., 1982].

2.2.3.2 Fusinite

Fusinite in coals originates from charcoal caused by forest fires and therefore it is the maceral that is highest in carbon content of all the constituents of coal, [Stach et al., 1982]. Fusinites are said to be commonly found in bituminous coals, but may also be present in peat and brown coals in varying quantities. However, peat and brown coals contain much less fusinite than hard coals. Starch and co-workers [1982] reported that the cell structure of fusinite is often well preserved and the cell cavities are usually filled with mineral matter such as calcite and ankerite. These minerals are believed to be responsible for preventing the collapse of the cells, thus keeping them intact [Stach et al., 1982]. The fusinite maceral may also be characterized by its high reflectance; high carbon and low hydrogen content [Stach et al., 1982]. It has also been reported that during carbonization, fusinite does not fuse. Its volatile matter yield decreases with increasing rank and generally, its physical and chemical properties only show small changes with increasing coal rank [Stach et al., 1982].

2.2.3.3 Semifusinite

Similar to fusinite, semifusinite is also reported to be due to forest fires. However, it originates from partly charred plant tissues [Stach et al., 1982]. Semifusinite is reported to be a transitional intermediate stage between fusinite and tellinite [Stach et al., 1982]. Its reflectance is less than that of fusinite and its plant cell structure is mostly less preserved than that of fusinite.

Semifusinite makes up the majority of the inertinite in Gondwana coals, and is reported to be the most common single constituent of inertinite in Gondwana coals [Stach et al., 1982]. In addition, the concentration of semifusinite has been observed to increase and decrease with the inertodetrinite maceral in coal. Semifusinites are poorer in carbon content and higher in hydrogen content than fusinites. However, they are richer in carbon and poorer in hydrogen compared to vitrinites [Stach et al., 1982].

2.3 Mineral matter in coal

The origin and depositional environments of coal result in different minerals being the main constituents in different types of coal. Mineral matter comprises all inorganic non-coal materials and inorganic elements present in coal as discrete (crystalline and non-crystalline) mineral particles [Gluskoter, 1975; Ward, 2002]; and may occur in coal as minerals, mineraloids and as organically-associated inorganic elements [Matjie et al., 2011]. All elements in coal are considered to fall under the term ‘mineral matter’ except for carbon (C), hydrogen (H), oxygen (O), nitrogen (N) and sulphur (S). However, the elements C, H, O and S may be present as an inorganic combination, for instance, H in free water and water of hydration; oxygen in water, oxides, carbonates, sulphate, silicates and sulphur in sulphides [Gluskoter, 1975].

According to Stach et al. [1982], the inorganic components may be classified in three groups according to their origin:

(i) inorganic matter from the original plant,

(ii) inorganic-organic complexes and minerals which formed during the first stage of coalification, or which were introduced by water or wind into the coal deposits as they were forming, and

(iii) minerals deposited during the second stage of the coalification process, after consolidation of the coal, by ascending or descending solutions in cracks, fissures or cavities, or by alteration of primarily deposited minerals.

The minerals that have formed together with the coal or have been introduced into the deposits are fine-grained and intimately intergrown with the coal. On the other hand, minerals which formed during the second stage of the coalification process are neither fine-grained nor intimately intergrown with the coal, because most of them were deposited in cracks and fissures [Stach et al., 1982].

Gondwana coals are generally known and are characterized by their high proportion of mineral matter content [Stach et al., 1982]. According to Stach and co-workers [1982], the high mineral matter content observed in these coals could be due to a combination of the following factors:

(i) the degree of the materials which drifted to the site of deposition i.e. allochthonous deposition, and

(ii) intrusion of minerals formed by crystallization to the seam after deposition due to a change in environmental conditions.

All minerals that were transported by wind or water and deposited in the coal swamp are termed allogenic or detrital, and those formed within the coal swamp, stemming from the original plant material, are known as authigenic or inherent minerals [Gluskoter, 1975]. Detrital minerals are reported to be the main cause of ash in higher-rank coals, whereas ash formation in lower-rank coals may be due to authigenic minerals and organics [Vassilev et al., 1996]. According to Vassilev et al. [1996], detrital minerals generally increase, while authigenic minerals decrease with increasing coal rank.

Mineral matter in Gondwana coals are reported to occur in two forms, dispersed throughout the coal as finely divided particles and in macroscopically visible bands and lenses. The latter may be easily removed from the coal by washing, whereas the former is not [Stach et al., 1982]. Mineral matter in coal is known to pose problems during coal use and is the main cause of ash formation in coals [Ward, 2002; Gluskoter, 1975]. However, even though the ash yield of coal is derived from the mineral matter during incineration, qualitative and quantitative determination of the amount of mineral matter that was originally present in the coal cannot be related to the remaining coal ash [Gluskoter, 1975; Vassilev and Vassileva, 1996]. This could be due to the inorganic matter originating from the organic matter that is fixed in the ash as newly formed phases and minerals [Vassilev and Vassileva, 1996].

Mineral matter is also associated with problems such as corrosion, fouling, slagging, stickiness, unwanted abrasion and pollution during coal handling and usage [Huffman and Huggins, 1986; Ward, 2002]. On the other hand, these minerals can also act as diluents (or dispersive agents) during coal conversion reactions [Matjie et al., 2011; Vamvuka, 2006; Kershaw and Taylor, 1992].

Different types of minerals have been reported for Gondwana coals, but over 90% of this mineral matter originates from clay minerals, carbonate minerals, sulphide minerals, silica minerals [Stach et al., 1982]. The most common minerals found in coal are clay minerals (kaolinite, illite, mixed-layer illite/smectite and feldspars), carbonates (siderite, calcite and dolomite), sulphide (pyrite) and quartz [Ward, 2002; Gluskoter, 1975]. Other important minor minerals present in coal are iron, sulphur, titanium, calcium, magnesium [Waugh and Bowling, 1984].

According to Gluskoter [1975], sulphates are not common in coals and are usually not found in fresh, unweathered coals; however, the oxidation of pyrite results in sulphates such as gypsum ($CaSO_4 \cdot 2H_2O$), and sulphur occurs with iron as pyrite [Waugh and Bowling, 1984]. Calcium and magnesium also occur in coal as carbonates and silicates, with titanium dioxide occurring as anastase or rutile [Waugh and Bowling, 1984]; and phosphates as apatite or alumino-phosphate [Gluskoter, 1975]. Listed in Table 2.2 are the most common minerals found in coal.

Table 2.2 Principal minerals found in coal and LTA. Adapted from Ward [2002]

Silicates	
Quartz	SiO_2
Chalcedony	SiO_2
Clay minerals:	
Kaolinite	$Al_2Si_2O_5\ (OH)_4$
Illite	$K_{1.5}Al_4(Si_{6.5}Al_{1.5})O_{20}(OH)_4$
Smectite	$Na_{0.33}(Al1.67Mg0.33)Si_4O1_0(OH)_2$
Chlorite	$(MgFeAl)_6(AlSi)_4O_{10}(OH)_8$
Interstratified Clay minerals	
Feldspar	$KAlSi_3O$
	$NaAlSi_3O_8$
	$CaAl_2Si_2O_8$
Tourmaline	$Na(MgFeMn)_3Al_6B_3Si_6O_{27}(OH)_4$
Analcime	$NaAlSi_2O_6{\cdot}H2O$
Clinoptilolite	$(NaK)_6(SiAl)_{36}O7_2{\cdot}20H_2O$
Heulandite	$CaAl_2Si_7O_{18}{\cdot}6H_2O$
Sulphides	
Pyrite	FeS_2
Marcasite	FeS_2
Pyrrhotite	$Fe_{(1\_x)}S$
Sphalerite	ZnS
Galena	PbS
Stibnite	SbS
Millerite	NiS
Phosphates	
Apatite	$Ca_5F(PO_4)_3$
Crandallite	$CaAl_3(PO_4)_2(OH)_5{\cdot}H_2O$
Gorceixite	$BaAl_3(PO_4)_2(OH)_5{\cdot}H_2O$
Goyazite	$SrAl_3(PO_4)_2(OH)_5{\cdot}H_2O$
Monazite	$(Ce,La,Th,Nd)PO_4$
Xenotime	$(Y,Er)PO_4$

Carbonates	
Calcite	$CaCO_3$
Aragonite	$CaCO_3$
Dolomite	$CaMg(CO_3)_2$
Ankerite	$(Fe,Ca,Mg)CO_3$
Siderite	$FeCO_3$
Dawsonite	$NaAlCO_3(OH)_2$
Strontianite	$SrCO_3$
Witherite	$BaCO_3$
Alstonite	$BaCa(CO_3)_2$
Sulphates	
Gypsum	$CaSO_4{\cdot}_2H_2O$
Bassanite	$CaSO_4{\cdot}1/2H_2O$
Anhydrite	$CaSO_4$
Barite	$BaSO_4$
Coquimbite	$Fe_2(SO_4)_3{\cdot}9H_2O$
Rozenite	$FeSO_4{\cdot}4H_2O$
Szomolnokite	$FeSO_4{\cdot}H_2O$
Natrojarosite	$NaFe_3(SO_4)_{2(}OH)_6$
Thenardite	Na_2SO_4
Glauberite	$Na_2Ca(SO_4)_2$
Hexahydrite	$MgSO_4{\cdot}6H_2O$
Tschermigite	$NH_4Al(SO_4)_2{\cdot}12H_2O$
Others	
Anatase	TiO_2
Rutile	TiO_2
Boehmite	$Al{\cdot}O{\cdot}OH$
Goethite	$Fe(OH)_3$
Crocoite	$PbCrO_4$
Chromite	$(Fe,Mg)Cr_2O_4$
Clausthalite	PbSe
Zircon	$ZrSiO_4$

Note: LTA = low temperature ashing

2.3.1 Mineral matter behaviour during coal processing

It has been shown that mineral matter reacts during coal heat treatments, resulting in newly formed phases [Vassileva et al., 2006]. According to Vassileva et al. [2006], during heat treatments in air, physico-chemical transformations of minerals occur due to various interactions between the solid, liquid and gas phases, and these interactions occur with both the original and the newly formed phases. Catalysts used during coal processing can also undergo secondary reactions with minerals present in coal to form new mineral phases [Formella et al., 1986]. It is therefore important to understand these reactions in order to be able to recycle the catalyst as well as to put in place environmentally acceptable methods for ash disposal.

Leaching of raw coal with hydrochloric and hydrofluoric acid has been shown to alleviate the problem of mineral matter associated with coal as it essentially removes all minerals that are chemically linked with carboxyl groups except for the pyrite [Strydom et al., 2011; Van Niekerk et al., 2008, Van Niekerk et al., 2010], thus reducing mineral interactions during coal processing. This method is known only to remove all of the inorganic constituents without causing any change in the carbonaceous material of coal [Formella et al., 1986; Strydom et al., 2011; Ye et al., 1998].

2.4 Potassium compounds

Potassium compounds are known to be among the most effective catalysts in coal gasification and have been shown to significantly enhance coal's reactivity during processing [Rivera-Utrilla et al., 1987; Kyotani et al., 1993]. These compounds are found in naturally occurring potassium-bearing minerals in coal and according to Spiro et al. [1986], these compounds are commonly found in clay minerals such as muscovite [$KAl_2(AlSi_3O_{10})(OH)_2$], illite [$K_{0.66}Al_2(Al_{0.66}Si_{3.33}O_{10})(OH)_2$], leucite [$KAlSiO_6$] and feldspar [$KAlSi_3O_8$].

Synthetic potassium compounds may, however, also be deliberately added to coal to enhance its reactivity and these potassium additives may include strong bases, organic salts and inorganic salts. The associated precursor anion of the catalyst has also been reported to play an important role as to how effective the catalyst would be during heating [Lang, 1986; Huttinger and Minges, 1986]. The catalytic effect of alkali metal chlorides is, however, generally very low compared to that of carbonates [Takarada et al., 1992], and according to Takarada and co-workers, this low catalytic activity is attributed to the affinity between alkali metal ions and

chloride ions. Veraa and Bell [1978] reported that oxides, hydroxides, bicarbonates and carbonates are more active than other salts.

Huttinger and Minges [1986] studied the reactivity of potassium salts during water vapour gasification and found that the potassium salt's catalytic effect follows the order: KOH ~ K_2CO_3 ($KHCO_2$, $K_2C_2O_4$, $KO_2C_2H_3$) ~ KNO_3 > K_2SO_4 > KCl. Marsh and Walker [1979] reported that the effect of addition of potassium salts to coal is attributed to the salts ability to destroy the coking and caking apparent in some coals, thus reducing the fluidity during heat treatments. In addition, the presence of potassium salts results in increased oxygen content in coal during heat treatments and as a result, reactivity is enhanced. Moreover, the reactivity of the resulting char is also enhanced because of the catalytic effect of the retained potassium. However, potassium compounds are known to react with mineral matter in coal, resulting in catalytically inactive silicates [Huttinger and Minges, 1986]. For instance, potassium reacts with clay minerals and pyrite forming inactive compounds such as $KAlSiO_4$ and $KFeS_2$, respectively [Lang, 1986], and according to Rivera-Utrilla et al. [1987], this behaviour may be overcome by increasing the catalyst loading.

2.4.1 Reactions of potassium compounds with mineral matter

Potassium carbonate is known to readily react with aluminosilicate compounds present in coal, producing catalytically inactive alkali aluminosilicates [Takarada et al., 1992; Rivera-Utrilla et al., 1987]. Bruno et al. [1986] reported that potassium carbonate reacts with kaolinite forming the product kaliophilite ($KAlSiO_4$) and muscovite ($KAl_2Si_3AlO_{10}$) in steam and nitrogen respectively. According to Formella et al. [1986], the formation of kaliophilite is due to changes that kaolinite and K_2CO_3 undergo, namely, the hydrolysis of K_2CO_3 [i.e. $K_2CO_3 + H_2O \rightarrow 2KOH + CO_2$] and dehydration and lattice destruction of kaolinite from crystalline kaolinite to amorphous metakaolinite [i.e. $Al_2O_3{\cdot}SiO_2{\cdot}2H_2O + K_2CO_3 \rightarrow$ metakaolinite]. According to Formella and co-workers [1986], the higher the amount of clay minerals in coal; the larger the amount of catalyst that must be added to increase the coal's reactivity.

2.5 Coal gasification

Coal gasification continues to receive a lot of attention after the oil crisis, and has been studied extensively over the past decades. Some of the advantages that this process offers are that different types of coal (lignite to anthracite) may be used. Depending on the type of coal and experimental conditions used, different product gas compositions can also be obtained; consequently various reactors may be used. Generally, coal gasification includes the following steps [Van Dyk and Waanders, 2007; Yu et al., 2007]:

(i) drying of the coal,

(ii) coal devolatilization producing char, tar and gases, involving devolatilization of organic constituents of coal and homogeneous reactions of volatile matter with the reactant gas,

(iii) gasification of the resultant char which involves heterogeneous reactions of the char with the reactant gases, and

(iv) combustion, resulting in ash formation.

Shown in Figure 2.3 are the various volatile products that are released when coal decomposes during coal pyrolysis.

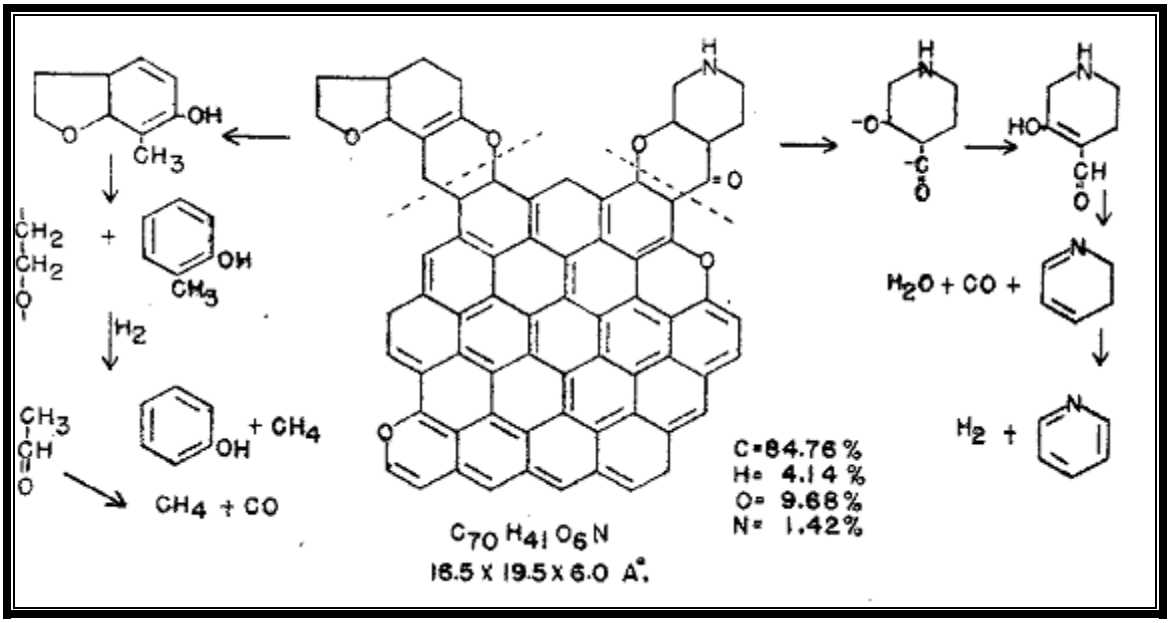

Figure 2.3 Model structure of coal during pyrolysis [Fuchs and Sandhoff, 1942].

2.5.1 Volatile product composition

The devolatilization of coal through heating is an important factor during coal processing. Since the structure of coal is made up of various functional groups of aromatic and hydroaromatic clusters that are linked by aliphatic bridges [Veras et al., 2002], during the devolatilization stage of coal, oxygen-containing complexes and other heterocyclic structures are broken in the temperature range of 400-700°C, followed by aliphatic carbon-carbon linkages and carbon-hydrogen linkages from 600°C. As a result, volatile products such as water, carbon monoxide, hydrogen, methane and other hydrocarbons are evolved [Fuchs and Sandhoff, 1942].

The whole process of devolatilization consists of two important stages, primary and secondary devolatilization. The decomposition of the individual functional groups to produce light species occurs during the primary devolatilization and smaller fragments released as tar occur during secondary devolatilization due to the decomposition of the macromolecular network [Veras et al., 2002]. Presented in Figure 2.4 are the molecular structure of coal and the volatile products evolved during the devolatilization of coal.

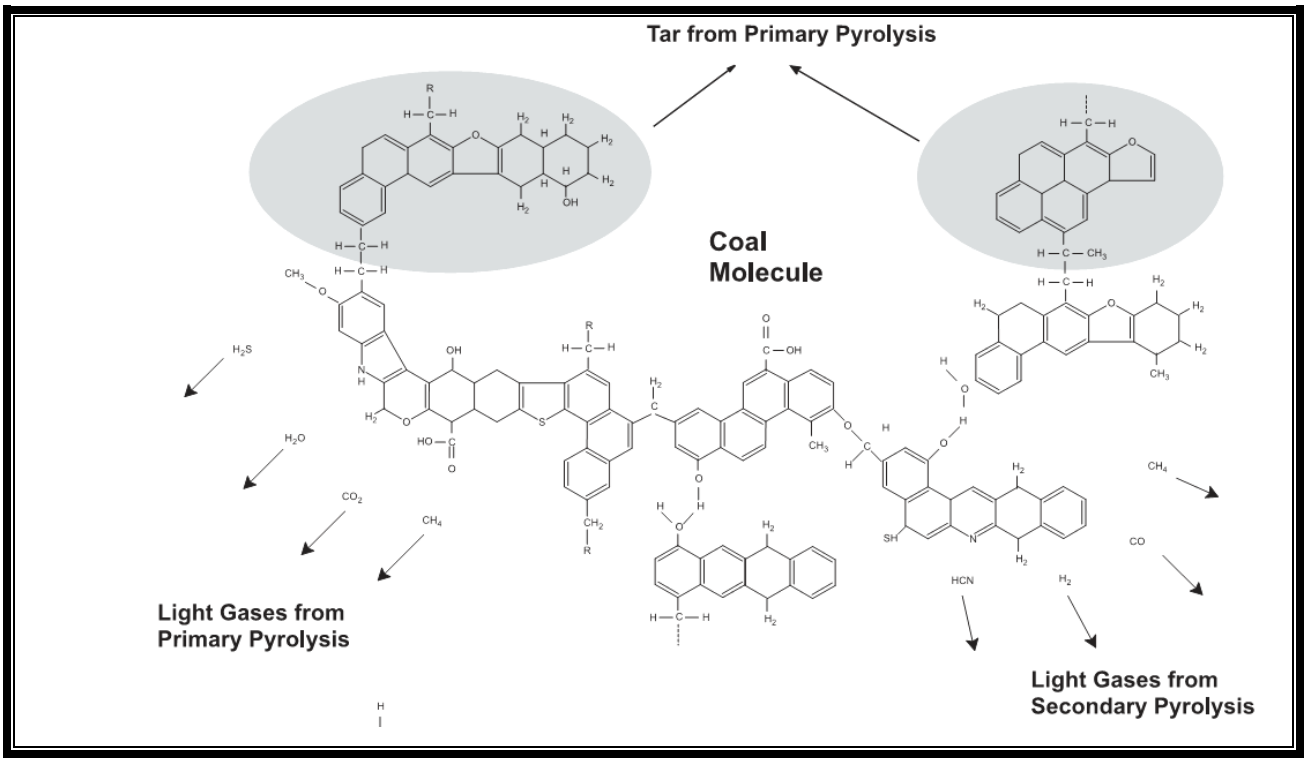

Figure 2.4 Volatile products evolved during the devolatilization of coal [Veras et al., 2002].

Irfan et al. [2011] observed that during pyrolysis of bituminous coal, volatile matter is released in streams and form condensed phase matter around a particle, and the volatile matter emitted contains mainly soot-producing heavy hydrocarbons.

Presented in Figure 2.4 is the three stage pyrolysis behaviour of softening coals [Ye et al., 1998]. The release of volatile matter and decomposition of oxygen-containing functional groups increase the porosity and total surface area of the particle. As a result, this may also increase the resultant char reactivity [Ye et al., 1998].

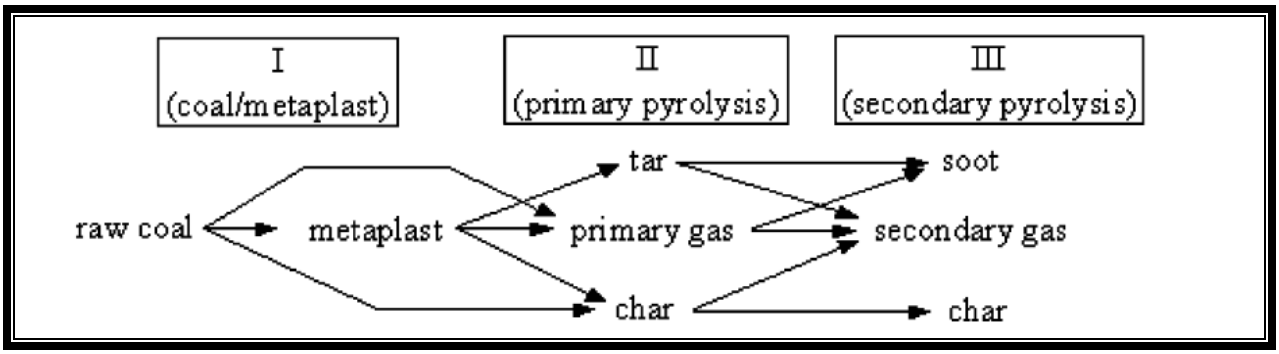

Figure 2.5 Pyrolysis process [Yu et al., 2007]

2.5.2 Coal-char gasification

Char gasification is controlled by factors such as the structural properties of the char, catalytic effect of inherent mineral impurities and pore structure [Ye et al., 1998]. In addition, the rank of coal, pressure, temperature, catalysts, minerals, heating rate and particle size of coal also play an important role in the rate of gasification. For instance, at higher temperatures, carbon conversion is increased and thus the reaction rate is increased [Irfan, 2011]. This implies that longer reaction times are required at lower reaction temperatures, observed by Everson and co-workers [2008]. As a result, char gasification is reported to be the rate determining step because it is the slowest step of the gasification process and thus controls the overall conversion process [Miura et al., 1989; Liu, 2006].

2.5.3 Mechanism of coal-char gasification in CO_2

During carbon gasification, two surface species (semiquinone and a carbonyl complex) are said to influence the gasification rate. The semiquinones, C(O), are as a result of a vacant carbon being oxidized and are reported to be a slowly desorbing species, whereas carbonyl complexes, C-(CO), desorb fast and are formed by oxidation of two adjacent vacant carbon sites which yield a di-ketone that readily breaks up into two carbonyl complexes [Kapteijn et al., 1992].

During gasification of small char particle sizes (< 300μm) in CO_2 at a lower temperature (< 1000°C), the char-CO_2 reaction takes place throughout the interior surface of the char particles and it is controlled by the chemical reaction rate [Irfan et al., 2011]. However, the char-CO_2 reaction of smaller pulverized char particles (< 100μm) at high temperatures (> 1000°C) is controlled by pore diffusion, indicating that temperature has the greatest effect on the gasification reactivity [Irfan et al., 2011]. According to Irfan et al. [2011], the reaction of non-catalytic char-CO_2 gasification may be presented by the following oxygen-exchange mechanism:

$$CO_2 \rightarrow CO + (O)$$
$$C_f + (O) \rightarrow CO + C(O)$$
$$CO \leftrightarrow (CO)$$

where C_f is the available active sites and C(O) is the occupied sites.

Many researchers have also proposed kinetic models consisting of elementary steps of the overall gasification reaction. Kapteijn and co-workers [1992] studied gas-solid reactions and reviewed these proposed kinetic models for carbon gasification in CO_2. A summary of their findings is presented in Table 2.3.

Table 2.3 Some of the proposed models for gasification of carbon in CO_2 [Kapteijn et al., 1992].

Ergun [1956]; Ergun and Menster [1965]

1. $CO_2 + C_f \leftrightarrow CO + C(O)$
2. $C(O) \rightarrow CO + C_f$

Key [1948]

1. $CO_2 + {-}C{-}C \leftrightarrow C{-}CO + CO$
2. $-C-CO \leftrightarrow CO + -C-$

Gadsby et al. [1948]

1. $CO_2 + C_f \leftrightarrow C(O) + CO$
2. $C(O) \rightarrow CO + C_f$
3. $CO + C_f \leftrightarrow C(CO)$

McCarthy [1986]

1. $CO_2 + C_f \leftrightarrow CO + C(O)$
2. $C(O) \leftrightarrow C{-}O$
3. $C(O) \rightarrow CO + C_f$

Blackwood and Ingeme [1960]

1. $CO_2 + C_f \leftrightarrow C(O) + CO$
2. $C(O) \rightarrow CO + C_f$
3. $CO + C_f \leftrightarrow C(CO)$
4. $CO_2 + C(CO) \rightarrow 2CO + C(O)$
5. $CO + C(CO) \rightarrow CO_2 + 2C_f$

Koening et al. [1985, 1986]

1. $CO_2 + 2C_f \leftrightarrow C^*$
2. $C^* \leftrightarrow C(O) + C(CO)$
3. $C(CO) \rightarrow CO + C_f$
4. $C(O) \rightarrow CO + C_f$

Where C^*/C_f = unsaturated carbon atom with a free sp^2 electron on the edge of the graphite, and C = saturated carbon atom in the graphite lattice.

2.5.4 Catalysed coal-char gasification in CO_2

Catalytic coal gasification has been studied for the past decades in order to gain more insight and understanding into the reactivity of coal-char; more so, catalysed coal gasification in a CO_2 atmosphere. The use of catalysts during char gasification has also been studied previously and has been shown to significantly lower high gasification temperatures, and to also overcome the slow reaction of carbon with CO_2 [Irfan et al., 2011]. Moreover, the addition of

catalysts to coal is reported to produce chars that have the desired pore structure, consequently enhancing char's reactivity with CO_2 [Moulijn et al., 1984]. However, these studies focused on vitrinite-rich coals and not the South African inertinite-rich coals.

Alkali and alkaline earth catalysts have been used in many studies and have shown to be effective towards catalysing the rate of gasification [Nishiyama, 1986]. Mineral matter naturally present in the carbonaceous matrix of coal has also been shown to have a catalytic effect on the rate of carbon gasification [Veraa and Bell, 1978]. Both the alkali/alkaline earth metals and mineral matter may be deliberately added to the coal/char, or may be naturally present in the coal. Matsuoka and co-workers [2008] reported that during pyrolysis, the alkali and alkaline earth metals from the coal matrix are released and undergo transformations into various species. The resultant species are dependent on the type of metals that were originally present in the coal, and in turn gasification is dependent on these types of metals [Matsuoka et al., 2008]. According to Matsuoka and co-workers [2008], potassium (K) and sodium (Na) vaporize during gasification, thus fewer interactions between K and Na take place and are insignificant. However, calcium (Ca) and magnesium (Mg) are reported to be the metals that are retained in the gasified char since they are converted into fine ash particles during the devolatilization stage, and these particles then react with inherent clay minerals in coal to form complex clay aluminosilicates [Matsuoka et al., 2008]. Ochoa et al. [2001] reported that a significant catalytic effect of mineral matter was detected only up to 1060°C during gasification of sub-bituminous chars, whereas a slight effect was detected at higher temperatures.

As mentioned, different parameters have an effect on coal-char during gasification in CO_2 atmospheres [Irfan et al., 2011]. Coal rank has an influence on the type of char that is formed and can therefore also influence subsequent char reactions. It has been observed that low-rank coals are more reactive than high-rank coals [Irfan et al., 2011; Garcia and Radovic, 1986]. The highly dispersed metals (resulting from mineral matter) present in the carbonaceous matrix of low-rank coals are said to be one of the causes of its high reactivity during gasification since these minerals are known to act as catalysts for the gasification rate. However, removal of mineral matter results in low-rank coals having the same reactivity as high-rank coal [Ye et al., 1998; Garcia and Radovic, 1986].

According to Takarada et al. [1985], the high reactivity of low-rank coal-chars is due to the high concentration of oxygen-containing functional groups (e.g. carboxylic and phenolic groups) that act as active sites where reactions can take place. These sites also act as exchangeable sites for mounting cations such as sodium, calcium, potassium and iron; and a

catalytic effect can only be observed when the active metals connect to the carboxylic and phenolic groups to form active sites on the coal surface [Nishiyama, 1986]. However these carboxylic and phenolic functional groups are thermochemically destroyed during heat treatments, thus influencing the catalytic effect of inherent mineral matter on char gasification reactivity [Ye et al., 1998]. As a result of these oxygen-containing groups, low-rank coals are therefore reported to be more sensitive to catalyst loadings than high-rank coals [Irfan, 2011].

The first step during char (carbon) gasification involves dissociative chemisorption of the reactant gas molecules on the active sites of the carbon [Lizzio et al., 1988]. These active sites are said to be located at the edges and imperfections within the turbostratic carbon crystallites [Lizzio et al., 1988]. Since some active sites are more active than others, the sites that are important for determining gasification rates are believed to be the ones that are sufficiently active to dissociatively chemisorb the reactant gas, but not to the extent that a stable C-O complex is formed [Lizzio et al., 1988].

Radovic and co-workers [1985] reported that the gasification reaction consists of the non-catalytic and catalytic process and therefore the gasification rate may be represented as a sum of both processes:

Gasification rate = Non-catalytic gasification rate + Catalytic gasification rate

The non-catalytic gasification rate is believed to be due to the chemical and physical properties of the char evident in higher rank coals. These physical and chemical properties include: active sites (which determine the accessibility of the reactant gas), nascent sites, dangling carbon atoms and edge carbon atoms [Radovic et al., 1985]. On the other hand, the catalytic gasification rate is said to be due to minerals in coal such as alkali and alkaline earth metals in the char (e.g. K, Na, Ca and Mg), particularly in lower rank coal. These metals are also known to act as catalysts during gasification, and their degree of dispersion is reported to be directly proportional to the amount of chemisorbed oxygen or CO_2 [Miura et al., 1989]. However, at certain concentration levels when the oxygen-containing functional groups are occupied by the added metal cations, further addition of cations results only in these cations being physically adsorbed and would therefore have little or no further catalytic effect on gasification [Ye et al.,1998].

It has also been shown that the presence of carbon monoxide can lower the gasification rate by either removing or decreasing the free active carbon complexes/sites. This happens by

blockage of the active sites, thus preventing insertion of the gas phase CO into the carbon matrix [Kapteijn et al., 1992]. The inhibition of gasification by CO may be shown by the following mechanism as indicated by Irfan et al. [2011]:

$$C(CO) + CO_2 \leftrightarrow 2CO + CO \qquad \text{where (CO) is the product gas}$$
$$CO + C(CO) \leftrightarrow C_f + CO_2$$

2.5.3.1 Potassium Catalysed CO_2 gasification

Potassium salts are known to act as catalysts for coal gasification of vitrinite-rich coals [Rivera-Utrilla et al., 1987]; with K_2CO_3 being the most effective in terms of its activity and cost [Kim et al., 1989]. According to Spiro et al. [1986], char has a high hydrogen contents compared to graphite and therefore during char CO_2 gasification, a hydride-hydroxide cycle takes place due to the oxygen transfer. Moulijn et al. [1984] reported that the oxygen transfer cycle between the gas phase and the surface of the carbon is due to the liquid film that results from the transformation of the carbonate, generating a molten layer of non-stoichiometric oxides containing an excess of the potassium metal. Consequently, aromaticity is decreased by formation of a covalent bond between the metal and the carbon, thereby speeding up the reaction. The active sites are therefore said to be oxygen-containing potassium species [Kapteijn et al., 1984].

Moulijn et al. [1984] concluded that during gasification, no bulk intercalation compounds are present and no metallic K-species are involved in the catalytic cycle. According to Formella et al. [1986], during potassium-catalysed steam gasification of coal, the catalysts undergo secondary reactions with the mineral matter present in coal, forming new mineral phases. Possible catalytic mechanisms have been proposed for the potassium-catalysed CO_2 gasification [Moulijn et al., 1984]. Shown in Figure 2.5 is an illustration of one of the many mechanisms for potassium catalysed CO_2 gasification that have been proposed [Wigmans et al., 1983].

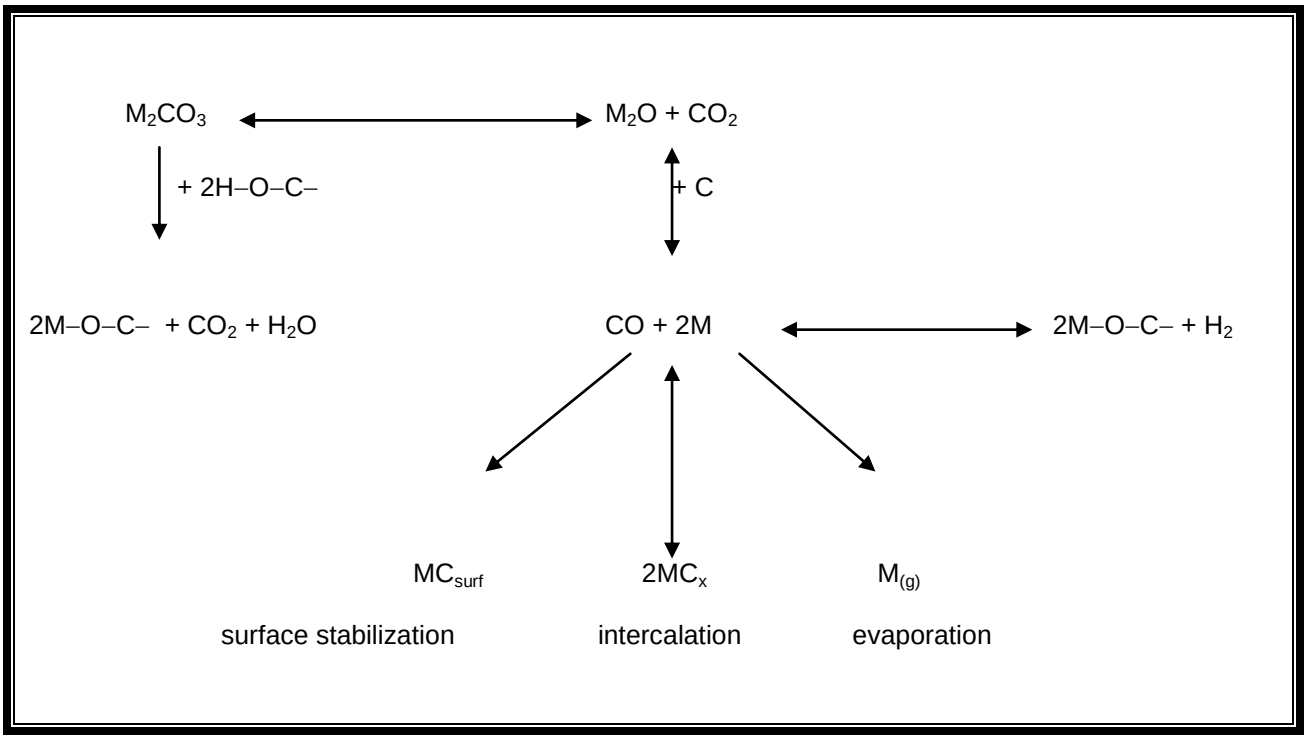

Figure 2.6 Mechanisms for potassium catalysed CO_2 gasification [Wigmans et al., 1983]

When a potassium carbonate catalyst is added to a char, a covalent M-C (M=K) bond is formed. This is a result of the oxygen supplied to the carbon by the catalyst via a redox cycle at the carbon-catalyst interface. The redox cycle is reported to involve three elementary reaction steps (shown below) and is evident in CO_2, H_2O, and O_2 gasification atmospheres [Rivera-Utrilla et al., 1987 and Moulijn et al., 1984]:

$K_2CO_3 + 2C \rightarrow 2K + 3CO$	Carbothermic reduction
$2K + CO_2 \leftrightarrow K_2O + CO$	Oxidation
$K_2O + CO_2 \leftrightarrow K_2CO_3$	Carbonate formation

Moulijn and co-workers [1984] reported that the decomposition of K_2CO_3 (between 500 K and 1000 K) takes place as follows: $K_2CO_3/C \rightarrow K_2O/C + CO_2$ (where K_2O/C denotes carbon supported potassium oxide). Reduction of the active species K_2O/C (between 900 K and 1200 K) takes place as follows: $K_2O/C + C \rightarrow 2K/C + CO$ (where K/C denotes carbon supported potassium).

Moulijn and co-workers [1984] also reported that the decomposition of the catalyst takes place below the melting temperatures of bulk K_2CO_3. However, Veraa and Bell [1978] reported four elementary steps (during gasification of coal char steam-helium mixture) of the decomposition of K_2CO_3, owing to the catalyst's superior catalytic activity. The reaction steps were as follows:

$$K_2CO_3 + 2C \rightarrow 2K + 3CO$$
$$2K + 2H_2O \leftrightarrow 2KOH + H_2$$
$$CO + 2H_2O \leftrightarrow CO_2 + H_2$$
$$2KOH + CO_2 \leftrightarrow K_2CO_3 + H_2O$$

According to Veraa and Bell [1978], metal chlorides react differently than K_2CO_3 in steam gasification of coal char. Their catalytic effect is reported not to be due to their conversion to a carbonate – due to the unlikelihood of the following reactions:

$$2MCl + 2H_2O \leftrightarrow M_2O + 2HCl \quad (M=Metal)$$
$$M_2O + CO_2 \leftrightarrow M_2CO_3$$

Veraa and Bell [1978] reported that the free energy of the metal chloride conversion to a metal oxide (first step) is strongly positive, thus the improbability of the reaction taking place. The metal chlorides act as inhibitors during the early stages of gasification, having an accelerating effect only in the last stages of gasification; during which only 20 to 25% of fixed carbon is present. Moreover, Veraa and Bell [1978] observed that for K_2CO_3 and metal chlorides, the production of CO and CO_2, H_2, CH_4 increases and decreases, respectively with increasing catalyst loading, at constant reaction temperature; whereas, at constant catalyst loading, the production of CO, CH_4, CO_2, and H_2 increases and decreases, respectively with increasing temperature.

From the literature that has been cited, most of the investigations were conducted on Northern hemispheric vitrinite-rich coals. Compared to the Northern hemispheric coals, limited studies have been conducted on South African coals. To date there is no work that has reported on how potassium salts affect the volatile product composition of the char derived from a South African inertinite-rich coal. Thus, the scope of this study was to investigate this unexplored area, using the coal from the Highveld coalfield. Some of the other important factors addressed in this

study were the effect of the potassium salts (K_2CO_3 and KCl) on the char conversion, as well as the effect of these salts on the reactivity of the coal-char when subjected to heat treatments in CO_2 atmosphere.

CHAPTER 3

Analysis and Characterization Techniques

This chapter gives a general overview of the analytical methods used in this study for sample characterization and chemical analysis. Detailed discussions of some of the theoretical bases of the techniques used are also presented.

3.1 Proximate Analysis

Proximate analysis is a technique that is used to determine the amount of fixed carbon (FC), volatile matter (VM), moisture and ash present in coal [Speight, 2005].

(i) Measurement of Moisture

The moisture content of the coal is determined by heating a weighed powdered coal sample to 106°C in an inert atmosphere. The sample is then cooled to room temperature and weighed again; and the weight loss observed represents the moisture content of the coal. Since the material driven off at this temperature is not collected and analyzed, the weight loss observed is generally said to be due to the moisture. The total moisture content in coal represents the surface moisture, inherent and crystalline moisture that is present in the coal matrix. No moisture from the volatiles is released at 106°C.

The moisture content in coal is reported to range from 2 to 15 weight % in bituminous coals and to nearly 45 weight % in lignite [Speight, 2005].

(ii) Measurement of Volatile Matter

The volatile matter in coal refers to the percentage of volatile products that vaporize when coal is heated. Determination of the volatile matter content involves heating the coal sample to 950 ± 20 °C in an inert atmosphere after the moisture content has been determined. The loss in weight is defined to be the volatile matter content of the coal, which is usually due to various gases such as CO_2, CO, water, light hydrocarbons and condensable organic compounds being driven off [Speight, 2005].

(iii) Measurement of Ash

The ash content is determined by heating the sample in a muffle furnace in the presence of air, to temperatures in the range of 850°C; leaving behind a non-combustible inorganic residue that is collected and weighed as ash. The ash is generally made of a complex mixture of oxides, silicates and aluminosilicates resulting from inorganic species formed from different elements such as sodium, potassium, magnesium, calcium, iron, titanium, aluminium and silicon [Speight, 2005].

(iv) Measurement of Fixed Carbon

The carbonaceous residue that did not vaporize with the volatile matter is defined as the fixed carbon. This is the carbon that is not reported in the volatiles as organic matter and it is not combined with other elements [Speight, 2005].

3.2 Ultimate Analysis

Ultimate analysis is used to determine the amount of elemental chemical constituents in coal; such as carbon, hydrogen, oxygen, sulphur and nitrogen present in the coal [Speight, 2005].

(i) Carbon

The carbon content includes the carbon present in the organic coal substance and any naturally occurring carbon present as the mineral carbonate.

(ii) Hydrogen

Determination of the amount of hydrogen includes organically associated hydrogen in coal and that found in all the water associated with the coal.

(iii) Nitrogen

All the nitrogen is assumed to be part of the organic materials in coal (i.e. nitrogen within the organic matrix of coal).

(iv) Sulphur

Determination of the total sulphur content includes organically-bound sulphur, pyrite and sulphate sulphur.

(v) Oxygen

The oxygen content is calculated by difference (i.e. the sum of the percentage of moisture, ash, carbon, hydrogen, nitrogen and sulphur are deducted from 100.0 to give the oxygen content).

3.3 Thermogravimetric (TG) Analysis

The decomposition of coal samples in this study were carried out in a thermogravimetric analyzer. The technique continuously records the variation in mass of a sample while the sample is in a controlled atmosphere and also subjected to a temperature program. The temperature of the sample is usually increased linearly with time; however, isothermal studies can also be conducted. A plot of mass or mass percentage as a function of time or temperature (called a thermogram or a thermal decomposition curve or TG curve) is then recorded, showing a decomposition pattern of the sample analyzed under a given atmosphere. The main components of a thermogravimetry instrument includes: a sensitive analytical balance or thermobalance, furnace, thermocouple, sample holder, a purge gas system for providing an inert or reactive atmosphere, a microprocessor and a computer for data acquisition and display.

The sensitivity of the thermobalance is usually of the order of one microgram, and samples ranging from 1 milligram to 100 grams may be analyzed. The sample holder is housed in the furnace; however it is thermally isolated from the furnace. The temperature of the thermogravimetric furnace ranges from ambient temperatures to 1500°C and higher, with heating rates to as high as 200°C/minThe temperature that is recorded during the analysis represents the actual temperature of the sample. The temperature of the sample is measured with a small thermocouple which is located as close as possible to the sample holder, and the temperature measured usually falls within ±2°C of the operating range [Skoog et al., 1998]. A schematic representation of the main components of a TG is presented in Figure 3.1.

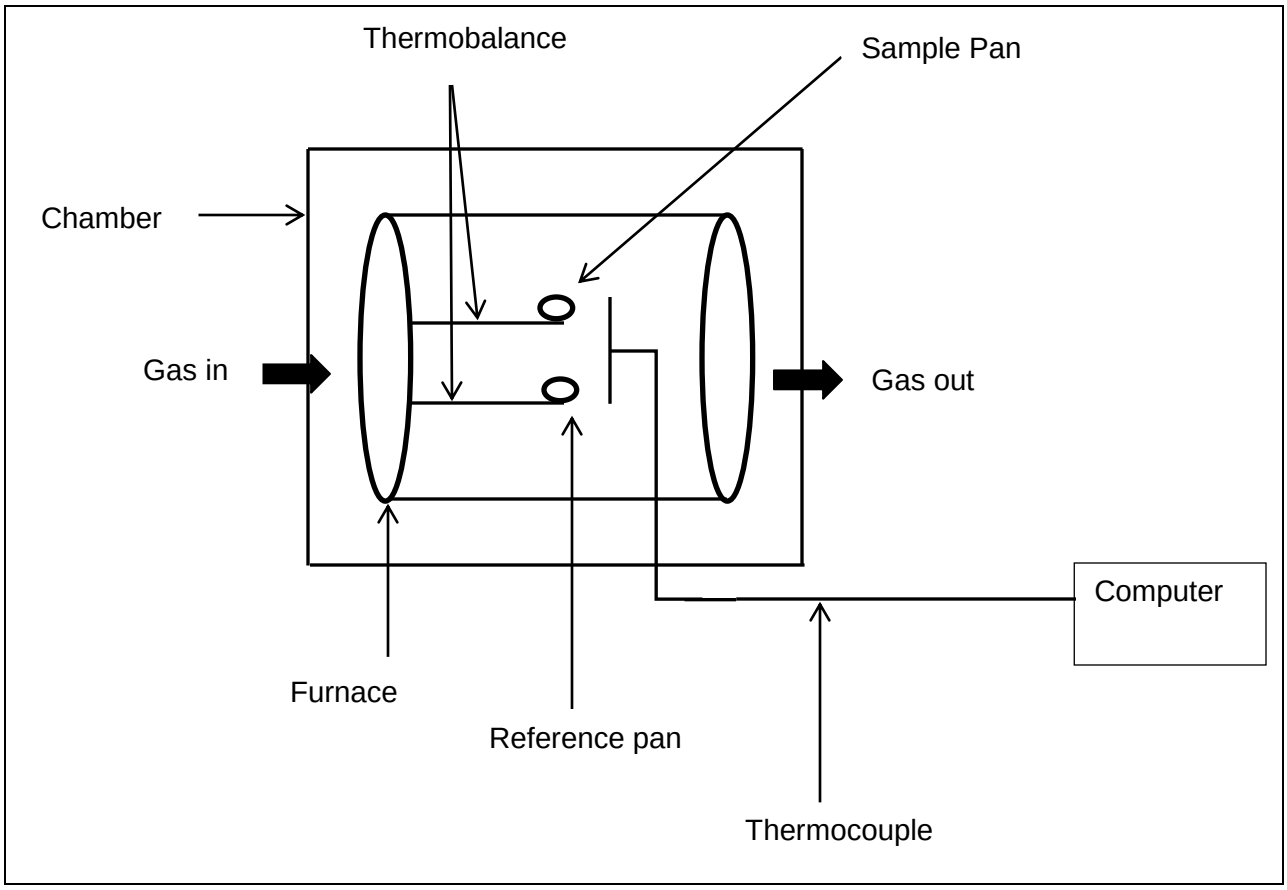

Figure 3.1 Components of a thermogravimetric (TG) analyzer

3.3.1 Derivative of Thermogravimetric (DTG) curves

DTG is the first derivative curve of the TG curve and can be used to more clearly reveal information that may not be detectable in a TG curve.

3.4 Mass Spectrometry (MS)

Mass spectrometry is an analytical technique that uses a mass spectrometer to measure and separate ions on the basis of their mass-to-charge ratios (m/z). The principal components of all types of mass spectrometers include: an inlet, ion source, mass analyzer and a detector. A schematic representation of a mass spectrometer is presented in Figure 3.2.

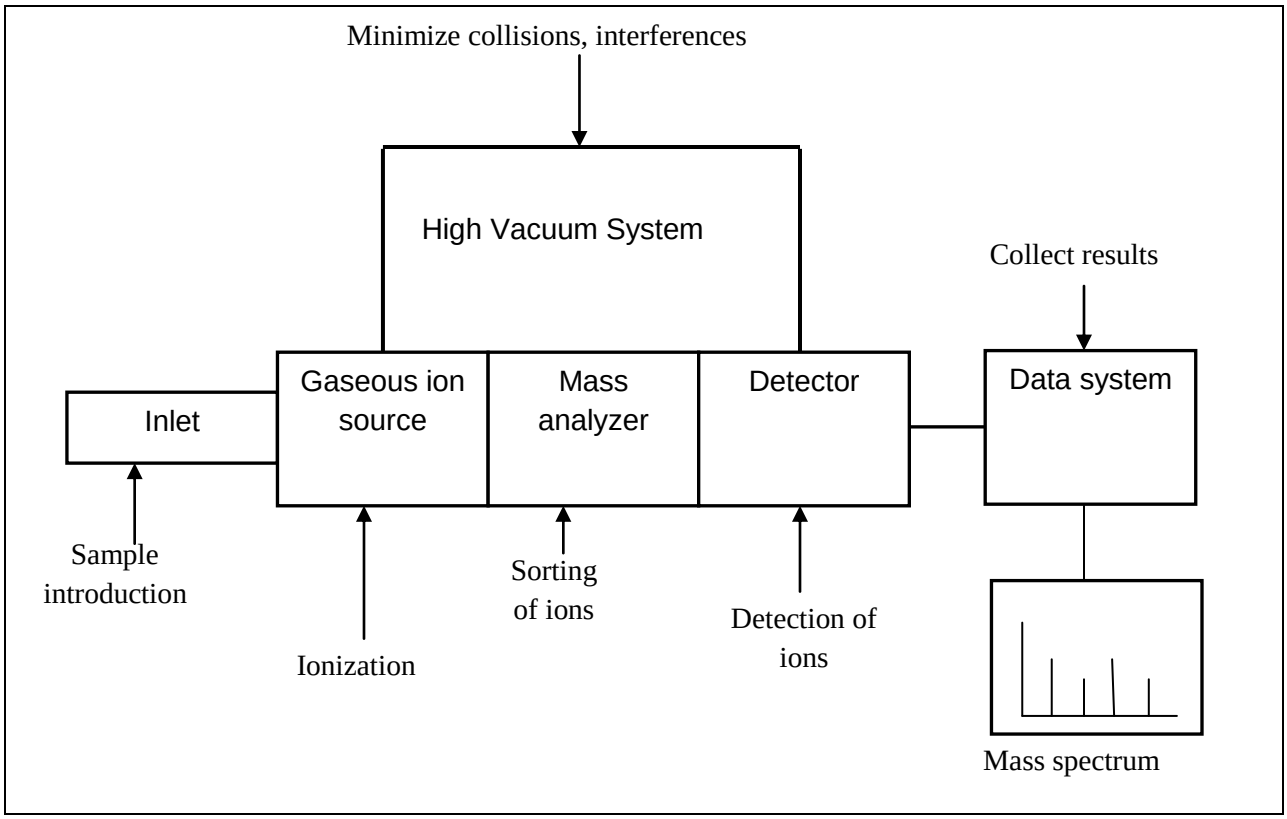

Figure 3.2 Components of a mass spectrometer

Micro amounts of the sample to be analyzed are introduced into the ion source where the components of the sample are ionized by bombardment with electrons, photons, ions and molecules; resulting in the formation of charged particles or gaseous ions. A stream of positive or negative gaseous ions is then accelerated into the mass analyzer where these ions are separated according to their mass-to-charge ratio by electromagnetic fields. The ion transducer converts the beam of ions into an electrical signal that can be processed by a signal processor, stored in the memory of a computer, and displayed as a mass spectrum [Skoog et al., 1998; Gunzler and Williams, 2002].

The X-axis of the mass spectrum indicates the m/z ratio of a given ion, where for singly charged ions; this corresponds to the mass of the ion. The Y-axis represents the height of the peak, which indicates the relative abundance of a given ion; however it is generally not reliable to use the height of the peak for quantitative analysis; and the peak intensity indicates the ability of the ion to desorb.

Some of the different types of mass spectrometers include time of flight (TOF) mass spectrometers and quadrupole mass spectrometers. The quadrupole mass spectrometer is the most commonly used spectrometer in atomic mass spectrometry. It uses a high frequency voltage to disperse the ions, and easily resolves ions that differ in mass by one unit. The TOF mass spectrometer measures the time required for ions to 'fly' down the length of a chamber.

The ions are periodically produced from sample bombardment with brief pulses of electrons, secondary ions, or laser generated photons. Ions from lighter sample particles arrive at the detector earlier than ions of the heavier particles [Skoog et al., 1998; Gunzler and Williams, 2002].

3.5 X-Ray Fluorescence

X-ray fluorescence (XRF) is a technique used for qualitative determination of major and minor elements in samples. A schematic diagram of XRF is shown in Figure 3.3.

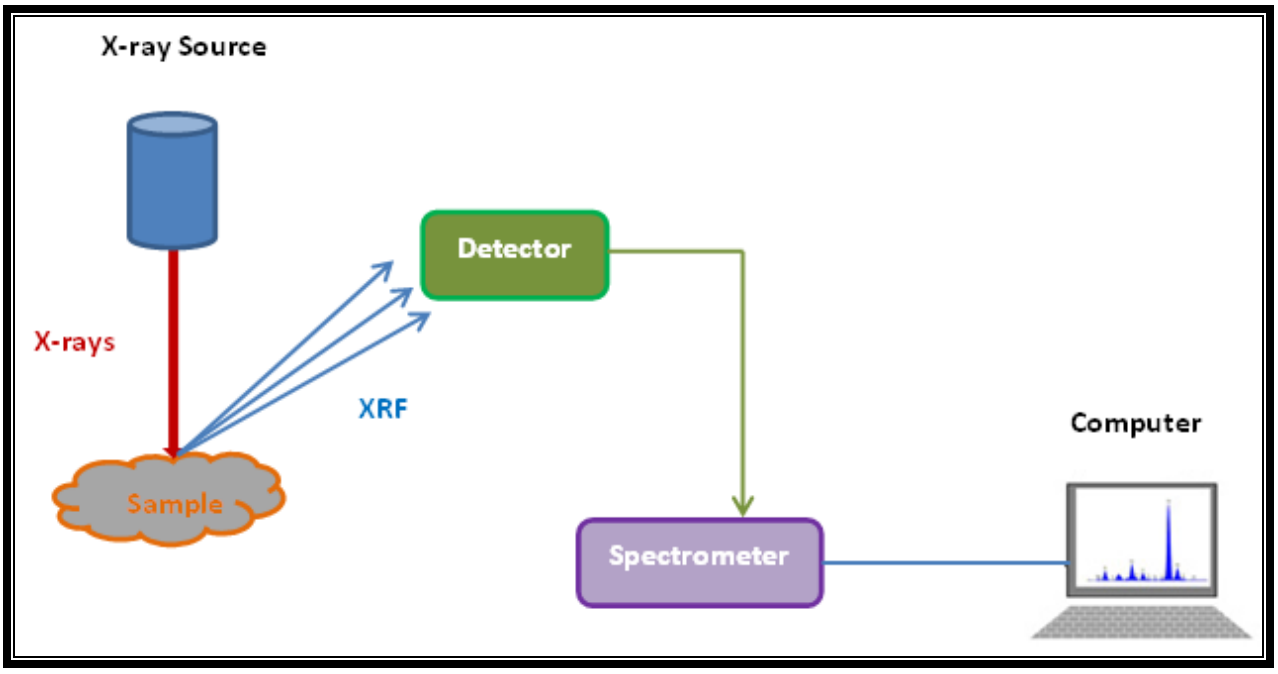

Figure 3.3 X-ray pathways during XRF analysis

During an XRF analysis, the sample is introduced into the target area of an X-ray tube. The sample is then irradiated with a beam of X-rays from an X-ray tube or a radioactive source.

The elements in the sample are then excited by absorption of the primary beam and emit their own characteristic fluorescence X-rays. These fluorescent x-rays are then detected and analyzed by the spectrometer. Because the relationship between emission wavelength and atomic number is known, isolation of individual characteristic lines allows the unique identification of an element; and elemental concentration can be estimated from characteristic line intensities. As a result, a qualitative and quantitative elemental analysis of the sample is obtained [Skoog et al., 1998; Gunzler and Williams, 2002].

3.6 X-Ray-Diffraction

The X-ray diffraction (XRD) technique is used to obtain qualitative and quantitative information of the crystalline compounds in samples.

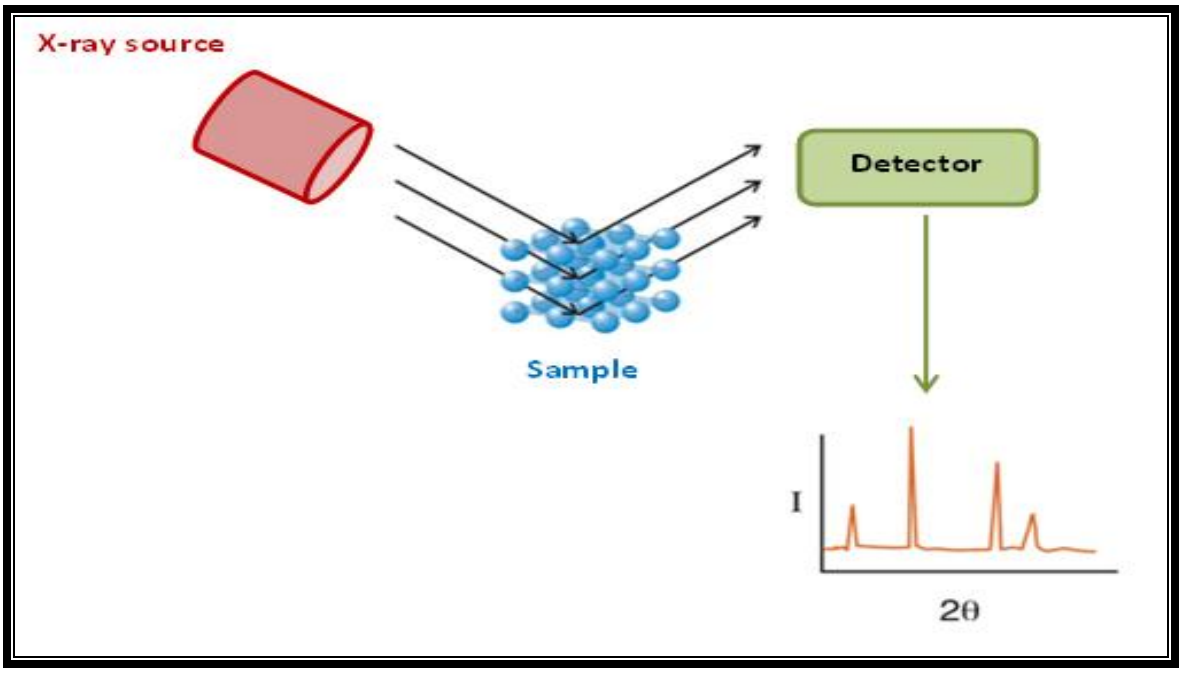

Figure 3.4 X-ray pathways during XRD analysis

For XRD analysis, the sample is ground to a fine homogeneous powder; in which form the small crystallites are randomly oriented in every possible direction. The X-ray beam is then passed

through the sample and the particles reflect the beam from all possible interplanar spacing positions, fulfilling the Bragg condition for reflection. The reflected beam is detected and a diffraction pattern is then obtained. The diffraction pattern is based upon the position of the diffraction lines, in terms of diffraction angles [theta (ɵ) or 2theta (2ɵ)]. These angles are determined by the spacing between a particular set of planes using Bragg's equation, shown below. A quantitative analysis of crystalline mixtures is obtained by the intensity of the diffraction lines, and comparing them with standards [Skoog et al., 1998].

Bragg's equation: $n\lambda = 2d \sin \theta$ [Skoog et al., 1998]

CHAPTER 4

Experimental Procedures

This chapter focuses on experimental methods specifically employed in this study and also clearly outlines the experimental conditions used and the steps followed for all the experiments conducted. General information on the coal used for the study is also provided.

4.1 Sample Preparation

4.1.1 Sequential leaching of coal

An inertinite-rich South African coal was chosen as most studies have focused mainly on Northern Hemispheric vitrinite-rich coals. Typical South African coals contain a large proportion of inorganic matter that may pose problems, such as slagging and fouling during coal processing [Matjie et al., 2011]. In order to obtain a residual coal sample with low mineral content, the coal was leached using an acid treatment method of HCl and HF. This method of leaching has a very small influence on coal characteristics, and only reduces the inorganic matter that is chemically linked with carboxyl groups in coal [Strydom et al., 2011; Van Niekerk, 2008].

A South African Highveld inertinite-rich medium rank C bituminous coal of particle size < 75 µm was used in this study. Sequential leaching of the coal with hydrochloric (HCl) and hydrofluoric (HF) was performed in a fume hood. The coal (500g) was leached with 4L of 5 M HCl solution for 24hrs and the solution filtered in a polypropylene Buchner funnel under vacuum. The residue was leached with 4L of 5 M HF solution for 24hrs and the solution was again filtered under vacuum using a Buchner funnel. The resulting residue was further leached with 4L of 5 M HCl for 24hrs, after which the product was filtered under vacuum and washed with large quantities of distilled water until approximately pH 7, to ascertain that most of the adsorbed acid was removed from the residual coal particles. The resulting product was then dried overnight in an oven at 80°C. All the leaching steps were carried out at room temperature. A total of 5kg of coal was leached. The leached sample is further referred to as demineralized coal. The leaching procedure is presented in Figure 4.1.

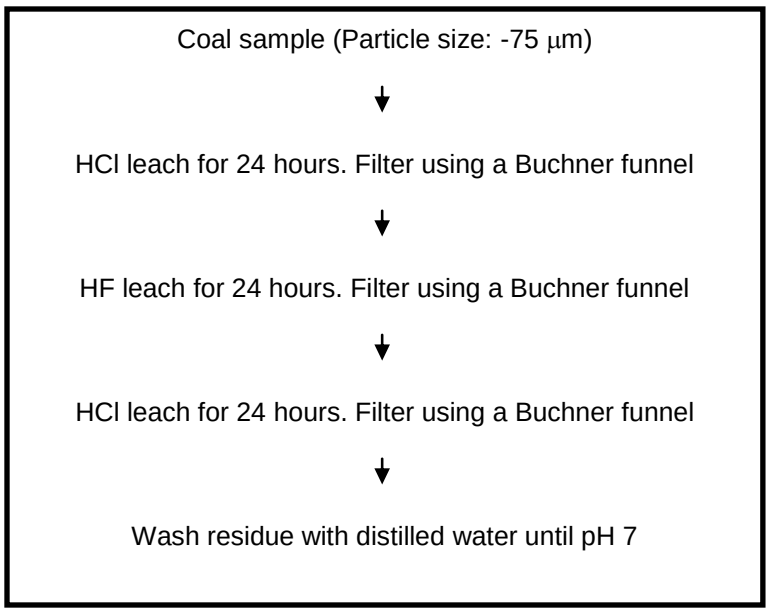

Figure 4.1 Sequential leaching procedure with HCl and HF

Proximate and ultimate analyses were conducted on the raw and demineralized coal. A total of three different samples of the same coal were prepared: (i) demineralized coal, (ii) raw coal, and (iii) demineralized coal with added mineral mixture. Various loadings of inorganic salts were added to the samples. The coal samples (with and without added dopants) were subjected to heat treatments in N_2 and CO_2 atmospheres.

4.1.2 Dopant addition

4.1.2.1 Model Mineral Mixture

A synthetic model mineral mixture made up of 25% kaolin clay, 20% quartz, 20% pyrite, 15% calcite, 8% siderite, 8% hydromagnesite and 4% anastase was prepared [Nel et al., 2011]. The components of the mineral mixture were chosen based on the most common and abundant minerals that occur in coal [Nel et al., 2011]. All the components of the mixture were pulverized and mixed together for several minutes using an electric blender/mixer to ensure thorough mixing. The purity of the chemical compounds in the mineral mixture are presented in Table 4.1.

Table: 4.1. Chemical compounds representing minerals included in the model mineral mixture.

Name	Formula	Purity	Supplier
Kaolin Clay	$Al_2Si_2O_5(OH)_4$	Ph. Eur. Bp	Riedel-de Haën
Quartz	SiO_2	Purum p.a. sand	Fluka
Pyrite	FeS_2	95 %	Strem Chemicals
Calcite	$CaCO_3.nH_2O$	98.0–100.5 %	Merck
Siderite	$FeCO_3.nH_2O$	Laboratory reagent	Qualikems
Hydromagnesite	$MgCO_3.nH_2O$	Meets USP testing specifications	Sigma
Anasatse	TiO_2	–	Sigma

The demineralized coal samples were then doped with 5wt% and the samples mixed for several minutes using an electric mixer until uniform mixing was obtained. Addition of the mineral mixture to the demineralized coal samples was done to mimic the behaviour of some of the naturally occurring minerals in coal, thus excluding some of the other minerals and their influences during heat treatments. The behaviour of the compounds of the mineral mixture during heat treatments in various atmospheres has been studied and is reported by Nel and co-workers [Nel et al., 2011].

4.1.2.2 Inorganic salts

Potassium carbonate (K_2CO_3) and potassium chloride (KCl) were chosen as the inorganic salt dopants in this study. Potassium compounds are known to exhibit a catalytic effect during coal gasification [Rivera-Utrilla et al., 1987]. Both the salts were first dried in the oven overnight at 120°C. Samples with loadings of 0.5, 1, 3 and 5 K-wt% for each of the salts were prepared.

Dopants were added to the raw coal, a demineralized sample of the same coal, and to the demineralized sample with added model mineral mixture. The doped samples were mixed together using a mortar and pestle and an electric mixer until uniform mixing was obtained.

4.2 Thermogravimetry-Mass Spectrometry (TG-MS)

Thermogravimetry coupled with a quadrupole mass spectrometer (TG-MS) was used to study the mass loss of the coal char samples with additives, as well as to analyze the gaseous composition products formed during heat treatment in a CO_2 atmosphere.

4.2.1 Thermogravimetric (TG) Analysis

Thermogravimetric (TG) studies of the coal samples were carried out using an SDT-Q600 thermogravimetric analyser, presented in Figure 4.2. The mass loss of the chars derived from the demineralized coal, raw coal and demineralized coal with added mineral mixture; with and without additives were investigated.

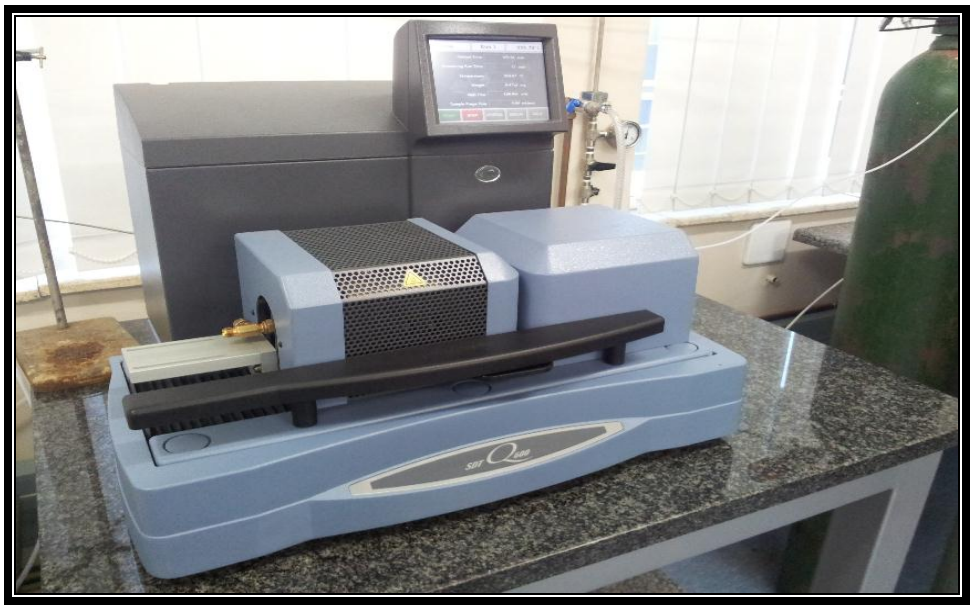

Figure 4.2 Thermogravimetric Analyzer (model SDT-Q600)

An empty alumina crucible was placed into the TG, onto the thermobalance and tared. The alumina crucible was then removed and about 10mg of sample was placed in it and loaded onto the thermobalance of the TG, as shown in Figure 4.3.

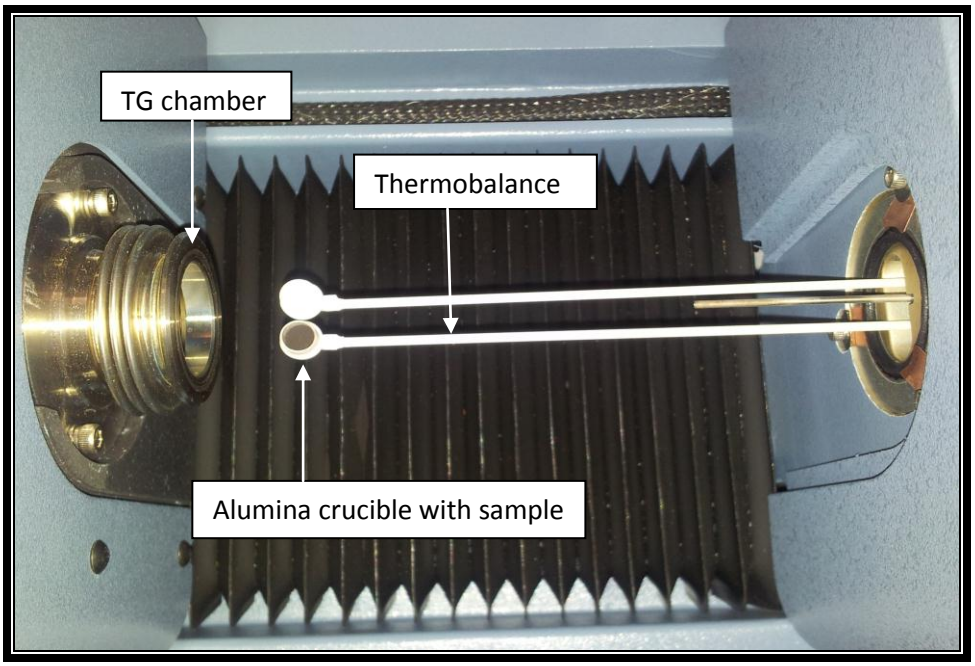

Figure 4.3 TG thermobalance onto which the sample was loaded

The TG chamber was closed and purged with nitrogen for 10 minutes to remove all the air present in the chamber. The temperature was allowed to equilibrate (at room temperature) and after the temperature stabilized, a char was prepared by subjecting the sample to a controlled temperature program where the sample was heated in a continuous flow of nitrogen to 900°C at a rate of 10°C/min and a nitrogen flow rate of 75ml/min; holding the temperature for 15 minutes at 900°C. The sample was then allowed to cool down (in-situ) to room temperature under the nitrogen atmosphere, to prevent the sample from oxidizing. Once the sample had cooled down to room temperature, the nitrogen flow was switched to CO_2. The temperature and the weight of the resulting sample were allowed to stabilize and after stabilizing, the sample was heated under CO_2 flow to 1200°C at a rate of 10°C/min and a CO_2 flow rate of 20ml/min. The mass loss as a function of temperature was recorded. All samples were subjected to the same experimental conditions, and two runs of each sample were performed to ensure repeatability.

4.2.2 Mass Spectrometer (MS)

A Cirrus mass spectrometer (model: LM92-00111019) with a Dual Faraday and multiplier detector was used to obtain MS results. The MS was connected to the TG as shown in Figure 4.3.

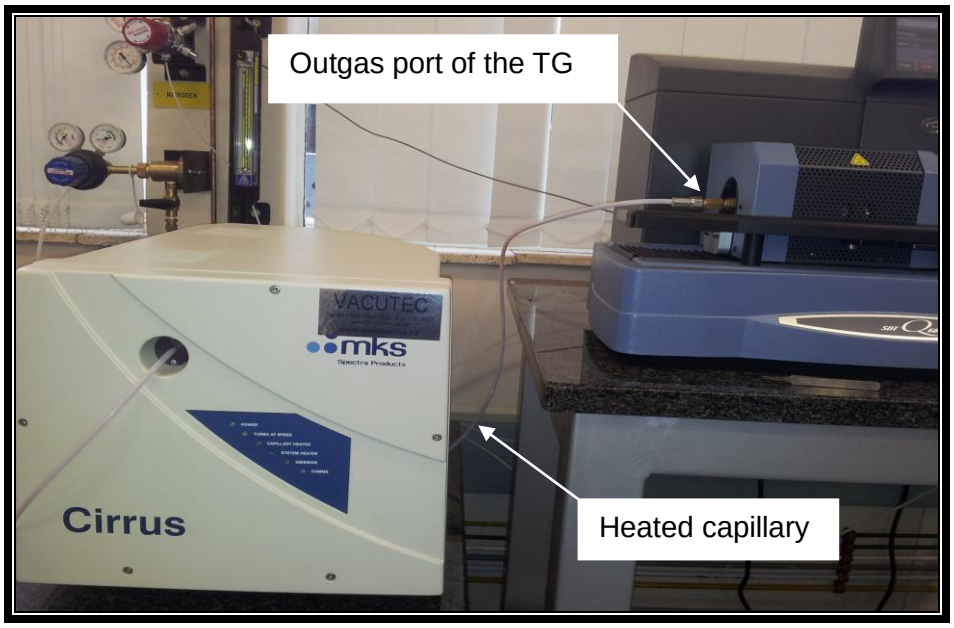

Figure 4.4 Mass Spectrometer connected to the TG instrument

The gas compositions of evolved gaseous species were identified by a mass spectrometer attached to the TG analyzer. Gaseous species evolved were detected and recorded from the beginning of the reaction under the CO_2 atmosphere. The MS was directly attached to the outgas port of the TG instrument and the evolved gases were simultaneously detected as the TG was scanning. The evolved gaseous species from the sample in the TG were fed through the outgas port via a heated capillary to the mass spectrometer.

The input gas is ionized by electron impact and the ions are sent through a mass filter and then onto a secondary electron multiplier that produces an output current proportional to the ion current. It should be noted that in this study, the mass spectrometer was used only to identify the reaction products from gases released during TG experiments, and the temperature ranges in which they were released. No quantitative analyses of the gaseous products were done.

4.3 Tube furnace experiments

Tube furnace experiments of the coal samples were carried out using a model TSH 12-75-610 Lenton horizontal tube furnace, presented in Figure 4.5. Only 5 K-wt% catalyst loaded samples were used for these experiments.

Figure 4.5 Horizontal tube furnace

4.3.1 Heat treatment in N_2

About 30g of sample was placed on the ceramic sample pan and loaded into the tube furnace, as shown in Figure 4.6. The furnace was closed and purged with nitrogen for 10 minutes to remove all the air present in the furnace. The sample was subjected to a controlled temperature program where it was heated in a nitrogen flow to 900°C at a rate of 10°C/min and a nitrogen flow rate of 75ml/min; holding the temperature for 15 minutes at 900°C. The sample was then allowed to cool down inside the furnace to room temperature under the nitrogen atmosphere to prevent oxidation. Thereafter, the sample was removed and stored under nitrogen until further analyses (i.e. XRD and XRF analyses) being conducted.

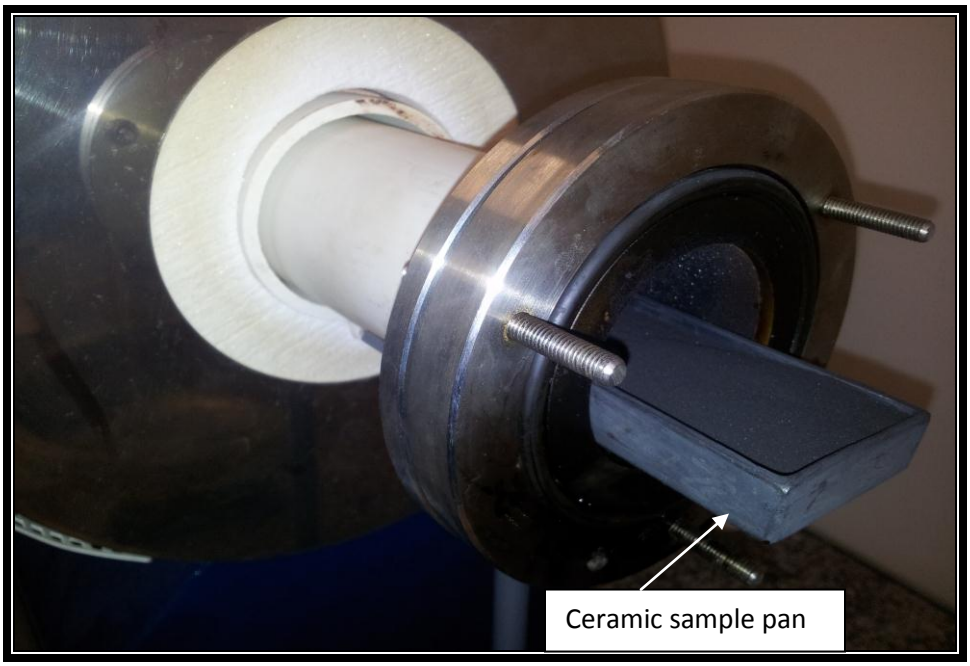

Figure 4.6 Sample loading into the tube furnace

4.3.2 Heat treatment in CO_2

About 30g of sample was placed on the ceramic sample pan and loaded into the tube furnace, and the furnace purged with nitrogen for 10 minutes. The sample was then heated in a nitrogen flow to 900°C at a rate of 10°C/min and a flow rate of 75ml/min, holding the temperature for 15 minutes at 900°C. The sample was then allowed to cool down inside the furnace to room temperature under the nitrogen atmosphere. Thereafter, the nitrogen flow was switched to CO_2, and heated to 1200°C at a rate of 10°C/min and a CO_2 flow rate of 20ml/min. The sample was then allowed to cool to room temperature inside the furnace, after which it was removed and stored until samples were sent for further analyses (i.e. XRD and XRF analyses).

4.4 Sample Analysis

The raw coal and the demineralized coal were sent to ACT (Advanced Coal Technology) labs for proximate and ultimate analyses. Samples from the tube furnace experiments (i.e. 5 K-wt% catalyst loaded samples) were submitted for XRF and XRD analyses. The XRF analysis

was conducted by Sci-ba Laboratories and Scientific Consultants, and the XRD analysis by XRD Analytical and Consulting.

4.4.1 Proximate and Ultimate Analyses

The raw and demineralized coal samples were submitted to ACT Labs for proximate and ultimate analyses. The analyses were crucial for the study in order to determine the effect of acid leaching on the reduction of the mineral matter in the coal sample. The proximate analysis was used to determine the amount of fixed carbon (FC), volatile matter (VM), moisture and ash present in the coal and the ultimate analysis to determine the amount of elemental chemical constituents (i.e. carbon, hydrogen, nitrogen, oxygen, sulphur) in the coal. The following analytical methods were used for analysis of the samples:

	Procedure / Method
Sample preparation	ACT-TPM-001 based on ISO 13909-4:2001
Moisture content (%)	ACT-TPM-010 based on SANS 5925: 2007
Ash content (%)	ACT-TPM-011 based on SABS ISO 1171: 1997
Volatile matter content (%)	ACT-TPM-012 based on SABS ISO 562: 1998
Total sulphur via IR spectroscopy (%)	ACT-TPM-013 based on ISO 19579: 2006
Ultimate analysis	ACT-TPM-027 based on ISO 12902

4.4.2 X-Ray Fluorescence (XRF)

X-ray fluorescence was used for qualitative determination of major and minor minerals in the 5 K-wt% catalyst loaded samples. Major element analysis was performed using a PANalytical Epsilon 3 energy dispersive X-Ray Spectrometer equipped with an Ag tube. XRF analysis was also performed for the potassium carbonate and potassium chloride catalysts, as well as for the mineral mixture that was prepared. For the 5 K-wt% loaded samples, XRF analysis was performed on samples before (i.e. after being devolatilized) and after reactions with CO_2. XRF analysis was done by Sci-ba Laboratories.

4.4.3 XRD (X-Ray-Diffraction)

Samples were submitted for XRD analysis to characterize and obtain qualitative and quantitative information of the 5 K-wt% catalyst loaded samples and mineral mixture. The samples were prepared for analysis using a back loading preparation method. They were analysed with a PANalytical X'Pert Pro powder diffractometer with X'Celerator detector and variable divergence and fixed receiving slits with Fe filtered Co-Kα radiation. The phases were identified using X'Pert Highscore plus software. The relative phase amounts (weight%) were estimated using the Rietveld method.

4.5 Experimental Plan

Listed in the tables below are the samples that were prepared for TG-MS experiments, as well as for the tube furnace experiments. The XRD and XRF analyses were performed on the 5 K-wt% catalyst loaded samples from the tube furnace experiments. Listed in Table 4.2 and Table 4.3 are the samples that were prepared for TG-MS experiments and tube furnace experiments, respectively. Listed in Table 4.4 are the experimental conditions employed in the study, for both TG-MS and tube furnace experiments.

Table 4.2 List of samples prepared for TG-MS experiments

Demineralized Coal (DC)					
Catalyst	Loading (K-wt%)	Sample name	Catalyst	Loading (K-wt%)	Sample name
None	0	DC			
K_2CO_3	0.5	DC + 0.5% K_2CO_3	**KCl**	0.5	DC + 0.5% KCl
	1	DC + 1% K_2CO_3		1	DC + 1% KCl
	3	DC + 3% K_2CO_3		3	DC + 3% KCl
	5	DC + 5% K_2CO_3		5	DC + 5% KCl
Raw Coal (RC)					
Catalyst	Loading (K-wt%)	Sample name	Catalyst	Loading (K-wt%)	Sample name
None	0	RC			
K_2CO_3	0.5	RC + 0.5% K_2CO_3	**KCl**	0.5	RC + 0.5% KCl
	1	RC + 1% K_2CO_3		1	RC + 1% KCl
	3	RC + 3% K_2CO_3		3	RC + 3% KCl
	5	RC + 5% K_2CO_3		5	RC + 5% KCl
Demineralized Coal with added mineral mixture (DC+MM)					
Catalyst	Loading (K-wt%)	Sample name	Catalyst	Loading (K-wt%)	Sample name
None	0	DC+MM			
K_2CO_3	0.5	DC+MM + 0.5% K_2CO_3	**KCl**	0.5	DC+MM + 0.5% KCl
	1	DC+MM + 1% K_2CO_3		1	DC+MM + 1% KCl
	3	DC+MM + 3% K_2CO_3		3	DC+MM + 3% KCl
	5	DC+MM + 5% K_2CO_3		5	DC+MM + 5% KCl

Table 4.3 List of samples prepared for tube furnace experiments

No heat treatment			
	Catalyst	Loading (K-wt%)	Sample name
Demineralized coal (DC)	None	0	DC
Raw coal (RC)	None	0	RC
Demineralized coal + mineral mixture (DC+MM)	None	0	DC+MM
Heat treatment in N_2			
	Catalyst	Loading (K-wt%)	Sample name
Demineralized Coal (DC)	None	0	DC (N_2)
	K_2CO_3	5	DC + 5% K_2CO_3 (N_2)
	KCl	5	DC + 5% K_2CO_3 (N_2)
Raw coal (RC)	None	0	RC (N_2)
	K_2CO_3	5	RC + 5% K_2CO_3 (N_2)
	KCl	5	RC + 5% KCl (N_2)
Demineralized coal + mineral mixture (DC+MM)	None	0	DC+MM (N_2)
	K_2CO_3	5	DC+MM + 5% K_2CO_3 (N_2)
	KCl	5	DC+MM + 5% KCl (N_2)
Heat treatment in CO_2			
	Catalyst	Loading (K-wt%)	Sample name
Demineralized coal (DC)	None	0	DC (CO_2)
	K_2CO_3	5	DC + 5% K_2CO_3 (CO_2)
	KCl	5	DC + 5% K_2CO_3 (CO_2)
Raw coal (RC)	None	0	RC (CO_2)
	K_2CO_3	5	RC + 5% K_2CO_3 (CO_2)
	KCl	5	RC + 5% KCl (CO_2)
Demineralized coal + mineral mixture (DC+MM)	None	0	DC+MM (CO_2)
	K_2CO_3	5	DC+MM + 5% K_2CO_3 (CO_2)
	KCl	5	DC+MM + 5% KCl (CO_2)

Table 4.4 Experimental conditions for TG-MS and tube furnace experiments

Heat treatment in N_2		Heat treatment in CO_2	
Temperature range:	ambient - 900 °C	Temperature range:	ambient - 1200 °C
Flow rate:	75 ml/min	Flow rate:	20 ml/min
Heating rate:	10 °C/min	Heating rate:	10 °C/min
Reactant gas:	N_2	Reactant gas:	CO_2

CHAPTER 5

Results and Discussion

Characterization of coal samples and additives

In this chapter, the results from various analysis techniques used to characterize the samples will be given and discussed. It is of great importance to be sure of the composition of the coal and additive samples before the influence of thermal treatment can be investigated properly.

5.1 Proximate and ultimate analyses

Proximate and ultimate analyses were used as characterization methods of the coal sample before and after sequential leaching with HCl-HF-HCl. The analyses were used to determine the general properties of coal and the extent to which the leaching process was effective. The normalized results are presented in Table 5.1.

A substantial reduction in the ash content (21.5% to less than 3%) was observed from the proximate results, indicating that a large proportion of the inorganic matter was removed by sequential leaching of the coal sample. The leaching method is known to reduce the inorganic matter that is also chemically linked with carboxyl groups in coal [Strydom et al., 2011], except for the pyrite [Formella et al., 1986]. The leaching method has been reported not to affect the carbonaceous matrix or the organic part of coal, except for a very small increase in –COOH content [Strydom et al., 2011]. The fixed carbon for the treated coal increased as expected and is indicative of the removal of inorganic components. The low total sulphur content is typical for the South African inertinite-rich bituminous coal utilized in this study [Falcon and Snyman, 1986].

The leaching process was crucial to validate the doping procedures (i.e. catalyst and mineral mixture additions) in this study. The inorganic matter associated with coal has been shown to undergo undesirable chemical transformation during heat treatments; as a result affecting the coal/char conversion [Formella et al., 1986]. Mineral-catalyst interactions have also been reported by Formella and co-workers [1986]. These interactions include secondary reactions of the catalyst with the mineral matter to form new mineral phases. Therefore it was

crucial to decrease the variables in the coal in order to reduce any interactions that might be due to the inorganic matter within the coal.

Table 5.1 Normalized Proximate and Ultimate analysis results of raw coal and demineralized

	Raw Coal (untreated coal)	**Demineralized Coal (treated/leached coal)**
Proximate Analysis	Moisture free basis (weight %)	Moisture free basis (weight %)
% Ash content	22.6	2.8
% Volatile matter	24.9	26.9
% Fixed carbon	52.5	70.3
Total	**100**	**100**
Ultimate Analysis	Dry-ash free basis (weight %)	Dry-ash free basis (weight %)
% Carbon content	77.1	79.2
% Hydrogen content	4.2	4.0
% Nitrogen content	2.1	2.3
% Oxygen content	15.3	13.5
% Total sulphur	1.3	1.0
Total	**100**	**100**

5.2 X-ray fluorescence (XRF)

Elemental analysis of the coal and char samples' ashes was performed by XRF. All the results were normalized to not include loss of ignition (LOI) values and are reported in weight percent (wt%), on an oxide basis. The LOI represents the amount of gaseous species (e.g. CO_2, H_2O and SO_x) that were given off during the decomposition of the samples and/or compounds. It is important to note that the XRF data presented were used solely for qualitative purposes and not for quantitative considerations.

It should be noted that, although the XRF output results are reported as simple oxides, they represent the ash elemental composition. In reality, ash consists of complex silicates and oxides [Xianglin et al., 1999].

5.2.1 Elemental analysis of the raw (untreated) and demineralized (treated/leached) coal

The coal samples' ashes were further characterized by XRF analyses in order to determine the major elemental composition of the coal ashes before and after sequential leaching. The normalized results are presented in Table 5.2. Minor and trace element analysis results are summarized in **Appendix A.**

It was also important to qualitatively determine the organically bound aluminium oxide (Al_2O_3) minerals as they have been reported to interact or react with potassium catalysts (used in this study) to form species that may affect coal/char conversion during heat treatments [Formella et al., 1986]. The Al_2O_3 minerals originate from clay minerals such as kaolinite ($Al_2O_3 \cdot SiO_2 \cdot 2H_2O$) which have been reported to be the most common mineral found in the type of coal (South African bituminous coal) utilized in this study [Ward, 2002, Stach et al.,1982]. Silica minerals such as quarts (SiO_2), as well as carbonate minerals (e.g. $CaCO_3$) have also been reported to be among the most common minerals found in this type of coal [Ward, 2002, Gluskoter, 1975, Stach et al., 1982].

The XRF results presented in Table 5.2 indicate that the raw untreated coal ash consists primarily of SiO_2, followed by aluminium oxide (Al_2O_3) and calcium oxide (CaO). The Al_2O_3 content was substantially reduced (26.30 – 5.22%) by the leaching process. The Al_2O_3 reduction might be due to the leached residue of kaolinite, where the leaching acids removed SiO_2 from the kaolinite [$(Al_2Si_2O_5(OH)_4$] structure. The SiO_2 content could be attributed to the silica mineral, quartz (SiO_2). The CaO present in the coal ash could be due to the carbonate minerals such as calcite ($CaCO_3$). The effect of leaching was also observed in the reduced SiO_2 (44.24 – 37.47%) and CaO (11.95 – 4.20%) minerals. These reductions indicate that the HCl/HF/Cl leaching process was effective, more so in removing the clay minerals and other elements associated with the clay minerals. The other components such as Na_2O, MnO, Fe_2O_3 and K_2O might be due to other minerals that were present in the original coal (listed in Chapter 2, Table 2.2).

Both the raw coal ash and the demineralized coal ash samples contained very low percentages of potassium (less than 0.6% K_2O). The effects of the addition of potassium

compounds may thus be ascribed to the additions and the influence of the potassium compounds in the samples can be regarded as negligible.

Table 5.2 Normalized XRF results for the raw (untreated) and demineralized coal. Results normalized to not include LOI values (weight %, oxide basis)

	Raw Coal	**Demineralized Coal**
SiO_2	44.24	37.47
TiO_2	1.35	11.18
Al_2O_3	26.30	5.22
Fe_2O_3	5.32	30.42
MnO	0.17	0.61
MgO	4.73	3.12
CaO	11.95	4.20
Na_2O	0.68	3.66
K_2O	0.38	0.61
P_2O_5	0.63	0.27
Cr_2O_3	0.21	0.95
SO_3	4.05	2.30
TOTAL	**100**	**100**

Note: LOI = loss of ignition

5.2.2 Elemental analysis of additives

The XRF analysis of the model mineral mixture ash and catalysts (i.e. K_2CO_3 and KCl) was performed in order to determine the major, minor and trace elements present. Potassium salts were chosen as catalysts since potassium compounds are found in naturally occurring potassium-bearing minerals in coal [Spiro et al.,1986]; and have been reported to exhibit a catalytic effect during coal heat treatments [Rivera-Utrilla et al., 1987, Kyotani et al., 1993].

The mineral mixture, prepared according to Nel et al. [2011], was made up of kaolin clay (kaolinite), quartz (SiO_2), pyrite (FeS_2), calcite ($CaCO_3$), siderite ($FeCO_3$), hydromagnesite (basic $MgCO_3$) and anastase (TiO_2). The minerals were added to the mixture in fixed ratios and the minerals were chosen based on the most common and abundant minerals closely

associated with coal ash (Table 5.2). The XRF analysis was performed on the ash of the mixture as a whole and not on each compound of the mixture, therefore minor and trace constituents in each of the compounds constituting the mixture are indistinguishable.

The normalized XRF results of the major elements of the ash mixture are presented in Table 5.3. The K_2O content of K_2CO_3 (99.56%) and KCl (99.14%) indicate that the potassium salts used were more than 99% pure.

Table 5.3 XRF results for the catalysts and mineral mixture, normalized to not include LOI values (weight %, oxide basis)

	Mineral Mixture	**K_2CO_3**	**KCl**
SiO_2	26.38	0.02	0.06
TiO_2	3.88	ND	ND
Al_2O_3	17.57	0.20	0.33
Fe_2O_3	21.09	ND	ND
MnO	0.02	ND	0.06
MgO	7.26	0.07	0.07
CaO	14.02	0.00	ND
Na_2O	0.29	0.13	ND
K_2O	0.42	99.56	99.14
P_2O_5	0.01	ND	ND
Cr_2O_3	0.01	ND	ND
SO_3	9.05	0.02	0.33
Total	**100**	**100**	**100**

Note: LOI = loss of ignition, ND = not detected, K_2CO_3 = potassium carbonate, KCl = potassium chloride

5.2.3 XRF results of raw and demineralized coal after heat treatment in N_2

Elemental analysis of the demineralized coal samples after heat treatment in N_2 (i.e. chars) from the tube furnace experiments was performed by XRF, in order to determine the elemental composition of the char ash. The chars prepared represent those that were formed during thermogravimetric (TG) experiments (**Chapter 6**), as similar experimental conditions

were simulated for both TG and tube furnace experiments. The XRF analysis was performed on the char ash produced from:

(i) raw, demineralized coal and demineralized coal with added model mineral mixture with no catalyst loadings.

(ii) raw, demineralized coal, demineralized coal with added model mineral mixture with ***5 wt%*** (i.e. ***K-wt%***) K_2CO_3 and KCl loadings.

The XRF results for chars derived from (i) and (ii) are presented in Table 5.4, as well as the product sample after heat treatments in CO_2. Minor and trace element analysis results of the samples are presented in **Appendix A**. The anticipated increase in K_2O content in potassium loaded samples was confirmed by the XRF results. It should be noted that an XRF analysis of the neat mineral mixture was not performed, but previous studies have indicated these values [Nel et al., 2011]. The XRF results will be discussed in Chapter 6, in comparison to the results obtained in following chapters**.**

Table 5.4 Normalized XRF results for samples with/without 5 K-wt% catalyst (K_2CO_3 and KCl) loadings before and after heat treatments in N_2 and CO_2 atmospheres (weight %, oxide basis)

	Heated in:	SiO_2	TiO_2	Al_2O_3	Fe_2O_3	MnO	MgO	CaO	Na_2O	K_2O	P_2O_5	Cr_2O_3	SO_3	Total
DC	**unheated**	37.47	11.18	5.22	30.42	0.61	3.12	4.20	3.66	0.61	0.27	0.95	2.30	**100**
	N_2	15.96	8.98	3.52	34.74	BDL	0.68	5.39	0.08	0.86	0.27	0.15	29.36	**100**
DC	**CO_2**	39.53	12.14	7.56	28.18	0.41	3.70	5.05	0.69	0.83	0.36	0.77	0.77	**100**
	N_2	5.54	3.94	1.72	12.75	BDL	0.44	3.08	0.01	59.69	0.07	0.06	12.70	**100**
DC + 5% K_2CO_3	**CO_2**	4.06	4.29	1.59	13.08	BDL	0.24	2.45	BDL	63.79	0.07	0.07	10.36	**100**
	N_2	6.01	4.36	1.39	14.26	BDL	0.45	3.33	BDL	57.95	0.08	0.07	12.10	**100**
DC + 5% KCl	**CO_2**	29.07	8.55	4.23	17.33	0.32	2.56	3.35	6.87	17.41	0.16	0.56	9.58	**100**
RC	**unheated**	44.24	1.35	26.30	5.32	0.17	4.73	11.95	0.68	0.38	0.63	0.21	4.05	**100**
	N_2	45.34	1.41	26.98	5.28	0.17	4.98	12.45	0.71	0.54	0.71	0.24	1.21	**100**
RC	**CO_2**	45.41	1.40	27.05	5.36	0.19	4.83	12.30	0.87	0.45	0.70	0.23	1.21	**100**
	N_2	32.76	2.04	18.53	7.79	0.21	4.08	9.33	1.37	13.57	0.42	0.25	9.66	**100**
RC + 5% K_2CO_3	**CO_2**	36.99	1.23	22.83	5.16	0.18	4.19	10.83	0.79	11.51	0.55	0.24	5.50	**100**
	N_2	39.37	1.27	24.18	5.19	0.18	4.43	11.15	2.38	7.33	0.57	0.24	3.71	**100**
RC + 5% KCl	**CO_2**	40.22	1.79	23.86	6.47	0.19	4.36	10.77	1.32	5.31	0.57	0.25	4.90	**100**
	N_2	37.47	11.18	5.22	30.42	0.61	3.12	4.20	3.66	0.61	0.27	0.95	2.30	**100**
DC + MM	**CO_2**	38.83	7.97	11.87	22.54	0.23	5.92	8.88	0.33	0.52	0.13	0.36	2.44	**100**
	N_2	30.88	6.57	7.97	17.83	0.23	4.61	7.43	2.74	16.81	0.08	0.39	4.46	**100**
DC + MM + 5% K_2CO_3	**CO_2**	7.41	3.98	3.64	18.97	0.00	0.96	5.98	0.00	42.97	0.04	0.04	16.01	**100**
	N_2	8.39	3.87	3.38	17.53	0.01	1.27	5.97	0.02	43.90	0.01	0.04	15.61	**100**
DC + MM + 5% KCl	**CO_2**	32.76	2.07	18.52	7.76	0.21	4.06	9.33	1.35	13.53	0.43	0.28	9.69	**100**

Note: DC = demineralized coal; MM = mineral mixture; DC+MM = demineralized coal with added mineral mixture; RC = raw coal; BDL = below detection limit, N_2 = nitrogen atmosphere, CO_2 = carbon dioxide atmosphere

5.3 X-Ray Diffraction of coal and char samples

The X-ray diffraction (XRD) analysis was performed on the coal ash and char ash samples with and without ***5 K-wt%*** catalyst additions; before and after heat treatments in N_2 and CO_2. The analysis was done in order to determine the crystalline phases that were present before and after heat treatments in N_2 and CO_2 atmospheres. The crystalline phases for the following samples were determined (i) demineralized coal ash with and without catalyst additions (ii) raw untreated coal with and without catalyst additions and (iii) demineralized coal ash with added mineral mixture plus catalyst loadings. The XRD results are presented below, as well as the XRD diffractograms from which the weight percentages of the mineral phases in the XRD results were determined.

The potassium mineral phases were of interest in this study, in order to determine the extent of interaction of K_2CO_3 and KCl with the coal and coal char, as well as with the compounds in the mineral mixture. It is important to note that the XRD results do not necessarily suggest that no potassium was retained or present in the samples after heat treatments in the N_2 and CO_2 experiments; since only the crystalline phases are given by the XRD analysis. The potassium compound may occur as an amorphous phase; therefore any amorphous potassium present in the samples will not be identified by the XRD analysis. The XRD results will be further discussed in Chapter 7.

5.3.1 Demineralized coal and char samples with/without catalyst loadings

The XRD results in Table 5.6 indicate that the mineral phases constituting the potassium compound in the coal samples were muscovite ($KAl_2(AlSi_3O_{10})(OH)_2$). However, no potassium-containing mineral phases were observed in the heat treated samples under both atmospheres; except for the mineral phase sylvite (KCl), which was observed in the KCl loaded samples and a relatively small amount of sylvite observed in sample K_2CO_3 loaded sample after CO_2 heat treatment. The small amounts of the mineral phase dolomite [$CaMg(CO_3)_2$] may be attributed to the reaction of CO_2 evolved from K_2CO_3, with some Ca and Mg in the samples to give this compound; thus suggesting that the Ca and Mg must have been present in small amounts in the sample.

Figures 5.1, 5.2 and 5.3 present the XRD diffractograms of the demineralized coal before heat treatments, and after heat treatments in N_2 and CO_2, respectively. Other XRD diffractograms of catalyst loaded samples before and after heat treatments in N_2 and CO_2 atmospheres are presented in **Appendix A**.

Table 5.5 XRD results of the demineralized coal and char samples with/without 5 K-wt% catalyst loadings (weight%)

		DC	DC		DC + 5 K-wt% K_2CO_3		DC + 5 K-wt% KCl	
Mineral phase	**Mineral formulae**	**unheated**	**N_2**	**CO_2**	**N_2**	**CO_2**	**N_2**	**CO_2**
Anastase	TiO_2	0.3	0.1	0.1	-	-	0.2	-
Dolomite	$CaMg(CO_3)_2$	-	-	-	0.2	0.3	-	-
Graphitic carbon	C	91.9	99.1	98.9	97.1	99.6	93.6	98.4
Iron alpha	α-Fe	-	0.1	0.1	0.0	-	0.1	0.0
Jadeite	$NaAlSi_2O_6$	-	-	-	1.5	-	-	-
Magnetite	Fe_3O_4	-	0.1	0.3	-	-	0.1	0.1
Muscovite	$KAl_2(AlSi_3O_{10})(OH)_2$	1.9	-	-	-	-	-	-
Pyrite	FeS_2	2.0	-	-	-	-	-	-
Quartz	SiO_2	3.9	0.7	0.7	0.6	0.0	1.0	0.6
Sylvite	KCl	-	-	-	-	0.1	5.0	0.9

Note: DC = demineralized coal; unheated = not subjected to any heat treatment; N_2 = heat treatment in nitrogen; CO_2 = heat treatment in carbon dioxide

Table 5.6 Normalized XRD results of the demineralized coal and char samples with/without 5 K-wt% catalyst loadings (weight%, ***carbon-free basis***)

		DC	DC		DC + 5 K-wt% K_2CO_3		DC + 5 K-wt% KCl	
Mineral phase	**Mineral formulae**	**unheated**	**N_2**	**CO_2**	**N_2**	**CO_2**	**N_2**	**CO_2**
Anastase	TiO_2	4.0	8.4	6.4	-	-	3.1	-
Dolomite	$CaMg(CO_3)_2$	-	-	-	7.6	78.6	-	-
Iron alpha	α-Fe	-	8.4	5.5	1.8	-	1.6	-
Jadeite	$NaAlSi_2O_6$	-	-	-	65.2	-	-	-
Magnetite	Fe_3O_4	-	14.7	29.1	-	-	1.6	6.3
Muscovite	$KAl_2(AlSi_3O_{10})(OH)_2$	23.5	-	-	-	-	-	-
Pyrite	FeS_2	24.5	-	-	-	-	-	-
Quartz	SiO_2	48.1	68.4	59.1	25.5	7.1	15.6	37.5
Sylvite	KCl	-	-	-	-	14.3	78.1	56.3

Note: DC = demineralized coal; unheated = not subjected to any heat treatment; N_2 = heat treatment in nitrogen; CO_2 = heat treatment in carbon dioxide

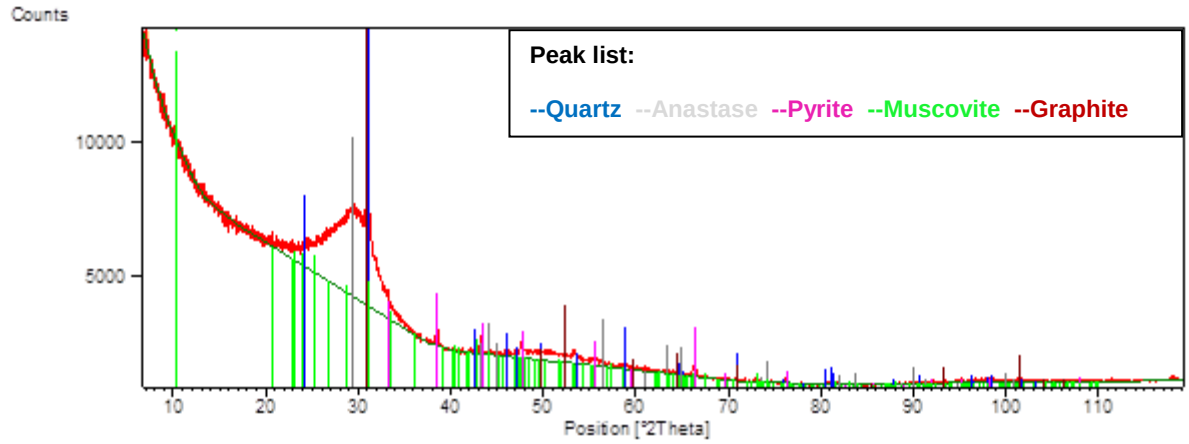

Figure 5.1 XRD diffractogram for the demineralized coal (DC) before heat treatment

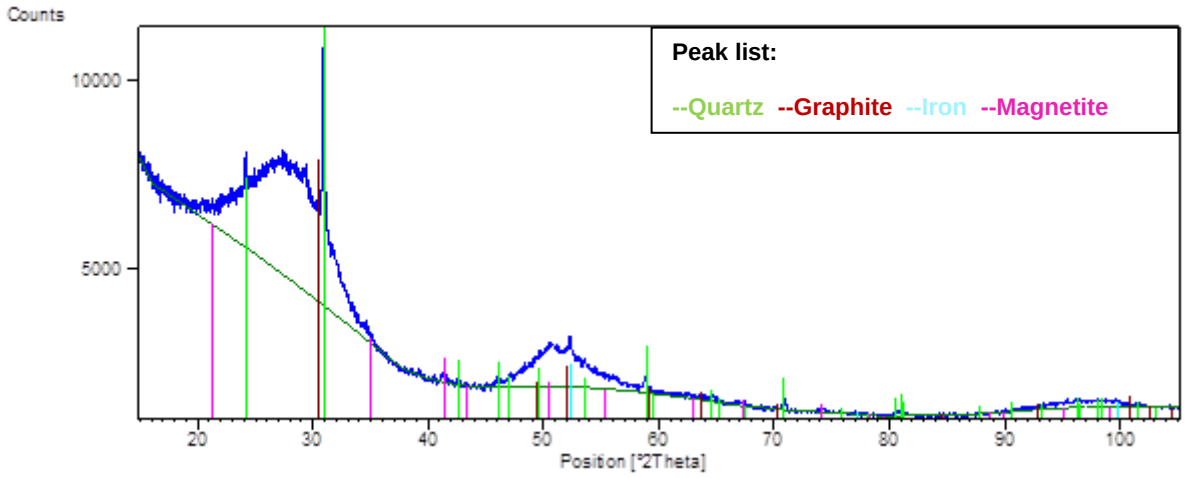

Figure 5.2 XRD diffractogram for the demineralized coal (DC) after N_2 heat treatment

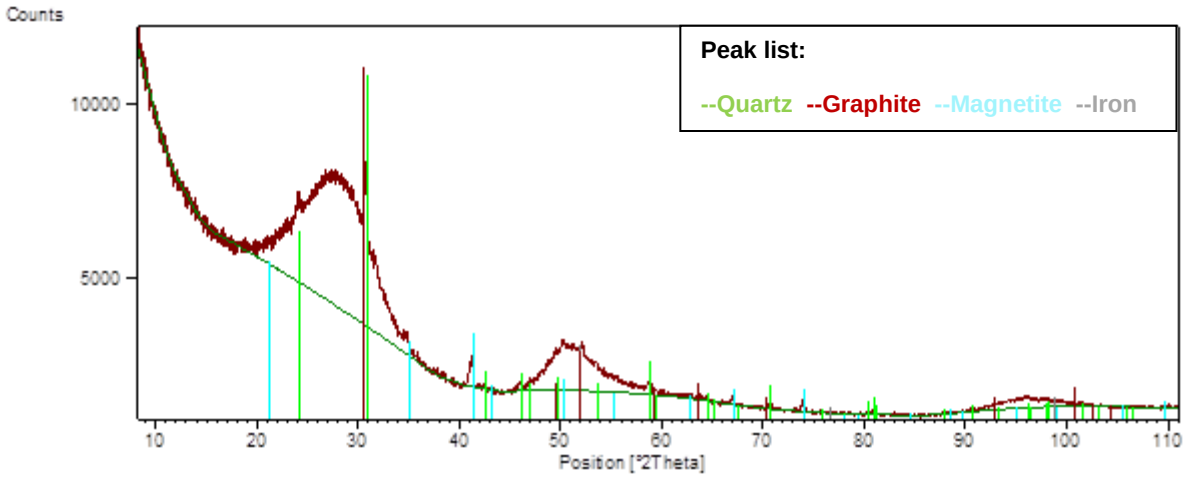

Figure 5.3 XRD diffractogram for the demineralized coal (DC) after CO_2 heat treatment

5.3.2 Raw coal and char samples with/without catalyst loadings

As it can be seen from the XRD results summarized in Table 5.7, the mineral phase constituting the potassium compound is muscovite ($KAl_2(AlSi_3O_{10})(OH)_2$) in the coal samples not subjected to any heat treatment. No potassium-containing mineral phases were observed in the samples with and without catalyst additions after heat treatments in N_2 and CO_2 atmospheres. Figures 5.4 – 5.6 present the XRD diffractograms of the raw coal and char before heat treatments, after heat treatments in N_2 and CO_2, respectively. Other XRD diffractograms of catalyst loaded samples before and after heat treatments in N_2 and CO_2 atmospheres are presented in **Appendix A**.

Table 5.7 XRD results of the raw coal and char samples with/without 5 K-wt% catalyst loadings (weight%)

		RC	RC		RC + 5 K-wt% K_2CO_3		RC + 5 K-wt% KCl	
Mineral phase	**Mineral formulae**	**unheated**	**N_2**	**CO_2**	**N_2**	**CO_2**	**N_2**	**CO_2**
Anastase	TiO_2	0.4	-	-	-	-	-	-
Calcite	$CaCO_3$	3.8	-	-	-	3.3	-	-
Dolomite	$CaMg(CO_3)_2$	7.5	-	-	0.4	-	-	-
Graphitic carbon	C	37.4	90.6	87.6	93.3	92.6	87.9	86.2
Iron alpha	α-Fe	-	0.3	0.01	0.4	-	0.03	0.1
Jadeite	$NaAlSi_2O_6$	-	-	-	-	-	-	-
Kaolinite	$Al_2O_3{\cdot}2SiO_2{\cdot}2H_2O$	30.0	-	-	-	-	-	-
Magnetite	Fe_3O_4	-	0.1	0.3	-	-	-	0.3
Mullite	$Al_6Si_2O_{13}$	-	0.7	2.6			-	-
Muscovite	$KAl_2(AlSi_3O_{10})(OH)_2$	5.0	-	-	-	-	-	-
Oldhamite	(Ca, Mg)S	-	1.0	0.6	1.6	1.5	-	-
Periclase	MgO	-	0.6	0.6	0.6	1.5	0.1	0.2
Plagioclase	$NaAlSi_3O_8$; $CaAl_2Si_2O_8$	-	-	2.3	-	-	3.9	8.1
Pyrite	FeS_2	2.2	-	-	-	-	-	-
Quartz	SiO_2	13.8	6.7	6.0	3.7	1.2	5.2	2.8
Sylvite	KCl	-	-	-	-	-	2.9	2.3

Note: RC = raw coal; unheated = not subjected to any heat treatment; N_2 = heat treatment in nitrogen; CO_2 = heat treatment in carbon dioxide

Table 5.8 Normalized XRD results of the raw coal and char samples with/without 5 K-wt% catalyst loadings (weight%, ***carbon-free basis***)

		RC	RC		RC + 5 K-wt% K_2CO_3		RC + 5 K-wt% KCl	
Mineral phase	**Mineral formulae**	**unheated**	**N_2**	**CO_2**	**N_2**	**CO_2**	**N_2**	**CO_2**
Anastase	TiO_2	0.7	-	-	-	-	-	-
Calcite	$CaCO_3$	6.0	-	-	-	45.1	-	-
Dolomite	$CaMg(CO_3)_2$	12	-	-	6.2	-	-	-
Iron alpha	α-Fe	-	3.0	0.08	5.3	-	0.3	0.8
Jadeite	$NaAlSi_2O_6$	-	-	-	-	-	-	-
Kaolinite	$Al_2O_3{\cdot}2SiO_2{\cdot}2H_2O$	48.0	-	-	-	-	-	-
Magnetite	Fe_3O_4	-	1.5	2.1	-	-	-	-
Mullite	$Al_6Si_2O_{13}$	-	7.5	21.0	-	-	-	-
Muscovite	$KAl_2(AlSi_3O_{10})(OH)_2$	8.0	-	-	-	-	-	-
Oldhamite	(Ca, Mg)S	-	11	5.0	24.0	19.6	-	-
Periclase	MgO	-	6.6	5.2	8.4	19.8	1.2	1.1
Plagioclase	$NaAlSi_3O_8$;	-	-	18.6	-	-	32.3	58.7
Pyrite	FeS_2	3.5	-	-	-	-	-	-
Quartz	SiO_2	22.0	70.5	48.2	56.2	15.6	42.5	20.6
Sylvite	KCl	-	-	-	-	-	23.8	16.7

Note: RC = raw coal; unheated = not subjected to any heat treatment; N_2 = heat treatment in nitrogen; CO_2 = heat treatment in carbon dioxide

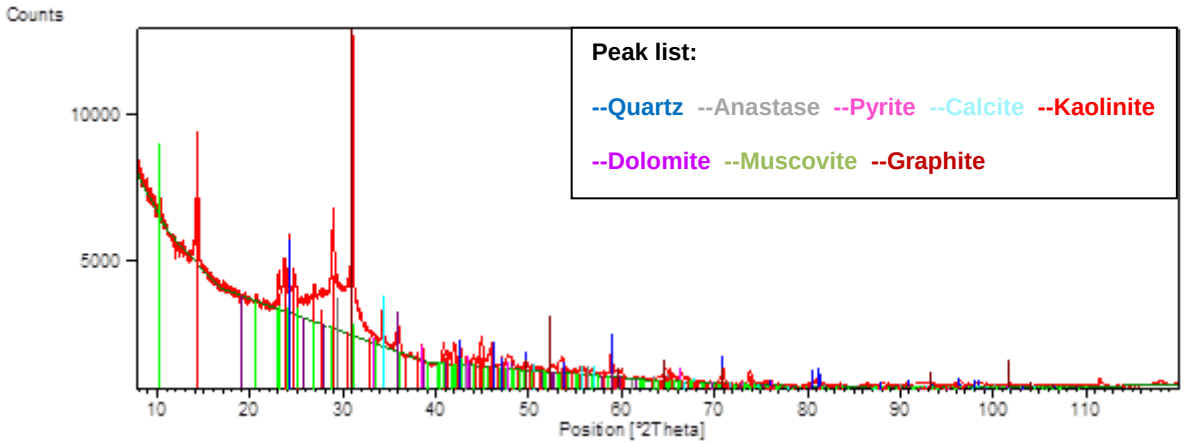

Figure 5.4 XRD diffractogram for the raw coal (RC) before heat treatment

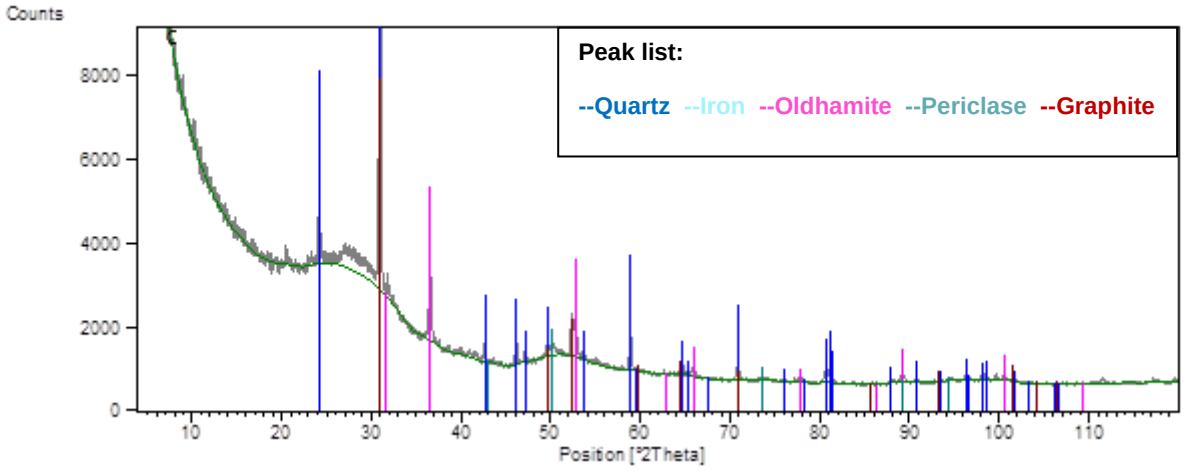

Figure 5.5 XRD diffractogram of the raw coal (RC) after N_2 heat treatment

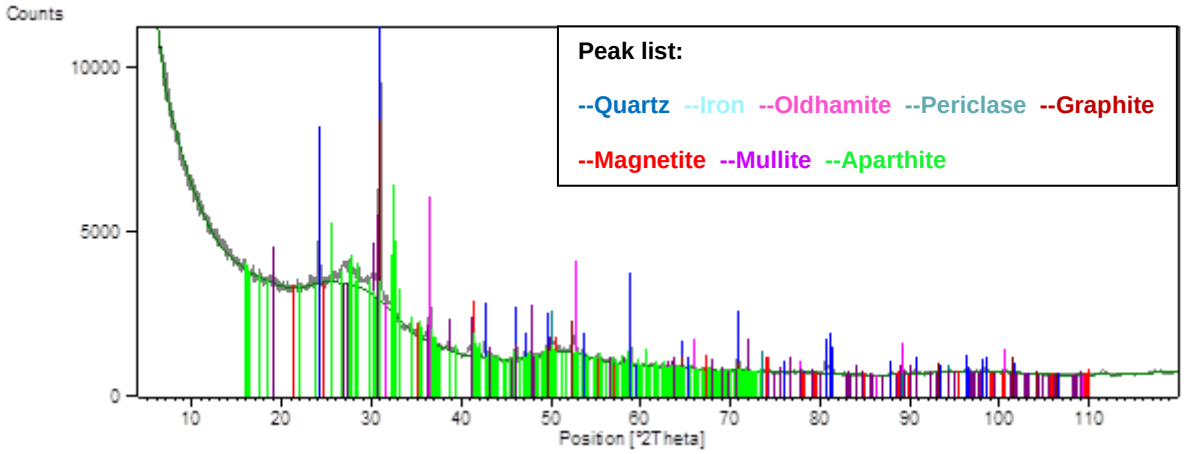

Figure 5.6 XRD diffractogram of the raw coal (RC) after CO_2 heat treatment

5.3.3 Demineralized coal and char samples with added mineral mixture, with/without catalyst loadings

The mineral phases constituting the potassium compound were muscovite ($KAl_2(AlSi_3O_{10})(OH)_2$) in the coal samples, as well as in the mineral mixture that was not subjected to heat treatments. However, no potassium-bearing mineral phases were observed in

the heated treated samples under both atmospheres, except for the mineral phase sylvite (KCl) which was observed in the KCl loaded samples after CO_2 heat treatment. Figure 5.7 - 5.8 presents the XRD diffractograms of the demineralized coal before heat treatments, after heat treatments in N_2 and CO_2 respectively.

It should be noted that the XRD diffractogram of the demineralized coal sample with the added mineral mixture where the sample was not subjected to heat treatment is not shown; because it is essentially the addition of the XRD results of the demineralized coal and mineral mixture. XRD diffractograms of catalyst loaded samples before and after heat treatments in N_2 and CO_2 atmospheres are presented in **Appendix A**.

Table 5.9 Semi-qualitative XRD results of the demineralized coal and char samples with added mineral mixture, with/without 5 K-wt% catalyst loadings (weight%)

		MM	**DC + MM**		**DC + MM + 5 K-wt% K_2CO_3**		**DC + MM + 5 K-wt% KCl**	
Mineral	**Mineral formulae**	**unheated**	**N_2**	**CO_2**	**N_2**	**CO_2**	**N_2**	**CO_2**
Ankerite	$Ca(Fe,Mg,Mn)(CO_3)_2$	-	-	-	0.4	-	-	-
Anastase	TiO_2	6.9	0.4	0.2	-	-	0.2	0.1
Calcite	$CaCO_3$	25.2	-	-	-	-	-	0.3
Dolomite	$CaMg(CO_3)_2$	1.6	-	-	-	0.6	-	-
Graphite	C	-	96.0	96.2	96.4	97.5	92.8	95.1
Fluorite	CaF_2	-	0.4	-	0.5	-	-	-
Iron alpha	α-Fe	-	-	-	0.04	-	-	-
Jadeite	$NaAlSi_2O_6$	-	-	-	0.6	0.8	-	-
Kaolinite	$Al_2O_3{\cdot}2SiO_2{\cdot}2H_2O$	33.5	-	-	-	-	-	-
Magnetite	Fe_3O_4	-	0.4	0.6	-	-	-	0.4
Muscovite	$KAl_2(AlSi_3O_{10})(OH)_2$	4.6	-	-	-	-	-	-
Perovskite	$CaTiO_3$	-	-	-	-	0.8		
Plagioclase	$NaAlSi_3O_8$; $CaAl_2Si_2O_8$	-	0.8	1.2	-	-	-	-
Pyrite	FeS_2	12.0	-	-	-	-	-	-
Quartz	SiO_2	16.3	1.9	1.4	1.5	0.2	1.4	1.0
Sylvite	KCl	-	-	-	-	-	4.6	2.6
Troilite	FeS	-	-	0.5	-	-	0.4	-

Note: DC = demineralized coal; MM = mineral mixture; DC+MM = demineralized coal with added mineral mixture; unheated = not subjected to any heat treatment; N_2 = heat treatment in nitrogen; CO_2 = heat treatment in carbon dioxide

Table 5.10 Normalized XRD results of the demineralized coal and char samples with add mineral mixture, with/without 5 K-wt% catalyst loadings (weight%, ***carbon-free basis***)

		MM	**DC + MM**		**DC + MM + 5 K-wt% K_2CO_3**		**DC + MM + 5 K-wt% KCl**	
Mineral	**Mineral formulae**	**unheated**	**N_2**	**CO_2**	**N_2**	**CO_2**	**N_2**	**CO_2**
Ankerite	$Ca(Fe,Mg,Mn)(CO_3)_2$	-	-	-	13.1	-	-	-
Anastase	TiO_2	6.9	10.0	4.5	-	-	2.3	1.8
Calcite	$CaCO_3$	25.2	-	-	-	-	-	7.7
Dolomite	$CaMg(CO_3)_2$	1.6	-	-	-	24.7	-	-
Fluorite	CaF_2	-	10.0	-	16.5	-	-	-
Iron alpha	α-Fe	-	-	-	1.3	-	-	-
Jadeite	$NaAlSi_2O_6$	-	-	-	19.5	31.7	-	-
Kaolinite	$Al_2O_3{\cdot}2SiO_2{\cdot}2H_2O$	33.5	-	-	-	-	-	-
Magnetite	Fe_3O_4	-	10.0	17.0	-	-	-	8.6
Muscovite	$KAl_2(AlSi_3O_{10})(OH)_2$	4.6	-	-	-	-	-	-
Perovskite	$CaTiO_3$	-	-	-	-	33.7	-	-
Plagioclas	$NaAlSi_3O_8$; $CaAl_2Si_2O_8$	-	19.7	30.5	-	-	-	-
Pyrite	FeS_2	12.0	-	-	-	-	-	-
Quartz	SiO_2	16.3	50.4	35.8	49.5	9.9	21.6	23.1
Sylvite	KCl	-	-	-	-	-	70.6	58.7
Troilite	FeS	-	-	12.2	-	-	5.5	-

Note: DC = demineralized coal; MM = mineral mixture; DC+MM = demineralized coal with added mineral mixture; unheated = not subjected to any heat treatment; N_2 = heat treatment in nitrogen; CO_2 = heat treatment in carbon dioxide

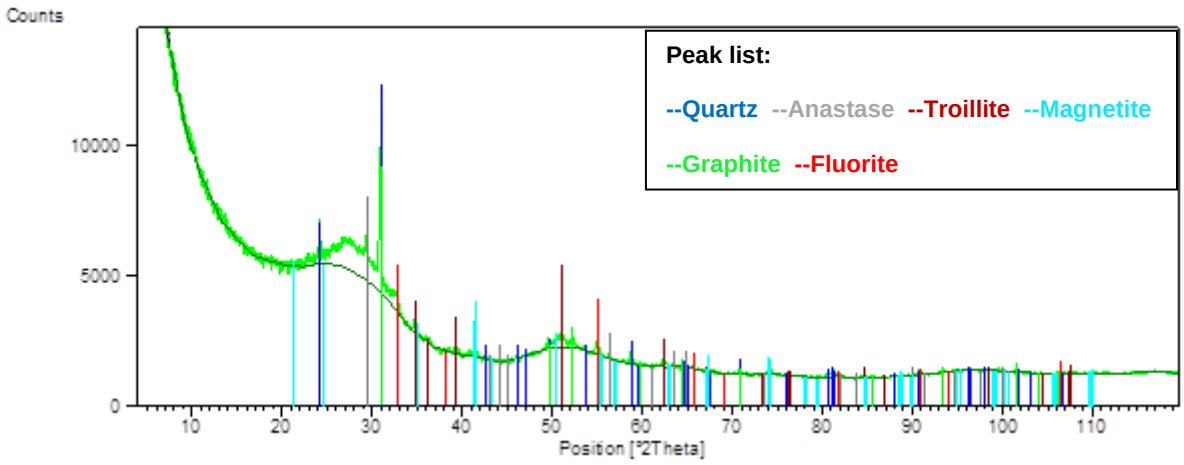

Figure 5.7 XRD diffractogram for the demineralized coal with added mineral mixture (DC+MM) after N_2 heat treatment

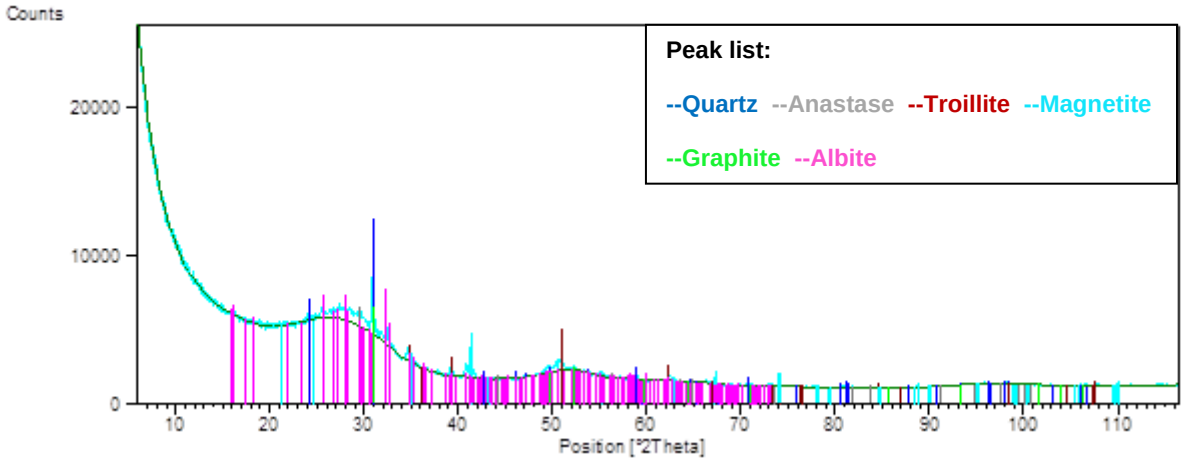

Figure 5.8 XRD diffractogram for the demineralized coal with added mineral mixture (DC+MM) after CO_2 heat treatment

From all the XRD results it is clear that no specific crystalline phases of potassium compounds formed before and after heat treatments in CO_2.

CHAPTER 6

Results and Discussion

Thermogravimetric (TG) analysis of coal-char samples

This chapter presents the TG results of the char samples derived from the demineralized coal, raw coal and the demineralized coal with an added model mineral mixture. The TG results are of the char samples during heat treatments in a CO_2 atmosphere. The chapter also looks at the relative reactivities due to K_2CO_3 and KCl loadings.

Thermogravimetric (TG) studies of the coal char were conducted in order to investigate the effect of the catalyst loadings on the mass loss of the samples during heat treatments in a carbon dioxide atmosphere.

Potassium carbonate (K_2CO_3) and potassium chloride (KCl) were used as catalysts in this study. Catalyst loadings of 0.5, 1, 3, 5 K-wt% were loaded to an inertinite-rich bituminous sample (i.e. raw or untreated coal), to an acid leached sample of the same coal (i.e. demineralized coal), and to the demineralized sample of the same coal with an added model mineral mixture. The catalyst loadings represent the initial K-wt% (calculated based on the K^+ content for K_2CO_3 and KCl) added to the coal samples prior to charring.

All samples were subjected to a heat treatment step up to 900 °C in a nitrogen atmosphere to produce the respective char samples. These char samples were then subjected to heat treatments in a CO_2 atmosphere up to 1200°C and the mass losses were determined from the TG curves. It has been reported that char reactivity is dependent on the heat treatment (or coal devolatilization) conditions on which the char was prepared [Liu et al., 2006]. All the samples were treated in the same manner and all the results are comparative between the samples.

Analysis and characterization of the chars prepared from the tube furnace experiments (i.e. before heat treatments in CO_2) are presented in Chapter 5 (Table 5.4 and 5.6). The characterization results provide information on the composition and mineral phase of the chars that were produced during TG studies, as they were prepared under similar experimental conditions (i.e. at 900°C). It should be noted that all the mass losses observed on the TG curves

are reported on a catalyst free basis (i.e. the mass loss observed is due to the coal alone); as explained in Section 6.1 below.

6.1 Thermochemistry of K_2CO_3 and KCl

Thermogravimetric (TG) analysis of the mass loss behaviour of the catalysts (K_2CO_3 and KCl), was carried out in a N_2 atmosphere in order to determine the behaviour and extent to which the catalysts decompose during heat treatments, as well as to determine the rough estimate of the amount of potassium that is retained in the char prior to char heat treatments in CO_2. The TG analysis was crucial in order to determine how much of the catalyst is lost during the charring phase (i.e. during heat treatment in N_2), before heat treatment of the prepared chars in CO_2 commences. The TG curves of K_2CO_3 and KCl during heat treatments (1200°C) are presented in Figure 6.1 and 6.2, respectively.

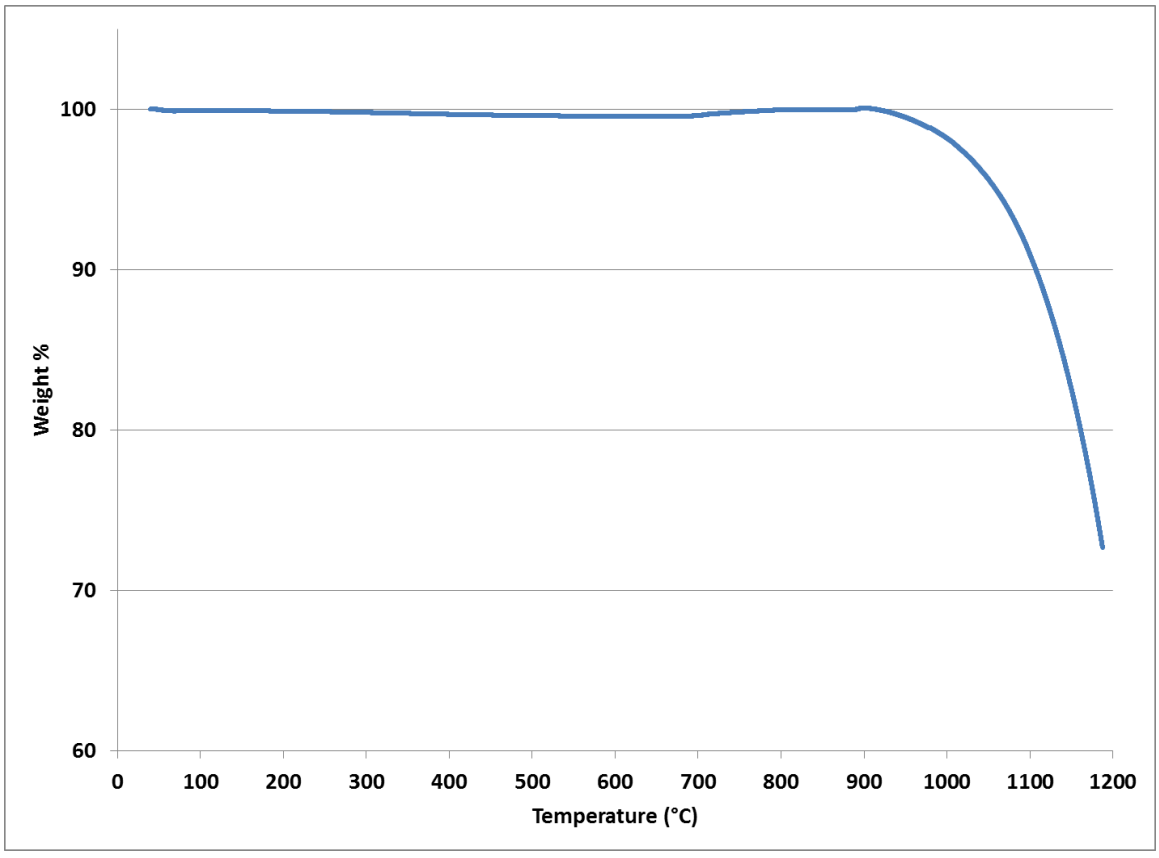

Figure 6.1 TG curve of K_2CO_3 in CO_2 atmosphere

Figure 6.1 indicates that no mass loss was observed for K_2CO_3 in N_2 up to 900°C. K_2CO_3 is known to decompose at high temperatures according to the reaction: $K_2CO_3 \leftrightarrow K_2O + CO_2$, however the reaction is negligible below the melting point of K_2CO_3 [Lehman et al., 1998]. Since the chars derived from K_2CO_3 loaded coal samples were prepared up to 900°C, the melting point of K_2CO_3 indicates that K_2CO_3 remained 'unchanged' in the char; and no decomposition of the carbonate took place until heat treatments of up to 1200°C in CO_2. However, instability of K_2CO_3 near its melting point has been reported [Lehman et al., 1998]. The TG curve of K_2CO_3, up to 1200°C, indicates that mass loss starts to occur just above 900°C and the decomposition does not go to completion under the temperature limits (1200°C) employed in this study. The temperature observed for the start of mass loss from K_2CO_3 is in agreement with the melting point of K_2CO_3 which is reported to be 900°C in N_2 and 905°C in CO_2 [Lehman et al., 1998].

Since K_2CO_3 decomposes into K_2O and CO_2 [i.e. K_2CO_3 (s) → K_2O (s) + CO_2 (g)], the mass loss observed on the TG curve is due to the release of CO_2. It is seen that only about 28% of the total CO_2 is evolved. Based on the latter, the mass loss of the K_2CO_3 loaded char samples were 'corrected' to take into account the mass loss due to CO_2 from the decomposition of K_2CO_3. Furthermore, the initial amount of the catalyst loaded to the coal prior to charring was 'subtracted' from the starting mass of the char during CO_2 heat treatments. Thus the mass loss curves are reported on a catalyst-free basis.

Figure 6.2 indicates that KCl experienced a mass loss just above 730°C, which is close to the reported melting point of 770°C [Atkins and Paula, 2006]. From the TG curve it can be seen that approximately a 40% mass loss occurs during the charring stage, suggesting that the char at the beginning of the CO_2 heat treatment only contains about 60% of the initially loaded KCl. It can be seen from the TG curve that by the time a temperature of 1200°C is reached, all of the KCl is lost; suggesting that some of the mass loss seen for the char samples is due to the mass loss of KCl. Therefore, the mass losses reported on a catalyst-free basis only take into account the initial amount of KCl loaded to the coal prior to charring and 60% of the mass loss during heat treatments to up to 1200°C. Thus the mass loss curves are reported on a catalyst-free basis.

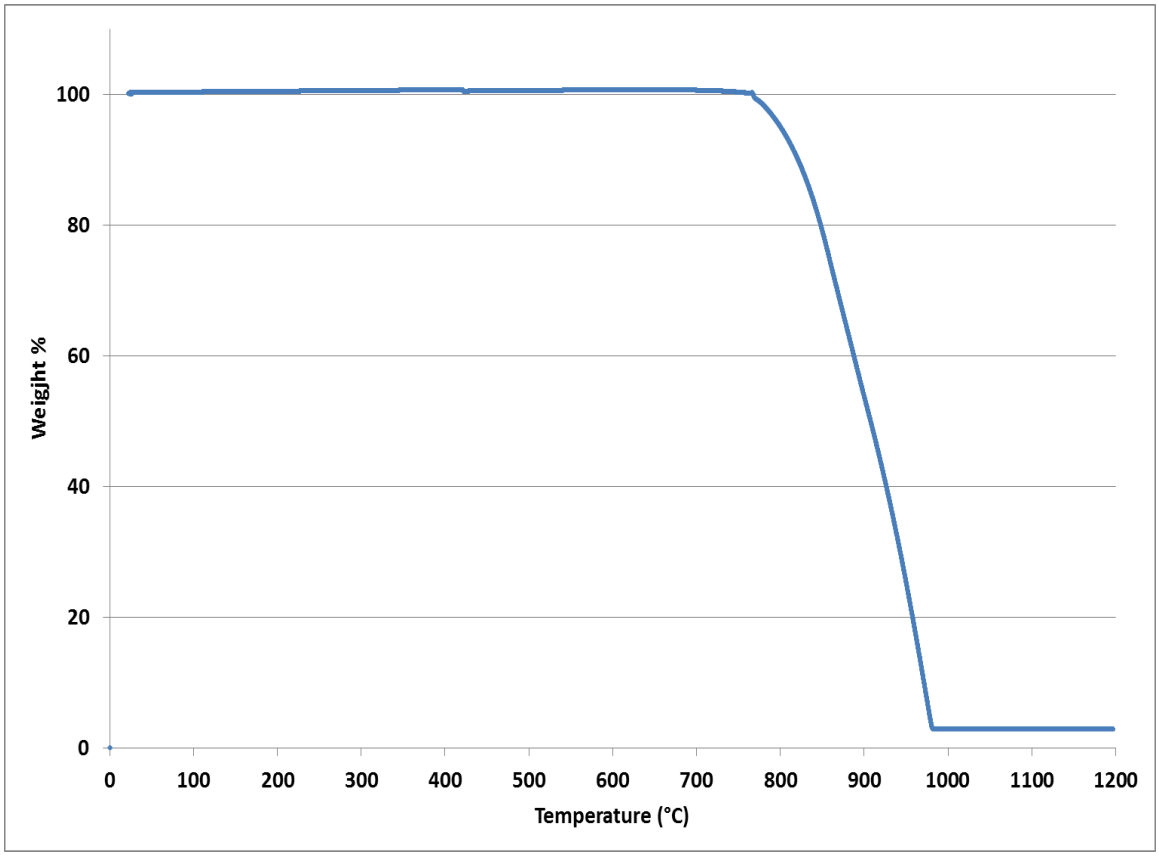

Figure 6.2 TG curve of KCl in CO_2 atmosphere

6.2 Effect of catalyst loadings on the coal-char derived from demineralized coal

6.2.1 TG curves

The TG curves for the K_2CO_3 and KCl loaded demineralized coal char samples are presented in Figures 6.3 and 6.4, respectively.

No significant mass loss was observed below 600°C for all the samples. This result is consistent with the fact that significant carbon gasification for C-CO_2 reactions occur at or near 700°C and above [Walker et al., 1959]. It was also observed that the conversion of the sample with no catalyst loading occurred over a broader temperature range than those with catalyst additions (i.e. conversion of the catalyst loaded samples occur over a narrower temperature range).

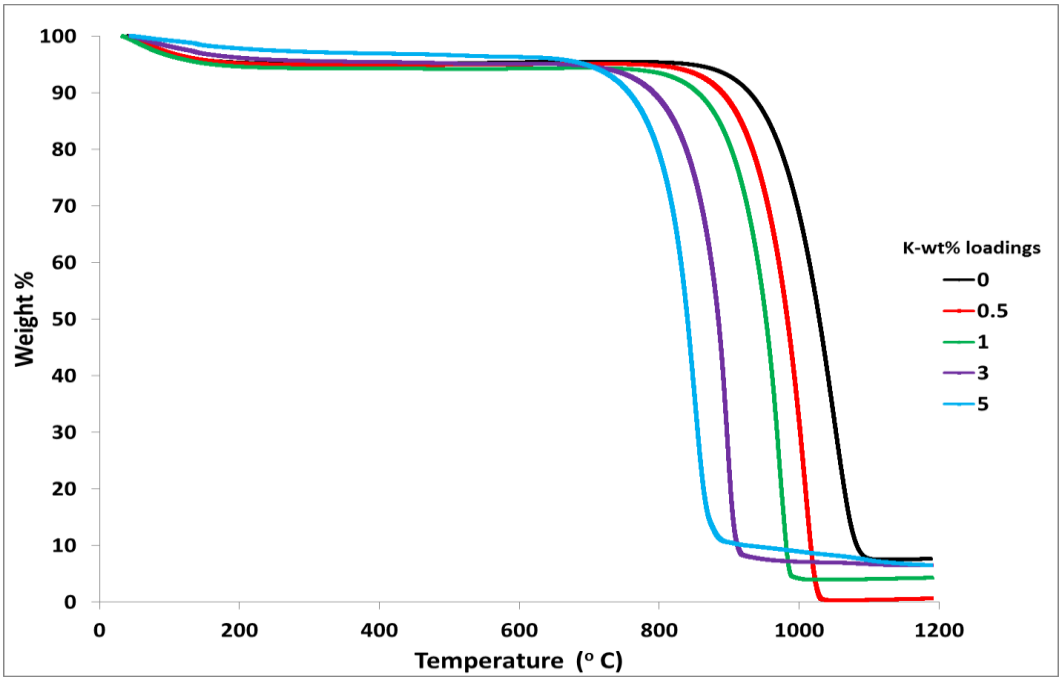

Figure 6.3 TG curves of char derived from demineralized coal (DC) with K_2CO_3 loadings during heat treatment in CO_2 atmosphere.

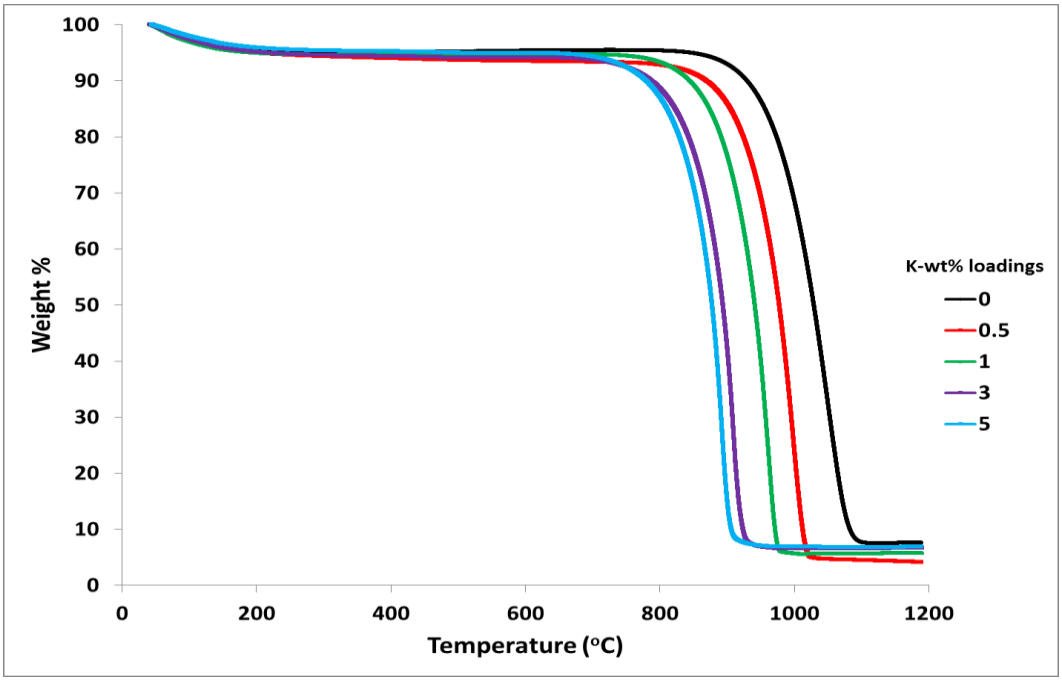

Figure 6.4 TG curves of char derived from demineralized coal with KCl loadings during heat treatment in CO_2 atmosphere.

A variation in the final ash content of the K_2CO_3 samples was observed. This observation may be attributed to some of the char not having reacted with the CO_2 reactant gas. Additionally, catalyst addition influences the reactivity of the char with CO_2 and this may have an influence in the final ash content. It was also observed that the final ash content of the 0.5 K-wt% loaded sample was about zero weight%, and this was noticed for all the repeat samples. No variation in the ash content of the KCl loaded samples (Figure 6.4). Therefore this is rather an interesting observation and may require further investigations in future studies.

Figure 6.4 indicates a similar catalytic behaviour by KCl loadings on the samples, where increasing KCl loadings have an effect on the mass loss of the samples. The mass loss started to occur at lower temperatures with increasing catalyst loadings when compared to the sample with no catalyst loading, suggesting an increase in rate of conversion with increasing catalyst loadings. Similarly, no significant mass loss was observed below 600°C for all the samples and the mass loss of the 'uncatalysed' sample occurred over a broader temperature range, whereas that of the catalyst loaded samples occurred over a relatively narrower temperature range.

6.2.2 DTG curves

The derivatives of the TG (DTG) for the K_2CO_3 and KCl loaded samples are presented in Figures 6.5 and 6.6, respectively.

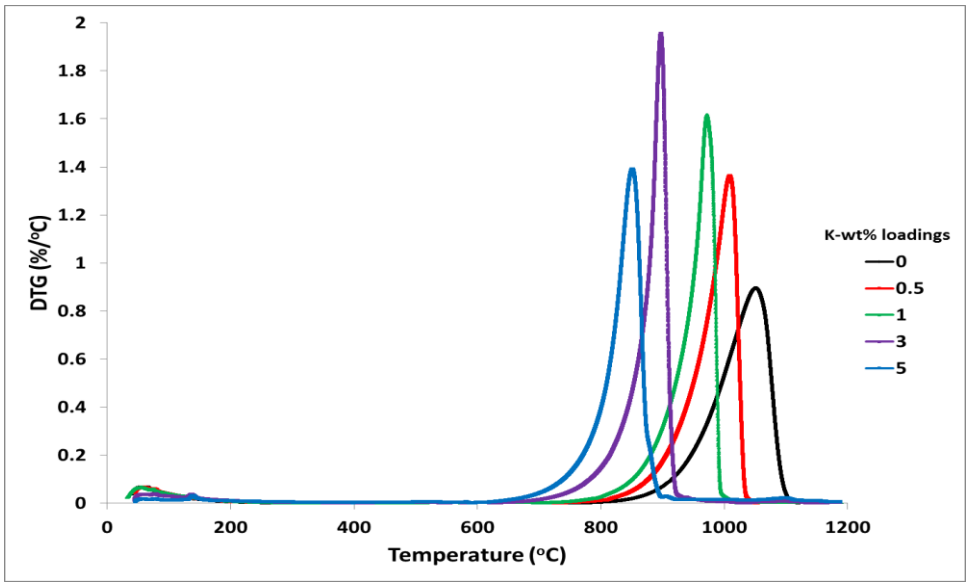

Figure 6.5 DTG curves of char derived from demineralized coal (DC) with K_2CO_3 loadings during heat treatment in CO_2 atmosphere.

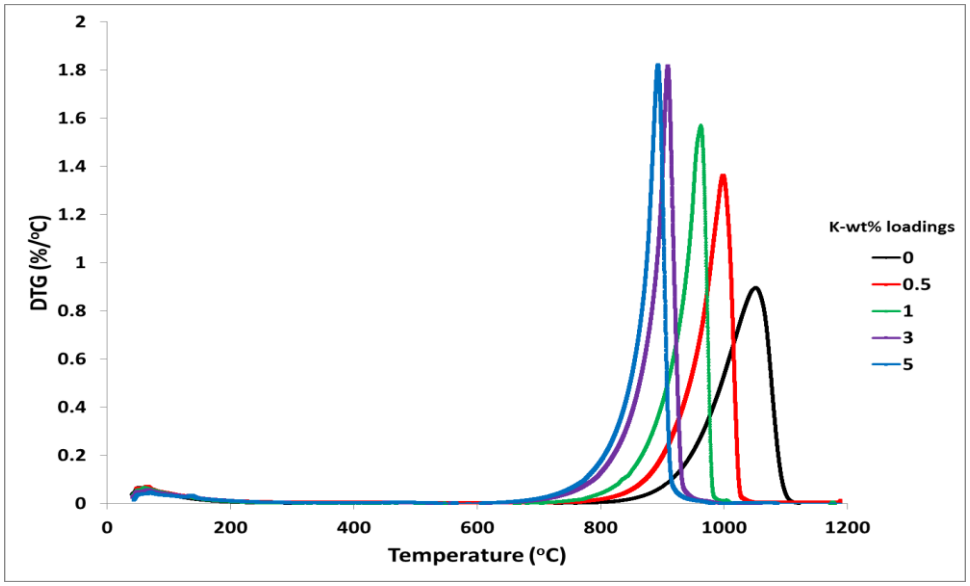

Figure 6.6 TG curves of char derived from demineralized coal (DC) with KCl loadings during heat treatment in CO_2 atmosphere.

The DTG curves enable accurate determination of the 'characteristic' temperatures of interest. These are the temperature at which maximum rate of mass loss (T_{max}) occurred,the temperature at the initial (T_i) mass loss and that at the termination (T_f) of mass loss. Figure 6.7 presents an illustration of how these temperatures were determined. It is important to note that the temperatures were determined by visual inspection from the DTG profiles as shown in Figure 6.7. These temperature values are listed in Table 6.1.

It was observed from the DTG curves that when the catalyst loading was increased, the temperature at maximum rate of mass loss was lower. In turn, the temperatures at the initial mass loss (T_i) and termination of mass loss (T_f) were also lower. These characteristic temperatures are listed in Table 6.1.

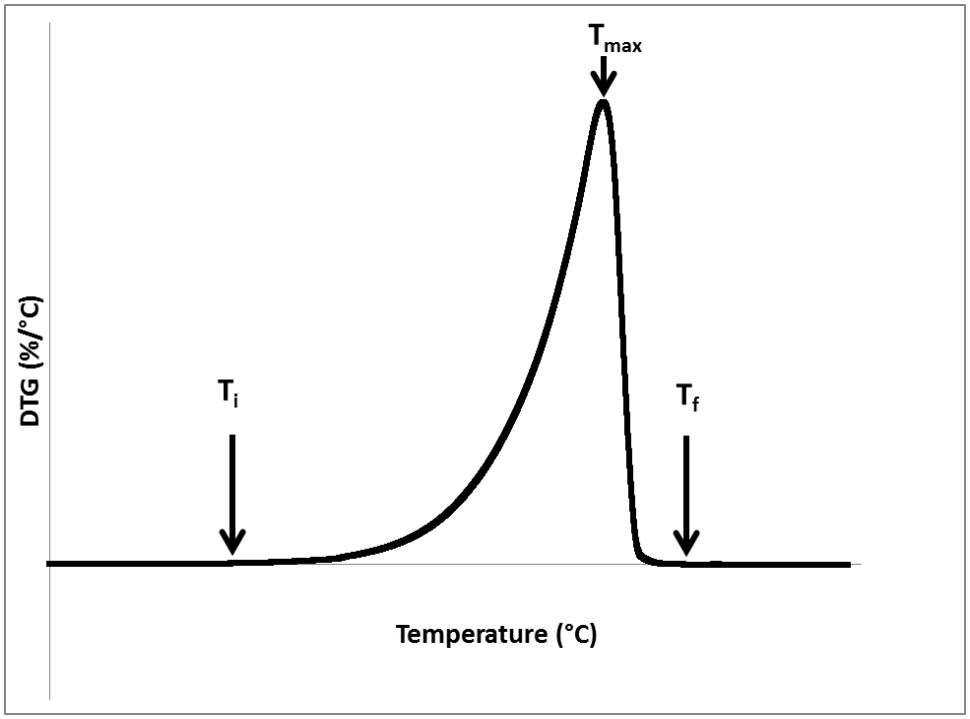

Figure 6.7 Illustration of characteristic temperatures by visual inspection of the DTG

Table 6.1 Characteristic temperatures (T_i, T_f, T_{max}) of the char derived from demineralized coal (°C)

Catalyst	Loading (K-wt%)	T_i	T_f	$\Delta T = (T_f - T_i)$	T_{max}
None added	0	748	1130	382	1047
K_2CO_3	0.5	732	1065	333	1006
	1	715	1030	315	970
	3	682	957	275	896
	5	617	945	328	848
KCl	0.5	744	1061	317	997
	1	721	1022	301	961
	3	668	984	316	908
	5	643	971	328	892

The temperatures at maximum rate of mass loss (T_{max}) were used to give an indication of the relative reactivity of the coal due to the different catalyst loadings used. The temperatures at 50% mass loss ($T_{50\%}$) were also used to give an indication of reactivity as a result of catalyst additions. The mass losses due to the catalysts were first deduced from the total mass loss to obtain the 50% mass loss position on the curve for only the char. An illustration of how the $T_{50\%}$ was determined is presented in Figure 6.8. Determination of $T_{50\%}$ was also by visual inspection and the list of temperatures are given in **Appendix A**.

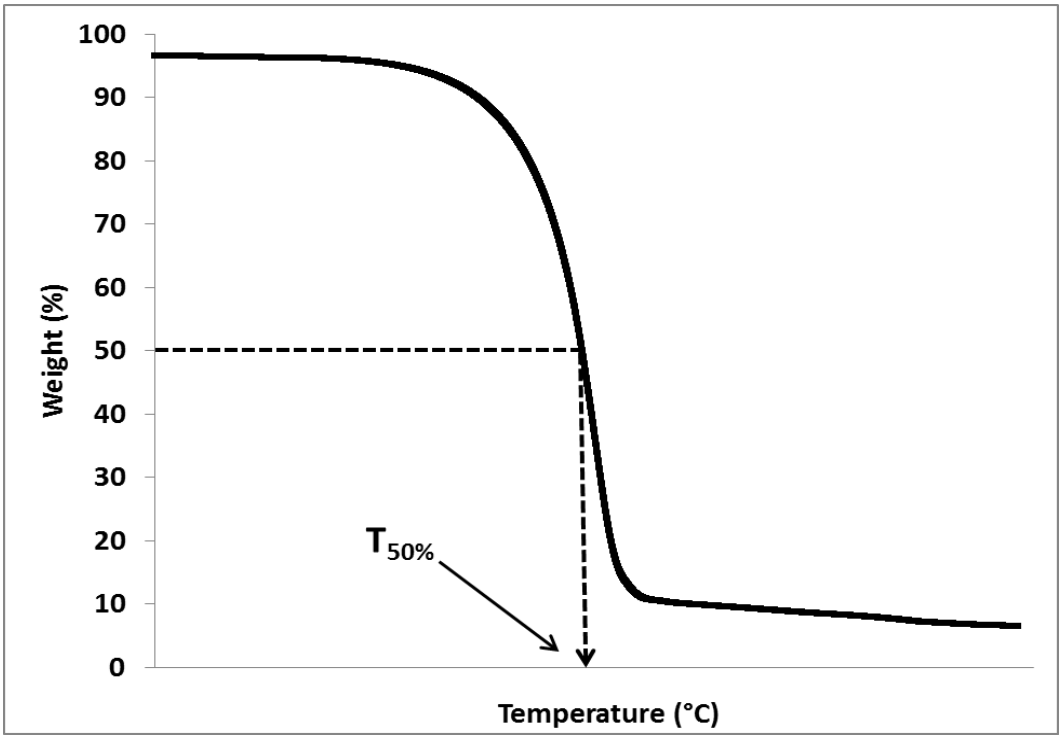

Figure 6.8 Illustration of the temperature at 50% mass loss ($T_{50\%}$) determination (by visual inspection)

The relative reactivity calculated from T_{max} and $T_{50\%}$ for K_2CO_3 and KCl loadings are presented in Figure 6.9 and 6.10, respectively. The relative reactivity was calculated by taking the reciprocal of T_{max} and $T_{50\%}$. Both Figures 9 and 10 show a similar trend in that the reactivity increases with increasing loadings of K_2CO_3 and KCl, indicative of an increase in rate of reaction with increased catalyst loading.

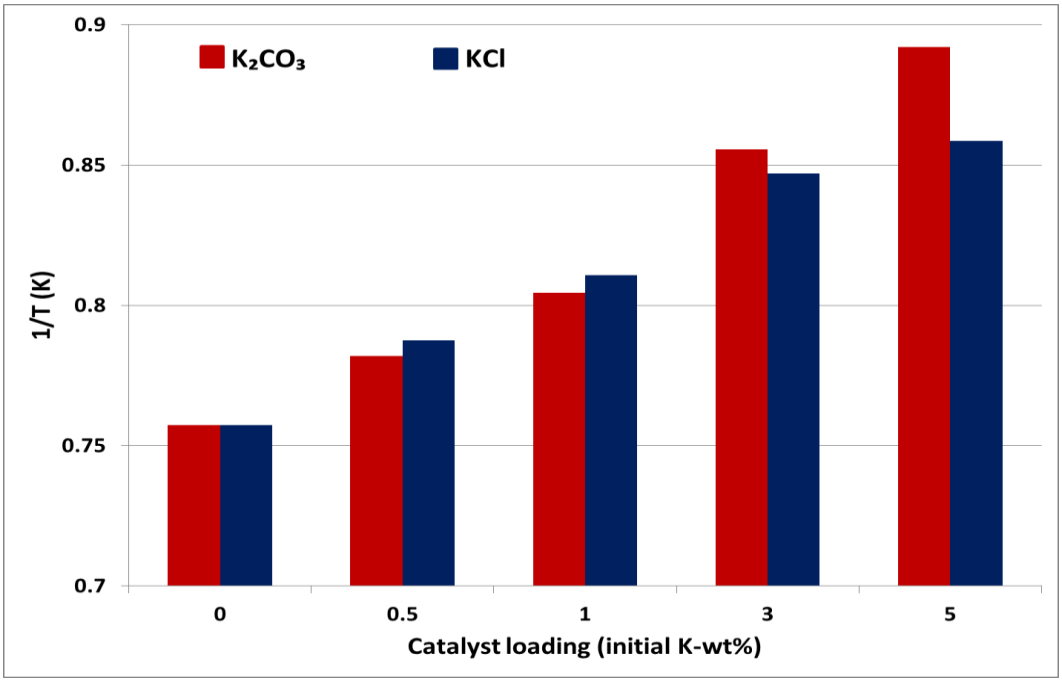

Figure 6.9 Reactivity at T_{max} of the char derived from the demineralized coal (DC) with K_2CO_3 and KCl loadings

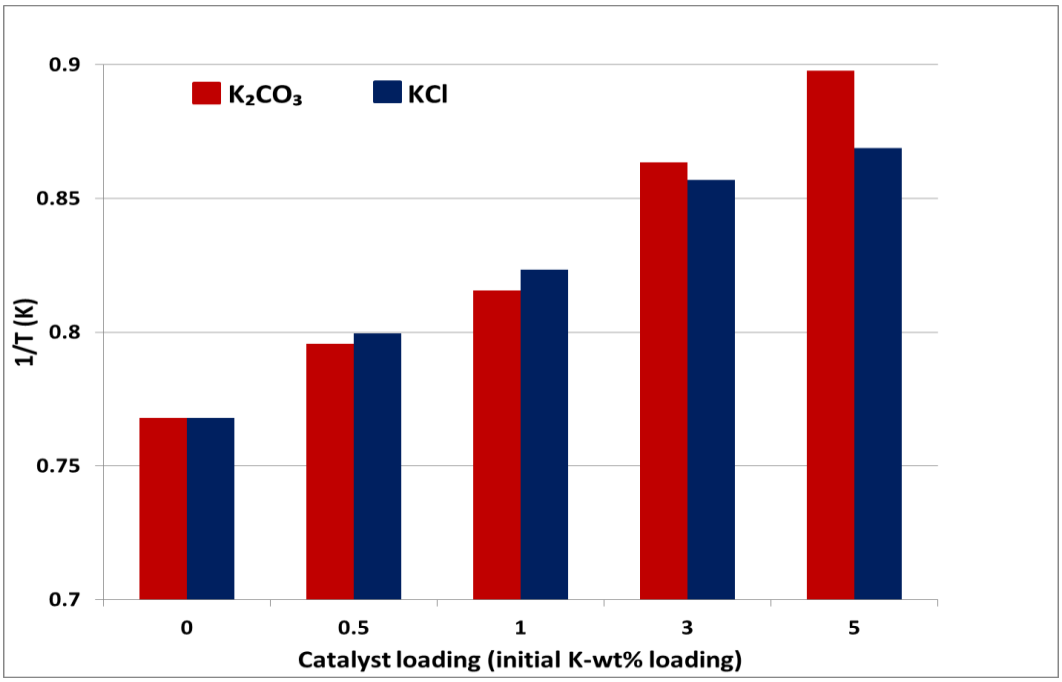

Figure 6.10 Reactivity at $T_{50\%}$ of the char derived from the demineralized coal (DC) with K_2CO_3 and KCl loadings

From the TG results it is clear that K_2CO_3 and KCl exhibit a catalytic effect during heat treatments of char derived from demineralized coal. The temperature ranges at which char conversion occurred for the K_2CO_3 loaded samples were lower than the temperature ranges of KCl loaded samples. This implies that the catalytic effect of K_2CO_3 is greater than that of KCl, and K_2CO_3 is a more effective catalyst than KCl considering the initial amounts added.

6.3 Effect of catalyst loadings on the coal-char derived from raw coal

6.3.1 TG curves

The mass loss of the raw coal char samples due to K_2CO_3 and KCl loadings were determined from the TG curves and are presented in Figures 6.11 and 6.12 respectively. It was observed from the TG curves for K_2CO_3 and KCl loaded coal char samples that catalyst addition has an effect on the mass loss of the samples. The mass loss occurred at lower temperatures with increased catalyst loadings, suggesting that catalyst addition enhances char conversion; when compared to the sample with no catalyst loading. The shift to lower temperatures is evident for both K_2CO_3 (Figure 6.11) and KCl (Figure 6.12) loadings. Therefore this implies that both K_2CO_3 and KCl have a catalytic effect and facilitate char conversion; and that conversion increases with increasing catalyst loadings. No significant mass losses were observed below 700°C for both K_2CO_3 and KCl loaded samples.

Figure 6.11 indicates that increasing loadings of K_2CO_3 caused the mass losses to occur over relatively narrower temperature ranges, which are more evident for the 3 and 5 K-wt% loadings. However, for lower loadings (0.5 and 1 K-wt%), the temperature range at which mass loss occurs does not differ as much from the raw uncatalysed coal char as that of the 3 and 5 K-wt% loadings. The ‘small’ shifts in the temperature observed for lower loadings could be that the initially active K_2CO_3 is deactivated by irreversible reactions in the ash that is present in the raw coal, as stated by [McKee et al., 1975]. According to McKee and co-workers [1975], this could then lead to K_2CO_3 being incapable of catalysing char conversion further as it has reacted with the mineral matter in the raw coal. However, for higher K_2CO_3 loadings, despite the occurrence of K_2CO_3 deactivation, the amount of available mineral matter to react with the potassium compounds is exhausted and the influence of the potassium compounds clear.

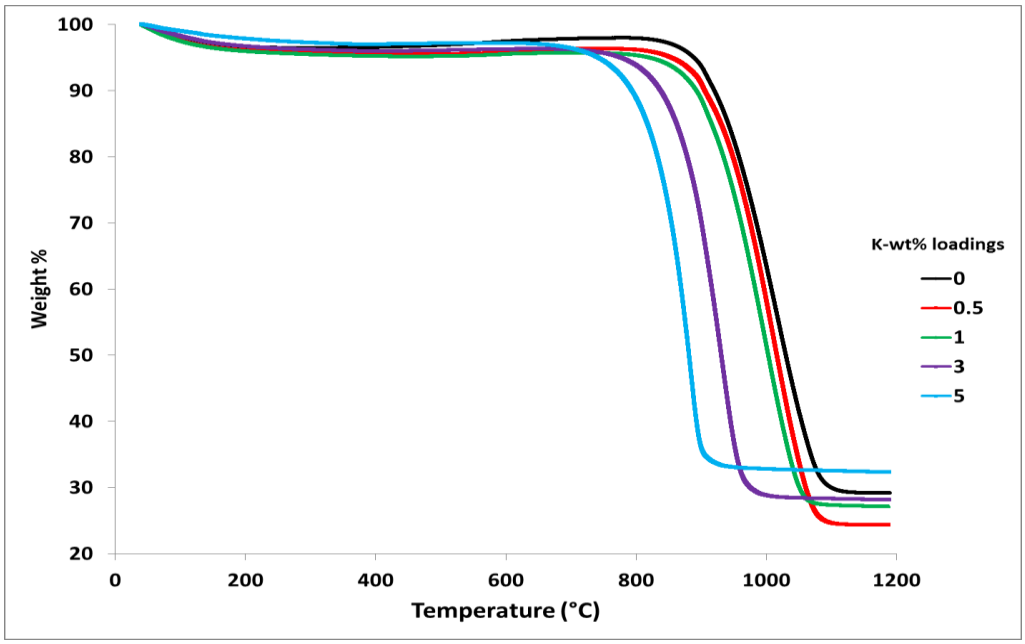

Figure 6.11 TG curves of the char derived from the raw coal (RC) with K_2CO_3 loadings during heat treatment in CO_2 atmosphere.

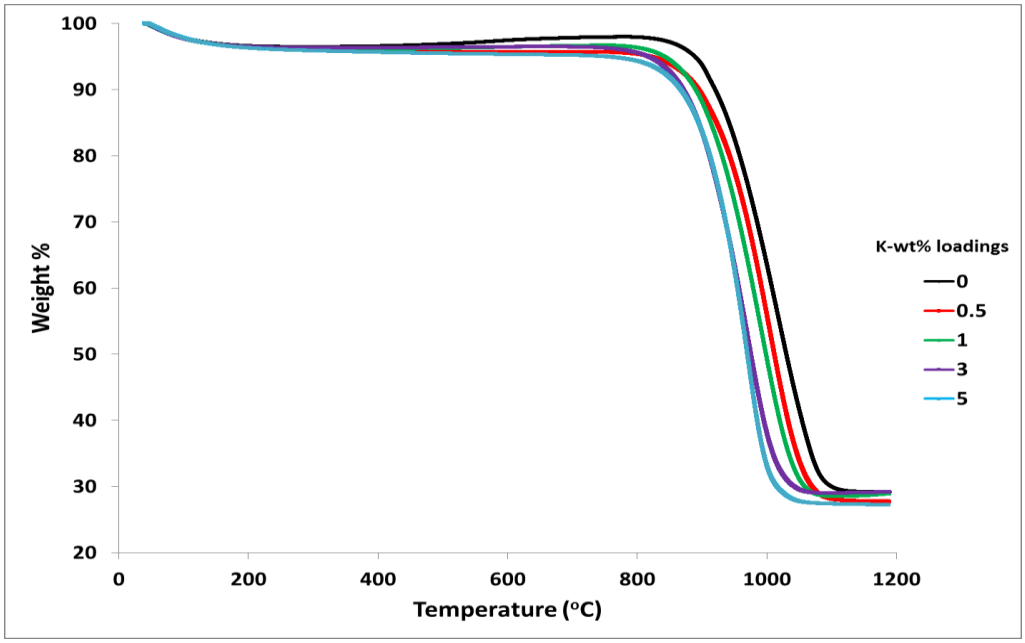

Figure 6.12 TG curves of the char derived from the raw (RC) with KCl loadings during heat treatment in CO_2 atmosphere

Similarly, a variation in the final ash content of the K_2CO_3 samples was observed and this observation may also be attributed to some of the char not having reacted with the CO_2. Additionally, catalyst addition influences the reactivity of the char with CO_2 and this may have an influence in the final ash content. It is also important to note that due to the heterogeneity of the raw coal, there is more ash content in the samples due to the high mineral matter content in coal. This may also play a role in influencing the final ash content after heat treatments. For future work, more replicates may be needed in order to minimize variability. No variation in the ash content of the KCl loaded samples (Figure 6.12) was observed.

Figure 6.12 indicates that the KCl loadings had an effect on the mass loss of the samples although the shifts in the temperatures ranges were not as pronounced as for the K_2CO_3 loadings (Figure 6.11).

A study done by Huttinger and Minges [1986] indicated KCl not to be as good a catalyst as K_2CO_3 during char gasification. With the raw coal containing a substantial amount of mineral matter that is known to have interactions with the catalyst causing catalyst deactivation, it could therefore be suggested that these smaller shifts observed in char conversion temperatures is due to the mineral matter deactivating the catalyst that is already not known to be a 'good' catalyst. The mass loss curve of the 3 and 5 K-wt% loadings were observed to be nearly the same.

6.3.2 DTG curves

The derivatives of the TG or mass loss profiles (DTG) for both K_2CO_3 and KCl loaded samples are presented in Figures 6.13 and 6.14.

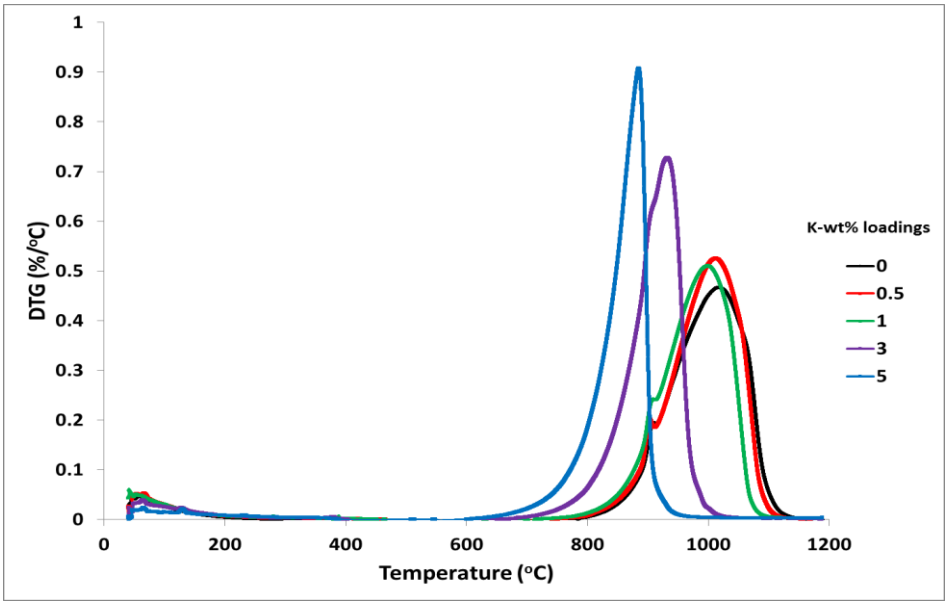

Figure 6.13 DTG curves of the char derived from the raw coal (RC) with K_2CO_3 loadings during heat treatment in CO_2 atmosphere.

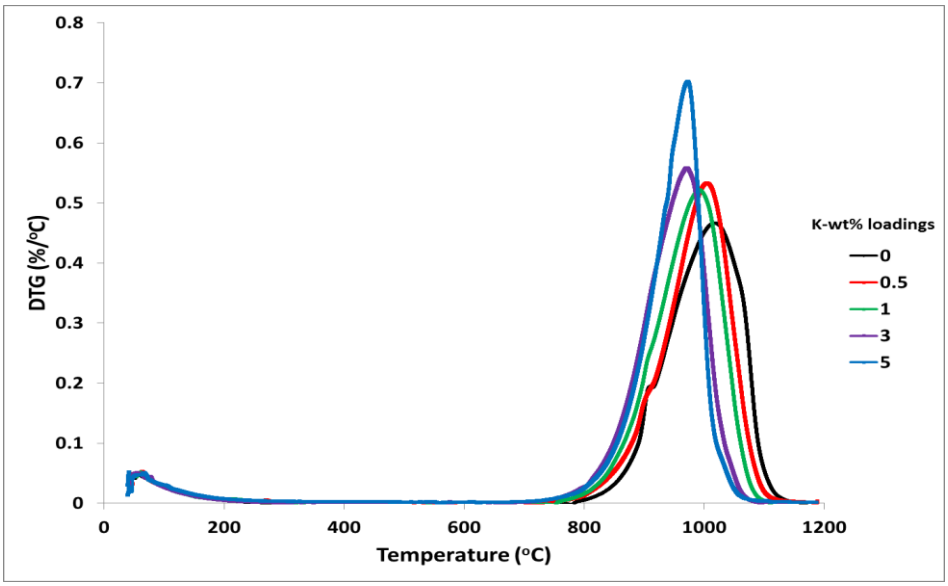

Figure 6.14 DTG curves of the char derived from the raw coal (RC) with KCl loadings during heat treatment in CO_2 atmosphere.

The temperature at which maximum rate of mass loss (T_{max}) took place, as well as the temperature at the initial mass loss(T_i) and at the termination (T_f) of mass loss were determined by visual inspection from the DTG curves as illustrated in Figure 6.7.

Table 6.2 Characteristic temperatures (T_i, T_f, T_{max}) of the char derived from raw coal (°C)

Catalyst	K-wt%	T_i	T_f	$\Delta T = (T_f - T_f)$	T_{max}
None added	0	749	1168	419	1011
K_2CO_3	0.5	738	1155	417	1008
	1	730	1120	390	994
	3	651	1038	387	927
	5	625	961	336	882
KCl	0.5	736	1136	400	1002
	1	736	1123	387	988
	3	729	1108	379	969
	5	708	1092	384	969

The characteristic temperatures (T_i, T_f and T_{max}) were determined by visual inspection and the values are presented in Table 6.2. It was observed that as the catalyst loading is increased, the temperatures at maximum rate of mass loss, as well as the temperatures at the initial (T_i) mass loss and termination (T_f) of mass loss are lower.

Similarly, the temperatures at T_{max} and $T_{50\%}$ were used to give an indication of the relative reactivity of the coal char due to catalyst loadings. An illustration of how $T_{50\%}$ was determined by visual inspection is presented in Figure 6.8. The relative reactivity was calculated by taking the reciprocal of T_{max} and $T_{50\%}$. The reactivity from T_{max} and $T_{50\%}$ for the K_2CO_3 and KCl loadings are presented in Figure 6.15 and 6.16, respectively. The $T_{50\%}$ values are listed in **Appendix A**.

A similar trend in reactivity was observed for both T_{max} and $T_{50\%}$, indicating that reactivity increases with increasing loadings of K_2CO_3 and KCl; which is indicative of an increase in rate of reaction with increasing catalyst loading.

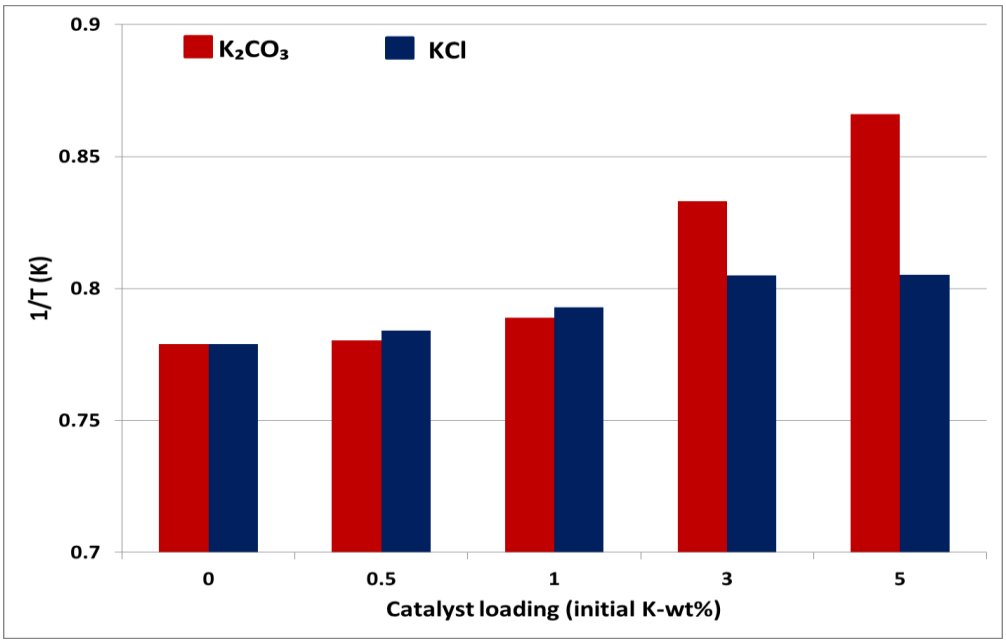

Figure 6.15 Reactivity at T_{max} of the char derived from the raw coal (RC) with K_2CO_3 and KCl loadings.

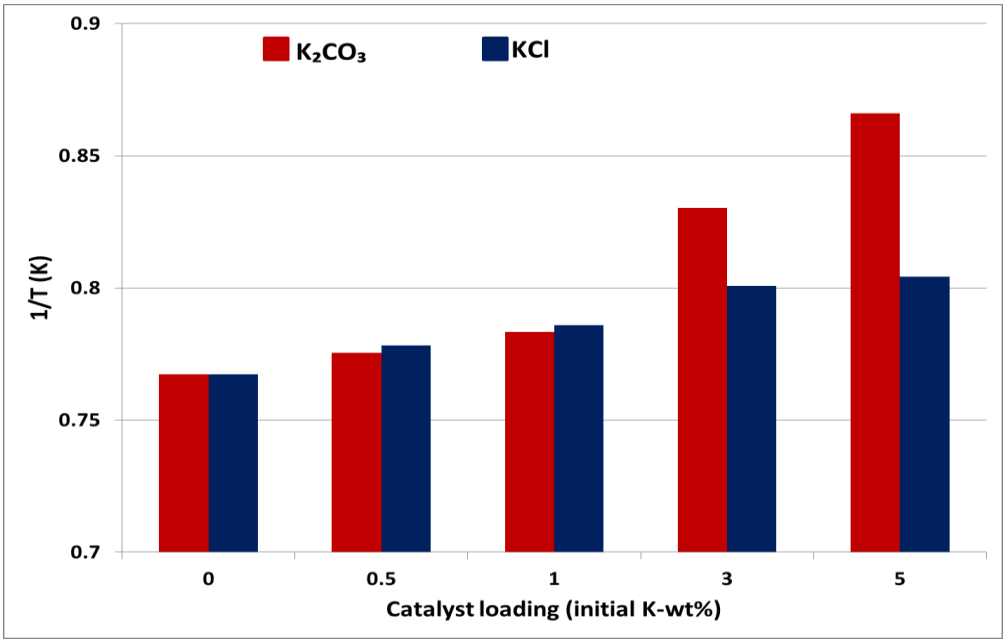

Figure 6.16 Reactivity at $T_{50\%}$ of the char derived from the raw coal (RC) with K_2CO_3 and KCl loadings.

The TG results clearly indicate that K_2CO_3 and KCl have a catalytic effect on char conversion during heat treatments in a CO_2 atmosphere. Char conversion increased with increased catalyst loadings for both K_2CO_3 and KCl. The temperature ranges at which char conversion occurred were lower for the K_2CO_3 loaded samples than for the KCl loaded samples. K_2CO_3 has been shown to be a more effective catalyst than KCl.

6.4 Effect of catalyst loadings on the coal-char derived from demineralized coal with added mineral mixture

6.4.1 TG curves

The mass losses of the demineralized coal with added mineral mixture samples due to K_2CO_3 and KCl loadings were determined from the TG curves and are presented in Figures 6.17 and 6.18, respectively.

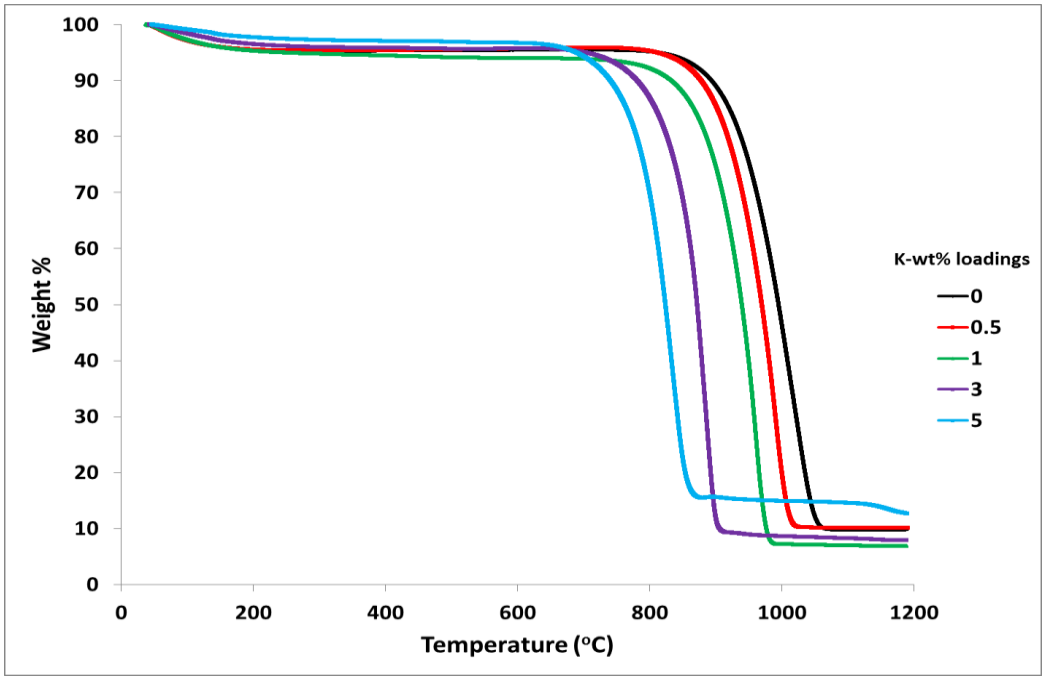

Figure 6.17 DTG curves of the char derived from the demineralized coal with added mineral mixture (DC+MM) with K_2CO_3 loadings during heat treatment in CO_2 atmosphere

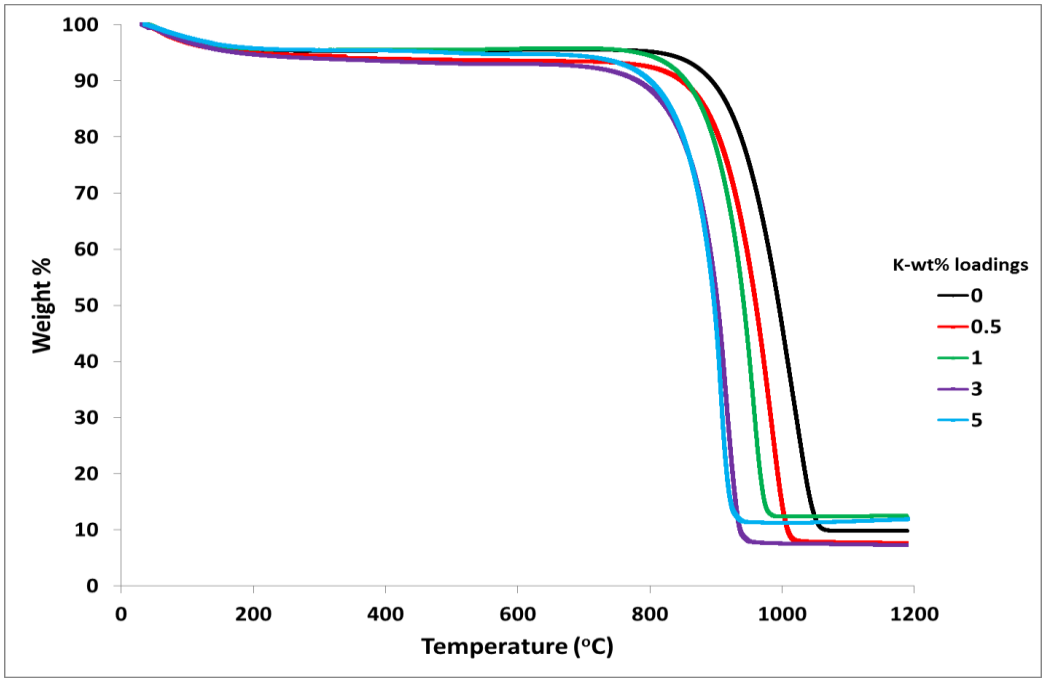

Figure 6.18 TG curves of the char derived from the demineralized coal with added mineral mixture (DC+MM) with KCl loadings during heat treatment in CO_2 atmosphere

It was observed from the TG curves that K_2CO_3 and KCl have a catalytic effect on the mass losses of the samples. The mass losses occurred at lower temperatures with increasing catalyst loadings, suggesting that catalyst addition enhances char conversion. The effect of the catalyst loadings is evident when compared to the sample with no catalyst loading. The shift to lower temperatures is evident for both K_2CO_3 (Figure 6.17) and KCl (Figure 6.18) loadings, and observed shifts in the temperature ranges during conversion indicate that the rate of char conversion is faster, hence the shift with increasing catalyst loadings. No significant mass losses were observed below 700°C for K_2CO_3, and below 800°C for KCl loaded samples.

Increasing loadings of K_2CO_3 caused the mass loss to occur over a relatively narrower temperature range for all the loadings. However for KCl loaded samples, overlapping of the mass loss curves for the 3 and 5 K-wt% loaded samples was observed. The insignificant change in the temperature ranges during which conversion takes place for the 3 and 5 K-wt% loadings could be due to catalyst accumulation and saturation of the surface with catalytic sites as a result of increased catalyst loadings, thus resulting in a maximum catalytic effect [Sams and Shadman, 1983]. According to Sams and Shadman [1983], this is caused by the large

amounts of catalyst on the surface consequently restricting CO_2 adsorption onto the surface of the micropores.

As observed previously, some variation in the final ash content of the K_2CO_3 and KCl samples was observed. This may be attributed to some of the char not having reacted with the CO_2. The ash content in the samples due to the model mineral mixture added to the coal may also influence the final ash content after heat treatments of the char. More replicates may be needed in order to minimize variability in future studies.

6.4.1 DTG curves

The derivatives of the TG or mass loss profiles (DTG) for both K_2CO_3 and KCl loaded samples are presented in Figures 6.19 and 6.20, respectively.

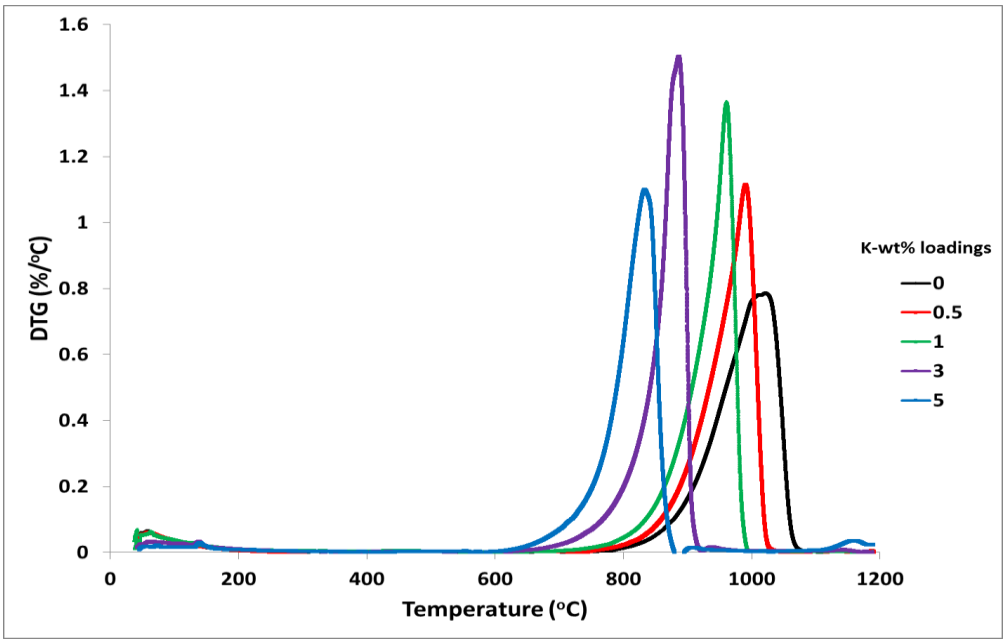

Figure 6.19 DTG curves of the char derived from the demineralized coal with added mineral mixture (DC+MM) with K_2CO_3 loadings during heat treatment in CO_2 atmosphere

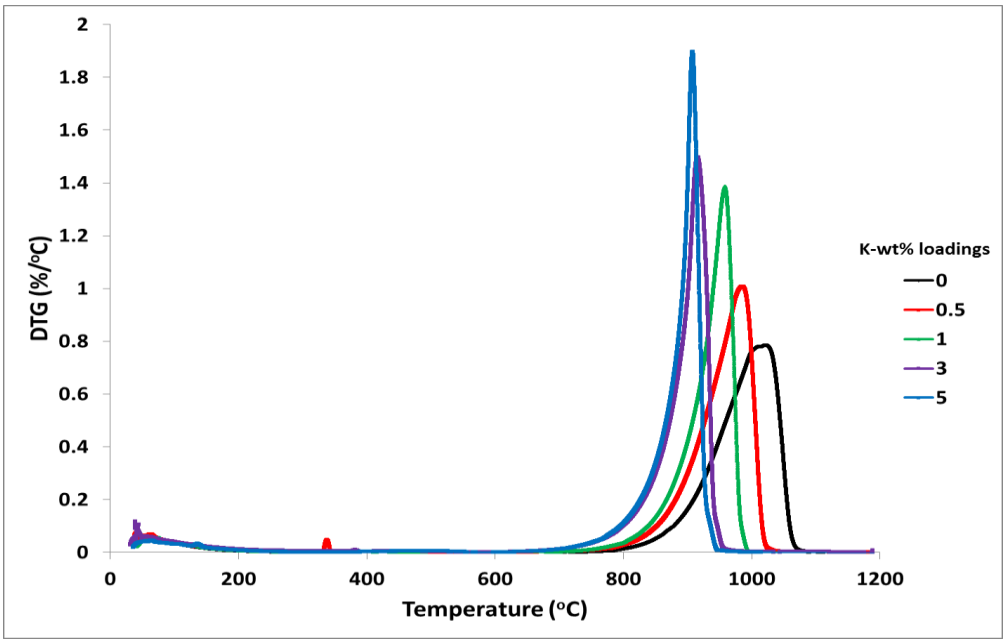

Figure 6.20 DTG curves of the char derived from the demineralized coal with added mineral mixture (DC+MM) with KCl loadings during heat treatment in CO_2 atmosphere.

The temperature at which maximum rate of mass loss (T_{max}) occurred; as well as the temperature at the initial mass loss (T_i) and termination (T_f) of mass loss were determined by visual inspection from the DTG curves as illustrated in Figure 6.7. The ΔT ($T_f - T_i$) and T_{max} values are listed in Table 6.3.

Table 6.3 Characteristic temperatures (T_i, T_f, T_{max}) of the char derived from demineralized coal with added mineral mixture (°C)

Catalyst	K-wt%	T_i	T_f	$\Delta T = (T_f - T_f)$	T_{max}
None added	0	770	1095	325	1011
K_2CO_3	0.5	727	1045	318	988
	1	725	1010	285	959
	3	673	936	263	884
	5	602	905	303	830
KCl	0.5	721	1055	334	981
	1	710	1004	294	957
	3	663	974	311	914
	5	646	955	309	907

It was observed that as the catalyst loading was increased, T_{max} for the K_2CO_3 and KCl loaded samples, as well as (T_i) and (T_f) were lowerThe relative reactivity of the samples with the K_2CO_3 and KCl catalyst loadings determined from T_{max} and $T_{50\%}$ are presented in Figure 6.21 and 6.22, respectively. An increase in reactivity with increasing loadings was observed for both catalysts.

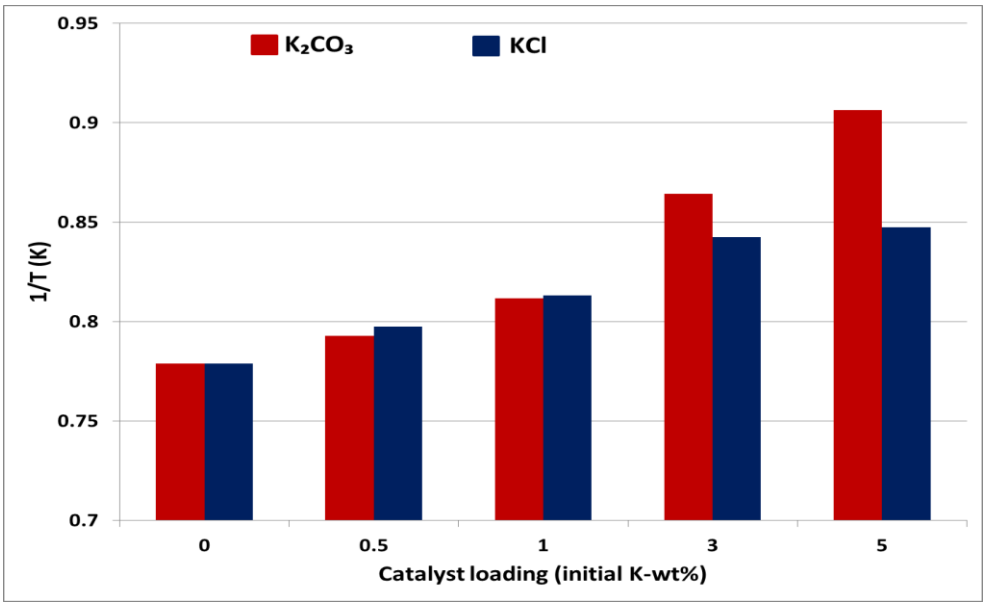

Figure 6.21 Relative reactivity at T_{max} of the char derived from the demineralized coal with added mineral mixture (DC+MM) with K_2CO_3 and KCl loadings.

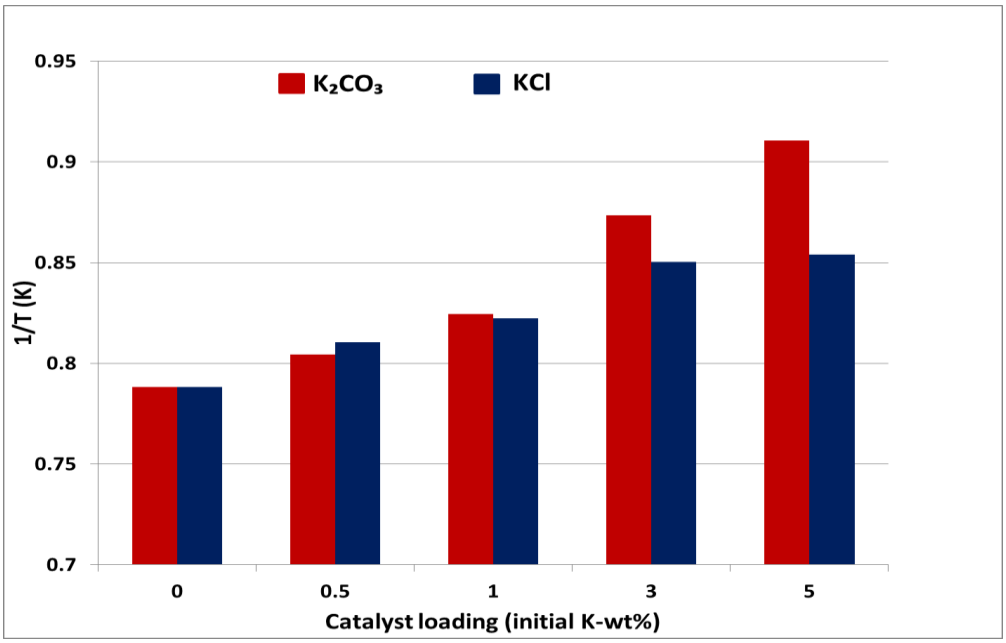

Figure 6.22 Relative reactivity at $T_{50\%}$ of the char derived from the demineralized coal with added mineral mixture (DC+MM) with K_2CO_3 and KCl loadings

The TG results of the char derived from the demineralized coal with added mineral mixture clearly indicate that K_2CO_3 is a more effective catalyst than KCl. Although both catalysts have a catalytic effect on char conversion, KCl seems to be more susceptible to mineral matter additions than K_2CO_3.

6.5 Comparisons of similar samples with/without K_2CO_3 and KCl loadings

The mass losses of the different samples with and without catalyst loadings were compared in order to determine the catalyst that had the better catalytic effect on the carbon conversion of the different samples. Only samples with the maximum (***5 K-wt%***) catalyst loadings were compared. The TG results are presented below.

6.5.1 Comparison of each char sample separately

Comparisons of the influence of K_2CO_3 and KCl on the mass loss curves of the demineralized coal, raw coal and demineralized coal with added mineral mixture samples are presented in Figure 6.23, 6.24 and 6.25, respectively.

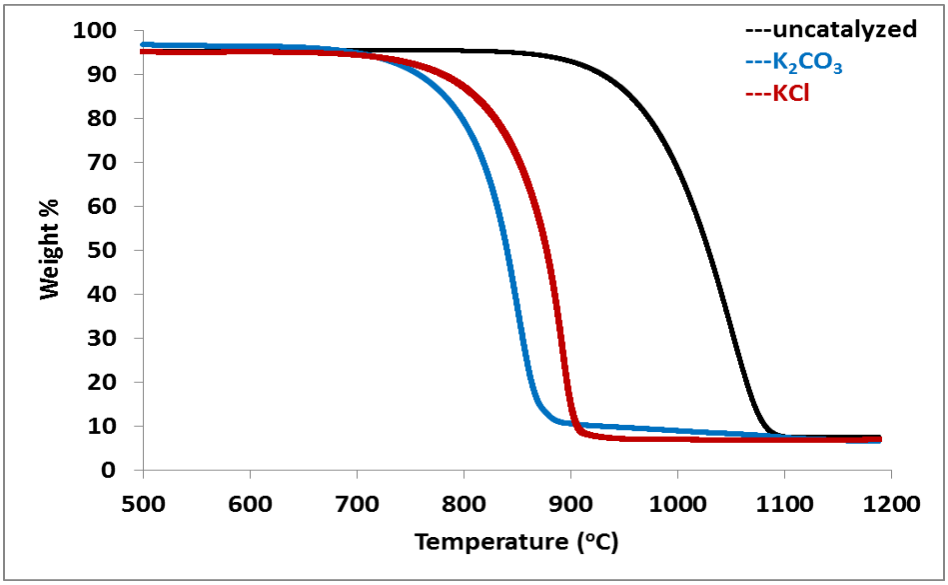

Figure 6.23 TG curves of the char derived from the demineralized coal with 5 K-wt% catalyst loading

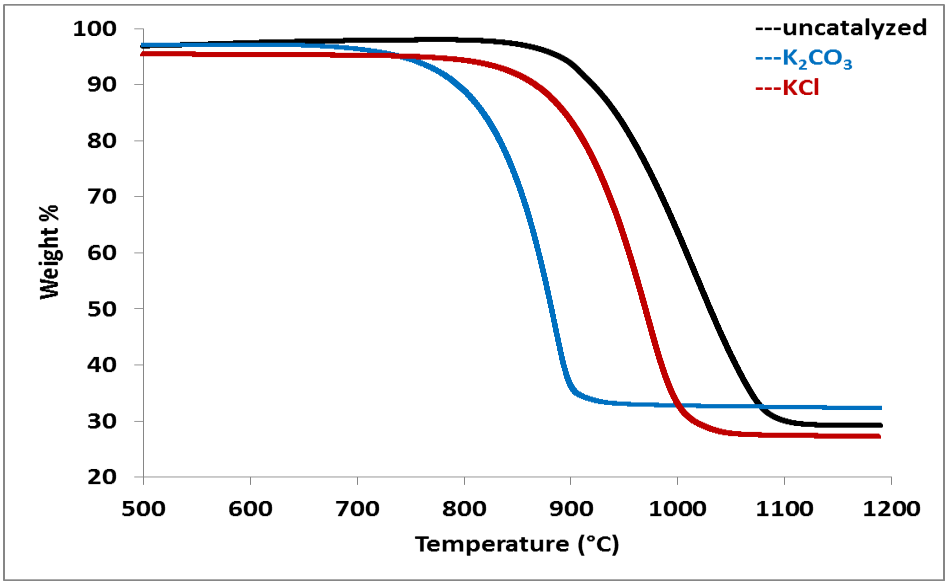

Figure 6.24 TG curves of the char derived from the raw coal with 5 K-wt% catalyst loading.

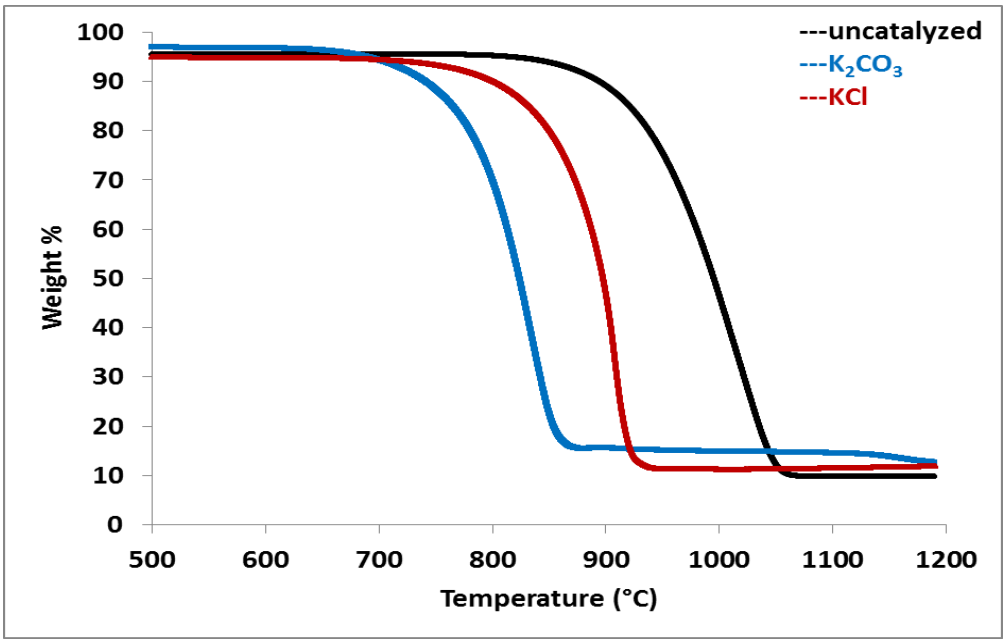

Figure 6.25 TG curves of the char derived from the demineralized coal with added mineral mixture with 5 K-wt% catalyst loading

It was observed that K_2CO_3 showed a more favourable catalytic effect on the samples compared to KCl. Mass losses of K_2CO_3 loaded samples occurred at much lower temperatures than that of the samples with KCl additions. This indicates that K_2CO_3 facilitates carbon conversion more effectively than KCl does. This behaviour is seen for all the different samples (i.e. demineralized coal, raw coal and demineralized coal with added mineral mixture). The presence of potassium salts has been reported to result in increased oxygen content in coal during heat treatments and subsequently enhancing reactivity. Furthermore, the reactivity of the resulting char is also enhanced because of the catalytic effect of the retained potassium [Marsh and Walker, 1979].

The low catalytic effect observed for KCl when compared to K_2CO_3 during heat treatments is in agreement with that reported by Takarada et al. [1992]. The associated precursor anion of the catalyst has been reported to play an important role as to how effective the catalyst would be during heating [Lang, 1986; Huttinger and Minges, 1986]. According to Takarada and co-workers, the catalytic effect of alkali metal chlorides is generally lower in comparison to that of carbonates, and the lower catalytic activity is attributed to the strong affinity between alkali metal ions and chloride ions. The alkali metal chloride catalysts have been reported to act as inhibitors during the early stages of gasification, but to improve the rate

during the later stages. Because of their accelerating effect during the gasification of the last 20-25% of the fixed carbon, the alkali metal chlorides cause a net reduction in the total time (or temperature) for complete gasification over that required for an 'uncatalysed' sample [Veraa and Bell, 1978].

6.5.2 Comparisons of char samples derived from a different coal sample

The influence of K_2CO_3 on the mass loss of the demineralized coal, raw coal and demineralized coal with added mineral mixture samples was compared, and the results are presented in Figure 6.26.

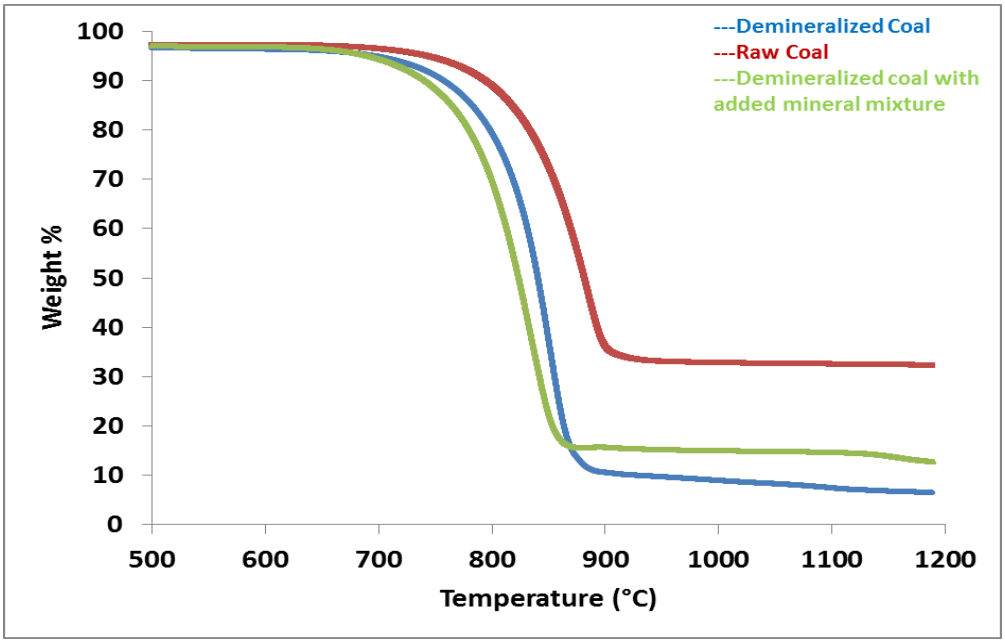

Figure 6.26 TG curves of the char derived from the 5 K-wt% K_2CO_3 loaded samples of the demineralized coal, raw coal and demineralized coal with added mineral mixture

Figure 6.26 indicates that the K_2CO_3 catalysed mass loss of the demineralized coal with added mineral mixture takes place at lower temperatures than that observed for the demineralized and raw coal. This suggests that carbon conversion occurs faster for the demineralized coal with added mineral mixture, followed by demineralized coal then the raw

coal. This could suggest that the mineral mixture may exhibit a catalytic effect and therefore there is a synergistic catalytic effect by the mineral mixture as well as the K_2CO_3, resulting in a more enhanced conversion of the char derived from the demineralized coal with added mineral mixture.

Similarly, the effect of KCl on the mass losses of the different coal samples was examined and the results are presented in Figure 6.27. However, Figure 6.27 indicates that the mass loss of the char derived from demineralized coal with a KCl loading occurred at lower temperatures than that of the raw coal and of the demineralized coal with added mineral mixture; suggesting that carbon conversion occurs faster for the demineralized coal char followed by demineralized coal char with added mineral mixture and then the raw coal char. This could be attributed to the deactivation of the catalyst by some compounds in the mineral matter, suggesting that the KCl is more prone to deactivation by the mineral matter than K_2CO_3 is.

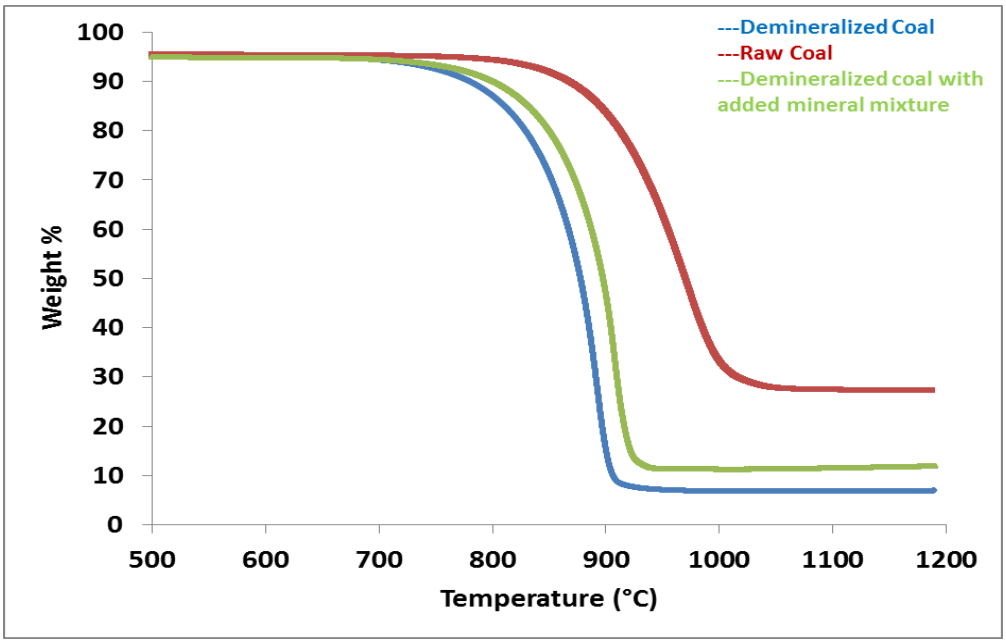

Figure 6.27 TG curves of the char derived from the 5 K-wt% KCl loaded samples of the demineralized coal, raw coal and demineralized coal with added mineral mixture

Thermogravimetric mass loss curves were used to successfully evaluate the influence of various loadings of K_2CO_3 and KCl on the char derived from the demineralized coal, raw coal and demineralized coal with added mineral mixture samples. These results will further be discussed in comparison to the gas analyses performed and are presented in the next chapter (**Chapter 7**).

CHAPTER 7

Results and Discussion

Mass Spectroscopy (MS) of evolved gaseous species from coal-char

This chapter presents the results of the mass spectrometry performed on the gaseous decomposition products from the 'undoped' and 'doped' samples of the coal char derived from demineralized coal, raw untreated coal, and the demineralized coal with added mineral mixture. The effect of the added mineral compounds on the gas evolution is also presented and discussed in this chapter, as well as the correlation between the MS and TG results.

7.1 TG-MS application

Thermogravimetric analysis coupled with mass spectroscopy (TG-MS) has previously been used to simultaneously record the temperature during mass loss or decomposition of the coal and the mass spectra of the evolved gaseous species [Otero et al., 2011; Li et al., 2003; Annamalai et al., 2003]. Some studies have been conducted concerning thermal analysis of volatile products from biomass [Huang et al., 2011; Barneto et al., 2009; Otero et al., 2002, Meszaros et al., 2007; Szabo et al., 1996; Varhegyi et al., 1988].

The TG-MS technique provides information on the thermal behaviour and product distribution of the gaseous species evolved from the sample of interest (i.e. char). The MS equipment records the mass-to-charge ratio (*m/z*), which corresponds to the volatile products evolved and detected, for example, a mass-to-charge ratio of 2 and 28 accounts for H_2 and CO, respectively, as the most probable molecules. One advantage of the TG-MS is that it allows real-time detection of evolved gases during thermal treatments.

7.2 Evolution of gaseous species during char heat treatments in a CO_2 atmosphere

The gas analysis of the coal char samples with and without mineral and inorganic loadings was performed during heat treatments in CO_2 atmospheres and the evolution profiles of the gaseous species investigated. The char samples were derived from the demineralized

coal, raw coal and demineralized coal with added mineral mixture, with and without loadings of K_2CO_3 and KCl. The mass spectroscopic results are presented in the sections below. It is important to note that only qualitative analysis studies of the evolution of some of the gaseous species (i.e. H_2, CO and C) was performed during the heat treatment in CO_2 for the samples with and without K_2CO_3 and KCl loadings.

7.3 Overview

7.3.1 Char formation

Figure 7.1 presents the model structure of coal-char after the devolatilization stage of coal. Coal char is primarily made up of aromatic clusters. However, structural studies of coal-char done by Fletcher [1992] have revealed that at the end of pyrolysis, the remaining char may still contain aliphatic carbons, which represent the presence of stable aliphatic bridge material and/or side chains that were not expelled during pyrolysis. As a result, the decomposition of coal-char during heat treatments results in these side chains being broken and released as various gaseous species, making up the composition of the gas product during further heat treatments of the char.

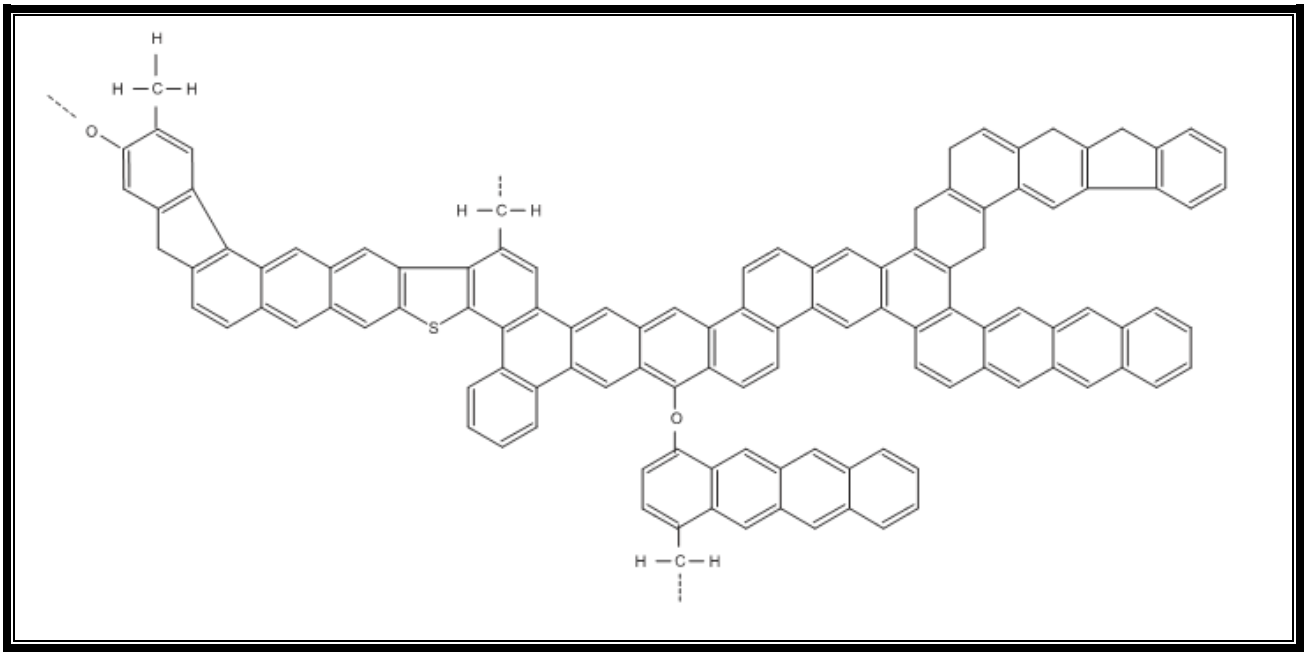

Figure 7.1 Model structure of coal char after pyrolysis [Veras et al., 2002]

7.3.2 Typical reaction mechanism of C-CO_2

The main focus of this study was to identify the composition of the gaseous product during coal-char heat treatments in a CO_2 atmosphere, up to temperatures of 1200°C. Presented in Figure 7.2 is an illustration of the proposed CO_2 chemisorption on a char and/or carbon surface during char/carbon gasification in a CO_2 atmosphere.

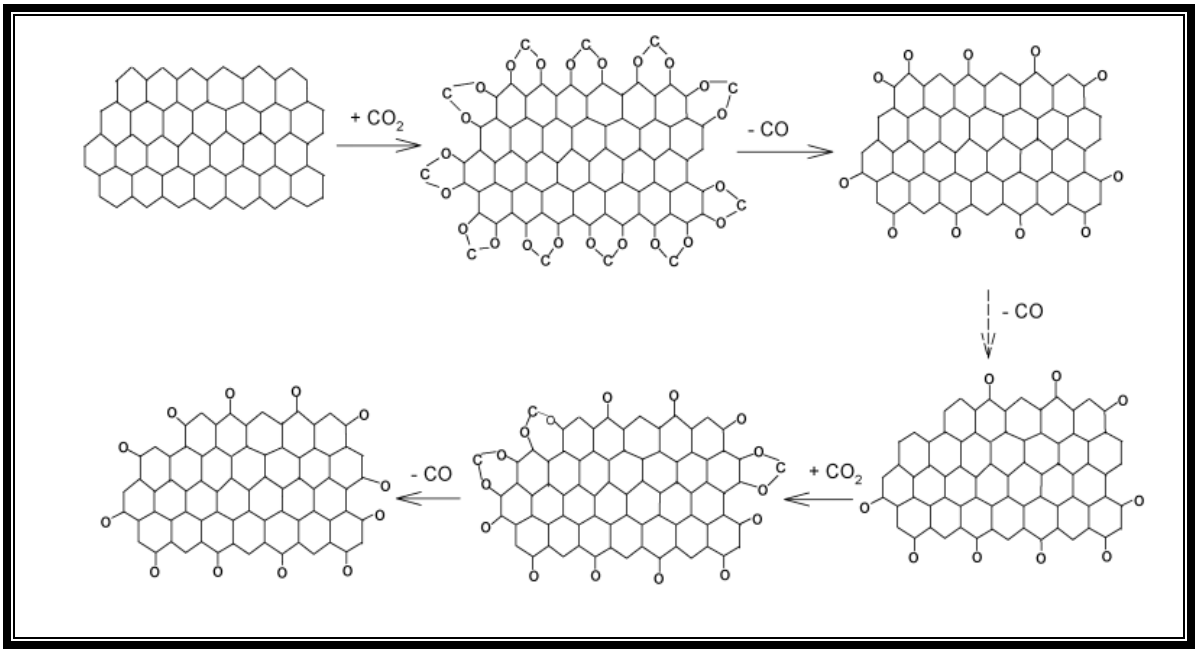

Figure 7.2 Illustration of CO_2 chemisorption during C-CO_2 reaction [Radovic, 2005]

CO_2 has been reported to be highly dissociative and to produce gas phase CO (carbonyl) and C-O (semiquinone) surface complexes [Moulijn and Kapteijn, 1995]. Chemisorption of the CO_2 gas molecule onto the char/carbon is reported to be the initial stage during coal gasification [Montoya et al., 2002; Radovic, 2009, Zhu et al., 2002].

The effect of the potassium (K) catalysts during heat treatment has been reported to be due to the ability of the potassium to spread over the char surface; combining with the char surface as surface complexes, C-O-K and C-K. Such mobility of the potassium catalyst may lead to rate enhancement of the coal char [Takarada et al., 1992].

7.4 H_2 evolution profiles

The hydrogen (H_2) evolution profiles of the coal char samples derived from demineralized coal, raw coal and demineralized coal with added mineral mixture, with and without catalyst loadings, are presented in Figures 7.4, 7.5 and 7.6, respectively. The H_2 evolution during the heat treatment of the char in CO_2 atmosphere for the samples with and without K_2CO_3 and KCl loadings was determined qualitatively. The H_2 identification was based on the key fragment H_2, corresponding to the mass number (m/z) of 2.

Hydrogen evolution during heat treatments of char may be associated with the different functional groups present on the surface of the carbon matrix in the char as shown in Figure 7.1. The production and release of H_2 during char heat treatment are due to H_2 reactions taking place at these temperatures during carbon conversion; resulting in hydrogen formation and hence its release. Possible sources of H_2 evolution observed could be due to the decomposition of functional groups.

The H_2 observed in the gas phase could also be attributed to the abstraction and removal of the hydrogen by the molecular gas phase from the carbons situated on the edges, as a means of creating carbon active sites as reported by Kyotani and Tomita [1999]. As a result, chemi-adsorption of the CO_2 gas molecule takes place at the free carbon site (C-C) due to the H_2 loss; where this has been reported as the initial stage during coal gasification [Montoya et al., 2002; Radovic, 2009, Zhu et al., 2002]. Removal of the edge hydrogen by the CO_2 gas phase is argued to take place at 700-900°C [Kyotani and Tomita, 1999].

Figure 7.3 presents an illustration of hydrogen abstraction by the gas phase, allowing CO_2 chemisorption.

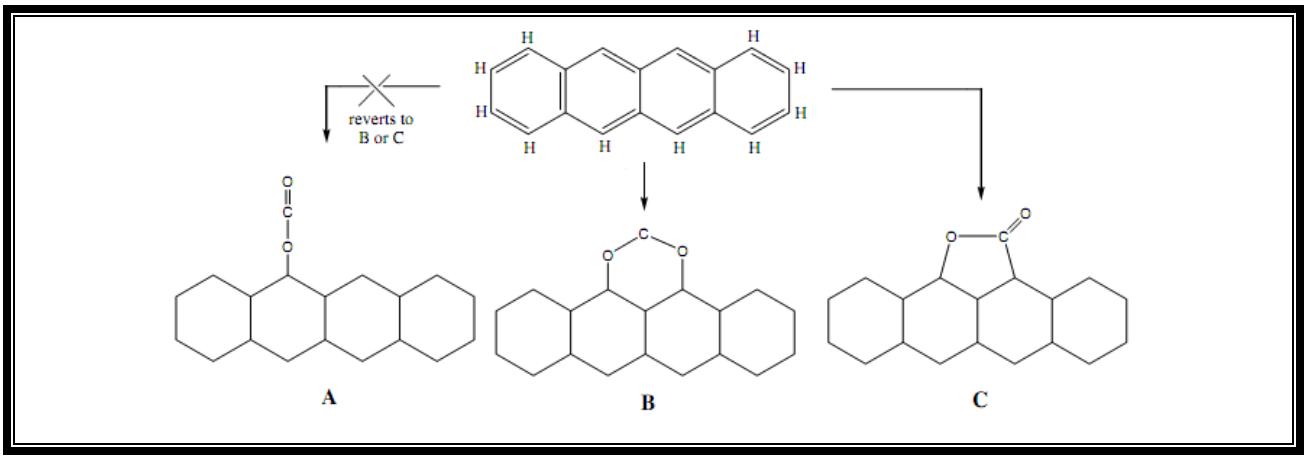

Figure 7.3 Abstraction of hydrogen by CO_2 molecular gas phase [Radovic, 2005]

Figures 7.4, 7.5 and 7.6 indicate that the temperatures at maximum rate of H_2 evolution for the 'uncatalysed' char samples were 1020°C, 1000°C and 980°C for the demineralized coal, raw coal and demineralized coal with added mineral mixture, respectively. It was observed that the addition of the catalyst facilitates the evolution of H_2 from the coal char samples.

As can be seen from Figures 7.4-7.6, addition of the catalysts to the samples shifted the temperature at which the maximum amount of H_2 was given off to lower temperatures. This shift to lower temperatures was observed with increasing catalyst loadings for both K_2CO_3 and KCl loaded samples. This implies that K_2CO_3 and KCl facilitate the evolution of H_2 by speeding up/enhancing the rate of the reaction steps and/or mechanisms where H_2 is given off, resulting in faster H_2 formation and release. As a result, lower temperatures are observed with increasing catalyst loadings. Enhanced amounts of H_2 in the product gas during K_2CO_3 catalysed steam gasification of coal char was reported by Kim et al. [1989]. Kim and co-workers also observed that increased amounts of K_2CO_3 enhanced H_2 in the product gas.

H_2 evolution for all the samples (Figure 7.4-7.6) began at approximately the same temperature of 800 °C; however, catalyst addition caused the H_2 evolution to take place over a relatively narrower temperature range than that observed for the sample without any catalyst loading. The 'narrowing' of the temperature range at which H_2 was released suggests that the rate of H_2 evolution was increased (i.e. H_2 was released faster) with increasing catalyst loadings.

Table 7.1 Temperatures at maximum rate of H_2 evolution (T_{max}) of the chars derived from demineralized coal, with/without catalyst loadings (°C)

Catalyst	Loading (K-wt%)	T_{max}
None added	0	1020
K_2CO_3	0.5	1000
	1	980
	3	900
	5	880
KCl	0.5	1000
	1	980
	3	920
	5	920

Table 7.2 Temperatures at maximum rate of H_2 evolution (T_{max}) of the chars derived from raw coal, with/without catalyst loadings (°C)

Catalyst	Loading (K-wt%)	T_{max}
None added	0	1000
K_2CO_3	0.5	1000
	1	980
	3	950
	5	900
KCl	0.5	1000
	1	1000
	3	1000
	5	980

Table 7.3 Temperatures at maximum rate of H_2 evolution (T_{max}) of the chars derived from demineralized coal with added mineral mixture, with/without catalyst loadings (°C)

Catalyst	Loading (K-wt%)	T_{max}
None added	0	980
K_2CO_3	0.5	980
	1	950
	3	900
	5	850
KCl	0.5	980
	1	950
	3	900
	5	900

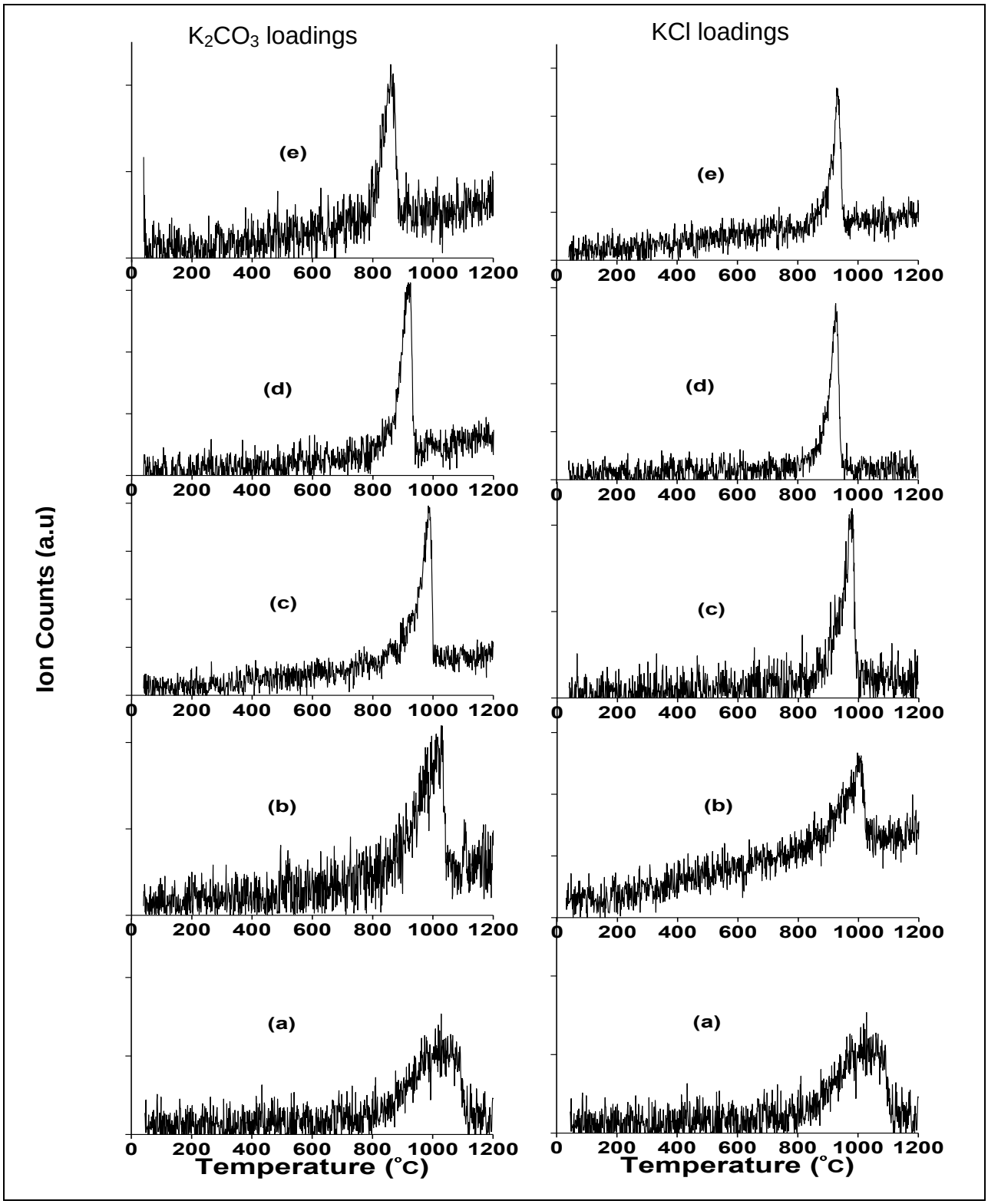

Figure 7.4 Mass spectra of H_2 (m/z = 2) for the char derived from demineralized coal with/without catalyst loadings: (a) 0% (b) 0.5% (c) 1% (d) 3% (e) 5%

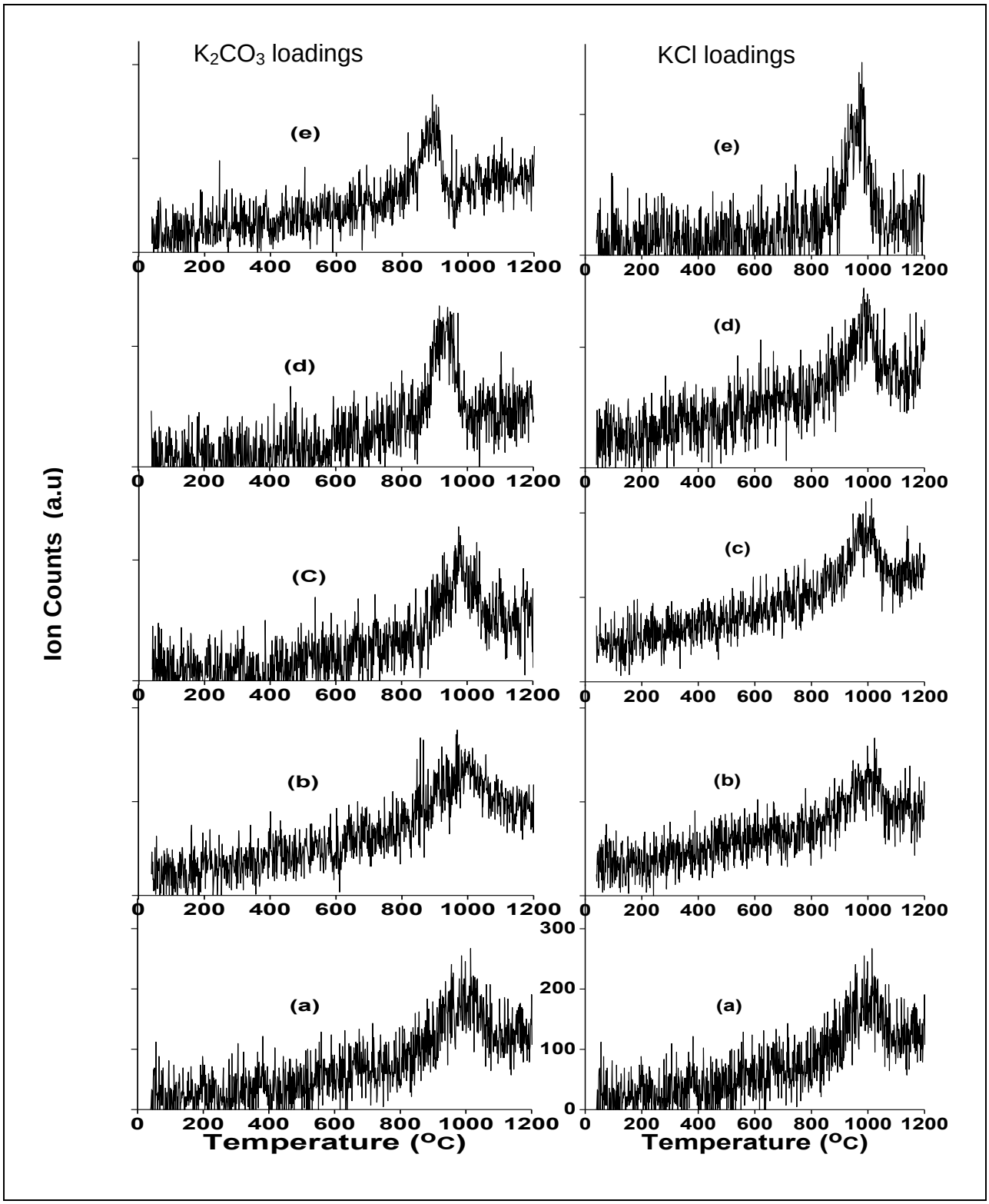

Figure 7.5 Mass spectra of H_2 (m/z = 2) for the char derived from raw coal with/without catalyst loadings: (a) 0% (b) 0.5% (c) 1% (d) 3% (e) 5%

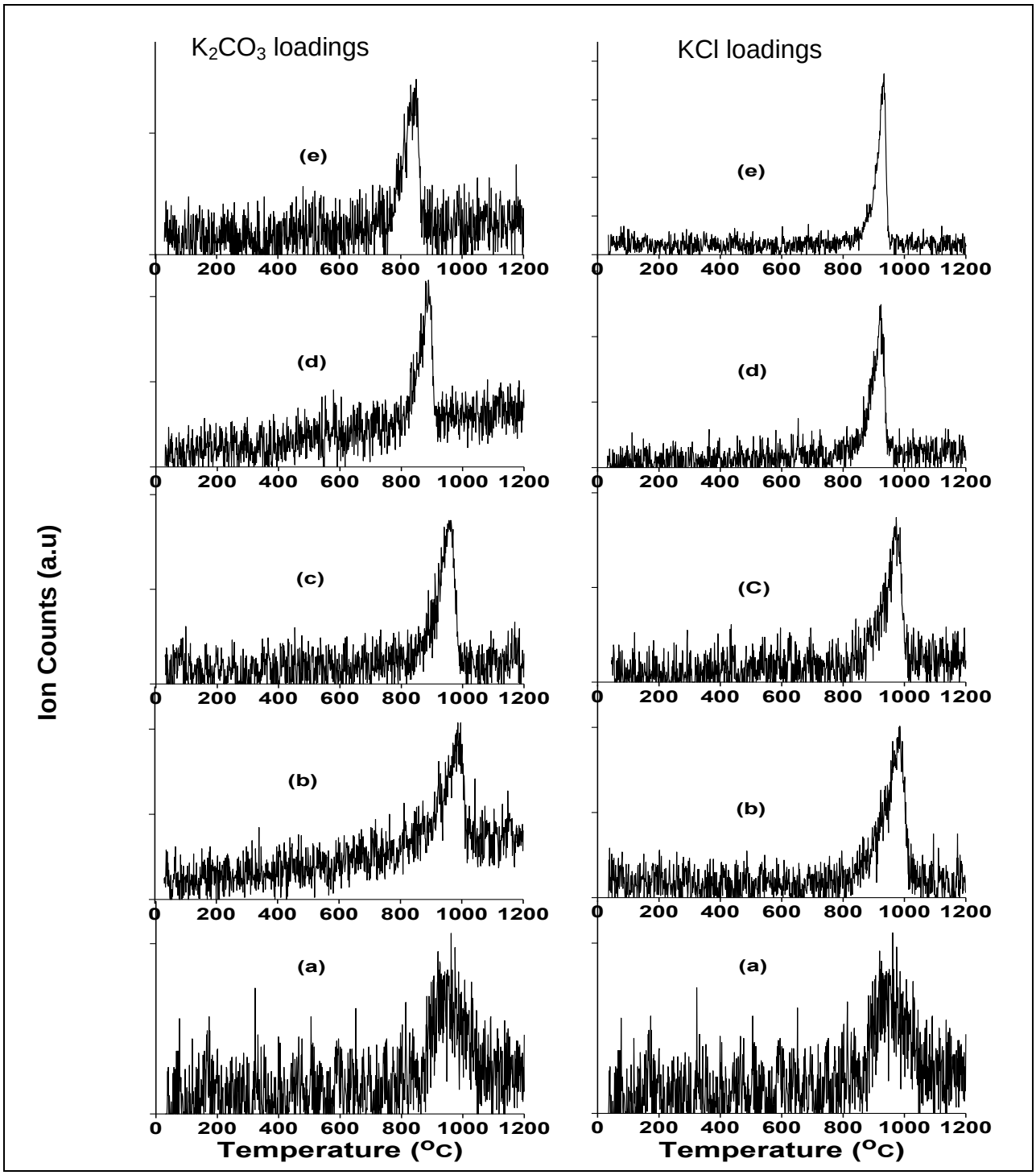

Figure 7.6 Mass spectra of H_2 (m/z = 2) for the char derived from demineralized coa lwith added mineral mixture, with/without catalyst loadings: (a) 0% (b) 0.5% (c) 1% (d) 3% (e) 5%

7.5 CO evolution profiles

The CO evolution patterns of the char samples prepared from K_2CO_3 and KCl loaded demineralized coal, raw coal and demineralized coal with added mineral mixture are presented in Figures 7.7, 7.8 and 7.9, respectively. The CO gas release is attributed to the key fragment CO^+, with the mass number (m/z) 28. The CO is proposed to be due to the parent molecule CO and/or CO_2 that is given off during coal char heat treatment, or thermal decomposition of the reactant gas CO_2.

From the CO evolution profiles (Figure 7.7-7.9), it was observed that the potassium compound dopants facilitate the evolution of CO and/or CO_2 from all the coal char samples derived from the demineralized coal, raw coal and demineralized coal with added mineral mixture. Additions of K_2CO_3 and KCl to the samples have shown to lower the initial and termination temperatures at which CO is evolved, as well as the temperature where CO evolution is maximal. This implies that K_2CO_3 and KCl facilitate the evolution of CO by increasing the rate of the reaction steps and/or mechanisms that produce CO; resulting in faster formation and release of CO. As a result, lower temperatures are observed with increasing catalyst loadings.

Kapteijn et al. [1991] proposed a C-CO_2 reaction mechanism and found that there were mainly two types of CO groups that may be responsible for CO desorption; a carbonyl type C-(CO) and a semiquinone type C(O). The semiquinones are as a result of a vacant carbon being oxidized and are reported to be a slowly desorbing species, whereas carbonyl complexes desorb fast and are formed by oxidation of two adjacent vacant carbon sites which yield a di-ketone that readily breaks up into two carbonyl complexes [Kapteijn et al., 1992]. The following mechanism was proposed by Kapteijn and co-workers [1991] for the reaction of carbon with all oxygen-containing gases:

$$CO_2 + C_f \leftrightarrow CO + C(O)$$
$$CO_2 + C_f + C(O) \leftrightarrow CO + 2C\text{–}(CO)$$
$$C\text{–}C(O) \leftrightarrow CO + C_f$$
$$C(O) \leftrightarrow CO + C_f \qquad \text{where } C_f \text{ is a free carbon active site}$$

According to Kapteijn and co-workers [1991], the carbonyl complexes (fast decay) ceased the moment when CO_2 could not be detected in the gas phase, suggesting that the fast

decay type is related to the presence of CO_2 in the gas phase. According to studies done by Chen et al. [1993] on the mechanism for carbon gasification reactions; the semiquinone and the carbonyl groups are stable and further bonding with oxygen from the reactant gas is necessary to weaken the surface carbon-carbon bonds in order to release CO. In addition, a dimeric CO molecule (O-C-C-O) may be released. However, it is not stable in the gas phase, thus two CO molecules will be released [Chen et al., 1993]. Figure 7.2 also gives an illustration of the possible formation and desorption/release of CO present in the gas phase.

The CO evolution spectra exhibited a CO desorption peak in the range of 900-1150°C, 850-1150°C and 850-1100°C for the char prepared from demineralized coal (Figure 7.6), raw coal (Figure 7.7) and demineralized coal with added mineral mixture (Figure 7.8); with no catalyst loadings. Temperature-programmed desorption (TPD) studies have been done on carbon treated with different gases (i.e. CO_2, O_2 and H_2O), and the results were a CO desorption peak around 950°C [Kyotani et al., 1988; Lizzio et al., 1988; Lizzio et al, 1990; Lizzio and Radovic, 1991; Radovic et al., 1991; Brown and Haynes, 1992]. The temperatures at which CO evolution is observed are to some degree comparable with that observed by Kyotani and others.

Table 7.4 Temperatures at maximum rate of CO evolution (T_{max}) of the chars derived from demineralized coal, with/without catalyst loadings (°C)

Catalyst	**Loading (K-wt%)**	**T_{max}**
None added	0	1100
K_2CO_3	0.5	1020
	1	980
	3	900
	5	850
KCl	0.5	1000
	1	980
	3	900
	5	900

Table 7.5 Temperatures at maximum rate of CO evolution (T_{max}) of the chars derived from raw coal, with/without catalyst loadings (°C)

Catalyst	Loading (K-wt%)	T_{max}
None added	0	1020
K_2CO_3	0.5	1020
	1	1000
	3	950
	5	900
KCl	0.5	1020
	1	1000
	3	990
	5	980

Table 7.6 Temperatures at maximum rate of H_2 evolution (T_{max}) of the chars derived from demineralized coal with added mineral mixture, with/without catalyst loadings (°C)

Catalyst	Loading (K-wt%)	T_{max}
None added	0	1000
K_2CO_3	0.5	990
	1	950
	3	900
	5	850
KCl	0.5	980
	1	970
	3	900
	5	900

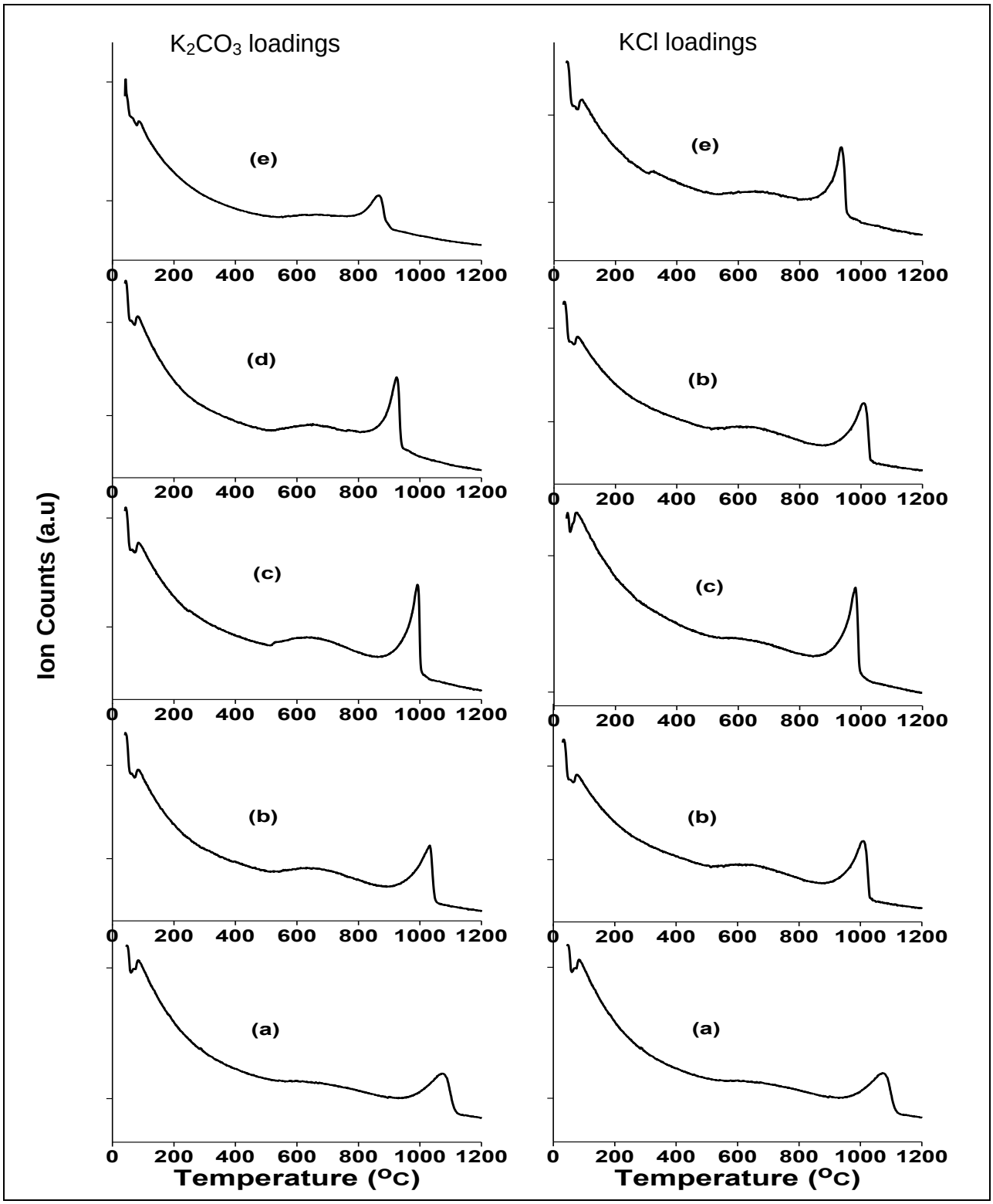

Figure 7.7 Mass spectra of CO (m/z = 28) for the char derived from demineralized coal with/without catalyst loadings: (a) 0% (b) 0.5% (c) 1% (d) 3% (e) 5%

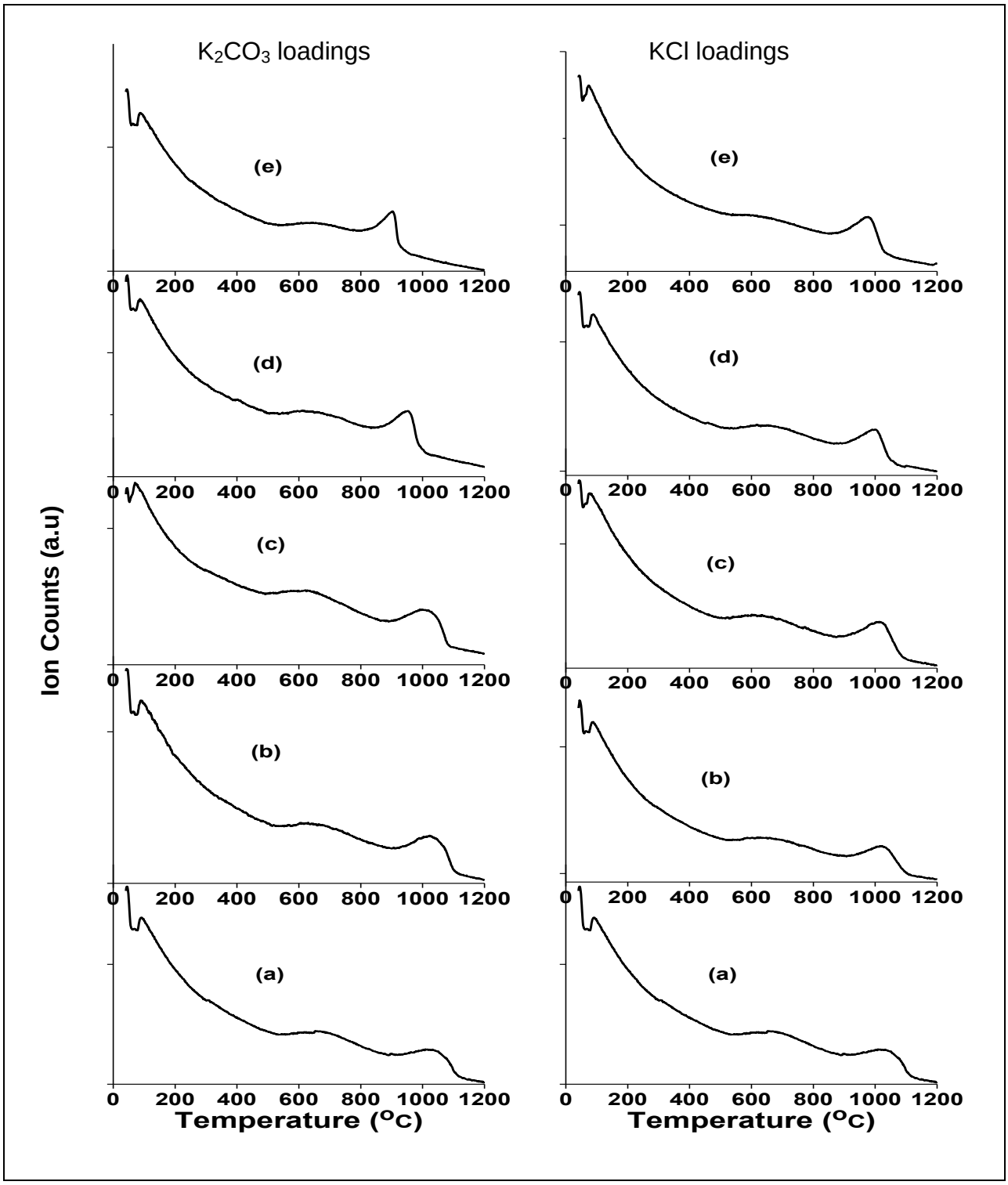

Figure 7.8 Mass spectra of CO (m/z = 28) for the char derived from raw coal with/without catalyst loadings: (a) 0% (b) 0.5% (c) 1% (d) 3% (e) 5%

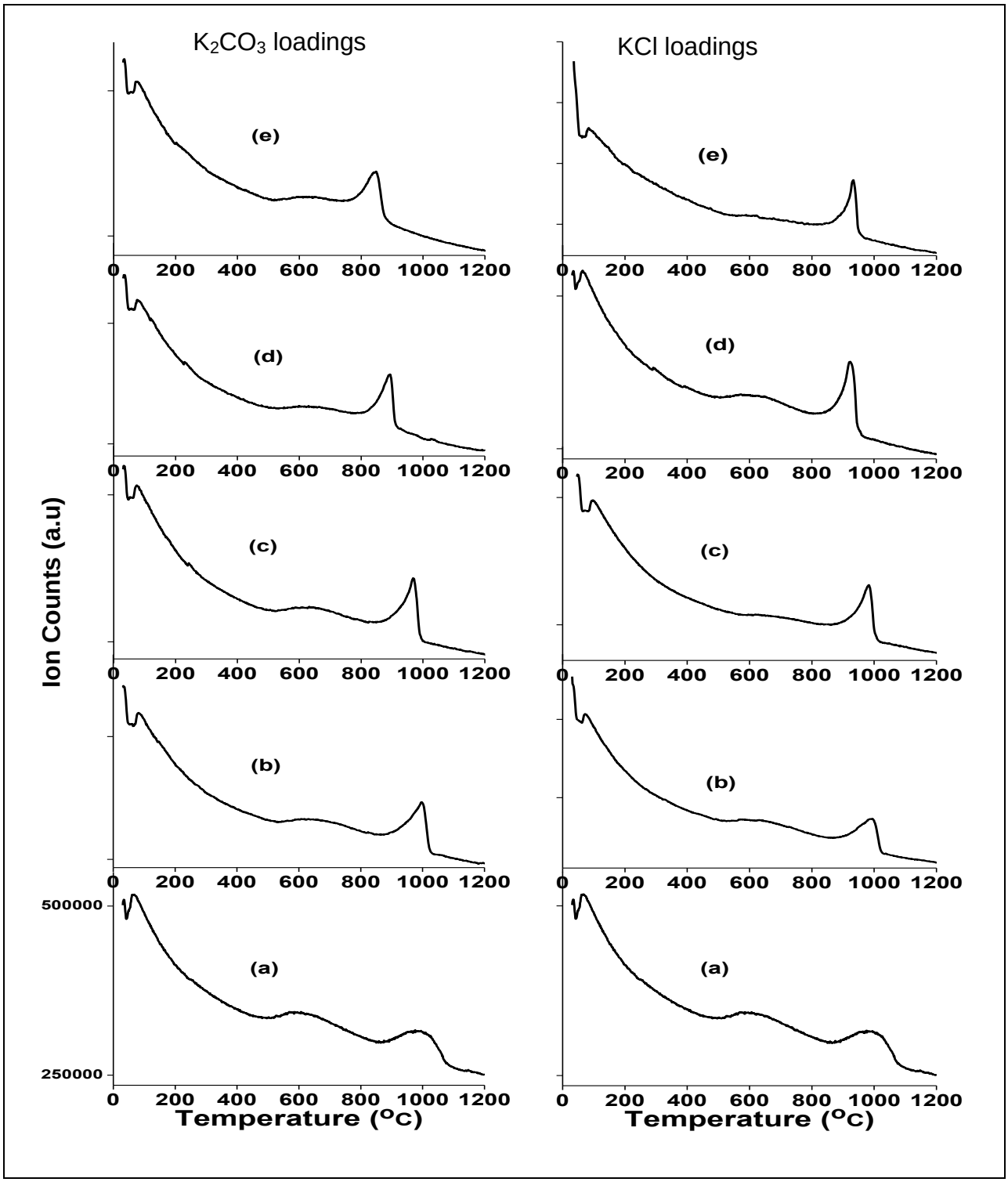

Figure 7.9 Mass spectra of CO (m/z = 28) for the char derived from demineralized coal with added mineral mixture, with/without catalyst loadings: (a) 0% (b) 0.5% (c) 1% (d) 3% (e) 5%

7.6 Gaseous carbon evolution profiles

The gaseous carbon evolution patterns of the char samples prepared from K_2CO_3 and KCl loaded demineralized coal, raw coal and demineralized coal with added mineral mixture are presented in Figures 7.10, 7.11 and 7.12, respectively. The C gas present in the gaseous phase is attributed to the key fragment C^+, with a mass number (m/z) of 12; and is proposed to be due to the parent molecules CO, CO_2, CH_4 and/or C_xH_y (aliphatics). Similarly, it was observed that the catalyst facilitates evolution of the gaseous C from all the coal char samples derived from the demineralized coal, raw coal and demineralized coal with added mineral mixture.

Addition of the K_2CO_3 and KCl to the samples have been shown to lower the initial and termination temperatures at which C is evolved, as well as the temperature where C evolution is maximal. This implies that K_2CO_3 and KCl facilitates the evolution of C by increasing the rate of the reaction steps and/or mechanisms that produce gaseous C containing gases, resulting in faster formation and release of gaseous C containing gases. As a result, lower temperatures are observed with increasing catalyst loadings. This catalytic effect for K_2CO_3 and KCl is in agreement with that observed in the TG results (Chapter 6), where an increase in char conversion was observed with increasing catalyst loadings.

The carbon evolution spectra for the char samples with no catalyst loadings exhibited a C desorption peak in the range 850-1150°C, 800-1150°C and 800-1100°C for the char prepared from demineralized coal (Figure 7.10), raw coal (Figure 7.11); and demineralized coal with added mineral mixture (Figure 7.12).

Table 7.7 Temperatures at maximum rate of gaseous carbon (C) evolution (T_{max}) of the chars derived from demineralized coal, with/without catalyst loadings (°C)

Catalyst	Loading (K-wt%)	T_{max}
None added	0	1050
K_2CO_3	0.5	1020
	1	990
	3	900
	5	850
KCl	0.5	1000
	1	980
	3	900
	5	900

Table 7.8 Temperatures at maximum rate of gaseous carbon (C) evolution (T_{max}) of the chars derived from demineralized coal with added mineral mixture, with/without catalyst loadings (°C)

Catalyst	Loading (K-wt%)	T_{max}
None added	0	1100
K_2CO_3	0.5	1020
	1	1000
	3	950
	5	900
KCl	0.5	1050
	1	1020
	3	1000
	5	980

Table 7.9 Temperatures at maximum rate of gaseous carbon (C) evolution (T_{max}) of the chars derived from demineralized coal, with/without catalyst loadings (°C)

Catalyst	Loading (K-wt%)	T_{max}
None added	0	980
K_2CO_3	0.5	980
	1	960
	3	900
	5	850
KCl	0.5	990
	1	980
	3	900
	5	900

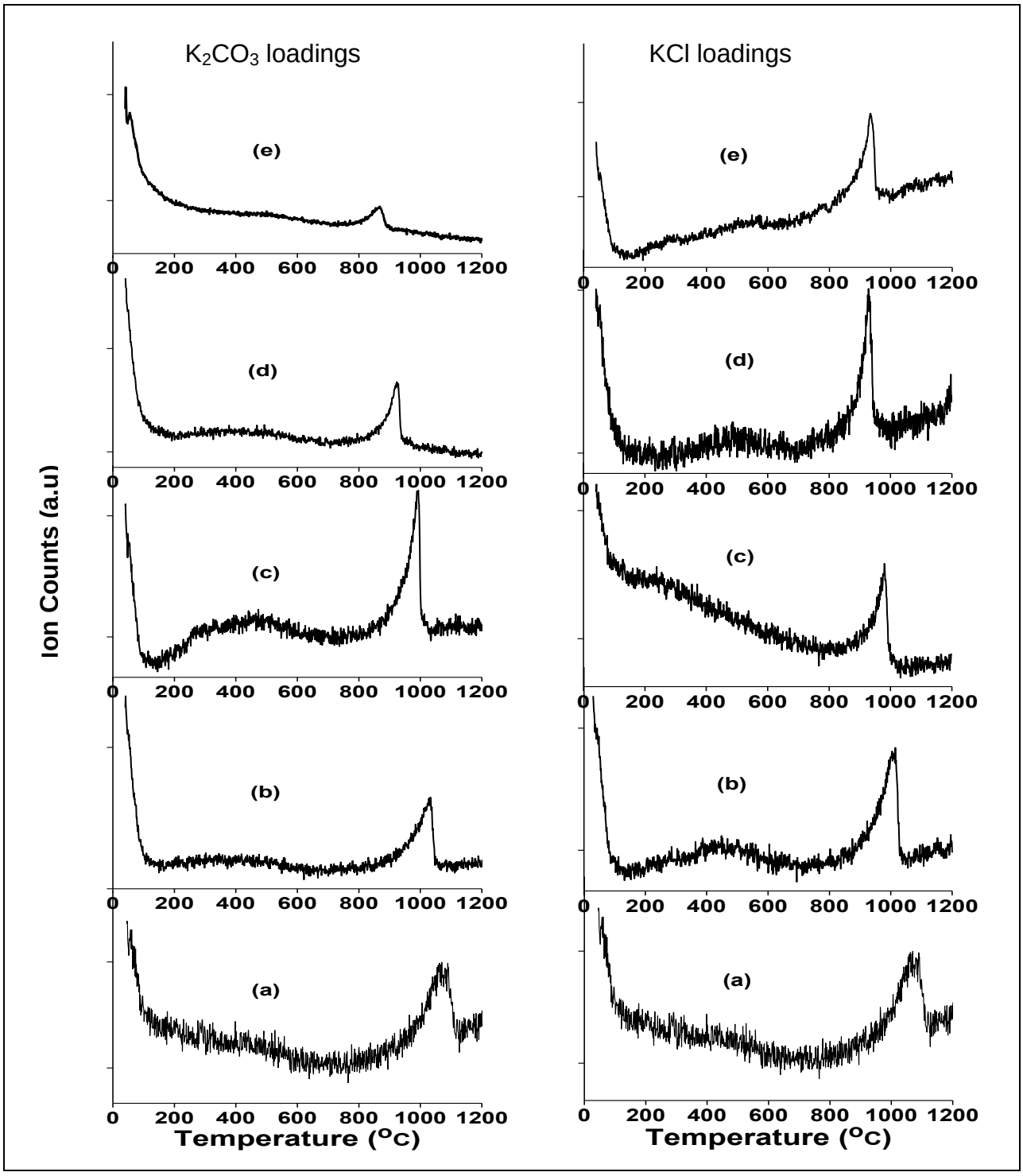

Figure 7.10 Mass spectra of C (m/z = 12) for the char derived from demineralized coal with/without catalyst loadings: (a) 0% (b) 0.5% (c) 1% (d) 3% (e) 5%

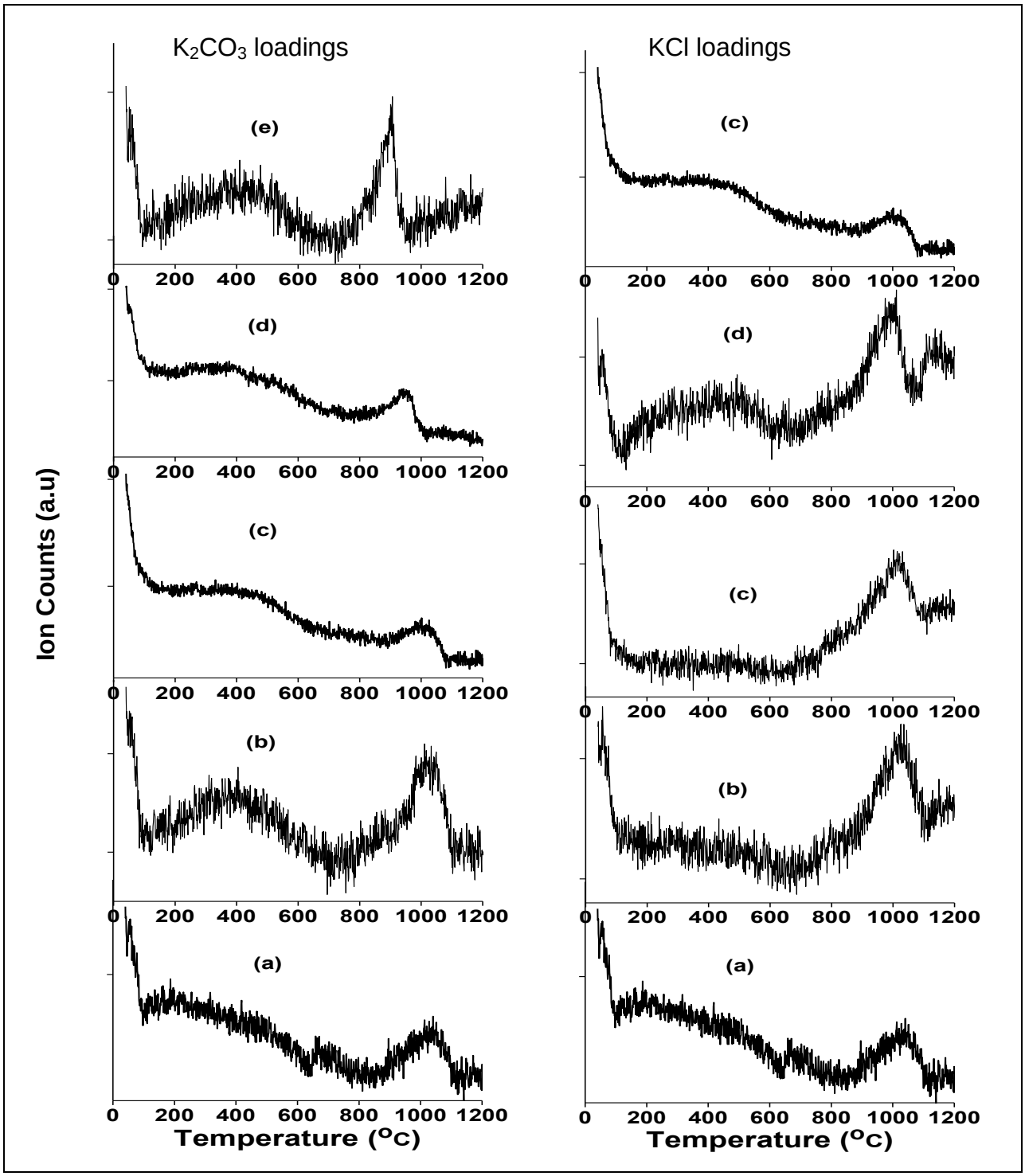

Figure 7.11 Mass spectra of C (m/z = 12) for the char derived from raw coal with/without catalyst loadings: (a) 0% (b) 0.5% (c) 1% (d) 3% (e) 5%

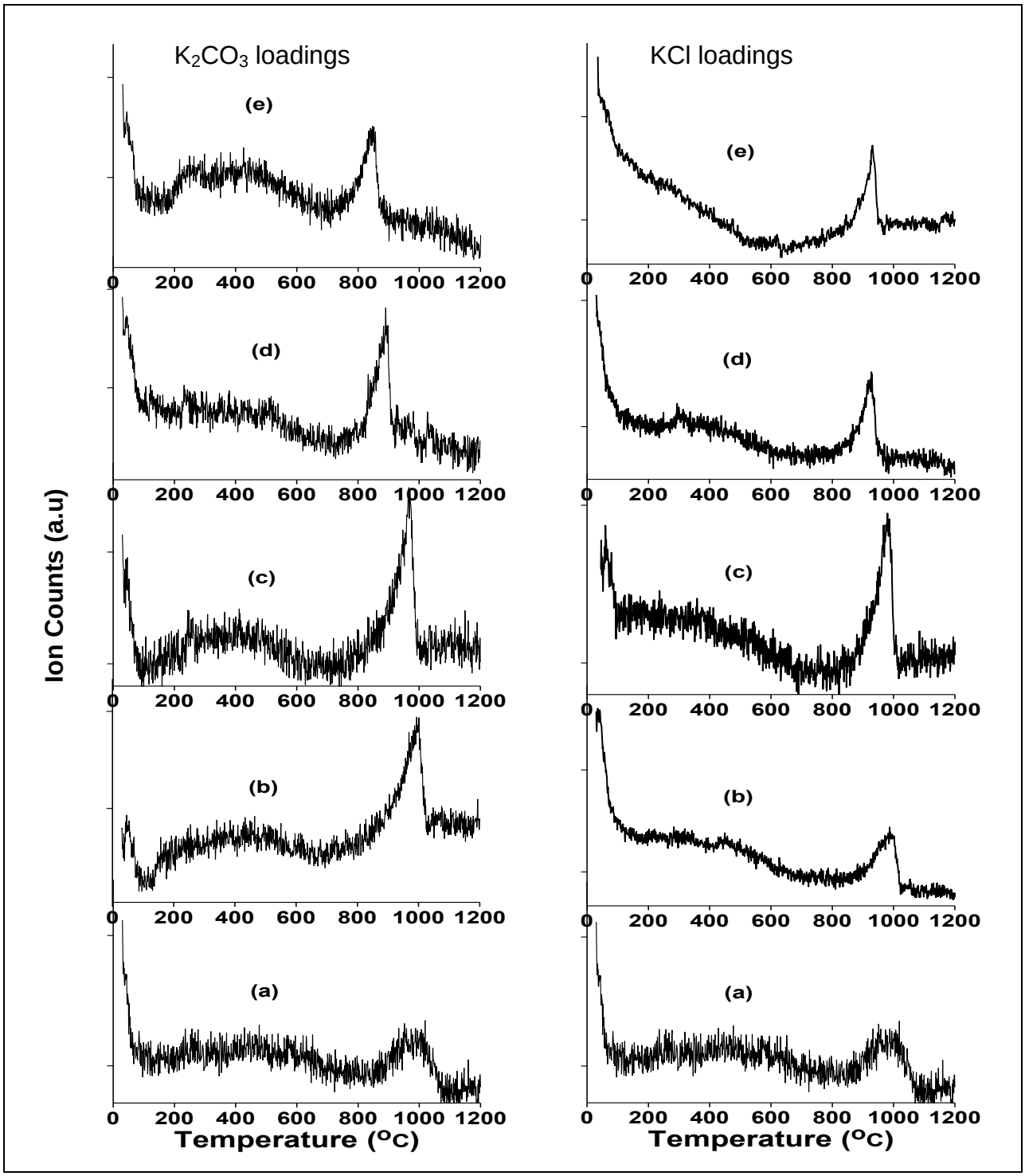

Figure 7.12 Mass spectra of C (m/z = 12) for the char derived from demineralized coal with added mineral mixture, with/without catalyst loadings: (a) 0% (b) 0.5% (c) 1% (d) 3% (e) 5%

7.7 The presence of potassium in the vapour phase of the product gas

The effect of K_2CO_3 and KCl loadings on the potassium loss during char heat treatments in a CO_2 atmosphere was investigated. The MS was used to determine whether any potassium from the catalyst loaded samples was identifiable in the product gas. It has been reported that, during heat treatments, the potassium from the catalyst is lost by at least three different mechanisms: (i) vaporization of potassium [Sams and Shadman, 1985]; (ii) irreversible reactions between the catalyst (e.g. K_2CO_3) and the ash component in the char [Formella et al., 1986; Bruno et al., 1986] and (iii) intercalation [Wigmans et al., 1983].

The m/z peak at 39 amu was used as an indication of the presence of potassium in the gaseous phase. However, as no peak was observed at this m/z ratio for all the MS results obtained, no potassium was observed in the gaseous products. This result implies that no vaporisation of potassium took place during heat treatments of the char in CO_2 atmospheres for all the catalyst loaded samples as well as the raw coal. This finding therefore suggests that the potassium from the catalyst was lost either via mechanism (i) and/or (ii). However, mechanism (ii) is more likely to take place for the char prepared from the raw untreated coal, followed by the char prepared from the demineralized coal with added mineral mixture. This is as the raw coal contains a large proportion of mineral matter relative to that present in the demineralized coal with added mineral mixture.

The XRF results (Chapter 5, Table 5.4) indicate a decrease in K_2O weight percentages relative to the presence of other inorganic compounds for the uncatalysed samples and 5 K-wt% KCl loaded samples after heat treatments in CO_2, suggesting catalyst loss during heat treatments of the char samples. However, an unexplainable increase in the wt% of K_2O was observed for the 5 K-wt% K_2CO_3 loaded samples of the demineralized coal and demineralized coal with added mixture after heat treatments in CO_2, which requires further investigations.

The XRD results (Chapter 5, Table 5.6-5.8) indicate that the main crystalline potassium compounds occurred as mineral phase sylvite (KCl) after heat treatments in CO_2. Sylvite was observed in the KCl loaded samples, as well as a relatively small amount in the 5 K-wt% K_2CO_3 loaded sample of the demineralized coal. No indication that kaliophilite or kalsilite ($KAlSiO_4$), which are known products of the reaction of K_2CO_3 with aluminosilicates, might be present in the char was revealed by the XRD results of the 5 K-wt% catalyst loaded samples. The absence of $KAlSiO_4$ in the demineralized coal samples after CO_2 heat treatments confirms that acid

leaching of the raw coal was effective in reducing inorganic matter, thus preventing mineral matter interactions during heat treatments.

As mentioned before, it is important to note that the XRD results do not necessarily suggest that no potassium was retained or present in the samples after heat treatments; since only the crystalline phases are obtainable by the analysis. The potassium may occur as an amorphous phase; therefore any amorphous potassium present in the samples will not be identified by the XRD analysis.

7.8 Comparisons of the MS results between 5 K-wt% loaded samples

Comparisons were done between the mass spectrometric results obtained when 5 K-wt% loadings of the potassium compounds on similar char samples were heat treated in the CO_2 atmosphere. The comparisons were done in order to determine the effect of the potassium compounds on the temperatures at which evolution of gaseous species are evolved. The results are presented below.

7.8.1 Effect of K_2CO_3 and KCl on the temperature ranges of evolution

7.8.1.1 H_2 evolution profiles

The effect of K_2CO_3 and KCl on the temperature range in which H_2 evolution was observed on the char derived from demineralized coal, raw coal and demineralized coal with added mineral mixture are presented in Figure 7.13, 7.14 and 7.15, respectively. The evolution profiles clearly indicate that K_2CO_3 reduces the range in which H_2 is evolved more than KCl. This indicates that K_2CO_3 exhibits a greater catalytic effect than KCl. This greater catalytic effect displayed by K_2CO_3 is also evident from the mass loss curves (Chapter 6), where the temperatures at which mass losses occured were lower than those observed for KCl loaded samples.

Figure 7.13 indicates that H_2 evolution for the 'uncatalysed' and catalysed char samples prepared from the demineralized coal begins at approximately the same temperatures. Termination of H_2 evolution is shifted from around 1150°C (for the 'uncatalysed' sample) to 1000°C and 950°C for KCl and K_2CO_3 loaded samples respectively. The temperature at which

maximum rate of evolution occurred were also shifted from 1020°C to 920°C and 880°C for KCl and K_2CO_3, respectively.

Figure 7.14 indicates that K_2CO_3 and KCl reduced the temperatures at which H_2 evolution was maximal for the char prepared from the raw coal, as well as the temperatures at which H_2 evolution ceased. The termination temperatures were reduced from around 1100°C to 1050°C and 950°C for KCl and K_2CO_3, respectively.

Similarly, a shift to lower temperatures at which H_2 evolution terminated, and where evolution was maximal was observed for the K_2CO_3 and KCl loaded char samples, prepared from the demineralized coal with added mineral mixture (Figure 7.15). The temperatures at maximum H_2 evolution shifted to lower temperatures of 925°C and 850°C for KCl and K_2CO_3, respectively. The maximum H_2 evolution for the uncatalysed sample occurred at temperatures of 950°C.

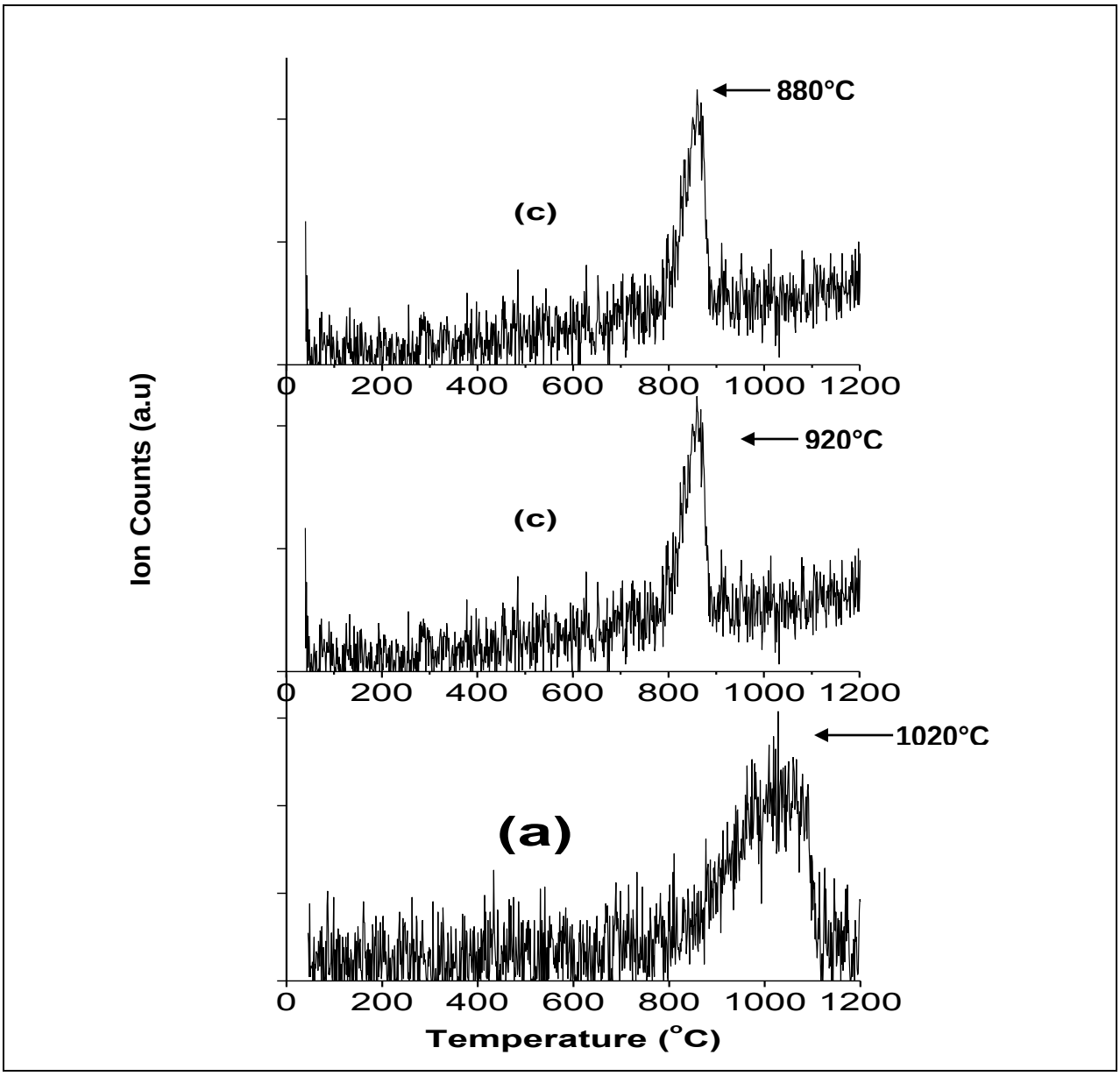

Figure 7.13 The effect of K_2CO_3 and KCl on the temperatures of H_2 evolution for the char derived from the demineralized: (a) uncatalyzed (b) 5 K-wt% KCl loaded sample (c) 5 K-wt% K_2CO_3 loaded sample

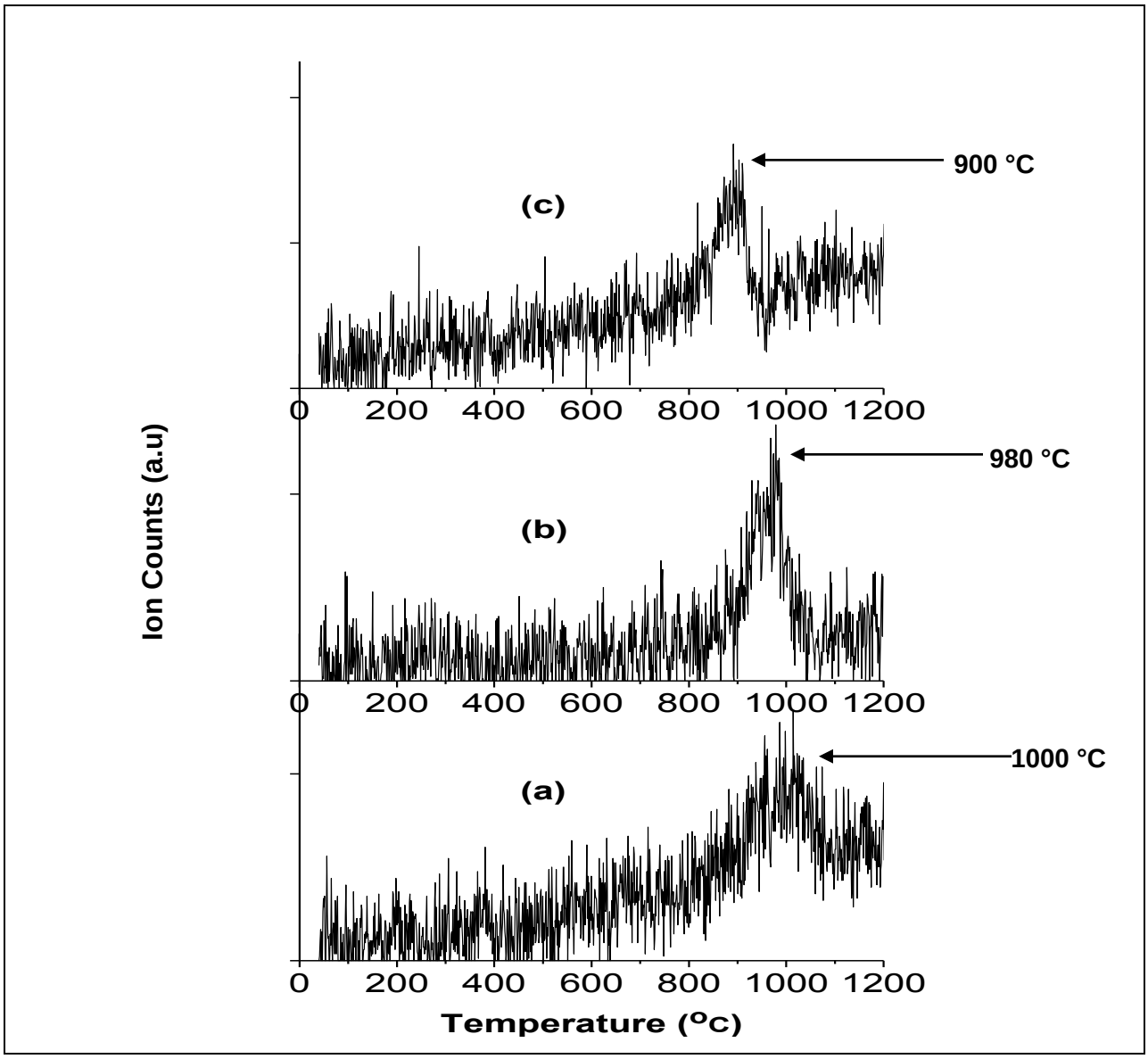

Figure 7.14 The effect of K_2CO_3 and KCl on the temperatures of H_2 evolution for the char derived from raw coal: (a) uncatalysed (b) 5 K-wt% KCl loaded sample (c) 5 K-wt% K_2CO_3 loaded sample

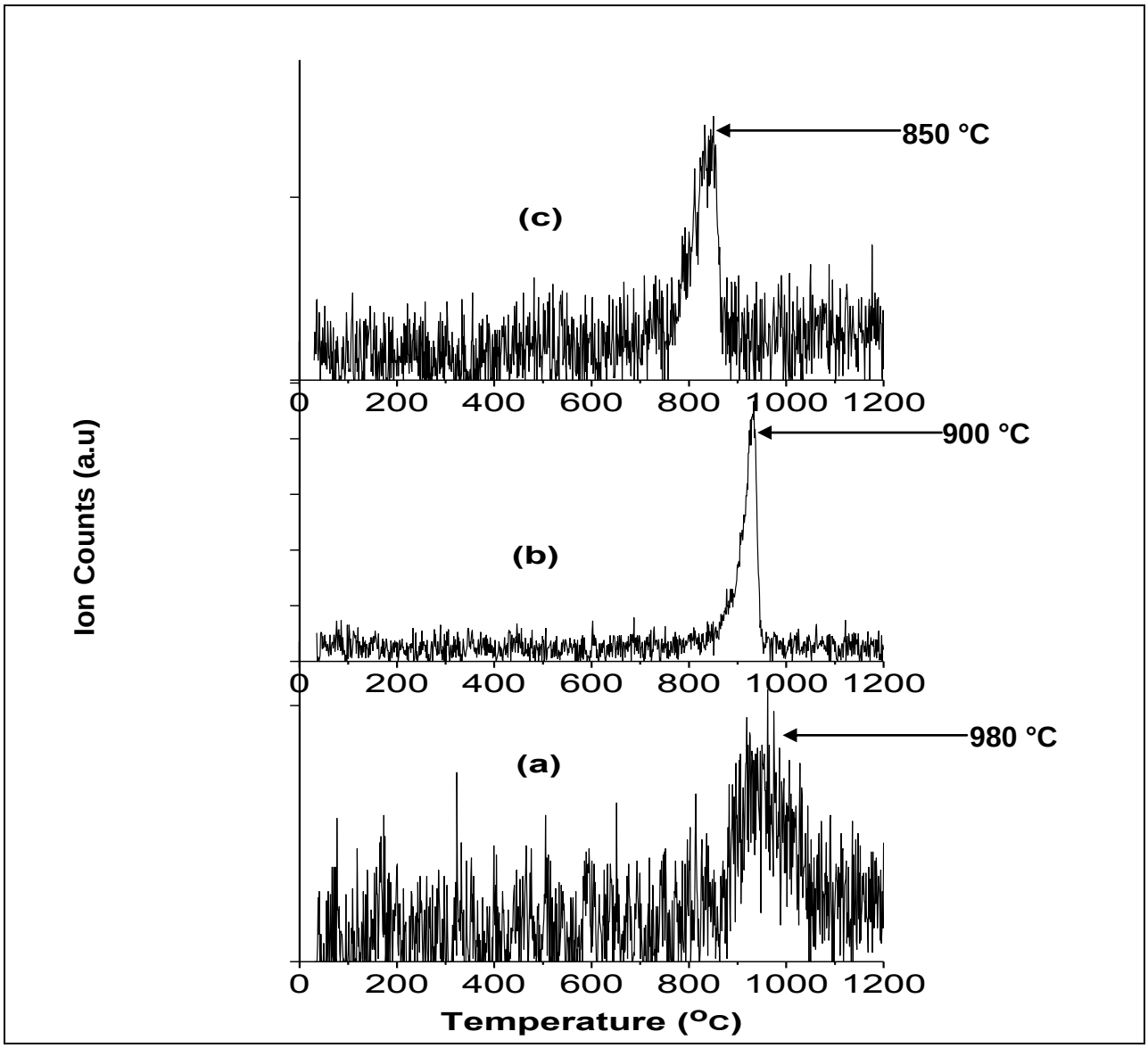

Figure 7.15 The effect of K_2CO_3 and KCl on the temperatures of H_2 evolution for the char derived from the demineralized coal with added mineral mixture: (a) uncatalysed (b) 5 K-wt% KCl loaded sample (c) 5 K-wt% K_2CO_3 loaded sample

The results obtained from the evolution of H_2 confirm that KCl and K_2CO_3 exhibit a catalytic effect on the CO_2 – char reaction.

7.8.1.1 CO evolution profiles

The effect of K_2CO_3 and KCl on the temperature range in which H_2 evolution is observed during heat treatment of the chars derived from demineralized coal, raw coal and demineralized coal with added mineral mixture are presented in Figures 7.16, 7.17 and 7.18, respectively.

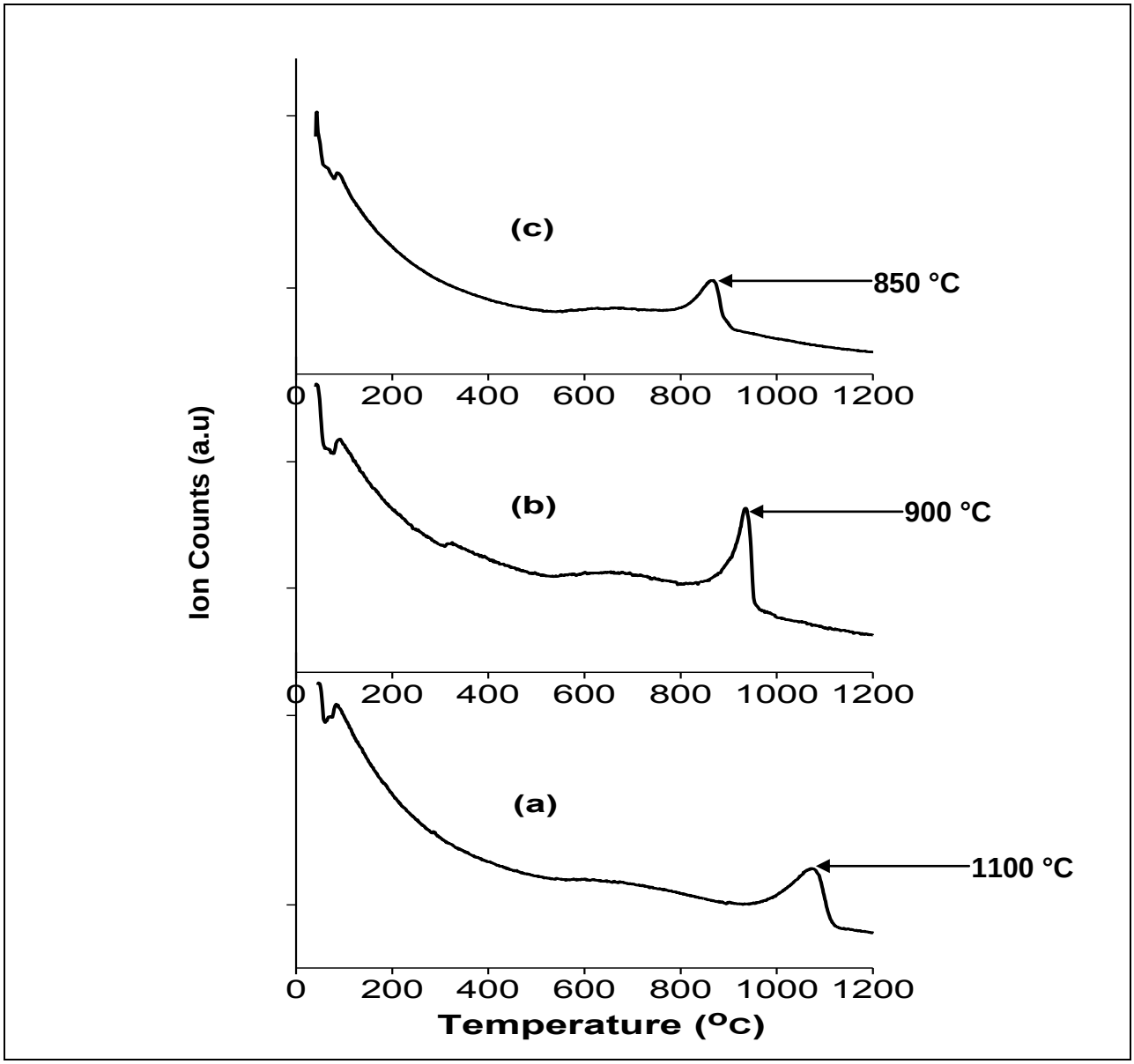

Figure 7.16 The effect of K_2CO_3 and KCl on the temperatures of CO_2 evolution for the char derived from the demineralized coal: (a) uncatalysed (b) 5 K-wt% KCl loaded sample (c) 5 K-wt% K_2CO_3 loaded sample.

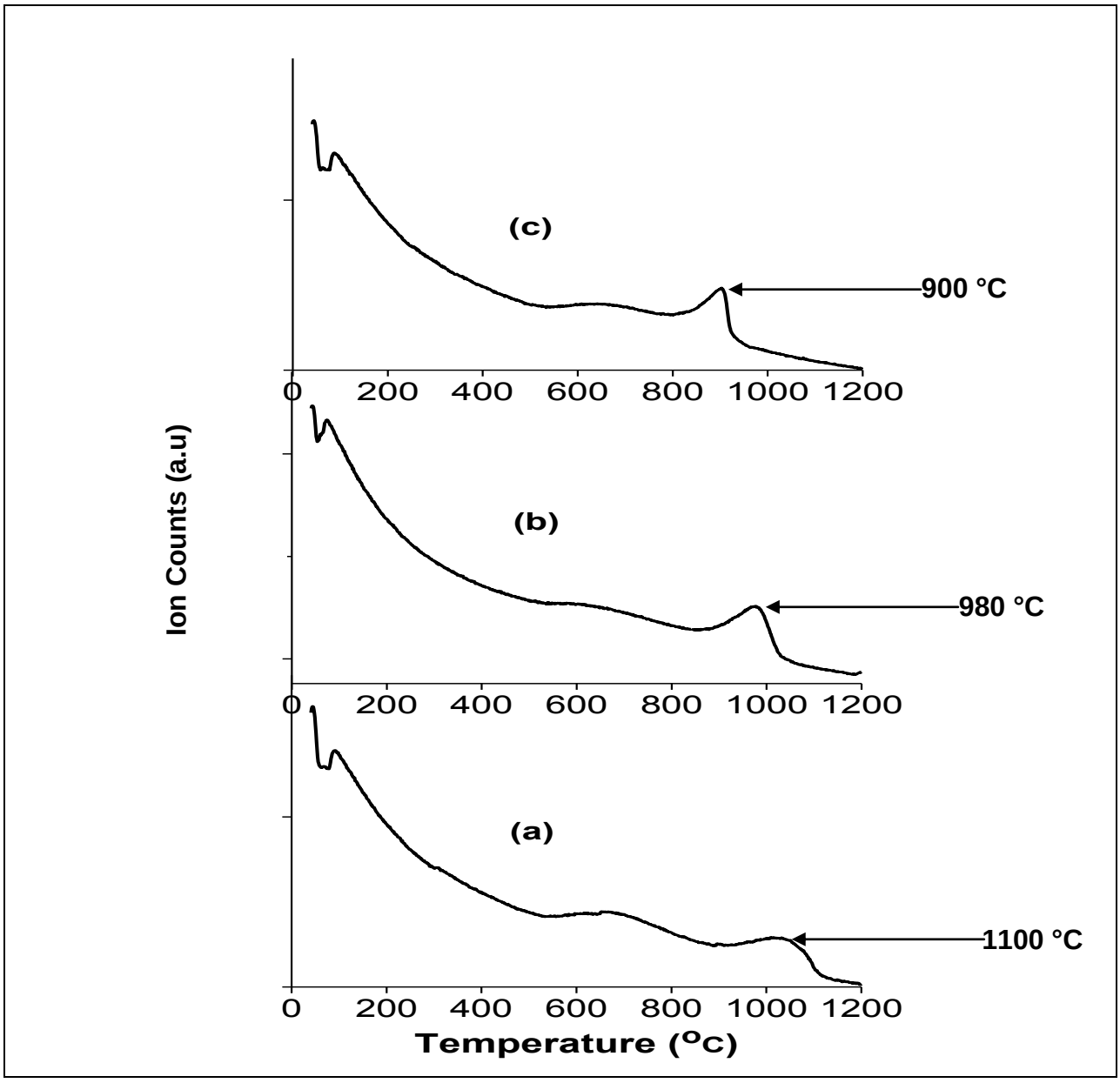

Figure 7.17 The effect of K_2CO_3 and KCl on the temperatures of CO_2 evolution for the char derived from the raw coal: (a) uncatalysed (b) 5 K-wt% KCl loaded sample (c) 5 K-wt% K_2CO_3 loaded sample.

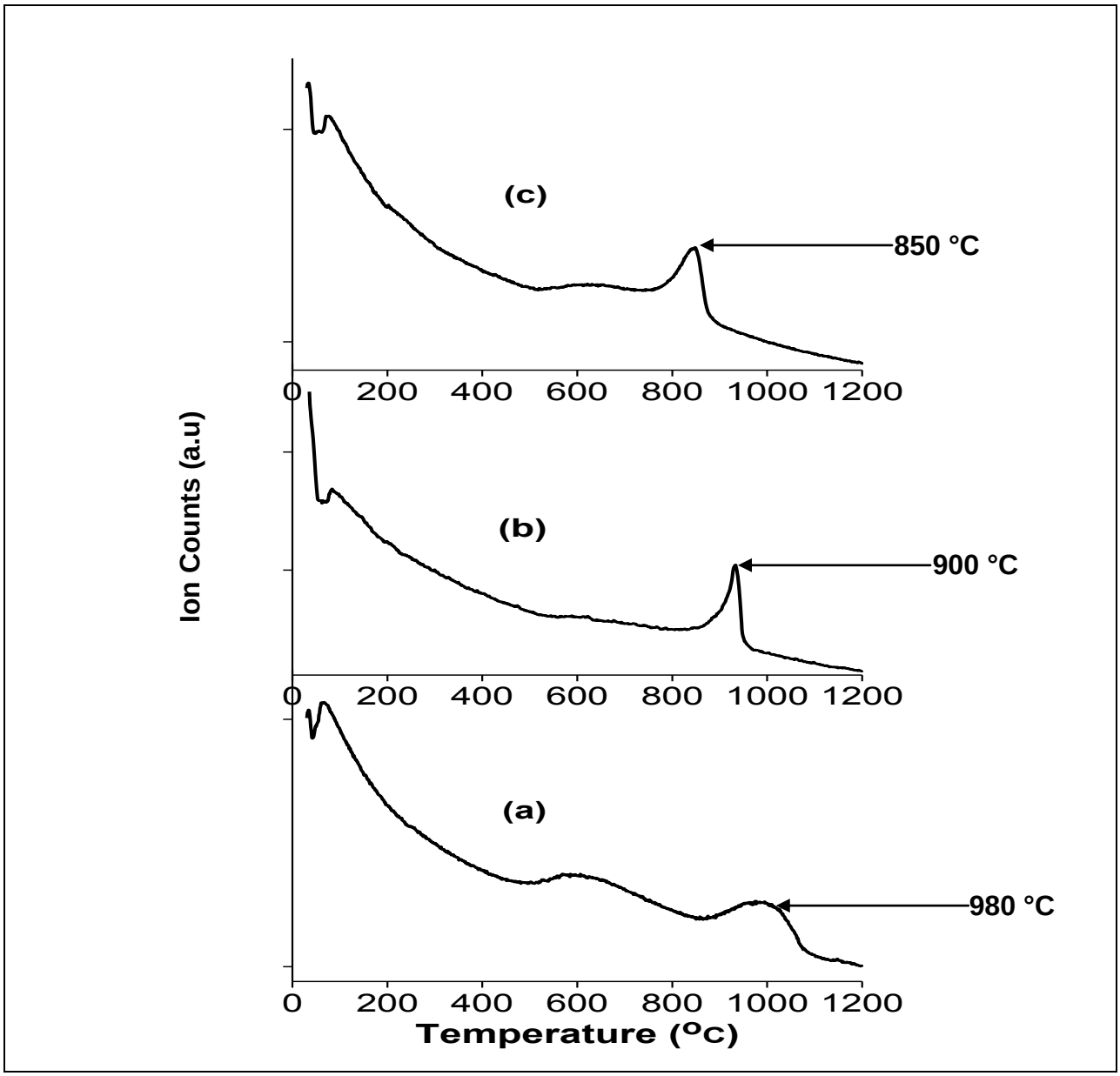

Figure 7.18 The effect of K_2CO_3 and KCl on the temperatures of CO_2 evolution for the char derived from the demineralized coal with added mineral mixture: (a) uncatalysed (b) 5 K-wt% KCl loaded sample (c) 5 K-wt% K_2CO_3 loaded sample

As seen from the evolution profiles, K_2CO_3 reduces the range in which CO_2 is evolved more than KCl. This indicates that K_2CO_3 exhibits a greater catalytic effect than KCl. This

greater catalytic effect displayed by K_2CO_3 is also evident in the mass loss curves (Chapter 6), where the temperature ranges at which mass loss occurred were shifted to much lower temperatures than those observed for KCl loaded samples.

Figure 7.16 indicates that CO_2 evolution for the uncatalysed, KCl and K_2CO_3 loaded char samples prepared from the demineralized coal begins at approximately 950 °C, 800 °C and 750 °C, respectively. Termination of CO_2 evolution is shifted from approximately 1150°C (for the 'uncatalysed' sample) to 1000°C and 950°C for the KCl and K_2CO_3 loaded samples, respectively. The temperature at which maximum rate of evolution occurred were also shifted from 1000 °C ('uncatalysed' sample) to 950 °C and 850 °C for the KCl and K_2CO_3 loaded samples, respectively.

Figure 7.17 indicates that K_2CO_3 and KCl reduced the temperature at which CO_2 evolution was maximal for the char prepared from the raw coal, as well as the temperatures at which H_2 evolution ceased. The temperature ranges for CO_2 evolution occurred at 900-1150 °C, 850-1100 °C and 800-1000 °C for the 'uncatalysed', KCl and K_2CO_3 loaded samples, respectively. The temperatures at maximum rate of evolution of CO_2 were reduced from approximately 1025 °C ('uncatalysed' sample) to 975 °C and 900 °C for the KCl and K_2CO_3 loaded samples, respectively.

A similar shift to lower temperatures at which CO_2 evolution occurs was observed for the KCl and K_2CO_3 loaded char samples derived from demineralized coal with added mineral mixture [Figure 7.18]. The temperatures at maximum CO_2 evolution were approximately 925 °C and 825 °C for KCl and K_2CO_3, respectively and the maximum CO_2 evolution for the 'uncatalysed' sample occurred at approximately 975 °C.

Similarly, the results obtained from the evolution of CO confirm that KCl and K_2CO_3 exhibit a catalytic effect on the CO_2 – char reaction.

7.8.2 Relationship between gas evolution temperatures and char conversion

The gas evolution profiles and the mass losses observed were compared for the 5 K-wt% catalyst loaded samples. This was done in order to determine whether the mass losses observed correspond with the onset of gas evolution and more importantly to investigate whether the temperature at maximum rate of mass loss corresponds with the temperature at which maximum rate of evolution is observed. In the figures below, the comparisons for the gaseous species H_2 are presented.

The DTG curves (instead of the TG curves) were used in order to clearly indicate the temperatures at which the onset and termination of coal char conversion takes place, as well as where maximum rate of conversion occurs.

H_2 evolution profiles

Figures 7.19 and 7.20 are the DTG-MS profiles of the coal char derived from the demineralized coal samples with 5 K-wt% K_2CO_3 and KCl loadings, respectively.

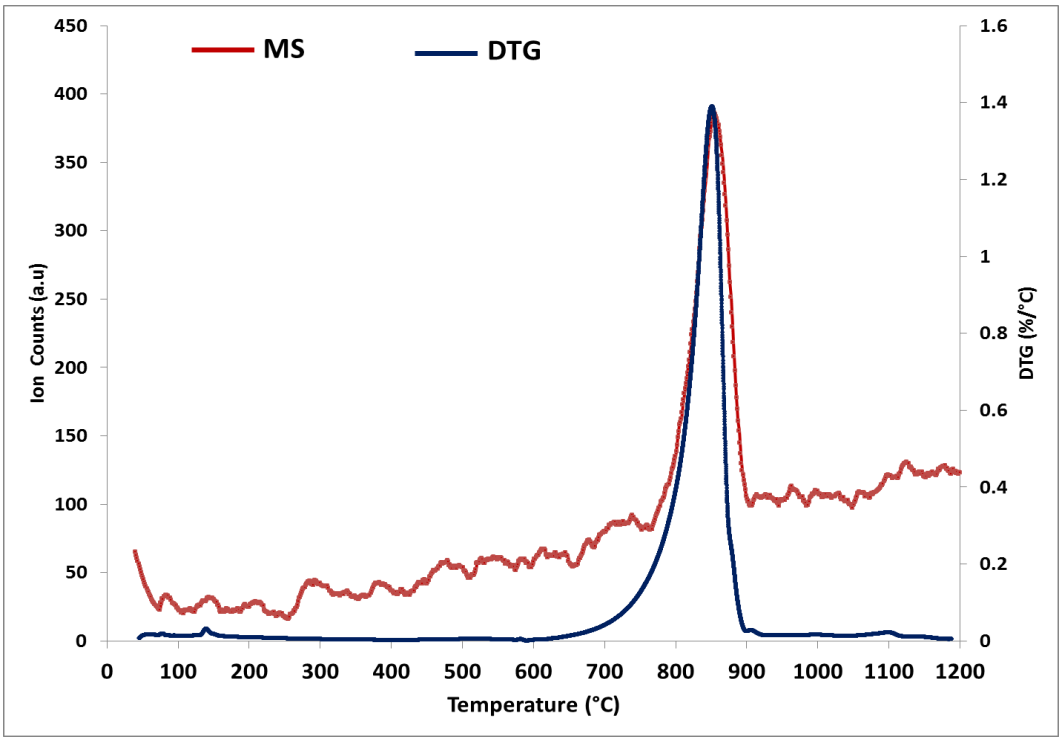

Figure 7.19 DTG-MS analysis of the char derived from demineralized coal with 5 K-wt% K_2CO_3 loading

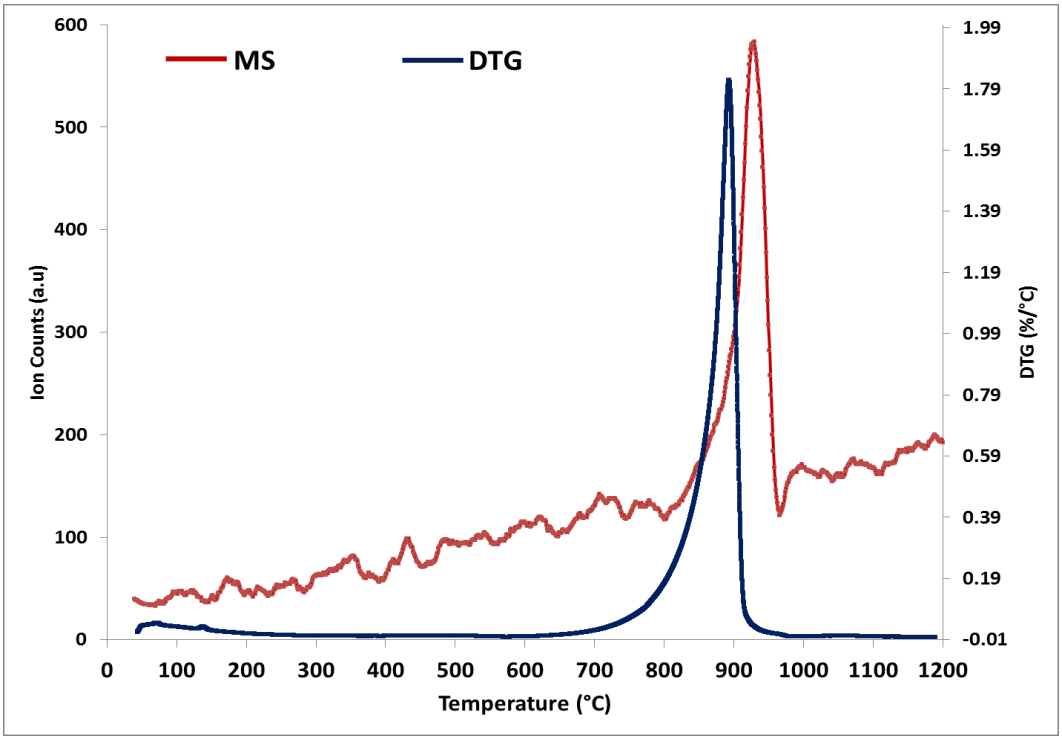

Figure 7.20 DTG-MS analysis of the char derived from demineralized coal with 5 K-wt% KCl loading

It was observed that the temperatures at which the onset and termination of char conversion occur correspond well with the onset of H_2 gas evolution. In addition, the temperature at maximum rate of mass loss also corresponds well with the temperature at maximum rate of H_2 evolution in the case where K_2CO_3 was used. A deviation of approximately 50 °C was observed between the temperature at maximum rate of mass loss and the temperature at maximum rate of H_2 evolution for the KCl loaded sample. The unexpected deviation observed is an interesting finding and therefore requires further investigations to study the reasons behind it.

Figures 7.21 and 7.22 present the DTG-MS profiles of the coal char derived from the raw coal samples with 5 K-wt% K_2CO_3 and KCl loadings, respectively. It can be seen that the char conversion temperatures correspond well with the onset, termination and the maximum temperatures where H_2 evolution occur.

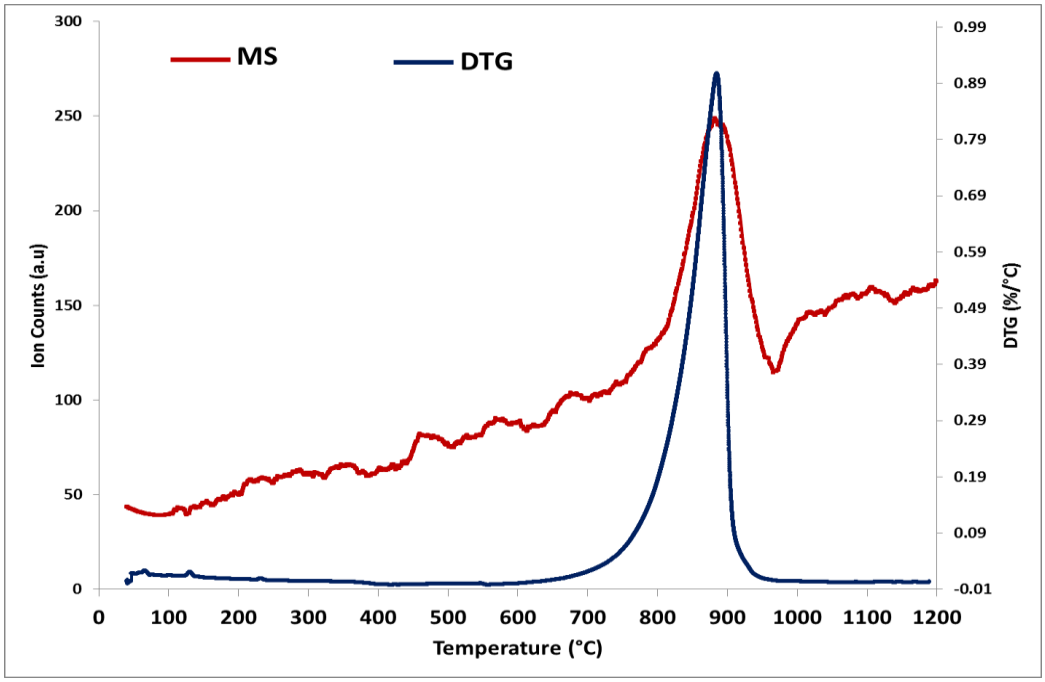

Figure 7.21 DTG-MS analysis of the char derived from raw coal with 5 K-wt% K_2CO_3 loading.

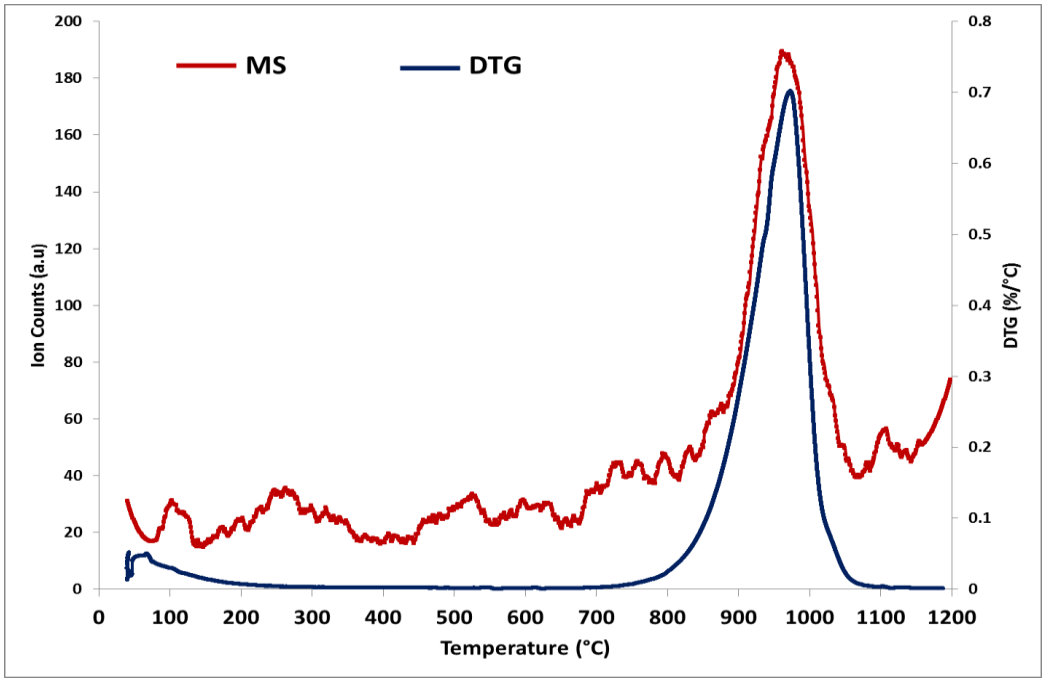

Figure 7.22 DTG-MS analysis of the char derived from raw coal with 5 K-wt% KCl loading

DTG-MS profiles of the coal char derived from the demineralized coal samples with 5 K-wt% K_2CO_3 and KCl loadings are presented in Figures 7.23 and 7.24, respectively. A similar trend was observed where temperatures at which the onset and termination of char conversion take place correspond well with the onset of H_2 evolution for the K_2CO_3 loaded samples. A deviation of approximately 40 °C was observed between the temperature at maximum rate of mass loss and the temperature at maximum rate of H_2 evolution for the KCl loaded sample. This unexpected behaviour should be investigated further in future work.

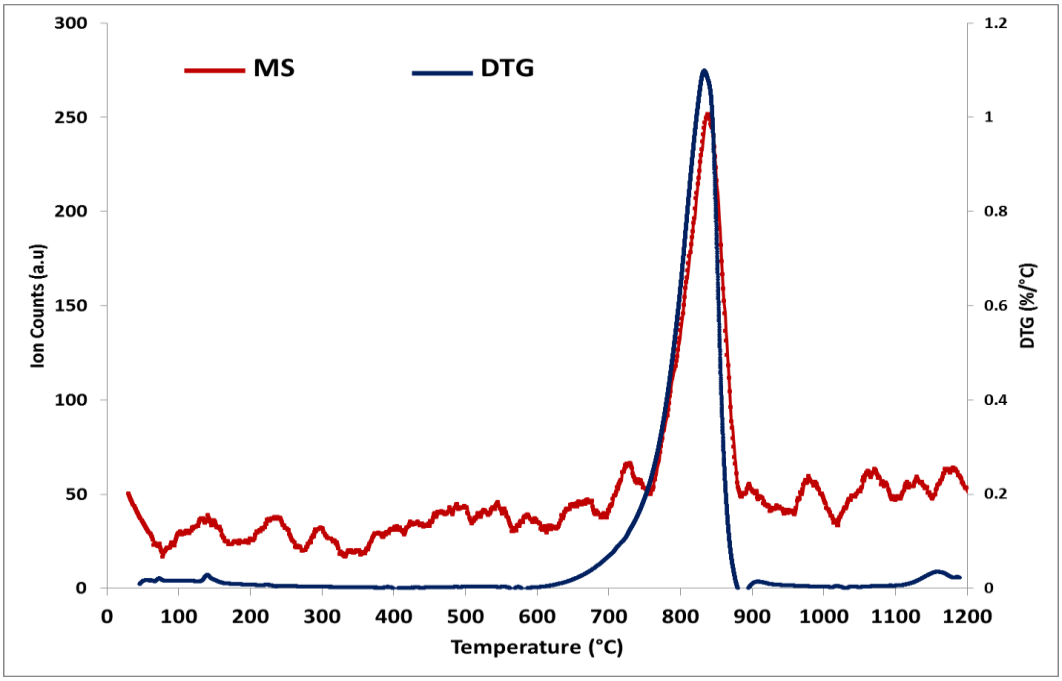

Figure 7.23 DTG-MS analysis of the char derived from demineralized coal with added mineral mixture and 5 K-wt% K_2CO_3 loading

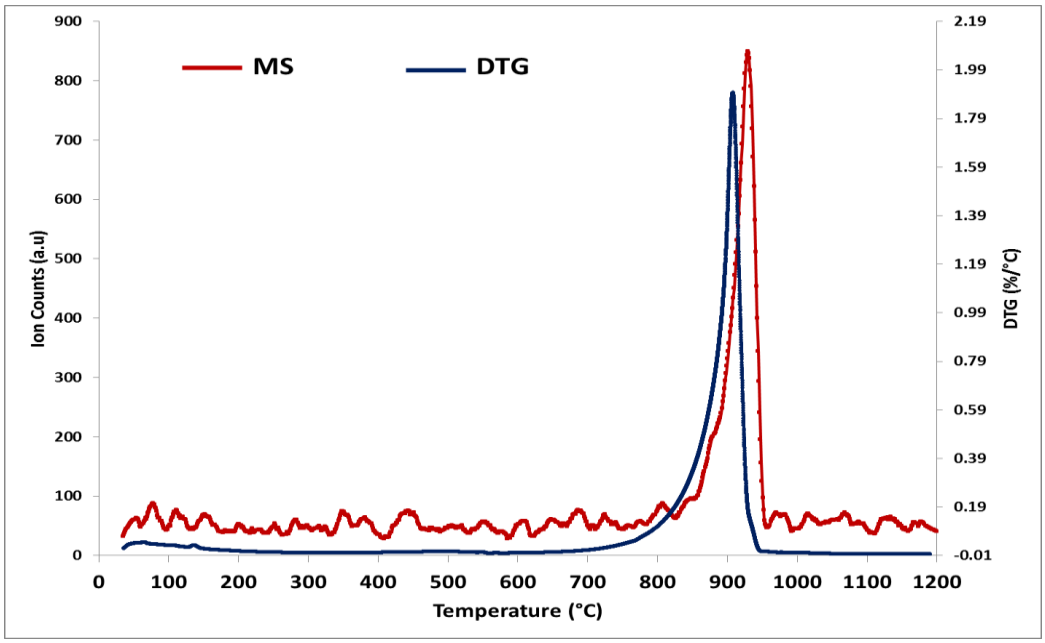

Figure 7.24 DTG-MS analysis of the char derived from demineralized coal with added mineral mixture and 5 K-wt% KCl loading

The DTG-MS profiles for the 5 K-wt% loaded samples clearly indicate that the mass losses correspond with the onset of gas evolution.

CHAPTER 8

Summary, Conclusions and Recommendations

Catalytic gasification of coal and char has been studied extensively worldwide, where the atmosphere was modelled by using CO_2. However, limited studies have been conducted on South African Inertinite coals. No TG-MS studies have been done to date on the effect of catalysts additions on the gas composition of a South African coal, thus this study investigated the gaseous product composition during the CO_2 reaction with the char from an inertinite-rich South African bituminous coal from a Highveld coalfield.

Thermogravimetric (TG) analyses were successfully used to evaluate the influence of various loadings of K_2CO_3 and KCl on the mass losses of the char derived from the demineralized coal, raw coal and demineralized coal with added mineral mixture samples. In addition, the catalytic behaviour of K_2CO_3 and KCl was successfully evaluated.

The TG-MS technique was successfully used to identify the evolved gas composition whilst simultaneously monitoring the mass losses or char conversion during heat treatments in a CO_2 atmosphere.

8.1 Coal Characterization

8.1.1 The proximate and ultimate analysis results indicated that the inertinite-rich South African bituminous Highveld coal contains a substantial amount of inorganic matter indicated by an ash content of 21.5%. Sequential acid leaching of the coal sample with HCl-HF-HCl significantly reduced the inorganic matter associated with the coal to less than 3%. The low total sulphur content typical in South African inertinite-rich bituminous coal was also confirmed. The XRF results revealed that a substantial proportion of the inorganic matter is associated with coal minerals in the form of quartz (44.24%), clay (26.30%) and carbonates (11.95%). The sequentially leached coal sample showed reduced amounts of quartz (37.47%), clay (5.22%) and carbonates (4.20%).

Conclusion

The decrease in ash content and the subsequent decrease in minerals indicate that the HCl-HF-HCl leaching process was effective, more so in removing the clay minerals and other elements associated with the clay minerals.

8.1.2 The XRF results indicated a decrease in K_2O content for the coal char samples after heat treatments in CO_2, where the K_2CO_3 compounds where added as catalyst.

Conclusion

The reduced K_2O content indicates at least some potassium loss during and after heat treatment in CO_2.

8.1.3 From the XRD results it was observed that the crystalline mineral phase constituting the potassium compound was muscovite ($KAl_2(AlSi_3O_{10})(OH)_2$) in the coal samples not subjected to heat treatments. No crystalline potassium-containing mineral phases were observed in the heat treated coal char samples under N_2 and CO_2 atmospheres. However, the mineral phase sylvite (KCl) was observed in the KCl loaded samples after CO_2 heat treatment.

Conclusion

The undetectable potassium crystalline phases suggest that most of the potassium retained in the coal-char samples after heat treatments in N_2 and CO_2 occurs as an amorphous phase and not in a crystalline phase.

8.2 Thermogravimetric (TG) analyses of coal char

8.2.1 From the TG curves, a lower catalytic effect was observed for KCl loaded samples when compared to K_2CO_3 loaded samples during heat treatments of the coal char in CO_2. Char conversion was observed to take place at lower temperatures for the coal char samples with K_2CO_3 loadings than for the KCl loaded samples. The temperatures at

maximum rate of mass loss for the coal chars derived from K_2CO_3 loaded samples were also lower than the temperatures of KCl loaded samples.

Conclusion

K_2CO_3 exhibits a greater catalytic effect than KCl during coal char heat treatments in CO_2.

8.2.2 The mass loss of the char derived from demineralized coal with 5 K-wt% KCl loading occurred at lower temperatures than that of the 5 K-wt% KCl loaded raw coal and of the demineralized coal with added mineral mixture. The mass loss of the char derived from demineralized coal with added mineral mixture plus 5 K-wt% K_2CO_3 loading occurred at lower temperatures than that of the raw coal and of the demineralized coal. These influences were discussed in Chapter 6, section 6.2 - 6.4.

Conclusion

KCl is more susceptible to deactivation by mineral matter than K_2CO_3.

K_2CO_3 seems not to be deactivated by addition of mineral matter.

Conclusion

The results obtained indicate that demineralized coal is more reactive in a CO_2 atmosphere than raw coal and demineralized coal with added mineral mixture. The K_2CO_3 catalyst seemed to have a greater catalytic effect than the KCl for all the char samples (i.e. char samples derived from the demineralized coal, raw coal and demineralized coal with added mineral mixture).

The char prepared from the demineralized coal samples showed a faster conversion with increasing K_2CO_3 loading. For the raw coal char, only high catalyst loads of 3 and 5 K-wt% seemed to yield a catalytic effect (increased reaction rates). Very little difference was observed between the studied other catalyst loading experiments.

The CO_2 conversion of the char derived from the demineralized coal and the demineralized coal with added mineral mixture do not differ significantly and is more than that of the raw coal char. The proposed ideal system to speed up the CO_2 catalytic reaction of coal char would be to use

a demineralized coal with loadings of 3 - 5 % K_2CO_3, but may not be possible for commercial applications.

8.3 Mass Spectrometry analyses

8.3.1 The evolved gases from the coal char samples with and without catalyst loadings were successfully identified using thermogravimetry coupled with a mass spectrometer (TG-MS). The evolution temperature ranges of gaseous products of interest, H_2, CO and C were identified during heat treatments of coal char in a CO_2 atmosphere. Catalyst addition to the samples shifted the temperatures at which the maximum rate of evolution of gaseous species occurs to lower temperatures. This shift to lower temperatures was observed with increasing catalyst loadings of up to 5 K-wt% for both K_2CO_3 and KCl loaded samples. The results thus indicate that the reaction rates are enhanced, with faster formation and release of these gaseous products.

Conclusion

K_2CO_3 and KCl loadings have an effect on the composition of the volatile reaction products formed at a specific temperature during heat treatments in a carbon dioxide atmosphere.

K_2CO_3 and KCl additions cause the evolution of gaseous products to take place over a narrower temperature range than that observed for the samples without any catalyst loading.

Mass losses correspond well with the onset and termination of gas evolution.

8.4 Catalytic activity of potassium compounds

It has been reported that the catalytic activity observed due to the potassium may be attributed to the chemical effect (i.e. the catalytic effect due to the changes in the chemistry of the reaction) and/or physical effect that the potassium salts have on the char samples [Attar and Baker, 1979]. According to Attar and Baker [1979], no simple mechanism is known as to how a solid can catalyse the rate of reaction of another solid, however, catalysis of char by K_2CO_3 may be attributed to the following mechanisms; where mechanisms (i) and (iii) suggest a chemical effect by the catalyst whereas (ii), (iv) and (v) suggest a physical effect by the catalyst:

(i) increased site activity

Oxygen functional groups in the char are required in order for any catalytic effect of $K_2CO_3$to be observed. Char contains some oxygen and hydrogen although it is predominantly carbon. The oxygen present in char may be present as surface bound –OH and –COOH groups and also as adsorbed O_2, CO_2, and CO. Therefore the catalytic effect due to K_2CO_3 may be attributed to the chemical interaction of K_2CO_3 with the oxygen functional groups, where the potassium atom (K^+) replaces the H^+ of the surface bound oxygen groups, thus generating more active sites that have more active surface dipole charges, allowing the reactant gas (CO_2) to be actively adsorbed and be in close contact with the char and thus enhance reactivity.

(ii) solid-solid polarization

With char being a good conductor and K_2CO_3 having electrical charges (negative surface charges); contact between the char and K_2CO_3 may generate more active sites of high activity due to an electric dipole created.

(iii) interaction between K_2CO_3 and the gas which forms more reactive species

Chemical interactions of K_2CO_3 with the gases and/or gaseous molecules produce more reactive gaseous species which subsequently react with the char.

(iv) interaction of K_2CO_3 with the temperature field

If the rate of gasification is limited by the rate of heat of transport, then the temperature of the char will be lower than the gas temperature or the measured temperature. Therefore if K_2CO_3 enhances the rate of heat transport to the char (i.e. by absorbing more heat as radiation), then the temperature of the char particles with the catalyst may effectively be larger than the temperature of the char without the catalyst at the same measured temperature. Therefore, since the rate of gasification is an increasing function of the temperature, enhanced rates of reactions will be observed.

(v) retaining the gas absorbed near the surface of the char

If K_2CO_3 has the ability to dissolve reactant gases such as CO_2, H_2O and H_2, then the gas may be absorbed and a thin layer coated on the surface of the char; implying an increased adsorption of the gas onto the char. This may result in the char having larger surface concentrations of the reactant gas hence enhanced gasification rates.

8.5 Recommendations

(i) Molecular modelling may provide some insight into the catalytic behaviour observed for K_2CO_3 and KCl during heat treatments of coal char. This can be used to enable better explanation of whether the catalytic effect observed is a physical and/or chemical effect.

(ii) Identification and quantification of the amorphous potassium (K) species retained in the ash after thermal treatment of the coal char.

(iii) For future studies, quantitative analysis of the evolved gaseous products may provide some insight into how catalyst loadings affect the amounts of gaseous products given off during heat treatment; as well as the rate at which evolution takes place. The use of internal standards for the spectroscopic analyses may be useful in order to enable accurate determination of the amounts of gaseous products given off.

(iv) Gas chromatography, as well as gas-phase FTIR spectroscopy may be used to further investigate the composition of the gas product (volatile inorganic and organic species) by collection of the volatile species from the tube furnace experiments.

References

Annamalai, K., Thien, B., Sweeten, J., 2003. Co-firing of coal and cattle feedlot biomass (FB) fuels. Part II. Fuel 82, 1183-1193.

Atkins, P., De Paula, J., 2006. Atkins' physical chemistry. Oxford university press. 8th edition.

Atter, A., and Baker, D.,1979. Catalytic coal gasification – Part I: Mechanism of the reaction of CO_2 with char. Unpublished.

Barneto, A., Carmona, J., Alfonso, J., Ferrer, J., 2009. Use of thermogravimetry/mass spectrometry analysis to explain the origin of volatiles produced during biomass pyrolysis. Industrial and Engineering Chemistry Resource 48. 7430-7436.

Blackwood, J., and Ingeme, A., 1960. The reaction of carbon with carbon dioxide at high temperature. Australian Journal of Chemistry 13. 194-209.

Brown, T., Haynes, B., 1992. Interaction of CO with carbon and carbon surface oxides. Energy & Fuels 6. 154.

Bruno, G., Carvani, L., Passoni, G., 1986. Correlation between potassium losses and mineral matter composition in catalytic coal steam gasification. Fuel 65, 1473-1475.

Cai, H., and Kandiyoti, R., 1995. Effect of changing inertinite concentration on pyrolysis yields and char reactivities of two South African Coals. Energy & Fuels. 956-961.

Chen, S., Yang, R., Kapteijn, F., Moulijn, J., 1993. A new surface oxygen complex on carbon: toward a unified mechanism for carbon gasification reactions. Industrial and Engineering Chemistry 32. 2835-2840.

Ergun, S., and Menster, M. 1965. Reactions of carbon with carbon dioxide and steam. In Chemistry and Physics of Carbon. Walker, P., Ed., Marcel Dekker: New York., Volume 1. 203-263.

Ergun,S., 1956. Kinetics of the reaction of carbon dioxide with carbon. Journal of Physical Chemistry 60. 480-485.

Everson, R., Neomagus, H., Kaitano, R., Falcon, R., du Cann, V., 2008a. Properties of high ash coal-char particles derived from inertinite-rich coal: II. Gasification kinetics with carbon dioxide. Fuel 87. 3403-3408.

Falcon, R., Snyman, C., 1986. An introduction to coal petrology: Atlas of petrographic constituents in the bituminous coals of Southern Africa. The Geological Society of South Africa. Review paper Number 2.

Fletcher, T., 1992. Chemical structure of char in the transition from devolatilization to combustion. Energy & Fuels 6. 643-650.

Formella, K., Leonhardt, P., Sulimma, A., Van Heek, K., Jüntgen, H., 1986. Interaction of mineral matter in coal with potassium during gasification. Fuel 65. 1470-1472.

Fuchs, W., and Sandhoff, A., 1942. Theory of coal pyrolysis. Industrial and Engineering Chemistry 34. 567-571.

Gadsby, J., Long, F., Sleightholm, P., Sykes, K., 1948. The mechanism of steam carbon reactions. Proceedings of the Royal Society 193. Series A. 377-399.

Garcia, X., and Radovic, L., 1986. Gasification reactivity of Chilean coals. Fuel 65. 292-294.

Glasspool, I., 2003. Palaeoecology of selected South African export coals from the Vryheid Formation, with emphasis on the role of heterosporous lycopods and wildfire derived inertinite. Fuel 82. 959-970.

Gluskoter, H., 1975. Mineral matter and trace elements in coal. In trace elements in coal; Babu, S. Advances in Chemistry. American Chemical Society. Trace elements in Coal.

Gunzler, H., Williams, A., 2002. Handbook of Analytical Techniques. Volume II.

Hagelskamp, H., and Snyman, C., 1988. On the origin of low-reflecting inertinites in coals from the Highveld Coalfield, South Africa. Fuel 67. 307-313.

Hattingh, B., Everson, R., Neomagus, H., Bunt, J., 2011. Assessing the catalytic effect of coal ash constituents on the CO_2 gasification rate of high ash, South African coal. Fuel Processing Technology 92. 2048-2054.

Hlatshwayo, T., 2009. The partition behavior and the chemical speciation of selected trace elements in a typical coal sample during pyrolysis. Masters dissertation. North-West University. Potchefstroom.

Huang, Y., Kuan, W., Chiueh, P., Lo, S., 2011. Pyrolysis by thermal analysis-mass spectrometry (TA-MS). Bioresource Technology 102. 3527-3534.

Huffman, G., and Huggins, F.,(1986). Reactions and transformations of coal mineral matter at elevated temperatures. Mineral Matter and Ash in Coal. American Chemical Society *Symposium Series* 301. Chapter 8. 100–113.

Huttinger, K., Minges, R., 1986. The influence of the catalyst precursor anion in catalysis of water vapour gasification of carbon by potassium. 2. Catalytic activity as influenced by activation and deactivation reactions. Fuel 65. 1122-1128.

ICCP (1994) System., 1998. The new vitrinite classification. International Committe for Coal and Organic Petrology (ICCP). Fuel 77. 349-358.

ICCP (1994) System., 2001. The new inertinite classification. International Committe for Coal and Organic Petrology (ICCP). Fuel 80. 459-471.

Irfan, M., Usman, M., Kusakabe, K., 2011. Coal gasification in CO_2 atmosphere and its kinetics since 1948: A brief review. Energy 36. 12-40.

Ishihara, A., Sutrisna, I., Finahari, I., Qian, E., Kabe, T., 2004. Effect of demineralization on hydrogen transfer of coal with tritiated gaseous hydrogen. Fuel Processing Technology 85. 887-901.

Kapteijn, F., Abbel, G., Moulijn, J., 1984. CO_2 gasification of carbon catalysed by alkali metals. Reactivity and mechanism. Fuel 63. 1036-1042.

Kapteijn, F., Meijer, R., Moulijn, J., 1992. Transient kinetic techniques for detailed insight in gas-solid reactions. Energy & Fuels 6. 494-497.

Kapteijn, F., Meijer, R., van Eck, B., Moulijn, J., 1991. Active sites in carbon gasification with CO_2 transient kinetic experiments. In Fundamental Issues in Control of Carbon Gasification Reactivity.Lahaye, J., Ehrburger, P., Eds. Kluwer: Dordrecht. 221-233.

Kershaw, J., Taylor, G., 1992. Properties of Gondwana coals with emphasis on the Permian coals of Australia and South Africa. Fuel Processing Technology 31. 127-168.

Key, A., 1948. Gas Research Board Communication, 40, 36.

Kim, K., Kim, K., Choi, J., 1989. K_2CO_3-catalysed steam gasification of coal char. Fuel 68. 1343-1346.

Klopper, L., Strydom, C., Bunt, J., 2012. Influence of added potassium and sodium carbonates on CO_2 reactivity of the char from a demineralized inertinite rich bituminous coal. Journal of Analytical and Applied Pyrolysis 96. 188-195.

Koening, P., Squires, R., Laurendeau, N., 1985. Carbon-carbon dioxide reaction: Kinetics at low pressures and hydrogen inhibition. Carbon 23. 531-536.

Koening, P., Squires, R., Laurendeau, N., 1986. Char gasification by carbon dioxide. Fuel 65. 412-416.

Kruszewska, K., 2003. Fluorescing macerals in South African coals. International Journal of Coal Geology 54. 79-94.

Kyotani, T., Kubota, K., Cao, J., Yamashita, H., Tomita, A., 1993. Combustion and CO_2 gasification of coals in a wide temperature range. Fuel Processing Technology 36. 209-217.

Kyotani, T., Tomita, A., 1999. Analysis of the Reaction of Carbon with NO/N_2O Using Ab Initio Molecular Orbital Theory. Journal of Physical Chemistry 103. 3434-3441.

Kyotani, T., Zhang, Z., Hayashi, S., Tomita, A.,1988. A TPD study on H_2O and O_2-chemisorbed coal chars. Energy & Fuels 6. 136.

Lang, R., 1986. Anion effects in alkali-catalysed steam gasification. Fuel 65. 1324-1329.

Lehman, R., Gentry, J., Glumac, N., 1998. Thermal stability of potassium carbonate near its melting point. Thermochimica Acta 316. 1-9.

Li, X., Matuschek, G., Herrera, M., Wang, H., Kettrup, H., 2003. A study on combustion of chinese coals by TA/MS. Journal of Analytical Applied Pyrolysis 67. 393-406.

Liu, H., Luo, C., Kato, S., Uemiya, S., Kaneko, M., Kojima., 2006. Kinetics of CO_2/Char gasification at elevated temperatures Part I: Experimental results. Fuel Processing Technology 87. 775-781.

Lizzio, A., Jiang, H., Radovic, R., 1990. On the kinetics of carbon (char) gasification: Reconciliation models with experiments. Carbon 28. 7-19.

Lizzio, A., Piotrowski, A., Radovic, L., 1988. Effect of oxygen chemisorption on char gasification reactivity profiles obtained by thermogravimetric analysis. Fuel 67. 1691.

Lizzio, A., Radovic, L., 1991. Transient kinetics study of catalytic char gasification in carbon dioxide. Industrial and Engineering Chemistry 30. 1735-1744.

Malumbazo, N., Wagner, N., Bunt, J., Van Niekerk, D., Assumption, H., 2011. Structural analysis of chars generated from South African inertinite coals in a pipe-reactor combustion unit. Fuel Processing Technology 92. 743-749.

Marsh, H., Walker, P., 1979. The effects of impregnation of coal by alkali salts upon carbonization properties. Fuel Processing Technology 2. 61-75.

Matjie, R., French, D., Ward, C., Pistorius, P., Li, Z., 2011. Behaviour of coal mineral matter in sintering and slagging of ash during the gasification process. Fuel Processing Technology. 1426-1433.

Matsuoka, K., Yamashita, T., Kuramoto, K., Suzuki, Y., Takaya, A., Tomita, A., 2008. Transformation of alkali and alkaline earth metals in low rank coal during gasification. Fuel 87. 885-893.

Matthews, J., Chaffee, A., 2012. The molecular representation of coal – A review. Fuel 96. 1-14.

McCarthy, D., 1986. The C-CO_2 reaction: A note on using transient state experiments. Carbon 24. 652-653.

McKee, D., Chatterji, D., 1975. The catalytic behavior of alkali metal carbonates and oxides in graphite oxidation reactions. Carbon 13. 381-390.

Meszaros, E., Jakab, E., Varhegyi, G., 2007. TG/MS, Py-GC/MS and THM-GC/MS study of the composition and thermal behavior of extractive components of Robinia psedoacacia. Journal of Analytical Applied Pyrolysis 79. 61-70.

Miura, K., Hashimoto, k., Silveston, P., 1989. Factors affecting the reactivity of coal chars during gasification, and indices representing reactivity. Fuel 68. 1461-1475.

Montoya, A., Mondragon, F., Truong, T., 2002. Formation of CO precursors during char gasification with O_2, CO_2 and H_2O. Fuel Processing Technology 77–78. 125–130.

Moulijn, J., Cerfontain, M., Kapteijn, F., 1984. Mechanism of potassium catalysed gasification of carbon in CO_2. Fuel 63. 1043-1047.

Moulijn, J., Kapteijn, F., 1995. Towards a unified theory of reactions of carbon with oxygen-containing molecules. Carbon 33. 1155-1165.

Narkiewicz, M., Matthews, J., 2008. Improved low-volatile bituminous coal representation: incorporating the molecular weight distribution. Energy Fuels 22. 104-111.

Nel, M., Strydom, C., Schobert, H., Beukes, P., Bunt, J., 2011. Comparison of sintering and compressive strength tendencies of a model coal mineral mixture heat-treated in inert and oxidizing atmospheres. Fuel Processing Technology 92. 1042-1051.

Nishiyama, Y.,1986. Catalytic behavior of iron and nickel in coal gasification. Fuel 65. 1404-1409.

Oboirien, B., Engelbrecht, A., North, B., du Cann, V., Verryn, S., Falcon, R., 2011. Study on the structure and gasification characteristics of selected South African bituminous coals in fluidized bed gasification. Fuel Processing Technology 92. 735-742.

Ochoa, J., Cassanello, M., Bonelli, P., Cukierman., A., 2001. CO_2 gasification of Argentinean coal chars: a kinetic characterization. Fuel Procsessing Technology 74. 161-176.

Otero, M., Diez, C., Calvo, L., Garcia, A., Moran, A., 2002. Analysis of the co-combustion of sewage sludge and coal by TG-MS. Biomass Bioenergy 22. 319-329.

Otero, M., Sanchez, M., Gomez, X., 2011. co-firing of coal and manure biomass: A TG-MS approach. Bioresource Technology 102. 8304-8309.

Radovic, L., 2005. The mechanism of CO_2 chemisorption on zigzag carbon active sites: A computational chemistry study. Carbon 43. 907–915.

Radovic, L., 2009. Active sites in grapheme and the mechanism of CO_2 formation in carbon oxidation. Journal of American Chemical Society. 17166–17175.

Radovic, L., Jiang, H., Lizzio, A., 1991. A transient kinetics study. References of char gasification in carbon dioxide and oxygen. Energy Fuels 5. 68-74.

Radovic, L., Steczko., K., Walker, P., Jenkins, R., 1985. Combined effects of inorganic constituents and pyrolysis conditions on the gasification reactivity of coal chars. Fuel Processing Technology 10. 311-326.

Rivera-Utrilla, J., Lopez-Peinado, A., Moreno-Castilla, C., Lopez-Gonzalez, J., 1987. Reactivity of Spanish coals in dry air. Effect of the addition of potassium carbonate and acetate. Fuel 66. 237-241.

Sams, D., and Shadman, F., 1983. Catalytic effect of potassium on the rate of char-CO_2 gasification. Fuel 62. 880-882.
Scott, A., 2002. Coal petrology and the origin of coal macerals: a way ahead. International Journal of Coal Geology 50. 119-134.
Shinn, J., 1984. From coal to single-stage and two-stage products: a reactive model of coal structure. Fuel 63. 1187-1196.
Skoog, D., Holler, F., Nieman, 1998. Principles of instrumental analysis. 5th edition.
Snyman, C.P., 1998. The mineral resources of South Africa. 6th edition. Council for Geoscience.
Speight, J., 2005. Handbook of coal analysis. Volume 166.
Spiro, C., Wong, J., Lytle, W., Greegor, R., Maylotte, D., Lamson, S., 1986. Forms of potassium in coal and its combustion products. Fuel 65. 327-336.
Stach, E., Mackowsky, M., Teichmuller, M., Taylor, G., Chandra, D., Teichmuller, R., 1975. Stach's textbook of coal petrology. 2nd edition.
Stach, E., Mackowsky M., Teichmuller, M., Taylor, G., Chandra, D., Teichmuller, R., 1982. Stach's textbook of coal petrology. 3rd revised edition.
Strydom, C., Bunt, J., Schobert, H., Raghoo, M., 2011. Changes to the organic functional group of an inertinite rich medium rank bituminous coal during acid treatment processes. Fuel Processing Technology 92. 764-770.
Szabo, P., Varhegyi, G., Till, F., Faix, O., 1996. Thermogravimetric mass spectrometric characterization of two energy crops, Arundo donax and Miscanthus sinesis. Journal of Analytical Applied Pyrolysis 36, 179-190.
Takarada, T., Ichinose, S., Kato, K., 1992. Gasification of bituminous coal with K-exchanged brown coal prepared from potassium chloride. Fuel 71. 883-887.
Taylor, G., and Liu, S., 1987. Biodegradation in coals and other organic-rich rocks. Fuel 66. 1269-1273.
Vamvuka, D., Troulinos, S., Kastanaki, E., 2006. The effect of mineral matter on the physical and chemical activation of low rank coal and biomass materials. Fuel 85. 1763-1771.
Van Dyk, J., Waanders, F., 2007. Manipulation of gasification coal feed in order to increase the ash flow temperature of the coal enabling the gasifiers to operate at higher temperatures. Fuel 86. 2728-2735.
Van Niekerk, D., Halleck, P., Mathews, J. P., 2010. Solvent swelling behavior of Permian-aged South African vitinite-rich and inertinite-rich coals. Fuel 89,19-25.
Van Niekerk, D., Mathews, J., 2010. Molecular representations of Permian-aged vitrinite-rich and inertinite-rich South African coals. Fuel 89. 73-82.
Van Niekerk, D., Mitchell, G. D., Mathews, J. P., 2010. Petrographic and reflectance analysis of solvent-swelled and solvent-extracted South African vitrinite-rich and inertinite-rich coals. International Journal of Coal Geology 81. 45-52.
Van Niekerk, D., Pugmire, R., Solum, M., Painter, P., Mathews, J., 2008. Structural characterization of vitrinite-rich and inertinite-rich Permian-aged South African bituminous coals. International Journal of Coal Geology 76. 290–300.
Varhegyi, G., Antal, M., Szekely, T., Till, F., Jakab, E., 1988. Simultaneous thermogravimetric-mass spectrometric studies of the thermal decomposition of biopolymers. 1. Avicel cellulose in the presence and absence of catalysts. Energy Fuels 2. 267-272.
Vassilev, S., and Vassileva, C., 1996. Occurrence, abundance and origin of minerals in coals and coal ashes. Fuel Processing Technology 48. 85-106.
Vassilev, S., Kitano, K., Vassileva, G., 1996. Some relationship between coal rank and chemical and mineral composition. Fuel 75. 1537-1542.
Vassileva, C., Vassilev, S., 2006. Behaviour of inorganic matter during heating of Bulgarian coals. 2. Subbituminous and bituminous coals. Fuel Processing Technology 87. 1095-1116.
Veraa, M., and Bell, T., 1978. Effect of alkali metal catalysts on gasification of coal char. Fuel 57. 194-200.
Veras, C., Carvalho, J., Ferreira, M., 2002. The chemical percolation devolatilization model applied to the devolatilization of coal in high intensity acoustic fields. Journal of Brazillian Chemical Society 3. 358-367.
Walker, P., Rusinko, F., Austin, L., 1959. Gas reactions of carbon. Advances in Catalysis 11. 133-221.

Wang, J., Jiang, M., Yao, Y., Zhang, Y., Cao, J., 2009. Steam gasification of coal char catalyzed by K_2CO_3 for enhanced production of hydrogen without formation of methane. Fuel 88. 1572-1579.

Ward, R., 2002. Analysis and significance of mineral matter in coal seams. International Journal of Coal Geology 50. 135-168.

Waugh, A., and Bowling, K., 1984. Removal of mineral matter from bituminous coals by aqeous chemical leaching. Fuel Processing Technology 9. 217-233.

Wigmans, T., Elfring R., Moulijn, J., 1983. On the mechanism of the potassium carbonate catalyzed gasification of activated carbon: the influence of the catalyst concentration on the reactivity and selectivity at low stem pressures. Carbon 21. 1-12.

World Coal Institute, Coal Facts 2008 edition, Coal Facts 2008 edition with 2007 data. Internet: (http://www.worldcoal.org/assets_cm/files/PDF/coalfacts08.pdf). Cited 23 May 2009.

Xianglin, S., Ying, C., Haibin, L., 1999. Reserach on the melting points of some chinese coal ashes. Impact of Mineral Impurities in Solid Fuel Combustion, edited by Gupta et al. Kluwer Academic/Plenum Publishers, New York.

Ye, D., Agnew, J., Zhang, D., 1998. Gasification of a South Australian low-rank coal with carbon dioxide and steam: kinetics and reactivity studies. Fuel 77. 1209-1219.

Yu, J., Lucas, J., Wall, T., 2007. Formation of the structure of chars during devolatilization of pulverized coal and its thermoproperties: A review. Progress in Energy and Combustion Science 33. 135-170.

Zhu, Z., Finnerty, J., Lu, G., Yang, R., 2002. A Comparative Study of Carbon Gasification with O_2 and CO_2 by Density Functional Theory Calculations. Energy & Fuels 16. 1359-1368.

APPENDIX A

Table A1 Minor and trace elemental analysis of samples with/without 5 K-wt% K_2CO_3 and KCl loadings before and after heat treatments in N_2 and CO_2 atmospheres (weight %)

	As	Ba	Bi	Br	Cd	Ce	Cl	Co
DC	BDL	BDL	BDL	3.77	16.5	35.39	6.43%*	11.4
DC (N_2)	BDL	BDL	BDL	2.72	13.1	36.75	BDL	18.7
DC ($C0_2$)	BDL	BDL	BDL	2.08	7.38	36.51	BDL	20.6
D-C + 5% K_2C0_3 (N_2)	BDL	BDL	0.96	3.1	24.3	45.14	2.15%*	9.33
D-C + 5% K_2C0_3 ($C0_2$)	BDL	BDL	0.37	3.09	25.9	48.03	1.84%*	10.2
D-C + 5% KCI (N_2)	BDL	BDL	0.18	6.26	BDL	44.61	14.77%*	11.3
D-C + 5% KCI ($C0_2$)	BDL	BDL	0.39	7.2	6.53	45.79	22.27%*	10.5
Raw - Coal	BDL	BDL	1.4	2.96	23.8	38.97	93.16	10.4
R-C (N_2)	BDL	BDL	0.39	2.99	BDL	38.62	0.83%*	12.6
R-C ($C0_2$)	BDL	BDL	BDL	2.21	21.7	39.45	0.04%*	13.2
R-C + 5% K_2C0_3 (N_2)	BDL	BDL	0.07	2.45	5.3	47.76	357.35	8.96
R-C + 5% K_2C0_3 ($C0_2$)	BDL	BDL	0.15	2.3	6.55	47.92	263.22	10.4
R-C + 5% KCI (N_2)	BDL	BDL	0.37	6.67	3.98	46.45	14.2%*	8.43
R-C + 5% KCI ($C0_2$)	BDL	BDL	0.18	6.26	BDL	44.61	14.77%*	11.3
D-C + MM (N_2)	3.96	BDL	BDL	2.07	34.8	37.29	BDL	31.5
D-C + MM (C02)	6.47	BDL	BDL	1.99	0.97	39.21	BDL	31.6
D-C + MM + 5% K_2C0_3 (N_2)	BDL	BDL	BDL	7.73	22.8	42.77	9.52%*	16.9
D-C + MM + 5% K_2C0_3 ($C0_2$)	7.76	BDL	BDL	2.8	4.21	45.21	1.38%*	19.6
D-C + MM + 5% KCI (N_2)	6.58	BDL	BDL	2.98	14.6	48.69	1.65%*	17
D-C +MM + 5% KCI ($C0_2$)	3.99	BDL	0.12	6.8	38.6	43.78	9.20%*	16.4

Note: DC = demineralized coal; MM = mineral mixture; DC+MM = demineralized coal with added mineral mixture; RC = raw coal; BDL = below detection limit

Table A1…continued

	Cr	Cs	Cu	Ga	Hf	Hg	La	Lu
DC	116.9	0.82	BDL	9.87	10.5	BDL	3.51	BDL
DC (N_2)	95.75	0.4	8.45	6.12	7.84	BDL	9.38	BDL
DC ($C0_2$)	113.5	0.32	10.7	BDL	11.1	BDL	7.1	BDL
D-C + 5% K_2C0_3 (N_2)	BDL	2.07	BDL	1.79	3.69	BDL	14.85	BDL
D-C + 5% K_2C0_3 ($C0_2$)	32.86	2.31	BDL	BDL	5.69	BDL	14.44	BDL
D-C + 5% KCI (N_2)	30.29	0.37	BDL	0.59	9.61	BDL	11.24	0.23
D-C + 5% KCI ($C0_2$)	BDL	0.86	BDL	0.08	11.6	BDL	8.37	BDL
Raw - Coal	51.96	2.07	BDL	12.03	5.19	BDL	11.2	2.75
R-C (N_2)	50.86	2.58	BDL	4.49	7.51	BDL	10.22	2.57
R-C ($C0_2$)	64.05	2.12	BDL	BDL	8.17	BDL	11.42	BDL
R-C + 5% K_2C0_3 (N_2)	BDL	1.68	BDL	2.12	5.88	BDL	12.87	BDL
R-C + 5% K_2C0_3 ($C0_2$)	37.13	2.15	BDL	1.84	4.52	BDL	13.03	BDL
R-C + 5% KCI (N_2)	BDL	0.35	BDL	5.14	7.59	BDL	11.79	1.79
R-C + 5% KCI ($C0_2$)	30.29	0.37	BDL	0.59	9.61	BDL	11.24	0.23
D-C + MM (N_2)	145.3	0.75	55.1	10.11	1.43	BDL	4.76	4.35
D-C + MM (C02)	153	0.78	56.4	7.09	7.46	BDL	9.03	1.23
D-C + MM + 5% K_2C0_3 (N_2)	48.31	0.9	21.1	11.44	2.92	BDL	10.3	BDL
D-C + MM + 5% K_2C0_3 ($C0_2$)	25.27	2.66	23.7	6.11	5.19	BDL	12.52	1.88
D-C + MM + 5% KCI (N_2)	11.07	2.32	20.2	10.12	5.39	BDL	15.6	BDL
D-C +MM + 5% KCI ($C0_2$)	BDL	0.96	20.2	3.71	4.88	BDL	8.08	BDL

Note: DC = demineralized coal; MM = mineral mixture; DC+MM = demineralized coal with added mineral mixture; RC = raw coal; BDL = below detection limit

Table A1…continued

	Mo	Nb	Nd	Ni	Pb	Rb	Sb	Sc
DC	1.45	9.79	74.7	212.7	BDL	BDL	BDL	6.14
DC (N_2)	1.56	13.6	79.1	210.7	BDL	BDL	BDL	5.02
DC ($C0_2$)	1.15	5.96	75.1	225.2	BDL	BDL	0.94	5.42
D-C + 5% K_2C0_3 (N_2)	1.6	10.7	74.9	171.9	BDL	8.05	1.08	1.96
D-C + 5% K_2C0_3 ($C0_2$)	1.57	10.6	76.9	193.6	BDL	12.28	0.82	1.8
D-C + 5% KCI (N_2)	0.91	BDL	75.9	158.1	BDL	17.17	0.95	0.11
D-C + 5% KCI ($C0_2$)	1.68	11.8	73.1	164.7	BDL	13.88	0.01	0.66
Raw - Coal	0.67	BDL	82.6	242	6.79	4.02	BDL	7.07
R-C (N_2)	0.59	BDL	79.1	220.3	BDL	6.62	BDL	12.7
R-C ($C0_2$)	0.44	BDL	77.8	237.7	BDL	8.6	BDL	8.29
R-C + 5% K_2C0_3 (N_2)	0.44	BDL	81.8	195.7	BDL	13.96	BDL	4.83
R-C + 5% K_2C0_3 ($C0_2$)	0.49	BDL	78	175.8	BDL	16.27	0.53	6.85
R-C + 5% KCI (N_2)	0.48	BDL	69.3	170.4	BDL	8.34	0.54	1.13
R-C + 5% KCI ($C0_2$)	0.91	BDL	75.9	158.1	BDL	17.17	0.95	0.11
D-C + MM (N_2)	1.55	10.6	54.9	100.8	6.01	3.16	BDL	9.75
D-C + MM (C02)	1.37	9.09	52.7	91.42	5.61	3.09	0.92	9.38
D-C + MM + 5% K_2C0_3 (N_2)	1.1	0.14	72	90.17	BDL	5.66	0.46	3.28
D-C + MM + 5% K_2C0_3 ($C0_2$)	1.42	5.9	65.2	113.9	BDL	13.18	BDL	5.51
D-C + MM + 5% KCI (N_2)	1.53	7.52	65.6	100.7	BDL	9.55	BDL	3.06
D-C +MM + 5% KCI ($C0_2$)	1.19	1.85	65.4	88.77	BDL	11.18	BDL	3

Note: DC = demineralized coal; MM = mineral mixture; DC+MM = demineralized coal with added mineral mixture; RC = raw coal; BDL = below detection limit

Table A1…continued

	Se	Sm	Sn	Sr	Ta	Te	Th	Tl
DC	1.58	2.87	1.09	215.8	0.35	0.01	6.27	0.3
DC (N_2)	1.18	12.5	1.46	291.1	0.3	0.01	7.9	BDL
DC ($C0_2$)	1.16	13.5	1.07	286.8	1.1	0.01	5.88	BDL
D-C + 5% K_2C0_3 (N_2)	1.21	7.91	1.32	194.6	3.34	0	5.71	3.83
D-C + 5% K_2C0_3 ($C0_2$)	1.27	10.9	2.25	211.2	4.36	0	8.37	1.67
D-C + 5% KCI (N_2)	0.64	11.6	1.43	511.6	4.86	0.01	7.94	1.04
D-C + 5% KCI ($C0_2$)	0.7	17.9	0.53	218.8	4.93	0.01	10.01	1.57
Raw - Coal	0.49	9.07	3.23	685.2	BDL	0.01	4.45	BDL
R-C (N_2)	1.09	0.84	1.89	819.4	0.14	0	4.79	BDL
R-C ($C0_2$)	0.92	1.3	3.57	870.8	4.21	0.01	8.14	BDL
R-C + 5% K_2C0_3 (N_2)	0.66	4.07	3.09	605.8	1.93	0	5.5	BDL
R-C + 5% K_2C0_3 ($C0_2$)	0.85	10.1	1.85	627.6	2.71	0	8.23	BDL
R-C + 5% KCI (N_2)	0.36	10.5	2.44	545.4	3.34	0.01	6.41	BDL
R-C + 5% KCI ($C0_2$)	0.64	11.6	1.43	511.6	4.86	0.01	7.94	1.04
D-C + MM (N_2)	0.71	34.1	3.56	224	1.07	0.01	5.25	BDL
D-C + MM (C02)	0.4	40.6	1.63	236.2	3.79	0.01	5.98	BDL
D-C + MM + 5% K_2C0_3 (N_2)	0.59	16.3	2.33	160.7	4.94	0.01	6.16	1.29
D-C + MM + 5% K_2C0_3 ($C0_2$)	1.17	28.6	2.17	179.1	2.99	0	7.26	1.49
D-C + MM + 5% KCI (N_2)	0.83	30	1.93	174.9	5.87	0	7.36	2.42
D-C +MM + 5% KCI ($C0_2$)	0.61	24.2	2.66	159.7	6.69	0.01	4.87	0.53

Note: DC = demineralized coal; MM = mineral mixture; DC+MM = demineralized coal with added mineral mixture; RC = raw coal; BDL = below detection limit

Table A1…continued

	U	W	Y	Yb	Zn	Zr
DC	8.17	3.37	BDL	1.32	12.6	52.2
DC (N_2)	17.39	2.57	10.8	3.33	BDL	128.4
DC ($C0_2$)	19.76	2.39	18	5.22	BDL	159.3
D-C + 5% K_2C0_3 (N_2)	5.68	3.45	2.93	0.62	BDL	65.86
D-C + 5% K_2C0_3 ($C0_2$)	2.47	3.33	3.81	0.4	BDL	78.31
D-C + 5% KCI (N_2)	17.4	2.46	BDL	2.56	BDL	BDL
D-C + 5% KCI ($C0_2$)	4	3.05	BDL	0.49	BDL	BDL
Raw - Coal	41.13	2.31	7.71	0.61	23.9	58.1
R-C (N_2)	43.03	2.98	11.5	1.49	BDL	81.86
R-C ($C0_2$)	43.77	3	18.2	0.32	BDL	106.3
R-C + 5% K_2C0_3 (N_2)	25.14	2.6	10.7	BDL	BDL	73.38
R-C + 5% K_2C0_3 ($C0_2$)	21.62	2.51	13	1.91	BDL	82.38
R-C + 5% KCI (N_2)	18.03	1.87	BDL	2.17	BDL	BDL
R-C + 5% KCI ($C0_2$)	17.4	2.46	BDL	2.56	BDL	BDL
D-C + MM (N_2)	6.52	1.64	13.5	4.93	4.15	119.9
D-C + MM (C02)	7.75	1.49	14.4	6.02	BDL	134.5
D-C + MM + 5% K_2C0_3 (N_2)	2.76	2.8	BDL	1.87	5.13	BDL
D-C + MM + 5% K_2C0_3 ($C0_2$)	1.36	2.99	4.51	3.16	BDL	74.59
D-C + MM + 5% KCI (N_2)	2.51	2.77	1.26	3.26	2.25	57.14
D-C +MM + 5% KCI ($C0_2$)	1.03	2.43	BDL	2.44	BDL	BDL

Note: DC = demineralized coal; MM = mineral mixture; DC+MM = demineralized coal with added mineral mixture; RC = raw coal; BDL = below detection limit

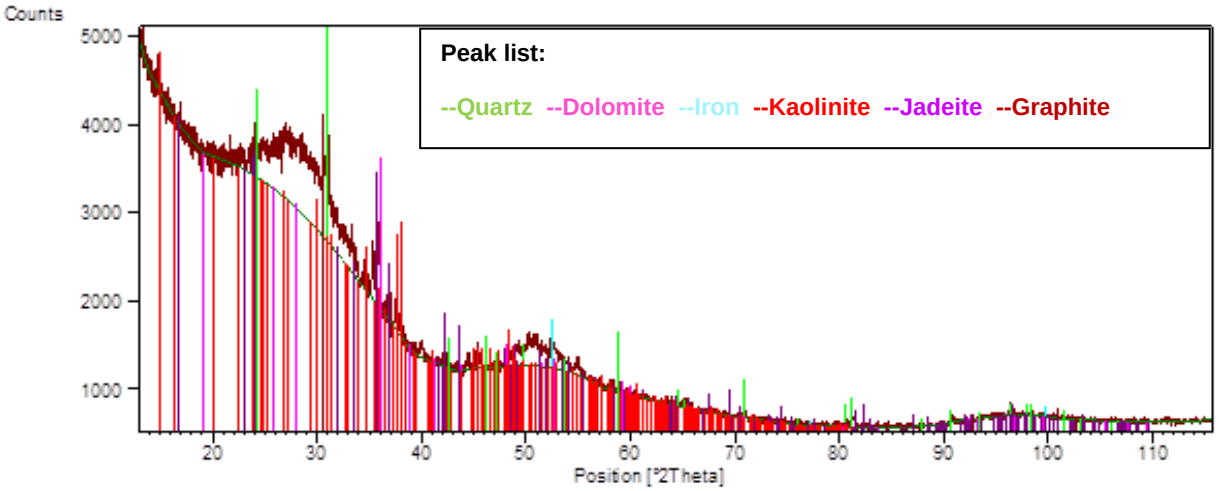

Figure A1 XRD diffractogram of DC + 5 K-wt% K_2CO_3 after heat treatment in N_2

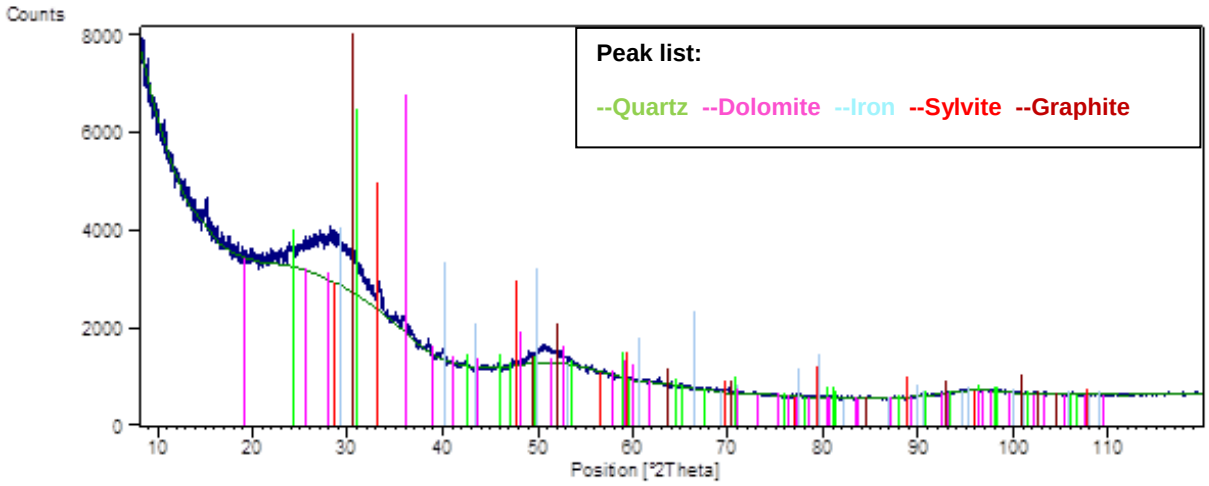

Figure A2 XRD diffractogram of DC + 5 K-wt% K_2CO_3 after heat treatment in CO_2

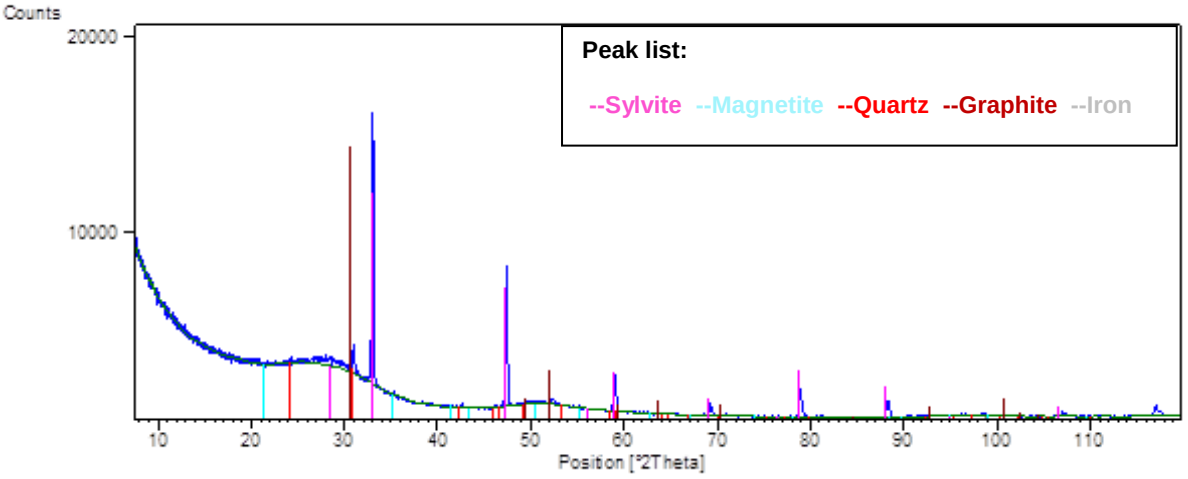

Figure A3 XRD diffractogram of DC + 5 K-wt% KCl after heat treatment in N_2

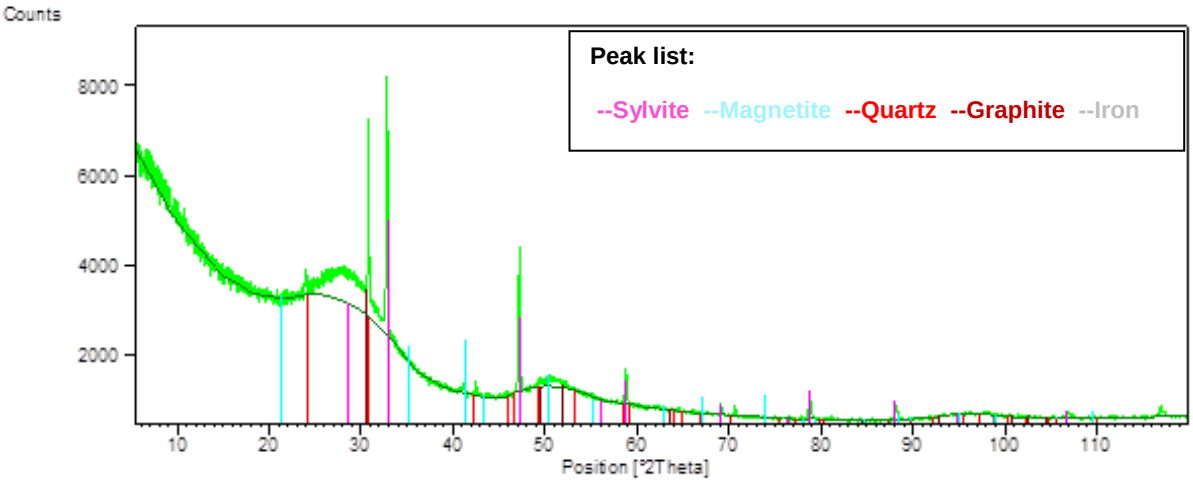

Figure A4 XRD diffractogram of DC + 5 K-wt% KCl after heat treatment in CO_2

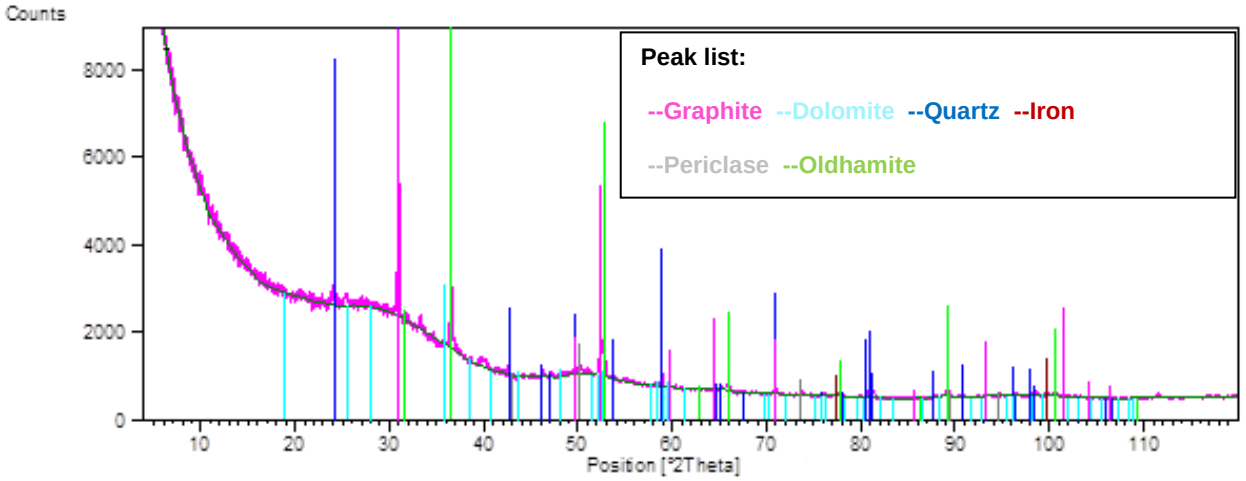

Figure A5 XRD diffractogram of RC + 5 K-wt% K_2CO_3 after heat treatment in N_2

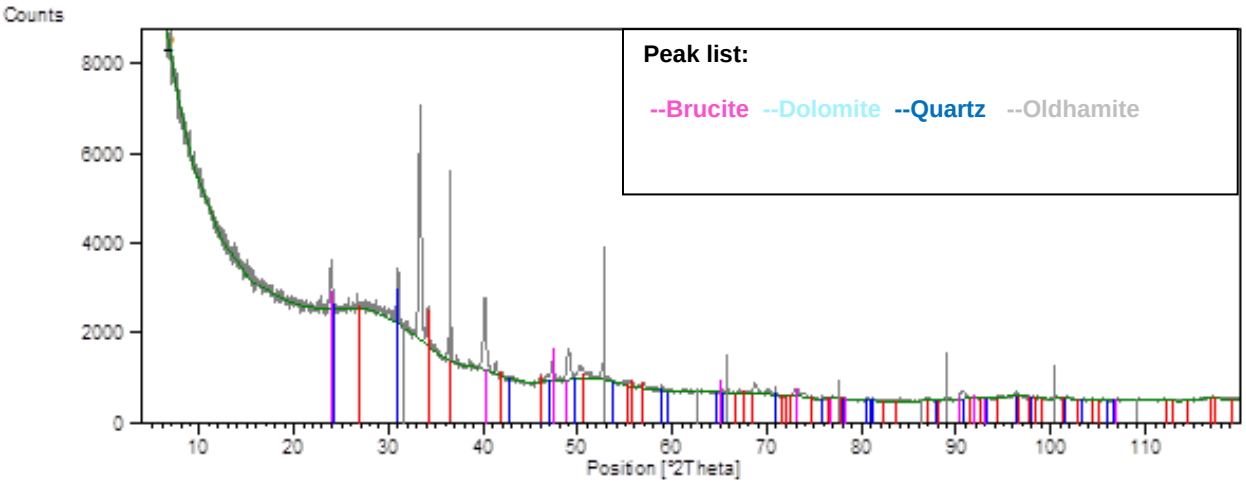

Figure A6 XRD diffractogram of RC + 5 K-wt% K_2CO_3 after heat treatment in CO_2

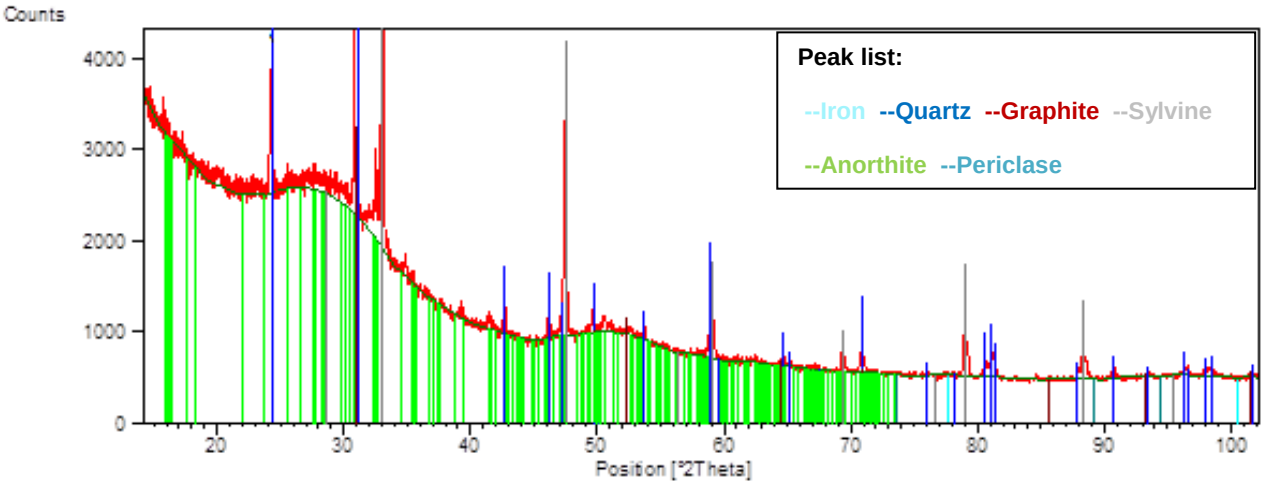

Figure A7 XRD diffractogram of RC + 5 K-wt% KCl after heat treatment in N_2

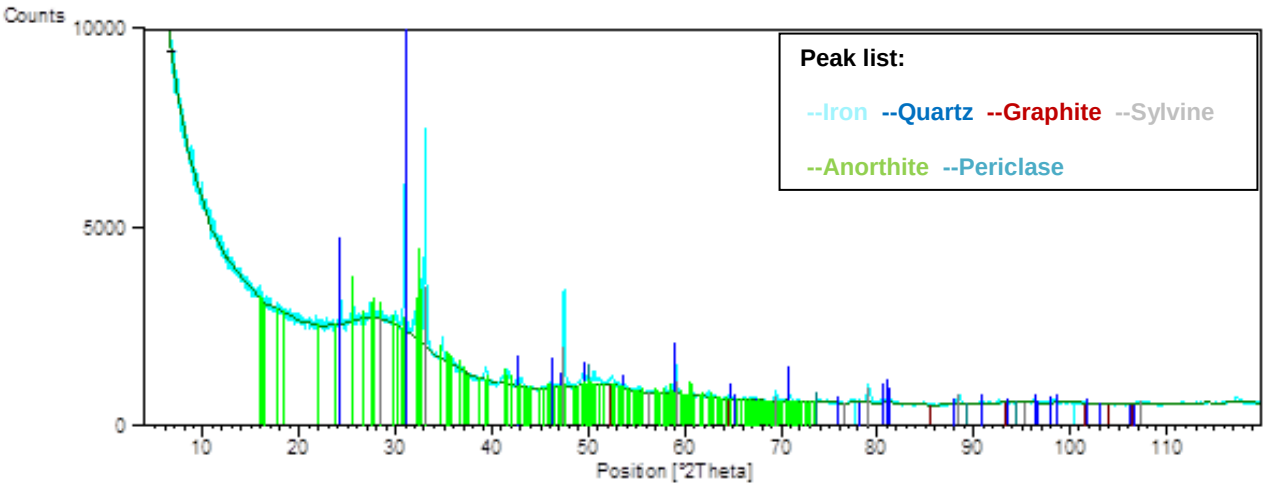

Figure A8 XRD diffractogram of RC + 5 K-wt% KCl after heat treatment in CO_2

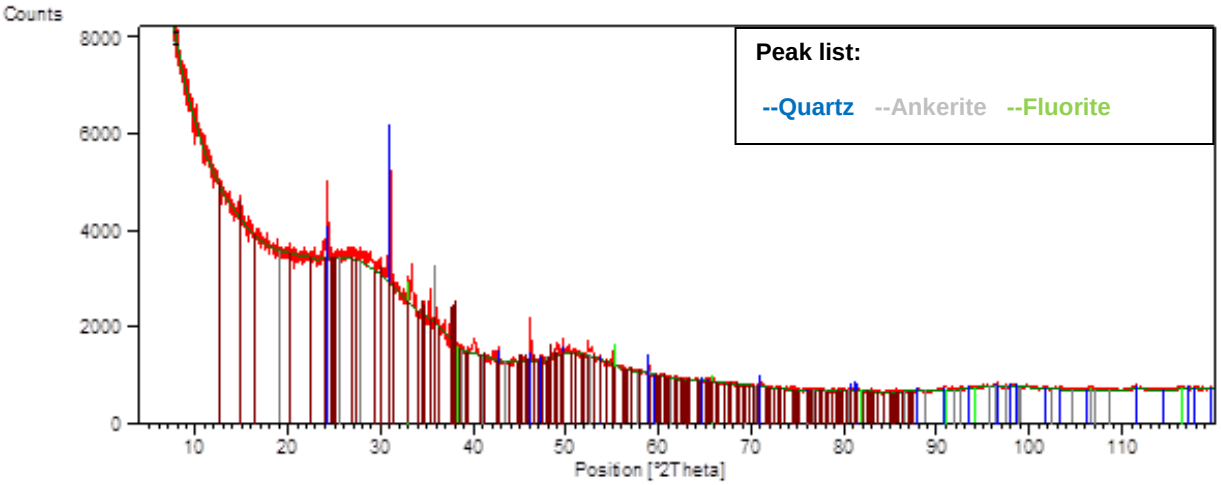

Figure A9 XRD diffractogram of DC+MM + 5 K-wt% K_2CO_3 after heat treatment in N_2

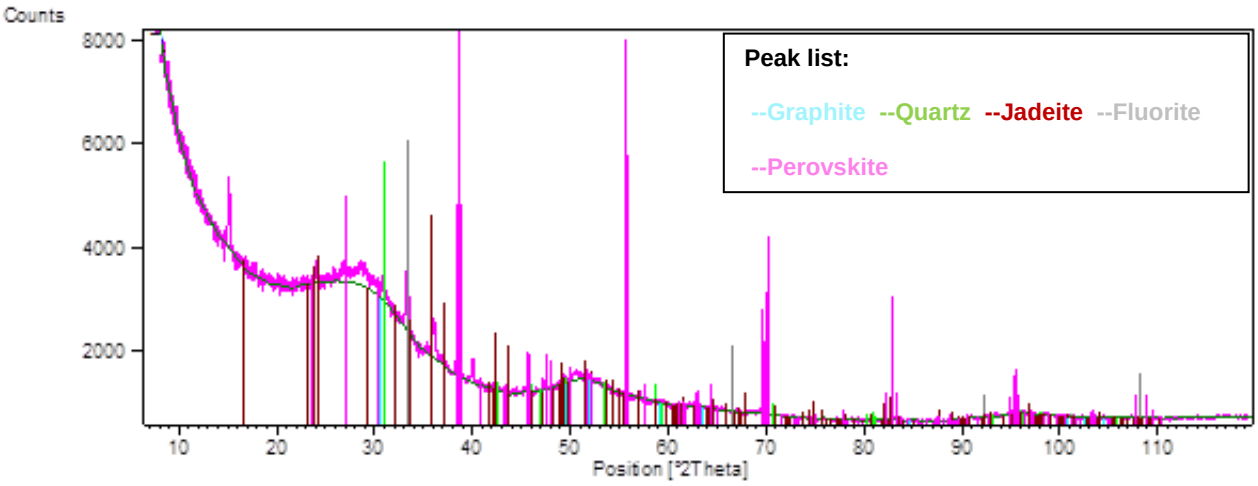

Figure A10 XRD diffractogram of DC+MM + 5 K-wt% K_2CO_3 after heat treatment in CO_2

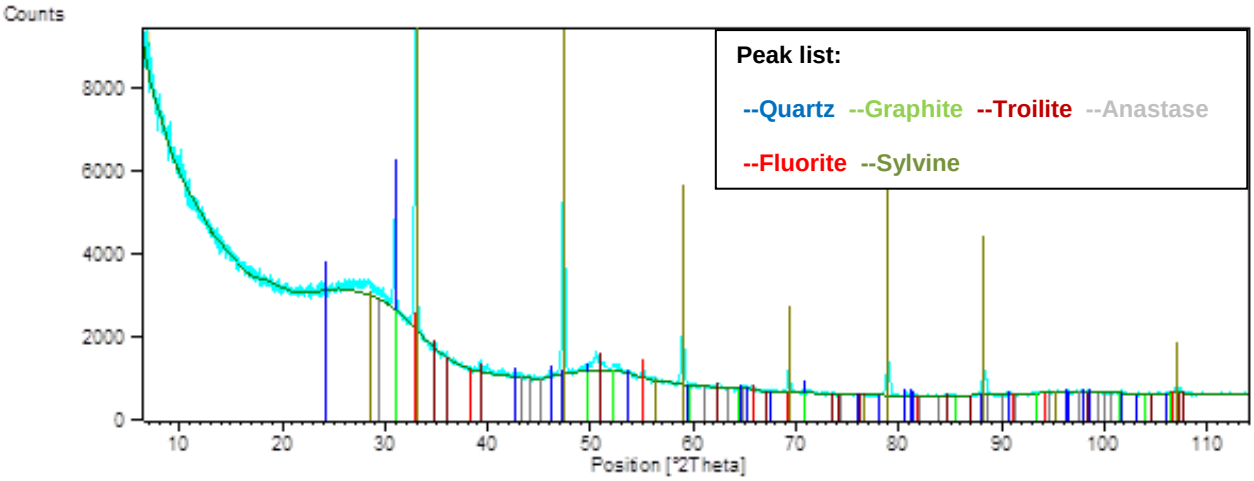

Figure A11 XRD diffractogram of DC+MM + 5 K-wt% KCl after heat treatment in N_2

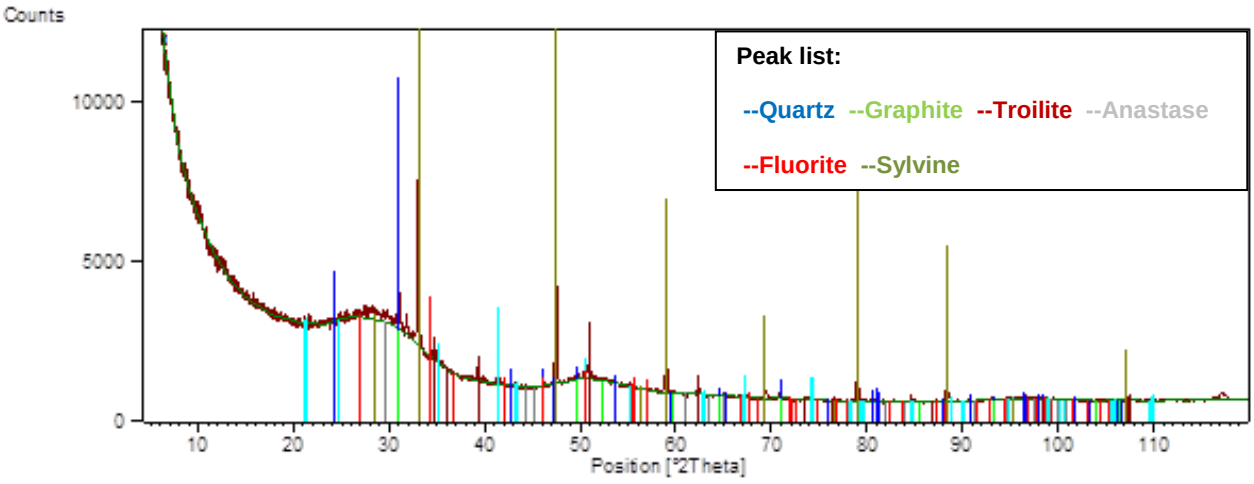

Figure A12 XRD diffractogram of DC+MM + 5 K-wt% KCl after heat treatment in CO_2

Table A2 Temperature values at $T_{50\%}$

	DC		RC		DC + MM	
K-wt% loading	K_2CO_3	KCl	K_2CO_3	KCl	K_2CO_3	KCl
0	1302	1029	1030	1030	995	995
0.5	1257	978	1017	1012	970	961
1	1226	942	1004	999	940	943
3	1158	894	931	976	872	903
5	1114	878	882	970	825	898

Note: DC = demineralized coal; DC+MM = demineralized coal with added mineral mixture; RC = raw coal